Soluble modulators of intermolecular interactions in proteins and lipid rafts

---

Thesis submitted to the University of Nottingham for the degree of Doctor of Philosophy

Jordan Lane, B.Sc. (Hons)

Abstract

The nonspecific binding of proteins to various biological and non-biological surfaces has limited the potential of several detection techniques such as surface plasmon resonance (SPR), Luminex and ELISA (among others). Plasma proteins have been shown to decrease the sensitivity of instruments when working with complex fluids such as blood samples. This study examines the binding properties of several plasma proteins to a range of surfaces and utilises reagents in the media to eliminate the nonspecific binding of the plasma proteins. This has created a set of conditions that can reduce the nonspecific binding interaction, without affecting the specific interactions which the various techniques measure.

These mechanisms were then applied to the assembly/disassembly of membrane microdomains. Membrane microdomains have been shown to be affected by from several factors such as acyl-chain length and temperature. This study demonstrates how reagents in the media can affect the assembly of these domains. We proposed a novel mechanism for the regulation of the domains, in which the reagents alter the intermolecular interactions between lipid head groups by altering the water network around these domains to promote domain assembly. These results that could have significant ramifications for the functional characterisation of membrane microdomains and the proteins that are known to associate with them.

Finally, membrane binding affinity and kinetics of different polypeptides with various lipid membrane composition were characterised and resultant microdomains were monitored. Demonstrating how the previously uncontrolled, soluble factors in a model system can control the intermolecular interactions that occur in the system that is being measured.

Abbreviation

AFM	Atomic Force Microscopy
bMFI	Background median fluorescence intensity
Chol	Cholesterol
D	Debye length (also dielectric increment)
ε	Dielectric constant
ε_0	Permittivity of free space
EDC	N-Ethyl-N'-Dimethylaminopropyl-Carbodimide
DAD	Detection antibody diluent
DCMR	Dielectric constant modifying reagent
DLPC	1,2-dilauroyl-sn-glycero-3-phosphocholine
DOPC	1,2-dioleoyl-sn-glycero-3-phosphocholine
DOPS	1,2-dioleoyl-sn-glycero-3-phospho-L-serine
DPPC	1,2-dipalmitoyl-sn-glycero-3-phosphocholine
DRM	Detergent resistant microdomains
DSPC	1,2-distearoyl-sn-glycero-3-phosphocholine
HSA	Human Serum Albumin
I	Ionisation potential
F	Force
FGF	Fibroblast growth factor
FI	Fluorescence intensity
Fib	Fibrinogen
FRAP	Fluorescence recovery after photobleaching
FPE	Fluoresceinphosphatidylethanolamine
G-CSF	Granulocyte-colony stimulating factor

GM-CSF	Granulocyte-macrophage-colony stimulating factor
IFN-γ	Interferon gamma
IL-1β	Interleukin 1-beta
IP-10	Interferon gamma induced protein 10
L_o	Liquid ordered phase
L_d	Liquid disordered phase
L_β	Gel phase
LOD	Limit of detection
LCSM	Laser Scanning Confocal Microscopy
MCP-1	Monocyte chemoattractant protein-1
MIP-1α	Macrophage inflammatory protein 1-alpha
MIP-1β	Macrophage inflammatory protein 1-beta
n	Refractive index
NHS	N-Hydroxysuccinimide
PBS	Phosphate buffered saline
PBST	Phosphate buffered saline Tween
PC	Phosphatidylcholine
PDGF-BB	Platelet-derived growth factor BB
PEG	Polyethylene glycol
PMT	Photomultiplier tube
PolyK	Poly-l-lysine
PolyQ	Poly-glutamine
POPC	1-palmitoyl-2-oleoyl-sn-glycero-3-phosphocholine
POPS	1-hexadecanoyl-2-(9Z-octadecenoyl)-sn-glycero-3-phospho-L-serine
PS	Phosphatidylserine

RANTES	Regulated on activation normal T cell expressed and secreted
ROI	Region of interest
SA-PE	Streptavidin-phycoerythine
SD	Standard deviation
Sig	Significant difference
SLB	Supported lipid bilayer
SM	Sphingomyelin
SPR	Surface plasmon resonance
ThT	Thioflavin T
TNF-α	Tumour necrosis factor alpha
T_m	Phase transition temperature
μ	Dipole moment
VEGF	Vascular endothelial growth factor
μ_0	Permeability of free space
μ’	Dipole self energy
$\Delta\Psi$	Transmembrane potential
Ψ_d	Membrane dipole potential
Ψ_s	Electrostatic membrane surface potential
λ	Wavelength

Publication List

RICHENS J.L., **LANE, J.S.**, MATHER M.L. AND O'SHEA, P. 2015. The interactions of squalene, alkanes and other mineral oils with model membranes; effects on membrane heterogeneity and function. *Journal of Colloid and Interface Science*, 457, 225-231.

RICHENS J.L., **LANE, J.S.**, BRAMBLE, J.P., AND O'SHEA, P. 2015. The electrical interplay between proteins and lipids in membranes. *Biochimica et Biophyisca Acta (BBA) – Biomembranes*. 1848(9), 1828-1836.

LANE, J. S., RICHENS, J. L., VERE, K.-A. & O'SHEA, P. 2014. Rational Targeting of Subclasses of Intermolecular Interactions: Elimination of Nonspecific Binding for Analyte Sensing. *Langmuir*, 30, 9457-9465.

VERE, K.-A., RICHENS, J. L., **LANE, J. S.**, HARRIS, H. J., DUGGAN, J. & O'SHEA, P. 2013. Evidence for sodium metasilicate receptors on the human osteoblast cell surface; spatial localization and binding properties. *Molecular Membrane Biology*, 30, 386-393.

Acknowledgements

During the years I have spent at the University of Nottingham there have been many people to whom I will always be grateful. Firstly, I must thank my supervisor, Paul O'Shea, for opening my eyes to the world of biophysics and offering guidance and support to build myself both academically and personally. The work carried out by himself, and the larger group, has been an enthralling task, in which he has facilitated several international trips and work with world-class collaborators on the EPSRC CAPTIALS project. Secondly, I would like to thank Simon Connell and Anders Aufderhorst-Roberts (University of Leeds), for their help with atomic force microscopy.

I also offer a great deal of thanks to the members of the Cell Biophysics Group, especially Jo Richens, for all the support, advice and technical excellence she has imparted me with. As well as Jonathan Bramble, who has offered a keen insight into other fields and Kelly-Ann Vere for her excellent management and support.

I would not be the person I am, or in the situation that I am in without the years of tireless support of my family, who have helped me every step along the road to this point, and to whom I can never be thankful enough. I would like to especially thank Amy Slater, who has been my balancing force throughout my life and especially at keeping me sane through the difficult times of writing my thesis. Alongside my host of friends who have been with me to enjoy every moment.

Table of Contents

1 Introduction 14

1.1 Preface 14

1.2 Proteins 16

1.2.1 Albumin 17

1.2.2 Fibrinogen 19

1.2.3 Poly-lysine 20

1.2.4 Poly-glutamine 21

1.3 Protein-protein interactions 24

1.4 Forces Involved in the Interactions between Biological Molecules 24

1.4.1 Charge-charge Interactions 25

1.4.2 Dipole interactions 27

1.4.3 Van der Waals forces 27

1.4.4 Hydrogen bonding 28

1.4.5 DLVO Theory 30

1.4.6 Bio-recognition 32

1.5 Protein-lipid and lipid-lipid interactions 35

1.6 Classes of molecules that can interfere with intermolecular interactions 36

1.6.1 Sodium Thiocyanate 36

1.6.2 Short Peptides that Modulate the Dielectric Constant 38

1.6.3 Different Factors of a Detection Instrument Medium 41

1.7 The complexity of the lipid bilayer 43
1.8 Membrane structure, formation and complexity 44
1.8.1 Assembly of Lipids into Membranes 47
1.8.2 Membrane Molecular Dynamics and Phase Formation 52
1.8.3 Lipid Rafts and their investigation 58
1.9 Measuring protein-lipid interactions: membrane potentials 65
1.10 Aims and Objectives 75
2 Materials and Methods 77
2.1 Lipid Compositions 77
2.2 Liquid Media Compositions 78
2.3 Proteins and Peptide Species 79
2.4 Unilamellar Lipid Vesicle Formation 79
2.5 Membrane Vesicle Labelling With FPE 80
2.6 Spectroscopic Analysis of Membrane Probe FPE 82
2.7 Fluorescence Analysis of FPE Probe 83
2.8 Stopped-flow rapid mixing and analysis 86
2.8.1 Kinetic data analysis 87
2.8.2 Protein Aggregation Studied by Thioflavin T 89
2.9 Supported Unilamellar Bilayers 90
2.10 Optical analysis of membrane bilayers 91
2.10.1 Confocal microscopy of supported lipid bilayers 91
2.10.2 Fluorescence Recovery After Photobleaching (FRAP) 92
2.10.3 Particle analysis quantification 94

2.11 Local spectroscopic analysis of supported lipid bilayer 96
2.12 Atomic Force Microscopy 96
2.12.1 Bilayer preparation for AFM 96
2.12.2 AFM image data capture and analysis 96
2.13 Surface Plasmon Resonance 97
2.13.1 Theory of SPR 97
2.13.2 SPR configuration 98
2.13.3 Antibody Attachment Protocol 99
2.13.4 Protein Binding Reactions 100
2.14 Bio-Rad Bio-Plex Bead-Based Multi-Analyte Detection 101
2.14.1 Detection of Analytes 101
2.14.2 Assay Performance Characteristics 103
2.14.3 Assay Accuracy 104
3 Rational Targeting of Sub-classes of Intermolecular Interactions 105
3.1 Assessing a Range of Soluble Reagents Effects on Nonspecific Binding 106
3.1.1 Protein-Membrane Binding Studies 106
3.1.2 The Effect of Media Reagents on the Membrane Binding of Albumin and Fibrinogen 108
3.1.3 The Synergistic Effect of Multiple Reagents on Membrane Binding 112
3.1.4 Further Synergistic Effect of Multiple Reagents on Membrane Binding 115

3.1.5 Summary of Membrane Binding Effect by Different Media 118

3.2 The Investigation of Nonspecific Binding between Proteins and Surfaces 118

3.2.1 Effects of Anti-nonspecific Binding Reagents on Specific Binding Reactions 128

3.2.2 Effect of Detergent Molecules on Binding Reactions 131

3.3 Validation of Anti-Nonspecific Media in Multiplex Immunoassays 134

3.3.1 Experimental design 135

3.3.2 Investigation of bead detection and separation 136

3.3.3 Identification of nonspecific binding 138

3.3.4 Specific binding of analytes 142

3.4 Discussion 145

3.4.1 The Interaction of Albumin with Model Membranes 145

3.4.2 The Interaction of Fibrinogen with Model Membranes 149

3.4.3 Interaction of Albumin and Fibrinogen to Antibodies and Surfaces . 151

3.4.4 Interaction of Multiple Analytes with Media Reagents 153

3.4.5 Summary of intermolecular forces 154

3.4.6 Future Work of Nonspecific Binding Reagents 154

4 Results 156

Regulation of membrane microdomain formation: Modulation of lipid head group interactions by targeting specific non-covalent molecular forces 156

4.1 Assessing the Membrane Organisation of Microdomains in the Presence of Soluble Reagents 158

4.1.1 Spatial Localisation of Membrane Microdomains with Various Lipid Compositions 158

4.1.2 Assessing factors that affect membrane microdomain formation with FPE-labelled SLBs 161

4.1.3 Assessing factors that affect membrane microdomain formation with Di-8-ANEPPS labelled SLBs 176

4.2 Quantification of Microdomain Formation in Supported Lipid Bilayers Assessed Using AFM 188

4.2.1 PC_{100} membranes 188

4.2.2 $DOPC_{60}Chol_{15}SM_{25}$ 192

4.2.3 Comparison of AFM and fluorescence microscopy techniques 201

4.2.4 Spectroscopic Analysis of FPE in Membrane Vesicles 205

4.2.5 Spectroscopic Analysis of FPE in Supported Lipid Bilayers 207

4.3 Discussion 209

4.3.1 Future Work for Membrane Microdomain Formation Processes 217

5 Polypeptide Control of the Assembly/Disassembly of Membrane Microdomains 219

5.1 Results 220

5.1.1 Membrane Interaction of Polypeptides 220

5.1.2 $PolyK_{10}$ Interaction with Various Membranes in Different Media 221

5.1.3 PolyK$_{cc}$ Interaction with Various Membranes in Different Media 238

5.1.4 PolyQ$_{28}$ Interaction to Membranes 253

5.2 Effect of Polypeptides on Membrane Microdomain Formation 265

5.2.1 Effect of PolyK$_{10}$ on Various Supported Lipid Bilayers in Different Media 265

5.3 Discussion 275

5.3.1 Effect of Ionic Strength on Polypeptide Binding 275

5.3.2 Dissection of the Membrane Binding Profile of Polypeptides in Various Media 277

5.3.3 PolyQ$_{28}$ interaction with Membranes 278

5.3.4 Membrane Specificity of Polypeptide Interactions 279

5.3.5 Effect of Chain Length of PolyK Interactions 282

5.3.6 β-Sheet Formation on Membrane Surfaces 283

5.3.7 Supported Bilayer Interaction of Polypeptides 285

5.3.8 Future Work into Membrane Microdomain Modulation by Polypeptides 290

6 General Conclusions 292

7 References 299

1 Introduction

1.1 Preface

Decades of development and optimisation have resulted in a toolbox to accurately depict and model protein-protein and protein-lipid interactions. The model systems within this toolbox have enabled the development of bottom-up synthetic biology; a novel approach that combines the simplest components of a living system, to construct model cells of ranging complexity to undertake and fulfil a given role.

The concept of bottom-up synthetic biology is relatively new. In terms of understanding biological membranes, the first experimental lipid monodisperse, unilamellar vesicle (or liposome) were described by Bangham in 1961 (published in 1964) [1, 2] which was shortly followed by the creation of the first model bilayer system 'the black lipid bilayer' created in 1962 [3]. In subsequent years, our increased understanding of lipid biophysics has yielded a great variety of lipid vesicle production and experimentation including: giant unilamellar vesicles, [4], nanodiscs [5], detergent micelles and bicelles [6] with added biological complexities such as the integration of membrane proteins [7, 8].

In parallel with increasing experimental complexity comes the challenge of modelling *in vivo* the complexity of the biological membrane. The classic fluid-mosaic model is widely supported as the current most accurate representation of the bilayer [9]. The delicate balance of membrane lipids, proteins, sugars and other components of *in vivo* biological membranes serves to undertake the intricate cellular processes including trafficking of proteins [10], signalling [11], differentiation [12] and apoptosis [13]. However, there is increasing *in vitro* [14] and *in silico* [15]

evidence for local heterogeneity in the biological membrane, broadly known as lipid rafts, linked with a host of functional roles. How we model the formation and activity of these domains is cause for much discussion and experimentation.

Sitting at the interface between biology and chemistry, this thesis explores how components in the aqueous phase can interact with synthetic lipid vesicles in order to mimic cell membranes more accurately.

Within the field of lipid biophysics, pure synthetic lipids in pure water are frequently used in defined binary or tertiary ratios to model the lipid bilayer. However, in reality the biological system is much more complex. As an initial step to overcome this simplistic approach, we have used naturally derived lipids to more closely mimic to the *in vivo* environment.

Secondly, interactions between the lipid bilayer and the media that surrounds it are generally overlooked, with the media assumed not to affect the lipid when investigating other binding interactions.

We then use a well-defined fluorescent probe in order to interrogate the binding between proteins and lipids and their lipid head groups. This may provide the understanding of the different intermolecular forces that underlie protein/lipid interactions and suggest ways in which these interactions may be manipulated. The interaction partners for the thesis have been chosen for a range of different reasons. Albumin and fibrinogen (represent globular and fibrillar proteins respectively) are in very high abundance in biological fluids, specifically blood. These proteins have been shown to nonspecifically bind to a range of different surfaces including interfaces directly involved in measuring a variety of biological processes, such as surface plasmon resonance and Luminex. The interactions of various polypeptides

are also assessed. Firstly, poly-lysine is frequently used in many cell and membrane based experimental systems. The effect of poly-lysine on the measurements made in these systems isn't full understood. The binding and aggregation of poly-glutamine has also been assessed, due to the pathological link of the polypeptide with Huntington's disease (discussed in more detail later).

Subsequently, the intermolecular forces that govern protein:protein and protein:lipid interactions will be discussed, followed by the formation processes and the forces involved in the lipid bilayer, followed lastly by the soluble reagents used to perturb and control these interactions.

Following the introduction, I will describe experimental systems that demonstrate the importance of reducing nonspecific binding without perturbing the specific binding. These results chapters will demonstrate that the components of a media can dramatically affect the binding parameter of proteins as well as lipid raft formation and ultimately affect complex biological systems involved in disease progression.

Uncovering the basic relationship between the aqueous media and lipid head groups at the biophysical level, could have major implications for bottom-up synthetic biology. By understanding these relationships, we could apply this understanding to influence and control the interactions within synthetic systems. Overlooked for decades, media conditions could hold the keys to the programming of synthetic systems.

1.2 Proteins

There are around 20,000 coding genes in the human genome. Assuming one protein per gene, it suggests that there should be approximately 20,000 proteins. However, the resultant proteins can differ substantially due to splice variation during translation

and later modified with a host of post-translational modifications (PMTs) such as, methylation, acetylation, phosphorylation, glycosylation to name a few.

In this study a number of protein-surface and protein-lipid interactions were investigated in order to different elucidate and minimise the intermolecular interactions present. The proteins selected in this study are: albumin, used to represent globular proteins, fibrinogen, used to represent fibrous proteins as well as different polypeptides frequently used in cell culture and another implicated in disease. These proteins offer a diverse range of physiochemical properties such as protein size, shape and charge distribution. When binding to the same target, their differential interactions allow us to elucidate the intermolecular interactions that govern their binding modes.

1.2.1 Albumin

Albumin was chosen due to being the most abundant protein in the human proteome as well as having well characterised binding parameters within the experiments used in this study. Physically, albumin is 67 kDa exhibiting a globular shape (9 x 6 x 5 nm). At physiological pH, it has a net negative charge, with an isoelectric point (PI) of pH 4.8 [16]. The various interactions of albumin with protein, lipids and surfaces has been well documented, with a full crystal structure and interactome and in fact, is the topic of a book in its honour [16].

Within human blood, albumin concentration ranges from 35-50 mg/ml, by contrast some cytokines used for biological detection in biomarker panels are 10^9 fold less abundant. Within the blood, the protein acts as a major contributor to colloidal osmotic pressure [16]. Albumin is known as a promiscuous binder and has been shown to associate with several different types of molecules, including fatty acids (Figure 1.2.1A), hormones (Figure 1.2.1B), drugs (Figure 1.2.1C) and ions (Figure

1.2.1D). The ability for albumin to bind such molecules reduces the bioavailability of several drugs *in vivo*, this has led to the expansion in the field of pharmacokinetics in order to predict these effects and the related drop in potency of different drugs. In some cases, albumin has been used as a drug carrier to increase drug selectivity and decrease off-target side effects [17]

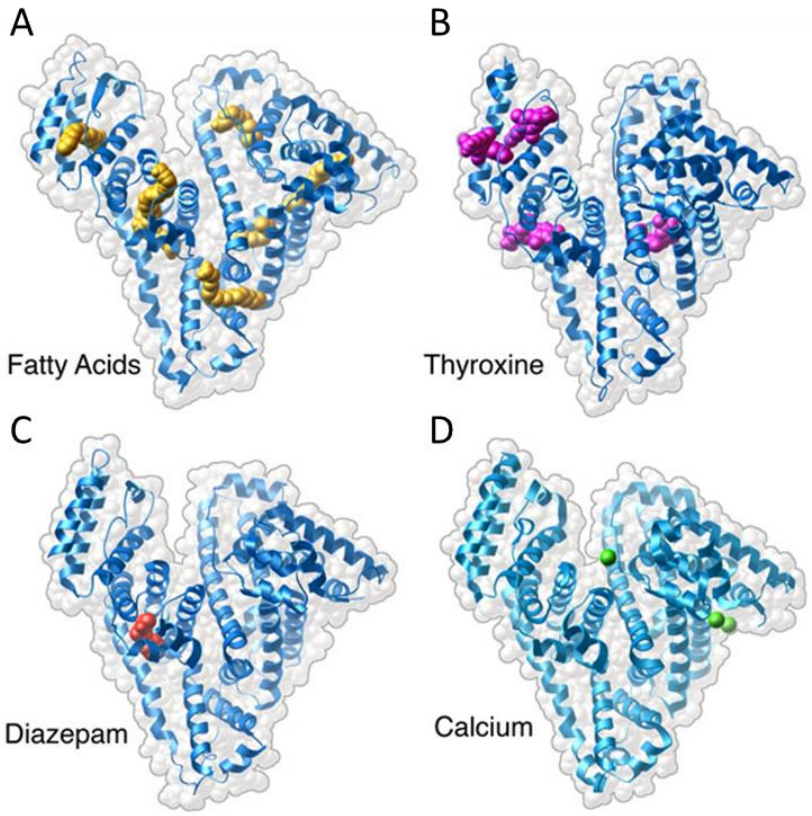


Figure 1.2.1. The complex of albumin with various bound molecules. (A) Fatty acid binds can bind in 6 different positions, (yellow) although the physiological relevance of all 6 poises is not clear [18]. Several different small molecules such as the hormone thyroxine (purple) (B), drug diazepam (red)(C) and calcium (green)(D) also bind. Adapted from [17].

Due to this promiscuous nature and abundance [19-21], albumin is frequently a problem protein when quantifying analytes in the blood [22, 23]. Several different methods have been used in the past to physically remove the albumin, such as albumin depletion kits; however, these kits have been shown to remove cytokines, which associate with albumin [23, 24]. This study aims to decrease the nonspecific

binding interactions of different proteins, without affecting the specific binding interactions. Therefore, the use of albumin will allow the work presented in this thesis to have a direct impact on the fields of biomolecular detection.

1.2.2 Fibrinogen

Fibrinogen is another abundant protein with characterised problems of nonspecific binding to various surfaces, such as biomedical devices, discussed in [25]. These binding interactions however, are different to albumin as the protein has very different physicochemical properties. Fibrinogen is a large and complex glycoprotein (340 kDa); the crystal structure shows a rod-like shape with dimensions of 9 x 47.5 x 6 nm. Like albumin, fibrinogen is negatively net charged at physiological pH (PI at pH 5.2) [26]. Fibrinogen is also highly concentrated in blood when compared to cytokines in blood, at 2-4 mg/ml.

The physical characteristics of fibrinogen vary significantly from that of albumin discussed previously. Where albumin is a globular protein with hydrophobic patches that are capable of binding multiple different analytes, fibrinogen is a linear protein that is relatively unstructured, with negatively charged domains connected by flexible α-helices.

Fibrinogen is synthesised in the liver and is involved in several different biological functions such as blood clotting and stabilisation of thrombi following vessel injury [27]. The presence of fibrinogen in blood has been used as a biomarker for deep vein thrombosis and can be radiolabelled and tracked to highlight the position of a thrombus [28].

Due to the mechanism of fibrinogen-mediated aggregation in the formation of a thrombus, characterisation of fibrinogen as a problem binder within detection

instruments is unsurprising. This makes fibrinogen specifically useful in this study, as the end-point goal would be to minimise/control the binding characteristics of all blood proteins in order to develop blood-based detections instruments for clinical use.

Previous studies, such as those by Rees and Lilley have shown that fibrinogen nonspecific binding was unaffected by NaSCN [29], which has previously been used to perturb nonspecific binding and hence is used as an exemplary protein for the further development of nonspecific binding media.

1.2.3 Poly-lysine

Poly-lysine (PolyK) was chosen for use in this study as it is commonly used in a variety of biochemical and cellular experiments. PolyK is used in cell culture to coat surfaces for improved cell adherence. As PolyK adsorbs to the surface, it enhances electrostatic interaction between the negatively charged ions on the cell membrane and positively charged ions on the culture surface [30]. In solution at physiological pH (as employed during this study), the structure of PolyK of all lengths has been shown to exhibit a random coil formation, this is expected to be due to electrostatic and steric repulsion from each positively charged residue to one another [31], giving it different physicochemical properties to folded proteins. PolyK association with membrane vesicles has been examined in the past, where it has been shown that PolyK binds to the membrane surface [30]. In this study, the interactions between the polypeptide and the membrane are examined to provide information about the binding forces involved, as well as to investigate any effect on polypeptide association with membrane microdomains. Elucidating the binding kinetics of these interactions may provide insight into the polypeptide associations of proteins such as

huntingtin with membranes, as well offer further information for those that use poly-lysine as a cell culture additive whilst studying membrane microdomains.

1.2.4 Poly-glutamine

Poly-glutamine (PolyQ) expansions have been linked with a membranes of neurological diseases, the most common being Huntington's disease. PolyQ diseases are characterised by being typically neuronal, with misfolded protein affecting normal cellular function [32]. PolyQ was chosen for the project due to the similar structure and physicochemical properties as PolyK. However has a fundamentally different charged residue. As such, PolyQ offers insight into the binding properties of these random coil peptides and potentially insight into the disease process as a whole.

The full-length huntingtin protein (Htt) is a 348 kDa protein comprised of 3144 amino acids and the sequence, structure and function has little in common with well-known proteins and hence its function is still incompletely understood [33]. The location of the protein was initially discovered to be in the nucleus of neural cells, where it was believed to regulate PolyQ transcription factors [34], however, it has since been shown to be expressed ubiquitously in humans and rodents, with the highest concentration in the CNS and testes [34]. Intracellularly, Htt is found throughout the cell, in the cytoplasm as well as specifically interacting with various organelles, including the nucleus, endoplasmic reticulum and Golgi apparatus [34]. This widespread location of the protein does not help define the purpose of the protein. The primary sequence of the protein also offers little evidence to define the function of the protein, with no known homology to motifs or binding domains. Due to the PolyQ expansion increasing in disease proteins, research has shown that the PolyQ region is responsible for functional activity in binding transcription factors

[35, 36]. Petruz *et al* [37], showed that the PolyQ expansion forms β-sheets and it was suggested that these β-sheets are functionally active as 'zippers' using the polar surfaces that are capable of binding transcription factors and are part of normal transcription regulation. When these expansions become too long, the affinity increases causing transcriptional dysregulation [33].

The mechanism for how mutant (or normal) huntingtin proteins affect cells is unknown, with a variety of different mechanisms being proposed, however, the various systems employed have been shown to have conflicting results (see Figure 1.2.2), reviewed in [38].

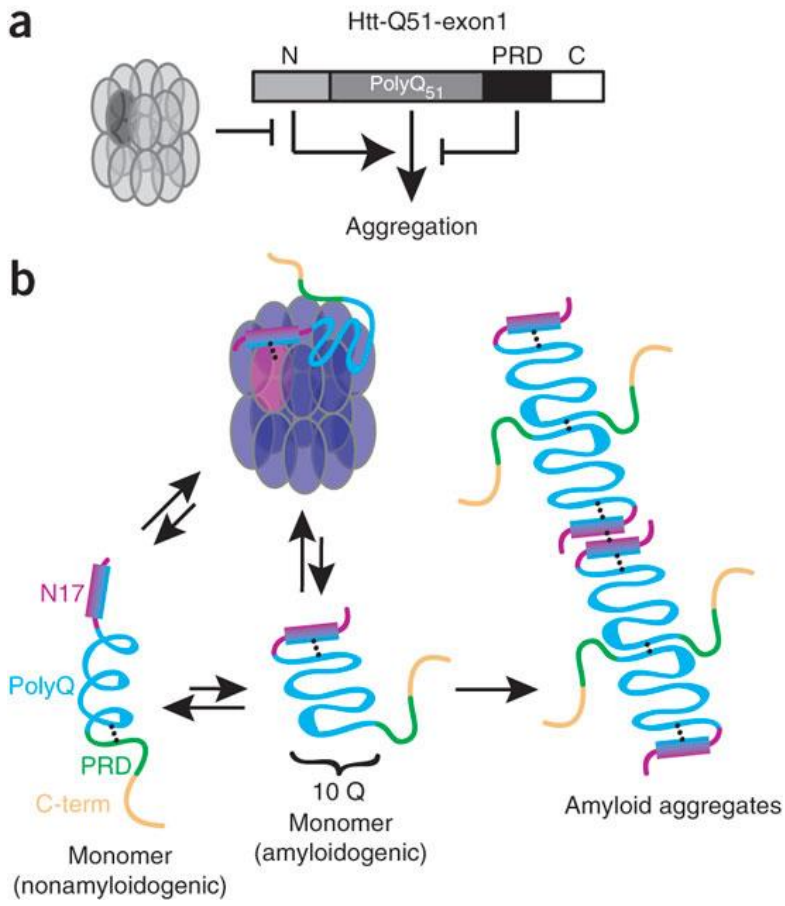


Figure 1.2.2. Mechanism of the amyloid formation with PolyQ. (A) The huntingtin exon contains an N-terminal localisation signal followed a PolyQ extension followed by the C-terminal domain. (B) The PolyQ expansions form β-sheets, these monomers then aggregate via β-sheet coupling, which forms insoluble aggregates. Adapted from [39].

The PolyQ expansion of the huntingtin (both pathological and non-pathological), forms β-sheets. With residues >40, these β-sheets form polymers and aggregate. These polypeptides then form large inclusions within the cell and on the cell membrane. These inclusions have been visualised by fluorescence microscopy of cells [35] and atomic force microscopy [40] with the volume of inclusions being proportional to the poly-glutamine expansion. Recent work has suggested that the formation of the inclusions is a cytoprotective mechanism from the cells, where smaller soluble aggregates are the cytotoxic component of the disease [32, 35]

The physiological relevance of the wild type protein is unknown. However, without the PolyQ expansion, there is no disease pathology. Therefore, there is a great need to understand the interaction of PolyQ expansion instead of the otherwise inert full length protein.

In this study, the binding characteristics of the PolyQ species will be examined in the presence of various soluble factors. The association of the polypeptide to various membrane vesicles will be examined the binding mechanism characterised.

In order to characterise the various binding parameters and kinetics of the aforementioned proteins to membranes and other surfaces, firstly, the basis of protein-protein interactions must be understood before an analysis of the binding surface to which they are interacting (i.e. a lipid bilayer).

1.3 Protein-protein interactions

The analysis of protein-protein interactions employs a vast array of biochemical and biophysical techniques. These range from using antibodies to detect their respective binding partners such as enzyme-linked immunosorbent assay (ELISA) and bead-based antibody immunoassay (tradename of Luminex) to fluorescent and biophysical techniques. The most sophisticated fluorescent techniques are: Förster resonance energy transfer (FRET), bioluminescence resonance energy transfer (BRET), -Amplified Luminescent Proximity Homogeneous Assay (alpha screen), which used fluorescence complementation in order to determine protein: protein interactions. Non-fluorescence studies have utilised the physical interactions to detect mass adsorption to a sensor surface, such as surface plasmon resonance (SPR). The work detailed in this thesis elucidates the intermolecular forces that underlie these interactions.

In order to complete this task, the environments in which these interactions take place must first be examined and understood.

1.4 Forces Involved in the Interactions between Biological Molecules

Within a biological system, the variety of different physical forces that are present are always in flux. These different forces, namely charge-charge (Coulombs forces), dipole forces, hydrogen bonding and dispersion forces (including Van der Waals forces) have different strengths, orientation and distance dependences. The physical underpinning of these forces has been well documented over several decades of research and forms the basis of several books, for example [41]. The distance dependence of the interactions is very important when trying to decipher the relative contribution of different intermolecular forces to an interaction. Figure 1.4.1

demonstrates the drop-off of interaction force with the different intermolecular forces present.

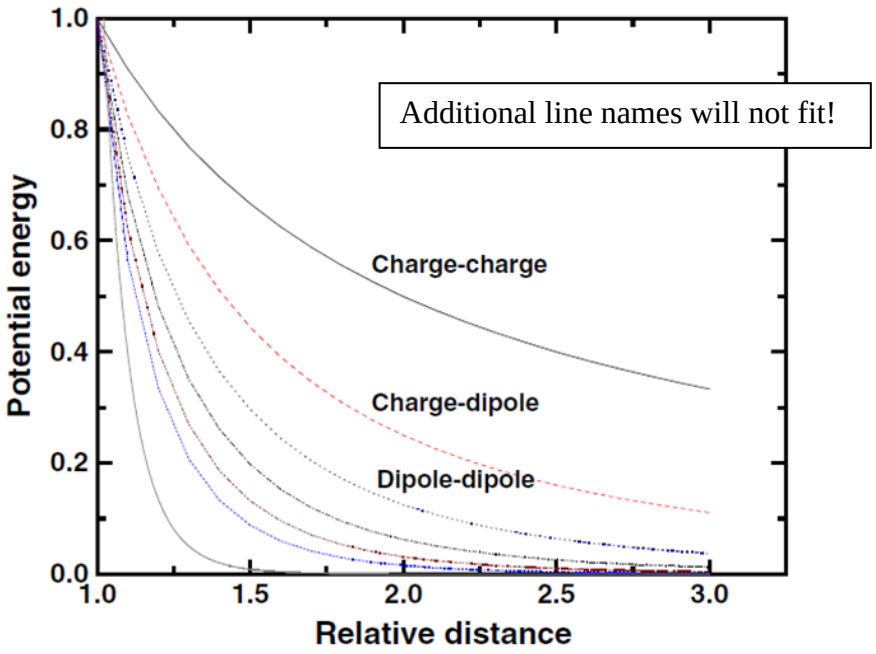


Figure 1.4.1. Relative distances of intermolecular forces between two molecules. Charge-charge interactions (1/r) are the longest distance, followed by charge-dipole ($1/r^2$), and dipole-dipole ($1/r^3$) (labelled), the other forces, induced-dipole interactions, Van der Waals forces, hydrogen bonding etc. all have shorter effective range (demonstrated with unlabelled lines). The relative distance between the interaction molecules is important in determining effects present [42-45]. Reproduced from [43].

In complex biological interactions, there is interplay between the various forces present and, depending on the situation, some will become more important at different times during a biological interaction. In this study, a brief overview of each force will be detailed with the relevance to biological interactions.

1.4.1 Charge-charge Interactions

Coulombic forces is the name given to charge-charge interactions. It is the strongest physical force and is sometimes stronger than covalent bonds.

The free energy of the Coulomb interaction between two charges Q_1 and Q_2 is given by:

$$w(r) = \frac{Q_1 Q_2}{4\pi\varepsilon_0 \varepsilon r} = \frac{z_1 z_2 e^2}{4\pi\varepsilon_0 \varepsilon r}$$

Equation 1.4.1.

The free energy (w(r)) of a Coulomb interaction can be described between two charges Q_1 and Q_2 (or two ions z_1 and z_2). Where ε is the dielectric constant of the medium and r is the distance between the two charges [41]. Coulomb forces are the longest-range intermolecular interaction studied, which manifests in the 1/r distance dependence or w(r) (Figure 1.4.1). This distance dependence is very important when dealing with intermolecular interactions between biological molecules (discussed more in Section 1.4.6.

1.4.1.1 *Factors that affect charge-charge interactions*

Within a biological system, the interactions between different species are in a medium instead of a vacuum and also in 3D instead of just between two interacting species. This means that the dielectric constant of a medium is very important. Typically, the dielectric constant (ε) of water is ~80, inside a protein core, the dielectric constant is 6-7, which increases to ~20 at the protein surface. The dielectric constant of a lipid bilayer is similar to that of a protein, in the hydrophobic core, the dielectric constant is ~1-2 and ~20 on the bilayer surface. The interaction of the medium with the ion's interaction species alters the associated Born energy (the energy required for an ion to maintain its charge) of the ions. This phenomenon explains how the strong charge-charge interactions of sodium and chloride in a salt are readily disrupted in water.

Charge-charge interactions between proteins can be altered by the medium between the proteins. If the medium contains a high salt concentration, there will be a multitude of charged ions between the proteins, which will interact with the relevant

charges. Therefore, this means the charge from the protein will be neutralised by the ions and will not affect the nearby protein. This is called ionic shielding.

1.4.2 Dipole interactions

Dipole interactions arise from the interaction of polar molecules, which have an uneven charge distribution in the bond of the molecule, resulting in one atom being slightly more electropositive and the other more electronegative. These charges then form charge interaction in a similar way to charge-charge interactions above. The strength of dipole interactions is dependent on the strength and duration of the dipole. As such, there is a hierarchy of dipole interactions from fixed ion-dipole interactions to permanent dipole-dipole interactions (of polar molecules) and finally to spontaneous dipole-dipole interactions. The dipole moment of a polar molecule is defined as:

$$u = ql$$

Equation 1.4.2. Dipole moment, u, of a polar molecule is defined as the distance, l, multiplied between two charges q+ and q- [41]

1.4.2.1 *Factors that affect dipole interactions*

Dipole interactions can be disrupted in a variety of ways. When discussing the interactions between proteins, the interaction of the proteins with the medium is important. The permanent dipole interactions present by ions in medium, hydrate with water molecules that are drawn to the surface of the ion. The degree to which the water molecules localise with ions affects the strength of the dipole.

1.4.3 Van der Waals forces

Van der Waals forces are formed by the spontaneous movement of charge in a molecule. This is quantum mechanical in nature, due to a spontaneous cluster of electrons in an otherwise neutral molecule. The formation of a transient charge

results in a chain-reaction of electromagnetic interactions. As the formation of the charges cannot be controlled, Van der Waals forces are always present even in nonpolar molecules.

1.4.4 Hydrogen bonding

Hydrogen bonds are the attractive force between hydrogen atoms attached to electronegative species (N-H and O-H). In the case of water, the polar nature of these interactions have been previously described above. Widespread hydrogen bonding in water creates unique physical properties such as strong surface tension, the boiling point of 100°C as well as ice formation structure that is less dense than the liquid form. The strength of hydrogen bonding is stronger than van der Waals forces, yet weaker than discussed electrostatic interactions [46].

In proteins, hydrogen bonding underpins a range of physical properties. In protein secondary structure, hydrogen bonding is responsible for the stabilisation of alpha helices, where the amino acid backbone interacts with itself every 5.4 angstroms (Å) (when each turn of the helix equates to 3.6 residues). Another form of secondary structure is the hydrogen bonding in β-sheet formation (Figure 1.4.2). These hydrogen bonds stabilise the protein in these fundamental configurations and lead to the development of more complicated secondary and tertiary structures, which form the basis of protein structure.

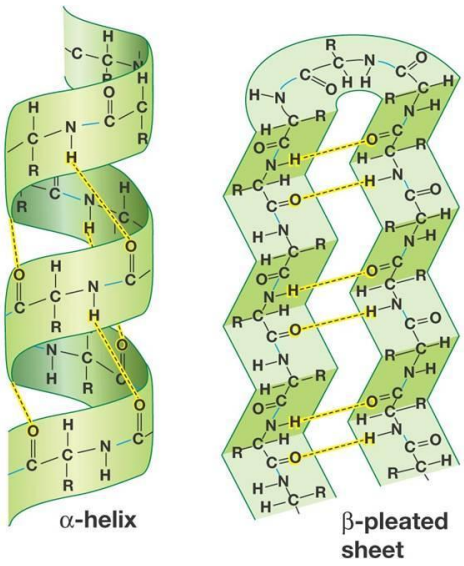


Figure 1.4.2. Protein secondary structures that are stabilised by hydrogen bonds. Hydrogen bonds are formed between the amino acid backbone of peptides to form an α-helix with a hydrophobic core and hydrophilic exterior. Hydrogen bonding can also occur between amino acids in a β-sheet formation. Reproduced from [31].

Hydrogen bonding is also important at the surface of membranes and proteins. The dielectric permittivity on the membrane surface (~20) is lower than in bulk solution (~80). This reduced dielectric permittivity correlates with a decreased degree of hydrogen bonding. The oxygen on the lipid head group can form a hydrogen bond with a free water molecule, however in doing so; it reduces the lifetime of the water from ~1 ps in bulk water to 6.3 ps. This creates a network of 'slow moving' water molecules across the membrane surface. This water network has been shown to differ between membrane compositions and organisations such as membrane microdomains [47].

The interplay between membrane proteins and lipids have been examined in a variety of contexts, with the different mechanisms reviewed in [43] and the underlying principles of membrane formation discussed in Section 1.8, followed by an examination of the physical forces that arise from these interactions in Section 1.4.5.

1.4.5 DLVO Theory

In aqueous solutions, VDW and electrostatic forces usually occur together, it is common practice to plot the two forces together when describing the net interaction between two surfaces, known as the Derjaguin-Landau-Verwey-Overbeek (DLVO) theory.

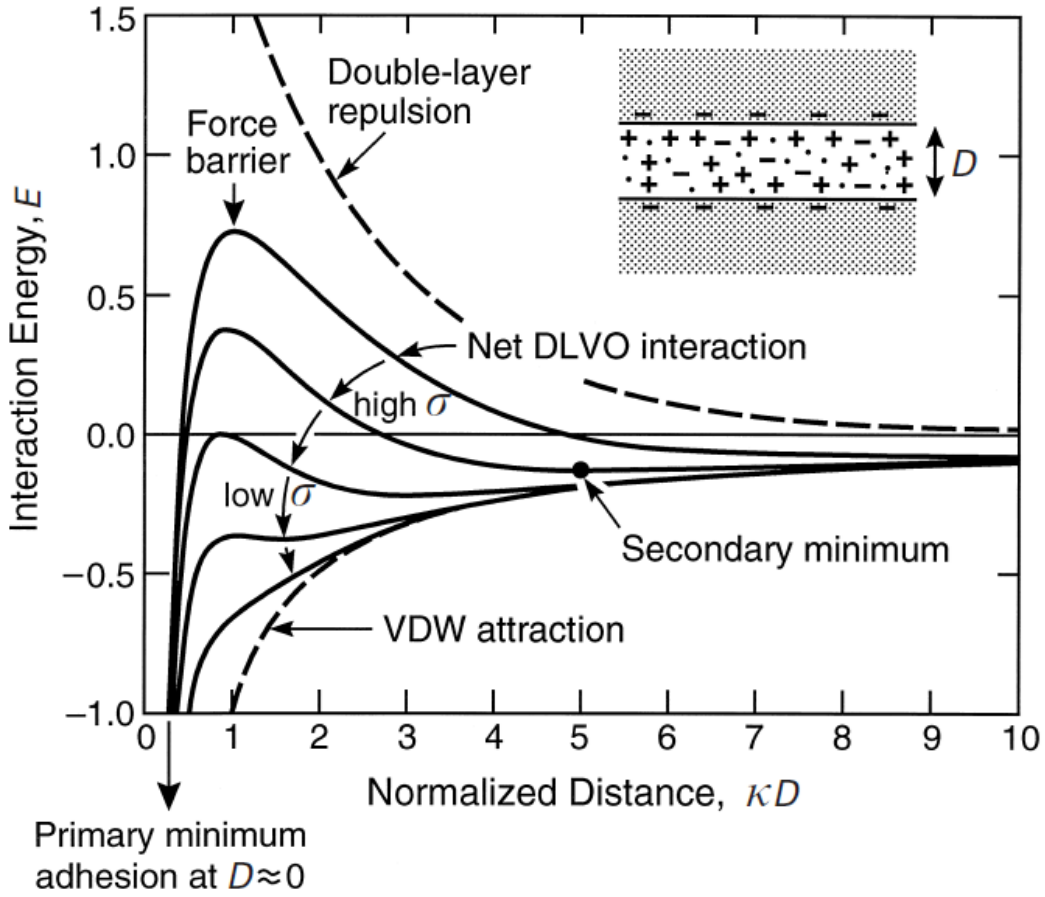


Figure 1.4.3. Schematic of DVLO theory. The DVLO theory describes the interactions between two sets of charged surfaces, separated by an aqueous or ionic solution at a given distance (D) (schematic insert). DLVO demonstrates how the attractive VDW and repulsive electrostatic double-layer forces together determine the total interaction potential between two charged surfaces in aqueous solutions at different surface charge densities (σ). In this example 1 κD = 1 nm. Adapted from [41].

The DLVO theory has been found to adequately describe the long-range forces between similarly charged colloidal and some bio-colloidal surfaces in aqueous solutions. At small and contact separations in liquids, continuum models such as Lifshitz theory of VDW forces and the Poisson-Boltzmann (PB) equation of

electrostatic interactions break down, and/or other forces take over to determine the final adhesion

Figure 1.4.3 shows how the various forces described can come together to determine whether interactions will be exclusively attractive or repulsive at a range of distances. Under certain conditions, the forces can be weakly attractive at some separation at the secondary minimum, with an energy barrier separating it from the more attractive primary minimum. This forms the various asymptotes shown in Figure 1.4.3. These forces are also differently affected by external factors such as the solution conditions, resulting in different surface charges (σ). The electrostatic forces in double-layer interactions are greatly affected, whereas VDW forces are reasonably unaffected. In the case of asymmetric interactions, such as the interactions of one negative (pI above pH) and a positive (pI below pH) the electrostatic double-layer interactions can be attractive (Figure 1.4.3). It clear from Figure 1.4.3 at a distance of >0.2 nm the electrostatic repulsion dominates VDW interactions. Once the distance is reduced to 0.2 nm; approximately one layer of water molecules between the surfaces VDW force dominates interactions, corresponding to the binding in the primary minimum [48]. DLVO forces are only expected to be attractive at both very small (<0.2nm) and very large separations (>5nm) distances.

The limitation of DLVO interactions due to a mean field approach to the interaction with the assumption that the membrane potential is uniform, whereas biological membranes are rarely simple, with complexities such as geometric complementarity.

The culmination in all of the forces discussed in this sections results in a complex nature of the energy profile shown in Figure 1.4.4. The combination of these forces governs the interaction between two interacting molecules. Understanding the

different forces involved in each interaction is vital in developing the ability to target the forces selectively for several purposes such as synthetic biology, development of detection machinery and dissection of disease pathologies.

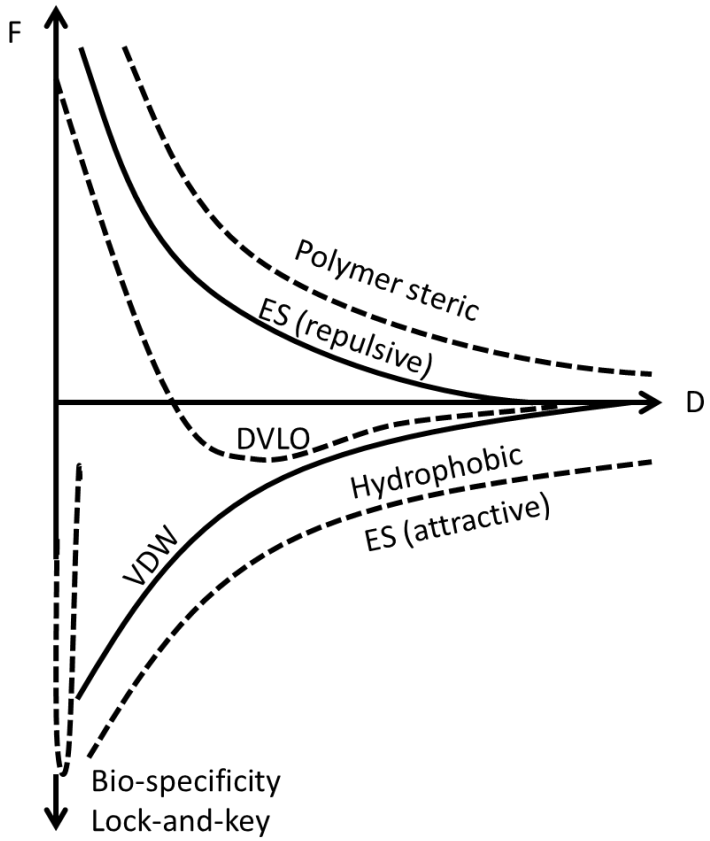


Figure 1.4.4. The interaction of different intermolecular forces. The interaction between two complex surfaces separated by distance (D), there are several forces that all concurrently occur. . Electrostatic (ES) repulsive and steric forces are negative interactions whereas VDW, hydrophobic and ES attractive forces are positive. Strength of the respective forces are shown as (F). Bio-specificity can increase the attractive forces dramatically. Adapted from [48].

1.4.6 Bio-recognition

All interactions mentioned so far are the culmination of different physical forces with various complexities (described by the DVLO theory). Bio-specific interactions are a particular class of highly complementary non-covalent bonds between biological molecules. The nature of these interactions can be shown through crystal structures of different receptor-ligand complexes. One of the strongest bio-specific forces is that shown between biotin and avidin (or the bacterial counterpart streptavidin),

which has an affinity of 10^{15} M^{-1}, which corresponds to a binding free energy of ~35 kT at room temperature. A protein interaction to a vesicle surface has been shown to be ~10 kT [49]. The interaction is stabilised and strengthened by seven amino acid residues of the biotin interacting with the avidin (Figure 1.4.5A) [50]. These involve ionic (electrostatic and hydrogen bonding) interactions, as well as van der Waals and hydrophobic interactions, dependent on the amino acid residue.

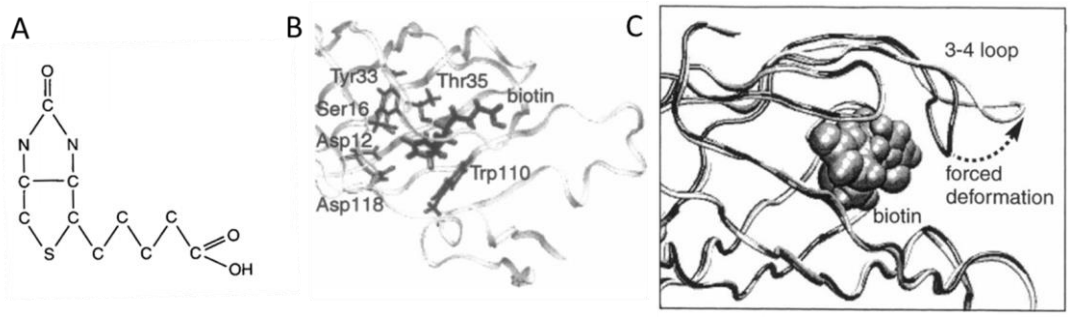


Figure 1.4.5. Binding pocket of biotin. (A) Chemical structure of biotin, (B) Biotin binding pocket in avidin protein. Key residues that interact are highlighted. When biotin binds to streptavidin, it induces a conformational change of the 3-4 loop, dramatically increasing the affinity of the interaction (C). Adapted from [50].

A common distinguishing factor that leads to bio-recognition of molecules is the close geometrical and chemical fit between the ligand and the binding pocket. The geometric fit is important due to the forces discussed decaying dramatically with distance (Figure 1.4.1), small decreases in the distance between the molecules increases the interactions strength greatly. For example, the ureido ring of biotin Figure 1.4.5A is positioned tightly to the binding pocket, and forms short-range hydrogen and electrostatic bonds with Asp 12, Asp 118 and Ser16. These effects are enhanced further in the case of Trp110 interaction with the ureido ring; upon interaction the biotin forces a conformational change in the avidin structure, reducing the distance of Trp110 from 0.5 nm to 0.2 nm, which increases the VDW attraction by nearly three orders of magnitude (Figure 1.4.5) [50].

The chemical fit of ligand and receptor refers to the interactions between the polar and ionic groups of the ligand and receptor (typically amino acid residues). The directional nature of hydrogen bonds means that the relative orientation of the polar chemical groups can increase the binding energy greatly [48].

The effect of cooperativity can be highlighted through an examination of the binding energies, given a typical hydrogen bond can form and break spontaneously and has lifetime of ~10^{-8} s. If three hydrogen bonds are formed under the same assumptions, the lifetime is calculated by 10^{-8} x e^{30} / e^{10} = 5 s, resulting in a ~500 million times longer lifetime with a mere three-fold increase of the binding energy [41]. This extrapolation fails to account for the sequential breaking of the hydrogen bonds, which would decrease the lifetime somewhat, yet remains orders of magnitude greater than the sum of its counterparts.

Here it has been clearly demonstrated that the strength of bio-specific bonds are heavily dependent on the geometry and chemistry of the binding pocket. The interactions are therefore typically short-ranged and often do not extend beyond the surface of the proteins, demonstrated by the binding force of avidin-biotin being eliminated after ~1nm [50]. Some binding sites have been examined that have strongly charged residues at the entry to the binding site, by virtue of long-range electrostatic forces, these residues can be envisaged as a long-range steering force or 'homing beacon' for molecules to interact [49]. The 'steering forces' alone are unable to distinguish between different charged molecules and hence do not directly contribute to bio-recognition.

The definition between non-specific and specific interactions is unclear as there is no mutual exclusivity of either the underlying physical forces. Biological ligands may

exhibit bio-recognition (such as those in Figure 1.4.5), but to a less efficient binding pocket, whereas some protein can adsorb strongly to a protein or surface 'nonspecifically'. This non-specific interaction can range from transient binding, or irreversible binding such as those in aggregation.

In this study, the selectivity of the interaction is used to select between the 'nonspecific' and 'specific' binding capacities. For example, the interaction between albumin and a lipid membrane does not have any specific bio-recognition and is therefore deemed nonspecific. If the lipid membrane was reconstituted with an albumin receptor, the interaction would be primarily driven by the specific interaction. Antigen-antibody interactions are able to discriminate between binding species and bind with high affinity due to the molecular recognition of the ligand and binding site as discussed, thus, in the context of the present study, this is deemed specific.

1.5 Protein-lipid and lipid-lipid interactions

The forces involved with protein-protein and protein surfaces have been detailed above. However, the surface with which the protein interacts can dramatically alter the intermolecular forces, which dominate the interaction.

The field of protein-membrane interaction is vast and the interaction, segregation, folding and translocation of membrane interacting proteins has been of interest for several decades [51].

In this study, model membranes were employed as a simplified version of a cellular plasma membrane. The complexities of the membranes were then increased to introduce different biophysical properties, such as phase separation into the system.

1.6 Classes of molecules that can interfere with intermolecular interactions

In the sections above, I have described the molecular forces that control the interactions of cellular macromolecules. Targeting intermolecular interactions have been undertaken in several different contexts for many years. One of the cornerstones of molecular medicine is the ability to design molecules that bind to therapeutic targets (such as agonists or antagonists binding to receptors). One example of targeting particular forces is the protocol of salting in or out proteins as part of purification protocols, (reducing or augmenting Coulombic interactions) [52]. However, reports of targeting other intermolecular interactions in a systematic fashion are rare and tend to be developed for a particular process of interest [53]. The use of soluble reagents in bulk phase media would allow a rational basis for a set of conditions that can be controlled to modulate interactions of a range of biological molecules. Subtle alterations in these reagents would allow particular forces to be reduced or eliminated altogether in order to assess their contribution to a particular interaction. A coarser approach was used previously with some success to evaluate the effects of separately reducing, the Coulombic and hydrophobic forces that take place in cell-cell interactions during cellular aggregation [53].

A range of different reagents could theoretically alter intermolecular interactions. The focus of this thesis will be on two classes of molecules; chaotropes such as NaSCN and dielectric constant modifying reagents. The efficacy of these reagents will be tested to modulate a range of different interactions, such as protein:lipid and protein:surface interactions.

1.6.1 Sodium Thiocyanate

Sodium thiocyanate (SCN) is a chaotrope and has been used to reduce nonspecific binding interactions [54]. Thiocyanate ions are classified as chaotropic agents in the Hofmeister series, which were initially classified due to their ability to salt in or out proteins ([55] Original work by F. Hofmeister (1880)). SCN has been shown in several different contexts to salt-in proteins such as ion-peptide group interactions [56], as well as water modulating effects [57-59]. This being said, the mechanism for all the Hofmeister series, specifically NaSCN is yet to be fully understood.

The qualitative order of the Hofmeister series is as follows:

Anions: $HPO_4^{2-} > SO_4^{-2} > C_2H_3O_2 > F^- > Cl^- > NO_3^- > Br^- > I^- > ClO_4^- > SCN^-$

Cations: $N(CH_3)_4^+ > Cs^+ > Rb^+ > NH_4^+ > K^+ > Na^+ > Li^+ > Ca^{2+} > Mg^{2+}$

The ions on the right-hand side of the order (i.e. SCN^- employed here) are categorised as a chaotropes and act to salt-in proteins, with ions on the left to salt-out proteins. Chaotropes disrupt the native hydrogen bonding between water molecules in a solution and impart stability to macromolecules by reduction of the hydrophobic effect. The ions in the Hofmeister series were initially thought to make or break the water structure of the bulk phase [60], [61] however more recent experiments [62, 63] and theoretical modelling [64, 65] have shown that the ions do not globally affect the water structure and the interactions are more sophisticated. The outcome of these experiments shows that the Hofmeister effect can be treated as an interfacial phenomenon [61]. Interfacial water structure plays a key role in the thermodynamic and kinetic properties of macromolecules. The chaotropic SCN^- ions have been shown to localise to the surface of proteins [66], this localisation is most likely to a key factor in perturbing intermolecular forces.

In this study, these reagents are employed to modulate nonspecific binding in different systems, firstly in a model membrane binding system in order to gauge their relative effectiveness. These reagents were then assessed to detection instruments in the form of label-free detection of SPR and widely used system multi-analyte system, Luminex, with representative effects being corroborated with specific binding exemplars to ensure that the specific molecular recognition, upon which the sensor systems relies is not diminished.

1.6.2 Short Peptides that Modulate the Dielectric Constant

The second class of intermolecular agents are the dielectric constant modifying reagents (DCMRs). Table 1.6.1 lists a range of common reagents and their effect on the dielectric constant. In this study, amino acids and peptides are employed to exclusively increase the dielectric constant of media (Table 1.6.1). Since the dielectric constant affects a number of the intermolecular forces, in particular Coulomb forces (Section 1.4.1) and dipole mediated interaction (Section 1.4.2), increasing the dielectric constant decreases these interactions and, in turn, reduces nonspecific binding.

The dielectric constant of a solution is a quantified as a measure of the ability of a substance (or solution) to store electrical energy in an electric field. The dielectric constant of water arises from the ability of water molecules to hydrogen bond and align their dipoles in a electrical field. Nonpolar molecules that can neither hydrogen bond or interact with electrical charges have little ability for electrostatic reduction (Section 1.4.3). Increasing the dielectric constant, decreases the attractive forces between molecules, therefore, decreasing the likelihood of binding and precipitation; enhancing the solubility of protein, macromolecules and drugs [67].

The relationship between solubility and nonspecific binding is interesting, historically there are various parameters that affect a protein's solubility and the several different examples of work solubilising proteins, such as: salting in proteins [52], pH changes [68], temperature-mediated solubility [69], the use of complex detergents (discussed in Section 3.2.2) and complexing with various carriers/chaperones etc. When proteins are in solution, several opposing processes can cause aggregation and precipitation [70-72]. With this in mind, it is unsurprising to expect that a medium with an increased dielectric constant and increased protein solubility has reduced nonspecific binding, so long as the magnitude of dispersion energy is small. If the dispersion energies are significant enough to induce binding, they can be overcome by the addition of other materials (e.g. detergents).

It is noteworthy that soluble reagents such as simple salts do not affect the dielectric constant of water [73]. This is somewhat surprising due to the characterised effect of ionic-shielding and hence decreased charge-charge interactions.

A number of different reagents have been identified which affect the dielectric constant of a given solution. The dielectric increments presented in Table 1.6.1 show the change in the dielectric constant of water ((D_o) ~80 at 20°C)) for a one molar solution of the reagent [42, 73].

Reagent	**Dielectric increment (δM^{-1})**
Molecules	
NaCl	0
EtOH	-2.6
Glycerol	-2.6
Mannitol	-2.6
Sucrose	-7.6
Phenol	-6.6
Urea	+2.7
Amino acids	
Glycine anhydride	-10
Glycine	+22.6

α-Alanine	+23.4
L/D-Valine	+25
L-Leucine	+25
L/D-Proline	+21
D-Glutamic acid	+26
L-Aspartic acid	+27.8
D-Glutamine	+20.8
L-Asparagine	+24.4
N-Phenylglycine	+30
Glycocyamine	+30
Creatine	+32.2
β-Alanine	+37.3
Arginine	+62
Peptides	
Diglycine	+71
Glycylalanine	+71.8
Alanylglycine	+71
Leucylglycine	+62.5
Glycylleucine	+72.3
Glycylphenylalanine	+67
Phenylalanylglycine	+70.4
Leucylglycylglycine	+56.7
Triglycine	+128
Tetraglycine	+159
Pentaglycine	+215
Hexaglycine	+234
Heptaglycine	+290 (in 5.14 M urea)
Double dipoles	
Lysylglutamic acid	+345
Cystinyldiglycine	+139
Cystinyldidiglycine	+250
Diglycylcystine	+139

Table 1.6.1 List of some molecules that affect dielectric constants of water. Dielectric increment $D = D_0 + \delta C$, $D_0 = 80$ for H_2O at 20 °C. C is molar concentration. Information from [42, 73].

Molecules with negative dielectric increments will decrease the ambient dielectric constant of water, enhancing the proximity energies, whereas positive dielectric increments will decrease the proximity energies. The ability for different molecules to impart a dielectric increment is dependent on the molecules dipole-self energy as discussed in Section 1.4.2). The dipole self-energy is dependent on the magnitude of the charge and the length of the dipole. Each molecule in Table 1.6.1 should elicit some effect; however, other considerations must be made in order to use a molecule

in a biological context. The strongest dielectric modifying peptide is that of lysylglutamic acid due to the strong double dipole. However, the molecule is likely to exhibit strong charge-charge interactions and irreversibly bind to negatively charged protein species, instead of remaining in the bulk solution to increase the ambient dielectric constant. Arg is zwitterionic, has a large dipole moment (+62 D) and has been shown to interact directly with proteins [74]. In the relationship defined in Equation 1.4.2 dielectric increment increases with dipole length (+71 D and +128 D for Gly-Gly and Gly-Gly-Gly respectively). The increasing dielectric increment of glycyl-peptides correlates to an increase in the dipole length (Gly-Gly-Gly-Gly, Gly-Gly-Gly-Gly-Gly, etc. (Figure 3.4.5)). Gly-Gly and Gly-Gly-Gly were chosen in this study due to their sufficient dielectric increment/ residue ratio in addition to practical considerations such as cost.

1.6.3 Different Factors of a Detection Instrument Medium

Several different technologies are able to detect analytes in complex biological fluids. One of the most complex biological fluids is that of blood plasma. Some medical diagnoses, such as the new field of biomarker detection in complex diseases hinge on the ability to detect pg/ml quantities of a protein target in a fluid that is comprised of different proteins in the tens of mg/ ml. Technologies created to detect these quantities such as ELISA, Luminex and more recently Surface Plasmon Resonance (SPR) all suffer from the nonspecific binding that has been shown to limit sensitivity and selectivity of the instrument [75, 76]. Details of the detection instruments are given in Section 2.13 and 2.14.

There are typically several different components of a detection instrument running buffer or sample diluent. Each medium is comprised of several different reagents

which fall into four main categories; the solvent, electrolytes, blocking agents and detergents.

In biological samples the solvent is almost exclusively water; however in some specific cases organic solvents are used [77]. The use of electrolytes has been discussed in detail in this chapter, offering the potential to reduce nonspecific binding. The ability of the different reagents to target different sub-classes of intermolecular interactions has been shown experimentally [54]. This approach has the potential to decrease electrostatic forces with the exception of dispersion forces (discussed later).

Blocking agents are commonly used to bind free active groups on a given surface following antibody immobilisation. Bovine serum albumin is commonly used as a blocking agent. However, the use of albumin is unfavourable. As discussed earlier (Section 1.2.1) albumin binds to several proteins and can contribute to nonspecific binding.

The final component of an assay buffer or protein diluent is a detergent. Detergents are used in order to solubilise and stabilise hydrophobic components that would otherwise aggregate or denature [78, 79]. Detergents physically interact with the surface of proteins and membranes, interacting with nonpolar regions. The detergent-bound nonpolar patches, therefore, have different properties and are no longer non-polar. The field of detergents has been studied by several different processes which have been extensively reviewed [80]. Tween-20 has been a long-standing detergent used initially in the development of western-blot techniques [81] and has been used widely since being non-ionic mild surfactant, that decreases non-specific binding, but

does not denature proteins and hence, can be used in the presence of a range of proteins including antibodies.

1.7 The complexity of the lipid bilayer

In this thesis, several types of membrane bilayers will be examined. `Biological lipid bilayers are complex. The fluid-mosaic model is generally accepted as a useful representation of a biological membrane (Figure 1.7.1) [9].

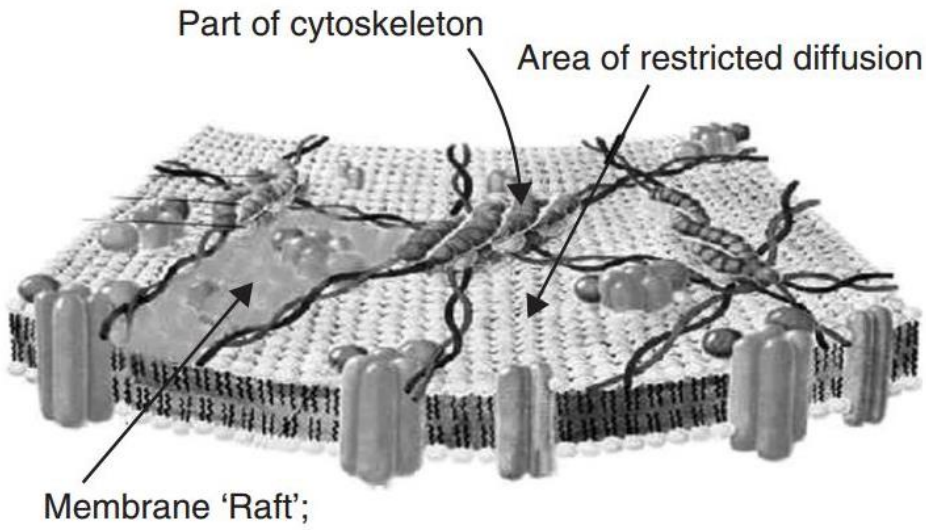


Figure 1.7.1. Fluid mosaic structure of the bilayer. Cellular membrane bilayers are very complex with a host of membrane proteins and cytoskeleton network. Reproduced from [82].

Biological membranes comprise a complex mix of membrane lipids and proteins, involved in a range of activities, including trafficking of proteins [10], signalling [11], differentiation [12] and apoptosis [13]. Some processes are performed by highly specialised intracellular membranes of organelles such as: liposomes, mitochondria and chloroplast. The formation of membrane rafts is an additional level of complexity. Such rafts restrict the diffusion of raft associated lipids and proteins in the plasma membrane.

The present study sets out to understand the different intermolecular forces that underlie various phenomena, including protein binding and membrane microdomain formation. Such studies may suggest ways to control these interactions providing information that may be exploited in the the field of synthetic biology further as well as giving insight into complex biological systems involved in health and disease.

1.8 Membrane structure, formation and complexity

In order to understand and control the full complexity of a cellular membrane, model systems are used to exemplify known physiochemical characteristics. When examined in turn, the complexity of the experiments can be developed to understand and try to control these systems.

Firstly, the fundamental forces to create the lipid bilayer must be examined and understood.

Membrane lipids are amphipathic molecules that possess a hydrophilic (polar) head and a hydrophobic tail (non-polar) tail. The amphipathic lipid molecules are broadly defined into three groups: (1) glycerophospholipids (referred to as phospholipids) (2) sphingolipids and (3) sterols. This study focuses on the self-assembly of phospholipids, which are the major contributors to the plasma membrane of the cell.

Glycerophospholipids (simple known as phospholipids) are the result of a phosphate group ester-linked to the *sn*-3 carbon of the glycerol backbone and two fatty acyl chains (Figure 1.8.2.).

Within a cell, the formation of acyl chains occurs by the successive addition of acetyl-CoA consisting of two carbon atoms; hence, acyl chains of odd numbered carbons are rare in biology. The fatty acyl chains in biological membranes are

generally between 14 and 24 carbons in length, with 16 and 18 carbons being the most common. The acyl chains also exhibit varying degrees of saturation, with double bonds (in *cis*-configuration) inducing a kink in the chain which can alter the properties such as packing which can determine their association with other lipids, (discussed further in Section 1.8.2) [83].

A further complexity arises from the lipid 'head group' of which, the phospholipid phosphate ester group can vary.

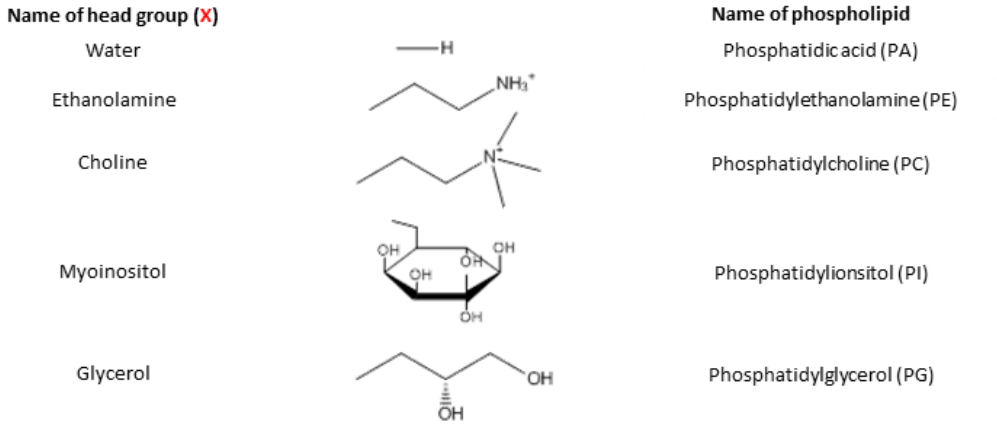


Figure 1.8.1. Chemical structure of lipid head group typically conjugated to phospholipid backbone. Adapted from [84].

The combination of the different lipid acyl chains and head groups (Figure 1.8.1) creates a systematic nomenclature of the various phospholipids employed in this study. DOPC 1,2-Dioleoyl-*sn*-glycero-3-phosphocholine is the formation of the most common unsaturated lipid in cell membranes with the phospholipid backbone, with two 18:1 oleic acid, fatty acids. DPPC, 1,2-dipalmitoyl-*sn*-glycero-3-phosphocholine is the most common unsaturated lipid in cell membranes [83].

Sphingolipids (generally called ceramides) are formed with a sphingosine backbone, which has a long saturated alkyl group connected to the C_1 and a free amine at C_2, subsequent fatty acids are attached through an amine link the C_2 and an H or

esterified phospho-X group is found at C_3. The subcategory of sphingolipids of three main types, sphingomyelins and glycosphingolipids are formed through of the attachment of choline or an oligosaccharide to the hydroxyl group of the sphingolipid backbone respectively. Gangliosides consist of an oligosaccharide chain that contains, at least, one sialic acid residue [83].

Sphingolipids are believed to be important in the formation of microdomains in biological membranes, discussed further in Section 1.8.2, as well as being involved in a range of biological functions, such as acting as second messengers in cell signalling pathways, [85] and other biological processes such as apoptosis [86].

The final category of biological membrane lipids are sterols, the previous two classes of membrane lipids have hydrophobicity inferred through relatively long aliphatic chains, sterols are composed of polycyclic structures. The most common sterol is cholesterol, which possesses a four-fused-ring structure in *trans* configuration, consisting of three six-atom rings and a fused five-atom ring, with a hydroxyl group in position 3, a double bonding between the carbon 5 and 6, as well as an iso-octyl lateral chain in position 17. The hydroxyl group is responsible for the amphiphilic nature of cholesterol, which orientates the cholesterol in the membrane. Cholesterol imparts different physiochemical properties in the membrane, such as increased rigidity, decreased fluidity and increased the membrane dipole potential (discussed later). Cholesterol in animal cells acts as a precursor for a range of different fat soluble vitamins and hormones [87].

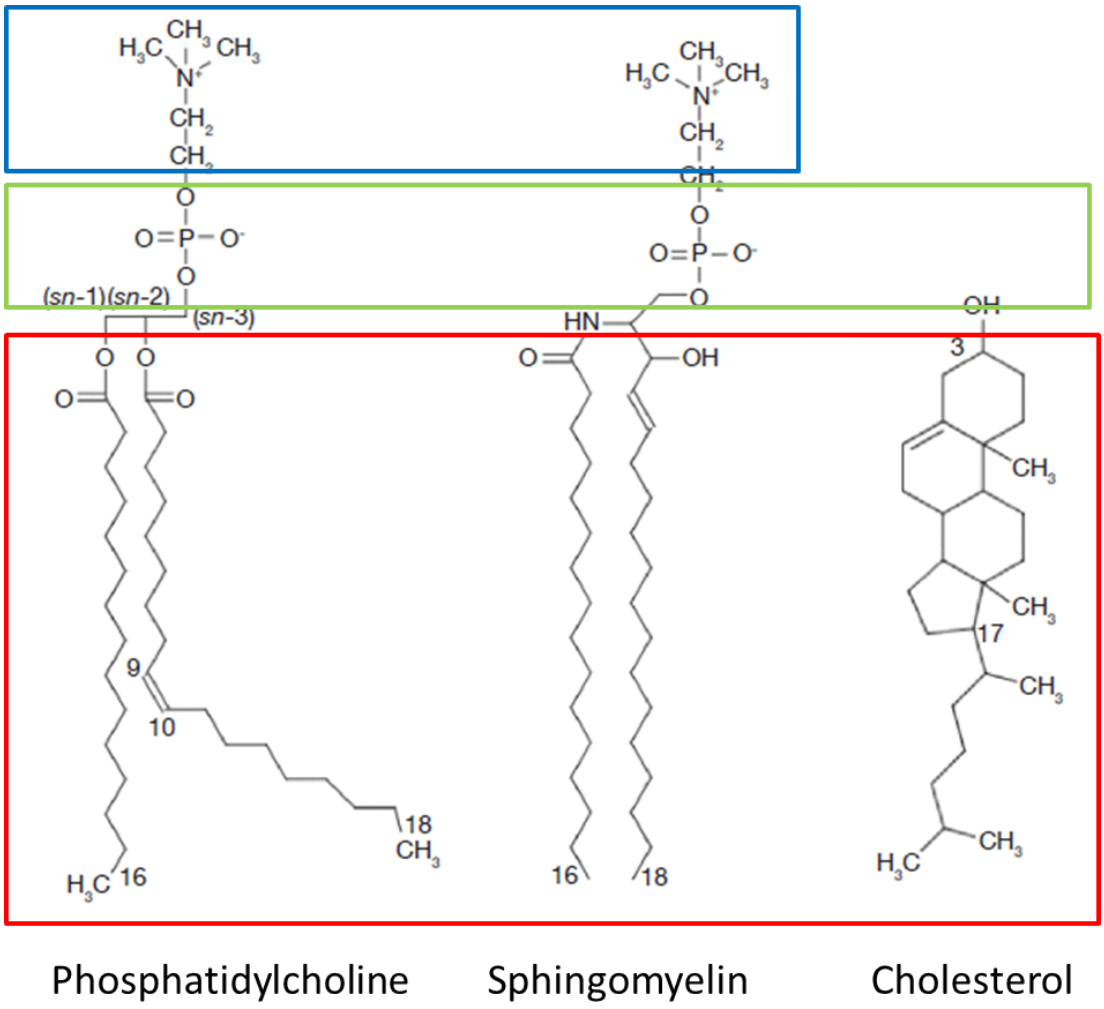


Figure 1.8.2. Structure and general orientation of the major components of the outer leaflet of mammalian plasma membranes. Choline head groups of phosphatidylcholine (PC) and sphingomyelin (SM) in blue. Hydrophilic structures of the phosphate group in PC, SM, and a hydroxyl group in cholesterol in green. Cholesterol α-face and β-face on the left and right side respectively. The hydrophobic region of each component in red. Structures are drawn with ChemDraw.

The properties of both the head group and the organisation of the chains can dramatically alter the biophysical properties of the membrane. In this study, these changes are exploited in order to produce membrane with surface charge or to create membrane with phase separation (discussed more in Section 1.8.2).

1.8.1 Assembly of Lipids into Membranes

The effect that underlies the formation of lipid components into membranes is called the hydrophobic force. Hydrophobic and hydrophilic interactions arise from the preferential inclusion or exclusion of water molecules dependent on the molecule's

ability to hydrogen bond. The segregation of hydrophobic molecules, such as hydrocarbons (in lipid acyl chains) arises as when a hydrophobic moiety is in water, the water molecules form a cage around the molecule, decreasing the entropy of water. When further hydrophobic molecules are present, the mean surface area of the solvent cage per hydrophobic molecule is reduced if the hydrophobic molecules are clustered together than if they are dispersed. The relative strength of the water-water interaction over the weaker hydrocarbon-hydrocarbon interaction results in the interior water being excluded forming a hydrophobic core.

The strength of the hydrophobic effect can be affected in several different ways. The hydrophobic force increases with temperature, however at very high temperatures, water molecules become more mobile, which decreases the hydrophobic force energy. Increasing the number of carbons in the hydrophobic moiety also increases the hydrophobic effect. More structured molecules (such as saturated acyl chains), can pack more tightly than unsaturated, increasing the interactions between them [88, 89].

Hydrophilic structures by definition preferentially interact with water molecules due to polar interactions. Amphipathic molecules, such as phospholipids, are part hydrophobic and part hydrophilic. The hydrophilic component is subject to preferential hydrogen bonding to water molecules, whereas the hydrophobic component excludes water molecules and preferentially forms self-self interactions. These opposing forces results in the self-assembly of lipid bilayers [46, 84].

The size and shape of lipid molecules within biological membranes can influence their localisation as well as the structure of the membrane itself. The shape of a can be defined by a simple geometric property of the molecule; Israelachvili-Mitchell-

Ninham packing parameter: $P = v/al$, where v is the molecular volume, a is the cross-section area of the head group, and l is the length of the molecules [90]. Figure 1.8.3 demonstrates that the approximation of P offers a simple comparison between lipid molecule size and relation to the built-in curvature stress. The surface area of PC and PS approximately matches the area occupied by the hydrophobic chains, giving rise to monomers with a crudely cylindrical shape (P = 1) (Figure 1.8.3B). The stacking of these lipids, therefore, leads to lamellar formations of membranes such as bilayers or liposomes. Certain lipid head groups (such as PE) have a smaller surface area than their acyl chains resulting in a conical shape of the lipid (P > 1), which results in negative curvature of the membrane and the formation of inverted hexagonal phases, also called inverted-micelles (Figure 1.8.3C), which are expected to form during membrane vesicle fusion [91]. If the head group has a much larger surface area than the hydrophobic moiety, such as lysophosphatidylcholine (P < 1) it is shaped like an inverted cone, which promotes micelle formation with the positive curvature (Figure 1.8.3A) [92].

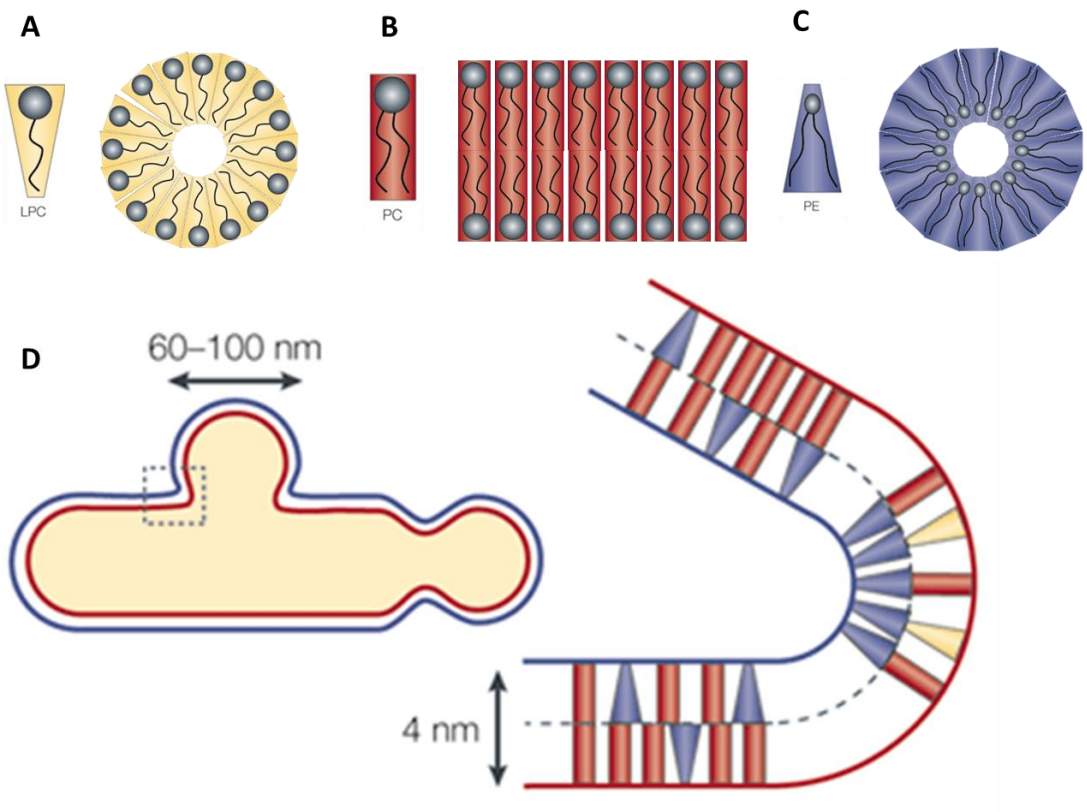


Figure 1.8.3. How lipid shape affects membrane curvature and formation. (A) Diagrammatic representation of lysophosphatidylcholine (LPS) as an inverted cone shape (P<1). Non-covalent aggregation of mono-acyl lipids form micelles, once the critical micelle concentration is reached in a given solution. The resulting micelle of positive curvature may be spherical, ellipsoid or discoidal with a hydrophobic interior. (B) Lipids with a cylindrical shape, such as phosphatidylcholine (PS) (P=1) organise into lamellar bilayers, with the hydrophilic head groups forming a 'sandwich' of the hydrophobic core. (C) Lipids with a conical shape (P>1), such as phosphatidylethanolamine (PE) induce negative curvature, these lipids can form type-II hexagonal liquid phase with an aqueous interior. (D) Bilayers in solutions form liposomes, consisting of an aqueous interior and exterior with a hydrophobic core between the bilayer leaflets. The presence of the negative and positive curvature lipids can promote the formation of structures such as invagination by PE or forming budding (adapted from [92]).

This physical difference between different components of the membrane relates to the heterogeneous and dynamic nature of lipid bilayers. The lipid composition of different membranes is linked to their function. In eukaryotic plasma membranes PE and PS are mainly found in the inner leaflet of the plasma membrane while PC and SM are primarily located in the outer leaflet [93]. Cholesterol is thought to be equally distributed in both membrane leaflets [94]. As the cholesterol does not contain a strong hydrophilic group like phospholipids, it can flip transversely across the bilayer. The lipid asymmetry is responsible for membrane curvature (Figure 1.8.3D),

which is essential for several biological processes such as vesicle budding and membrane fusion [91].

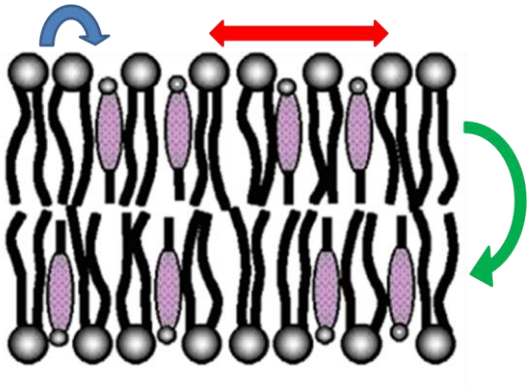


Figure 1.8.4. Phospholipid lipid molecules (grey) in a bilayer have three potential freedoms. The blue arrow represents molecule rotation within the bilayer. The red arrow represents lateral diffusion within a bilayer. The green arrow represents transversal diffusion. Due to their planar nature, cholesterol molecules (purple) do not rotate in the bilayer.

Lipid molecules within a bilayer are highly mobile in both rotational, translational dimensions (lateral diffusion). Lipid molecules rotate in space around their axis perpendicular to the plane of the membrane in the order of nanoseconds (Figure 1.8.4) [95]. Lipids in a bilayer also exhibit transversal diffusion (also called flip-flop) in which a lipid molecules 'flips' from one bilayer to another (Figure 1.8.4). The time phrase in which transverse diffusion occurs is highly contested; originally these processes were thought to be rare and slow, in the order of hours to days [96], due to the energetically unfavourable passage of the polar lipid head group forcing through the hydrophobic core of the bilayer. Cholesterol, as mentioned above, only has a small hydroxyl group as the hydrophilic moiety, has been previously measured to diffuse transversally in approximately 1 s (Figure 1.8.4). Controversially, recent literature has suggested that the rate of lipid flip-flop is much faster than previously anticipated, with the rate at the transitional temperature of lipids 'too fast to measure', with results shown 5°C below the transition temperature to be in the range of microseconds [97]. These results have arisen due to experimental techniques such

as sum-frequency generation spectroscopy, which uses the vibration sum frequency of two input lasers to deduce information from monolayers and droplet interface bilayers, such as lipid composition, structure and orientation without the use of fluorescent or paramagnetic lipid [96, 97]. In the past decade, this work has come under scrutiny, with some labs attributing the results to pore formation in the membranes, or the overheating of the membrane [98].

The existence of flippases and scramblases, proteins that have been shown to specifically transport phospholipids from one side of the membrane to the other [99], suggests that the historical view of slow lipid flip-flop.

1.8.2 Membrane Molecular Dynamics and Phase Formation

Lipid bilayers exist in several different physical phases. These different phases impart different properties of the bilayer but are frequently the product of the same lipids in various environments such as temperature, pH, and ionic strength. The chemical structure of the lipid components, alongside the presence or absence of cholesterol, strongly influences the phase of the bilayer (Figure 1.8.5). Each structure shown in Figure 1.8.5 has been deduced by x-ray diffraction [84]. The most ordered lipid organisation is that of gel phase (L_β or $L_{\beta'}$), which is also called solid-ordered (S_o) phase. The classical gel phase is characterised by the tight ordering of the lipid acyl chains all in *trans* configuration and is elongated to the maximum, which severely restricts the molecular rotation as well as diffusion of the lipids, with lateral diffusion reduced to 10^{-3} μms^{-1}. In Figure 1.8.5 the domains are displayed as tilted with respect to the plane of the membrane, this gives rise to differences between tilted $L_{\beta'}$ and not tilted L_β domains. The degree of tilt associated with the gel phase is dependent on the hydration of the lipid; increasing water content enhances the angle of the tilt and decreases the thickness of the bilayer [84].

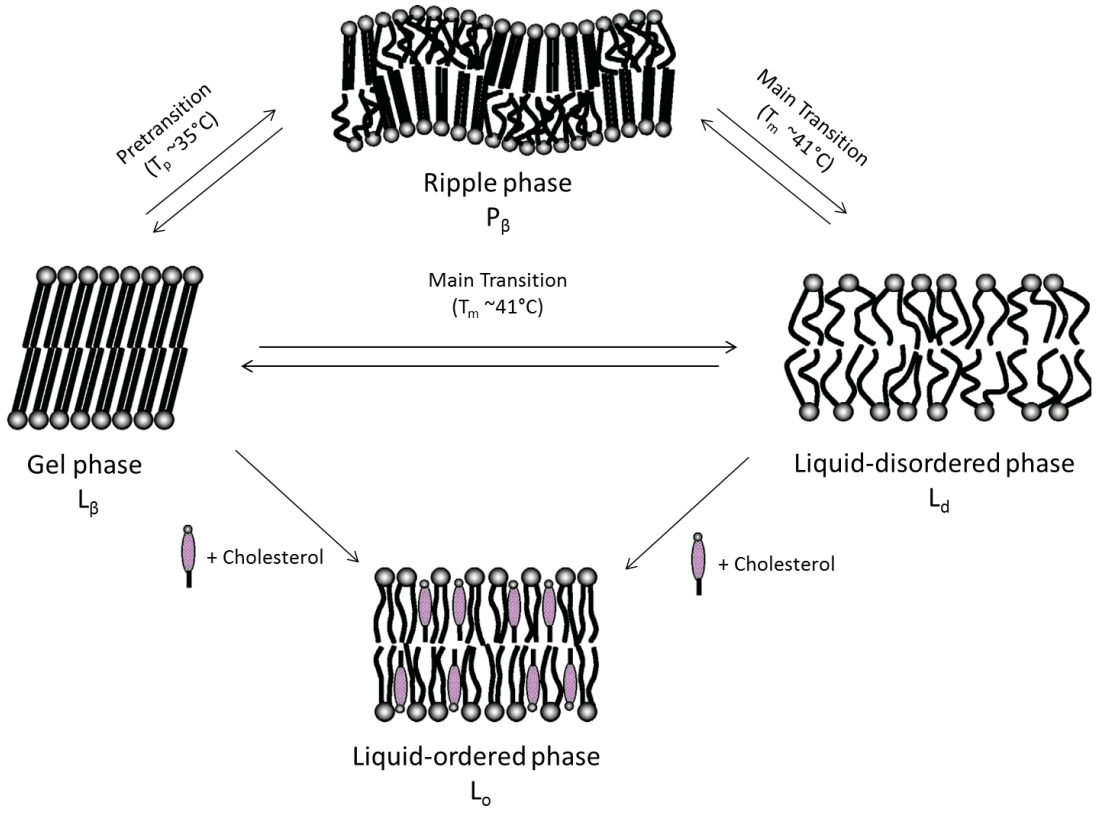


Figure 1.8.5. An illustration of the phase transitions adopted by a DPPC bilayer in an aqueous medium. Adapted from [87]. Transition temperatures were initially derived from [100] in DPPC bilayers.

The tilt of lipid acyl chains is also dependent on the nature of the head groups and the relative levels of hydration of the head groups. PC has a larger head group than PE, hence, associated with more water. Hence, PC lipids exhibit a tilt compared to the bilayer, whereas PE lipids are perpendicular [101].

Increasing the temperature of gel phase forms a pre-transition to ripple phase P_β. The ripple phase is characterised as a 'half-way' point of gel transition to the other extreme of lipid organisation, liquid-disordered phase (L_o). Pre-transition is dependent on two different mechanisms; firstly partial melting of the acyl chains which forms partial liquid disordered phase, and secondly changes to the vicinity of the polar head groups. Due to the increase head group size of PC and the greater interactions with the solvent, the lipids are more likely to enter ripple phases than PE

lipids. These phases form periodic one-dimensional undulations on the surface of the bilayer [87].

The transition between the gel and the liquid-disordered phase is termed the thermotropic phase transition temperature (T_m). Once T_m is reached, the acyl chains melt, the T_m of each lipid is different depending on the nature of its hydrophobic moiety. The T_m of different lipids decreases non-linearly with the length of hydrocarbon (due to decreased van der Waals interactions) as well as the degree of saturation, for example, stearate 18:0; (i.e. 18C chain with no double bonds) has a T_m of 58°C. The introduction of a double bond in oleate, however, leads to a decrease of the T_m to -22°C. Incorporation of unsaturated lipids into the bilayer disrupts the lipid packing of the saturated lipids, causing a destabilisation of the gel phase. A mixture of saturated and unsaturated lipids forms the liquid-disordered phase, which is well hydrated and the lipid head groups are organised in a loose hexagonal lattice. The incorporation of unsaturated chains (or gauche-configuration saturated chains) that are unable to pack together results in more space between the different lipid molecules. This increases the molecular rotation of the lipids as well as increasing lateral diffusion dramatically to ~1 μms^{-1}, hundreds of times faster than in the gel phase [102].

The fourth lipid phase is that of liquid ordered phase (L_o) (Figure 1.8.5). Liquid-ordered phases are created through the presence of cholesterol in the membrane [103]. Cholesterol destabilises the gel phase by decreasing the packing order and disrupting the triangle lattice formation. Cholesterol integration into liquid disordered phases has the opposite effect, where the cholesterol imparts stability to the membrane by ordering the lipids to bring them closer to the gel phase. As the hydrocarbon moiety of cholesterol is formed through polycyclic structures, the

molecule is rigid and planar. The cholesterol intercalates between the lipid chains and favours a *trans* chain conformation [104], furthermore the cholesterol forms a hydrogen bond between the 3-β-hydroxyl of the cholesterol and the *sn*-2 carbonyl of the phospholipid. Cholesterol increases the rate of axial rotational diffusion of the phospholipids that it associates with due to the reduction of entanglement between the acyl chains. However, the cholesterol molecule itself undergoes slower axial rotation, attributed to its planar shape [95]. The lateral diffusion of liquid-ordered phases has been shown by pulsed-field NMR on a stack of ~1000 macroscopically aligned bilayers to be in the region of three to five times slower than liquid disordered DOPC lipids [95]. The exchange of lipids between the L_o and the L_d phases was slower than the lateral diffusion of the L_d phase.

The lipid compositions of different membranes are the main contributing factor to the number of domains that can exist in a bilayer. Phase diagram are useful for explaining the different states of membranes *in vitro*. Membrane microdomains *in vivo* are subject to several external factors such as temperature, pH, pressure and osmolarity that can all influence the formation of different lipid phases.

Phase diagrams aim to document the possible phases of a membrane at thermodynamic equilibrium. Initially, the phase behaviour of cholesterol in binary systems was examined, the prevalence of the various lipid phases, gel phase (P_β), liquid ordered phase (L_o) and liquid disordered phase (L_d) were observed, with the use of differential scanning calorimetry and NMR [105] to match the theoretical studies of Ispen et al. [103] (Figure 1.8.6), With increasing temperature, there is more vibrational and rotational energy in the membrane, which results in the formation of L_d. These phase diagrams can then be applied using natural lipids such as those derived from lecithin egg PC as part of model membrane compositions. A

binary mixture of egg PC and cholesterol would be represented by the ternary phase diagram of those such as Figure 1.8.7. Egg lecithin PC has a combination of different lipids that fall broadly into two categories of high T_m lipids, with long saturated chains and low T_m lipids of short saturated chains or mono- or polyunsaturated lipids. The broad categorisation of the lipids allows the use of ternary phase diagrams as analytical tools to assess the probable phases present in the membranes.

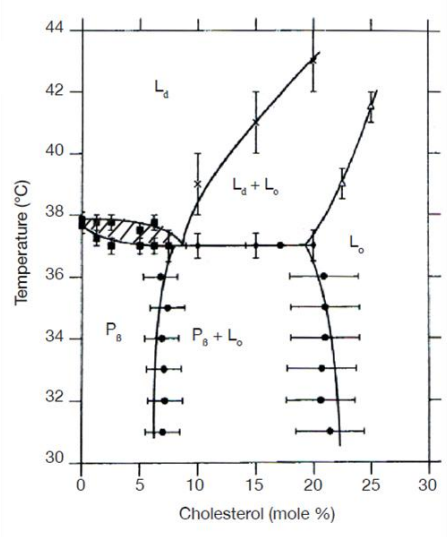


Figure 1.8.6. Phase diagram for binary DPPC-Cholesterol. Vist et al. demonstrated with different molar ratios of DPPC and Cholesterol, there are distinct lipid phases, gel phase (P_β), liquid ordered phase (L_o) and liquid disordered phase (L_d). X-axis; with increasing cholesterol L_o phase is more prevalent. Y-axis; with increasing temperature L_d becomes more prevalent. Lipid phases and phase boundaries (black spots), observed by nuclear magnetic resonance [105]

Since the production of the phase diagram, the field has expanded dramatically with an ever-increasing array of different lipid compositions such as the formation of DOPC/DPPC/Cholesterol phase diagrams and the introduction of sphingolipids such as sphingomyelin, which has been shown to co-localise with cholesterol in microdomains (Figure 1.8.7) [106].

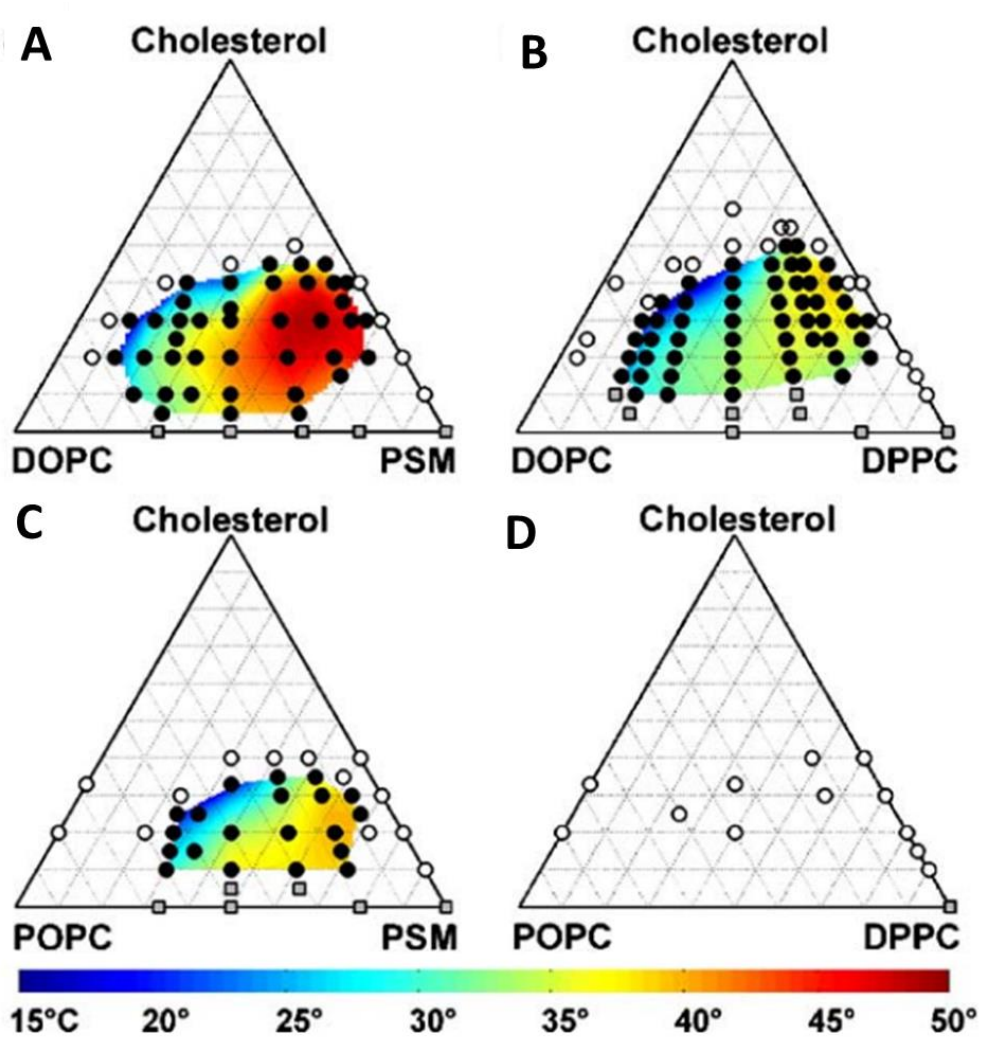


Figure 1.8.7. Phase diagram of different lipid mixture reported by fluorescence microscopy for giant unilamellar vesicles containing ternary mixtures. (A) DOPC/PSM (sphingomyelin)/Cholesterol, (B) DOPC/DPPC/Cholesterol, (C) POPC/PSM/Cholesterol and (D) POPC/DPPC/Cholesterol. Over a range of temperatures; decreasing the temperature increased the formation of microdomains. Filled circles represent microdomain forming mixture, open circles represent homogenous mixture. Adapted from [107].

Increasing the temperature of a lipid system may result in more raised above lipid their melting temperature. Once lipids are above their melting temperature the acyl chains are more likely to undergo trans-gauche isomerisation and induce liquid disordered phase, hence decreasing the population of L_o microdomains (Figure 1.8.7). In membranes containing saturated sphingolipid such as sphingomyelin (PSM) (instead of saturated phospholipid DPPC), the transition temperatures are shifted to a lower temperature when the low T_m lipid component has a higher chain melting temperature (e.g. POPC vs. DOPC) [107].

1.8.3 Lipid Rafts and their investigation

The initial fluid mosaic model proposed by Singer-Nicolson published in 1972 proposed a long-range model in which all membrane lipids and proteins were randomly distributed in cell membranes [9]. Recent experiments have shown the environment to be much more complex with the formation of distinct lipid rafts comprised of different proteins and lipids. Lipid rafts in cells were first isolated by Brown et al. [108], in which isolated fragments of the membrane that were not fully solubilised by non-ionic detergents such as Triton X-100 (TX100) or CHAPS at low temperatures. These fragments, termed detergent-resistant membranes (DRMs) are composed of cholesterol, sphingolipids, ganglioside and glycophosphatidylinositol (GPI) anchors, to which we know now to be L_o phase lipids. To confirm the presence of DRMs, an L_o phase different sterol-rich mixtures containing various lipid organisations was defined and subsequently subjected to TX100 extraction, where DRMs could only be detected in L_o containing mixtures [109].

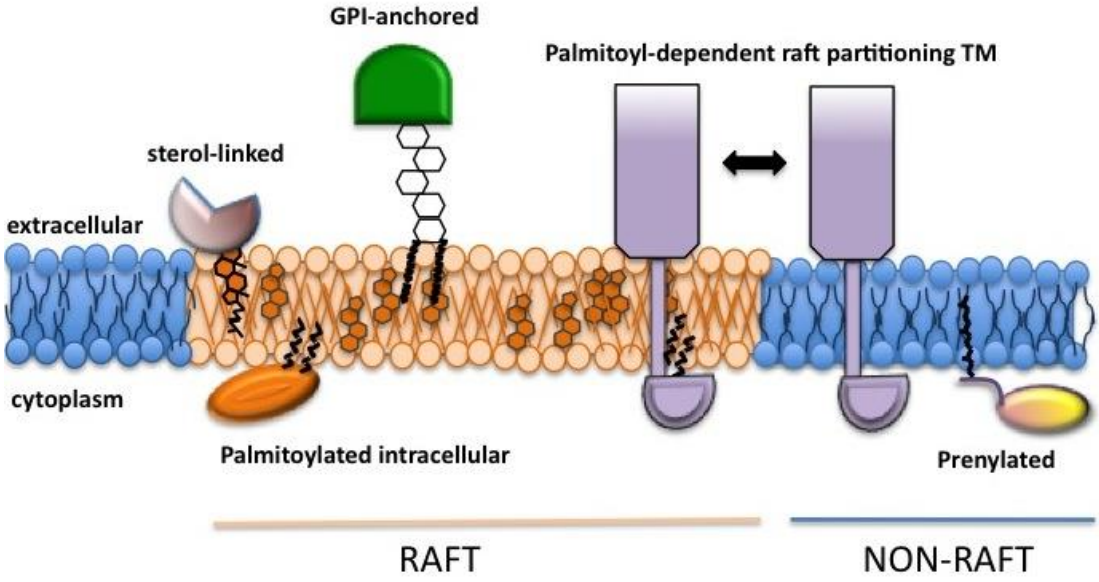


Figure 1.8.8. Proteins localise to membrane rafts through a variety of different functional groups. Proteins are localised to rafts though GPI-anchors, sterol linkers and palmitoylation, Adapted from [110]

The role of DRMs was expanded greatly in a range of different studies that have linked the presence of various cell signalling pathways. The best-understood mechanism of protein targeting to rafts is with proteins that do not contain transmembrane domains. Glycophosphatidylinositol (GPI) anchors are well known raft-targeting signals (Figure 1.8.8)[111]. A tandem NH_2-terminal myristate/palmitate motif has been shown to target peripheral peptides to lipid rafts. This motif is prominent in Src-family kinases and some G protein α subunits, which targets them to the membrane [110]. This principle was demonstrated with a GFP recombinant protein tagged with a raft-targeting motif, where it was shown by fluorescence microscopy to co-localise with lipid rafts within cells [112].

Transmembrane domains of proteins and transmembrane peptides can insert themselves into the membrane dependent on the properties of the bilayer. The 'rough' surfaced α-helices pack better with disordered lipids to minimise molecular

space between the helices and the acyl chains (Figure 1.8.9) partition into L_d phases in preference to L_o domains (Figure 1.8.9). Hydrophobic mismatch was also expected to change the preferential binding of transmembrane domains to L_d domains. L_o domains are thicker, therefore longer transmembrane domains were expected to localise into ordered, membranes, to negate the hydrophobic mismatch of the thinner L_d phase compared to the thicker L_o; however, given the unfavourable packing, the domains are shown to tilt in L_d phase rather than integrated into the more ordered L_o phase (Figure 1.8.9) [113].

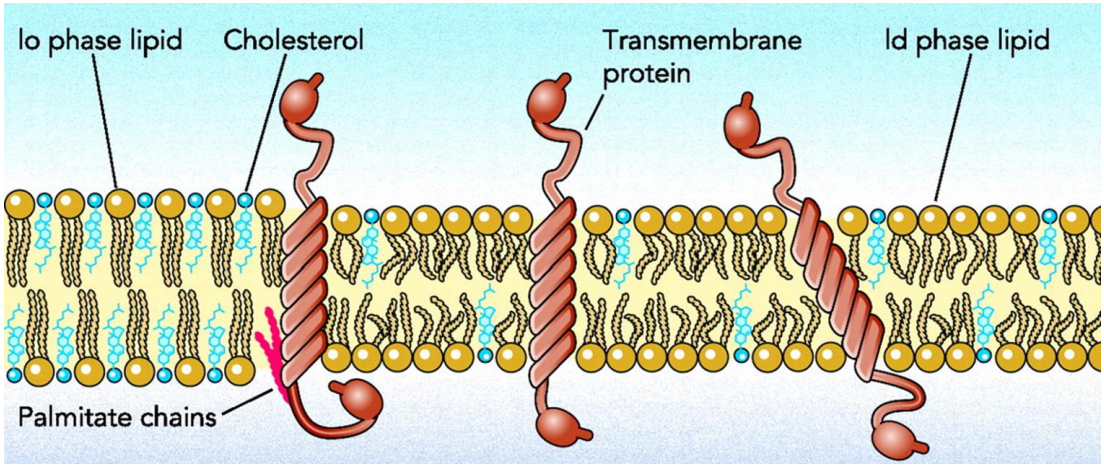


Figure 1.8.9. The position of transmembrane domains differs with each lipid organisation. Transmembrane domains can associate with the periphery of L_o domains (left-hand domain). Transmembrane domains in L_d domains tilt to balance the hydrophobic mismatch (middle and right domains). Adapted from McIntosh et al., 2003.

Further studies, however, did start to show the preferential inclusion or association to lipid rafts through different linkages. Palmitoylation, consisting of two or more linked palmitoyl chains localises proteins to the cytoplasmic leaflet of the bilayer, close to the membrane interface (Figure 1.8.8). Several proteins have been shown to need palmitoylation in order to function, highlighting the physiological relevance of lipid rafts within different systems. Raft targeting by palmitoylation has been most characterised in T-cells, where it been shown that palmitoylation aids raft targeting and function of the co-receptors CD4 [114] and CD8 [115] and the raft targeting of

the T-cell scaffolding protein LAT for signalling [116]. There are many examples of a functional role for palmitoylation in cell signalling, such as the targeting of palmitoylated-APP to lipid rafts enhancing amyloidogenic processing on cell membranes [117]. The basic mechanism of palmitoylation increases the hydrophobicity of the protein to target it to the membrane organisations that have saturated acyl chains; hence preferentially localising to L_o domains to L_d domains. However, not all palmitoylated transmembrane proteins associate with DRMs, for reasons that are unclear [72].

The model membrane systems of different lipid compositions such as illustrated in Figure 1.8.5 suggest that lipid rafts within cells are stable, long-lived structures that may be purified. The plasma membrane is known to contain significant amounts of order-preferring sphingolipids and sterols in combination with disorder preferring phospholipids [110, 118]. The balance of these components in model membranes gives rise to accurate predictions of possible phase behaviour at 37°C in cells. Furthermore, the evidence that particular the proteins are enriched in experimentally derived DRMs is substantial, and the existence and properties of the described lipid rafts are at the route of our understanding of several different processes, such as T-cell antigen receptor-mediated signalling [119, 120]. Despite this, the detergent procedure for isolating DRMs from live cells has many flaws, which questions how representative DRMs from live cells are. The major flaw is that the TX100 extraction requires cooling of the cells before the detergent solubilises the L_d phase. At lower temperatures, the percentage of L_o increases (Figure 1.8.7), especially around transmembrane domains. During the formation of DMRs, TX100 may solubilise the outer edges of the L_o phase of larger rafts or entire rafts if the raft is only moderately ordered, leading to an underestimate of domain numbers. The use of different

concentrations of detergent, or different detergent species has been shown to affect the degree to which proteins assemble into DRMs [121].

The visualisation of lipid rafts in living cells is a contentious issue. Some studies, such as the study by Hammond *et al*. [122] have tried to demonstrate the a potential lipid raft system in living cells, that of induced raft formation. This study simulated a model membrane in which gangliosides are monodispersed the membrane, however maintained close to a phase transition (Figure 1.8.10A). Upon an external stimulation of cholera toxin, the phase boundary was shifted into the large-scale formation of L_o and L_d phases (Figure 1.8.10B).

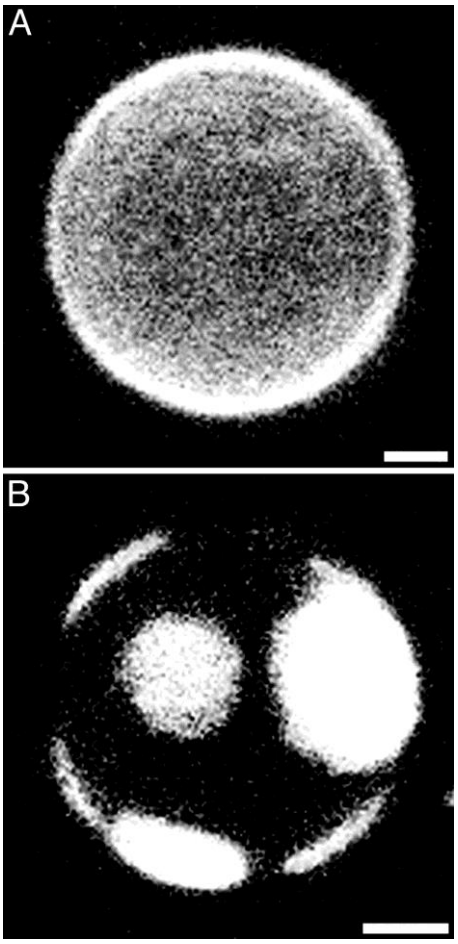


Figure 1.8.10. Cholera toxin B binding to GM_1 in the membrane indirectly changes the distribution fluorescent probe by changing the phase state of the lipid bilayer, scale bar 5 µm. Reproduced from [122]

Given the presence of induced structures in the plasma membrane, such as the immune synapse it is reasonable to suggest that the plasma membrane may be maintained close to a phase transition so that small changes in the protein or lipid composition allows large-scale changes needed for processes such as signalling.

The size of membrane microdomains has been shown to vary dependent on the system employed, as well as the technique used to visualise them. Imaging of live cells has been shown to be difficult, without a clear consensus of microdomain morphology. Live cell membranes, are by definition live and are not in equilibrium, although local equilibrium may exist. The formation of domains in cells is therefore expected to be transient dependent on the processes that the cell is undertaking or when exposed to an external stimulus. The size of *in vivo* domains are still contested but are generally accepted to be in a range of 10-400 nm [118, 123]. The size restriction of these domains has been attributed to the cytoskeleton of the cell confining the different lipid phases to sections of the membrane [121]. The best way to predict the nature of the microdomains and to characterise the processes responsible for their maintenance is to start by studying model membranes. Understanding these systems then provides hypotheses that may be tested in biological membranes.

Fluorescence microscopy of membrane microdomains has been valuable in the development of models of lipid raft formation and the examination of the processes in membrane microdomains. Fluorescence microscopy allows the observation of model systems such as GUVs [122], supported lipid bilayers (SLBs) [124, 125] as well as cell systems [126]. The field of fluorescence microscopy has been developed in two different ways. Firstly, with the development of a range of fluorescent probes, suitable for an array of biological processes, such as imaging the nucleus,

mitochondria, the extracellular membrane, cytoplasm etc. In the field of membrane imaging, there are probes categorised for preferential inclusion or exclusion in L_o or L_d lipid phases [127]. The probe employed in this study, fluoresceinphosphatidylethanolamine (FPE) has been long used to interrogate the electrostatic potential of the membrane [128] as well supported lipid bilayer (SLB) systems [124]. Secondly, the development of more sophisticated microscopy techniques, such as confocal microscopy and recently, super-resolution microscopy can increase the spatial resolution and hence the accuracy of membrane detection [129]. In this study confocal fluorescence microscopy is used in combination with of atomic force microscopy. Confocal microscopy allows visual interrogation of a large area of lipid bilayer surface with the incorporation of FPE and atomic force microscopy (AFM) interrogates the physical membrane structure below the diffraction limit.

AFM was invented by Binnig et al. [130], and allows interrogation of a membrane bilayer with Ångstrom resolution [131]. AFM has been used to obtain images of sub-micron sized domains [107, 132], ranging from 10 nm in critical fluctuations to hundreds of nanometres in long-lived structures. AFM can accurately depict the topography of a lipid bilayer with height differences between the L_o being raised 0.5-1 nm above the L_d background. AFM protocols and techniques have now been developed in which, ultra-fine AFM is possible, which has shown there to be distinct hydration layers across different formations of membrane lipids [131].

With the existence of three types of lipid raft formation; phase lipids in model membranes, experimentally derived DRMs, and critical fluctuations of the phase boundary, the terminology for what constitutes a ‘raft’ is confused [133]. For the purposes of this thesis, the term membrane microdomain is used to describe regions

of a membrane bilayer that are separated into distinct domains. When possible, further distinctions to the membrane microdomains will be discussed, such as the formation of L_o phases rich in sphingomyelin and/or cholesterol and L_β phase of saturated lipids.

Technique	Protein/ Membrane	Size of Microdomains	Reference
Live confocal	GFP–GPI & other components/ Jurkat and HL60 cells	Several μm	[134]
Live Confocal	GPI anchored proteins – CHO cells	<5 nm	[126]
Two-photon microscopy	Macrophages	<1 μm	[135]
Molecular simulations	In Silico	3-5 nm	[125, 136]
Atomic Force Microscopy	Lipid bilayers	~200 nm	[15, 124],
Confocal Microscopy	Supported lipid bilayers, giant unilamellar vesicles	2 – 3 μM	[15, 124]
Microscopy	GM1 – model membranes	10-15 μM	[122, 124]

Table 1.8.1 Summary of evidence for lipid raft formation with different techniques and types of membranes.

1.9 Measuring protein-lipid interactions: membrane potentials

Clearly, the lipid bilayer is a highly complex and dynamic structure, and its interactions with other cellular components, most notably, proteins, will be similarly complex. Being able to measure and quantify these interactions is vital to the understanding membrane biology and therefore a discussion of these interactions is now warranted.

The lipid molecules that make up the plasma membrane directly affect the electrochemical properties of the membrane and therefore, the molecular interactions with the cell surface. The three most significant membrane potentials are; the transmembrane potential ($\Delta\Psi$), the electrostatic surface potential (Ψ_s), and the dipole potential (Ψ_d).

1.9.1.1 *The Transmembrane Potential Difference (Δψ)*

The ΔΨ is created by two different bulk phases being separated by a membrane. The membrane is, under standard conditions, impermeable to charged molecules, differences in the anion/cation concentration of the different bulk phases results in a gradient across the membrane. The difference between the phases in cells is maintained by the active transport of ions across the membrane [82]. In non-excitable resting cells, the ΔΨ is typical between -40 mV and -80 mV. The plasma membrane is maintained at -70 mV, with a negative charge in the cell interior [137]. The potential is imparted by the distribution of Na^+, K^+ and Cl^- across the membrane, primarily driven by the Na^+K^+ ATPase, which is embedded in the cell membrane. Each cycle of the pump results in the exchange of three Na^+ ions from the intracellular compartment in exchange for two K^+ ions from the extracellular compartment. Due to the three-out, two-in nature of the pump, the electrical gradient is maintained across the membrane [138].

The electrochemical gradient of the plasma membrane is linked to chemical reactions within the cell. One of the most notable example is such as the propagation of an action potential in neuronal cells. Action potentials result from the opening of voltage-gated Na^+ channels, one the membrane potential reaches a voltage of +55 mV, all the Na^+ channels open, resulting in further depolarisation until reaching +70 mV at which point the Na^+ channels are inactivated. The action potential then propagates down the axon until the synapse to convert the electrical signal into a chemical response. The membrane is then repolarised by K^+ channels that release K^+ down its concentration gradient and out of the cell, restoring the -70 mV membrane potential. [139]

1.9.1.2 *The Membrane Surface Potential (Ψ_s)*

The membrane surface potential is dependent on the interaction of ions to the lipid bilayer surface. The water interface of a lipid bilayer is complex and includes a host of different lipid polar and ionised lipid head groups and proteins. The adsorption of bulk ions from the aqueous phase onto the membrane surface results in a net excess charge at the surface, resulting in Ψ_s. This potential exists from the lipid/aqueous interface and decays as a function of distance from the membrane until an electroneutral point has been reached a point infinitely distant from the membrane. The electrostatic theory in relation to the lipid bilayer has been extensively discussed in reviews [82, 137, 140].

The existence of Ψ_s results in the redistribution of aqueous ions; this leads to electrostatic attraction of counter ions to the membrane surface. This layer is described as the Stern layer (Figure 1.9.2). The forces involved in the ion-membrane interactions are thought to be primarily electrostatic and van der Waals in nature and are strong enough to immobilise the ions on the surface (i.e. larger than the thermal motion of the ions to diffuse into bulk). The formation of the Stern layer at the membrane surface reduces the net negative potential of the lipids and proteins, however not completely, leading to a surface potential of ~30 mV [82]. The manifestation of this charge has been shown to be essential in the formation and stabilisation of the membrane [138].

Classical electrostatics describe the interactions of the ions beyond the Stern layer. The electrostatic potential of the Stern layer is called the Stern potential. Coulombic interactions between the ions and the membrane surface, along with the thermal motion of the ions themselves, results in the 'diffuse double layer' (Figure 1.9.2).

The diffuse layer can be approximated by the Debye length (λ), which is ~1 nm under physiological conditions (37°C with the ionic strength of 154 mM) [137]. Increasing the concentration of the ions in solution enhances the ionic screening and hence increases the thickness of the diffuse layer (Figure 1.9.1) [82]. This concurrently, reduces the electrostatic surface potential due to increased ionic shielding (Figure 1.9.1).

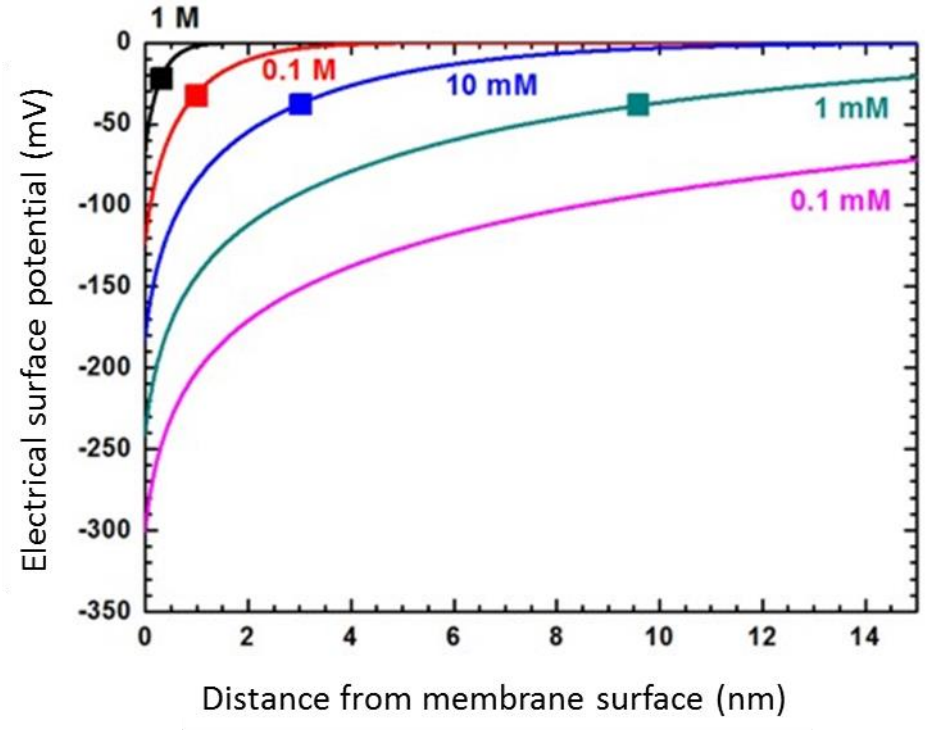


Figure 1.9.1. The effect of electrolyte concentration on the surface potential of the membrane. Values were determined by a fixed surface charge of -0.2 C/m^2, which corresponds to one elementary charge per 0.8 nm^2, the approximate size of a phospholipid head group. Temperature 25°C and ε_r=78. Adapted from [82].

Upon movement of a particle, such as a membrane vesicle, a proportion of the diffuse layer also migrates with it. The fraction where the diffuse layer separates from the bulk is termed the shear boundary (Figure 1.9.2).The electrochemical potential between the shear boundary and the bulk water is called the zeta potential (ζ). The magnitude of the zeta potential is used as a measurement of dispersion, aggregation in a variety of colloid solutions. If there is a large positive zeta potential

the molecules will tend to repel each other. If the zeta potential is low, there is no repulsive force resulting in aggregation [138].

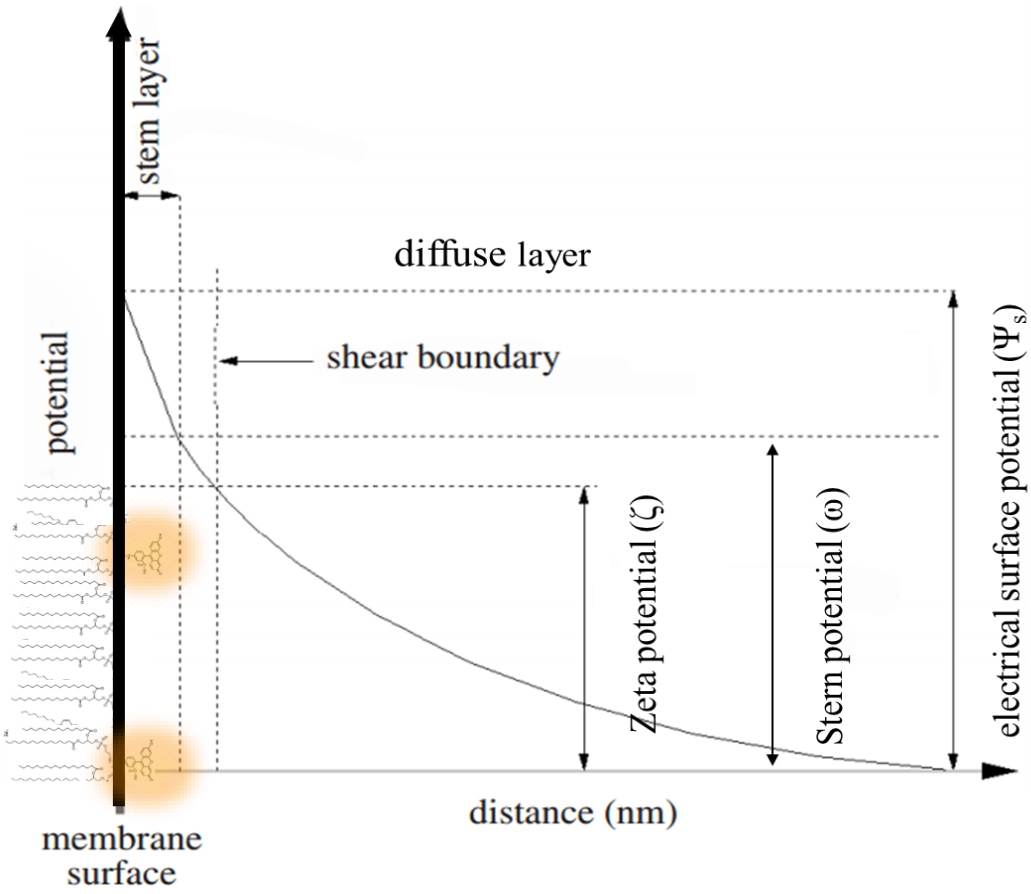


Figure 1.9.2. Contributions to the magnitude of the membrane surface potential. Illustration of the decay of membrane surface potential (Ψ_s) between the negatively charged membrane surface and the electroneutral point at infinity. Membrane and FPE probe situated in the Stern layer Adapted from [141].

Understanding the principles of Ψ_s allows it to be utilised for a variety of different purposes, for example, molecule sizing using the zeta potential with such instruments as the Zetasizer (Malvern Inc.).

Several fluorescent probes utilise the properties of the membrane surface potential as an indicator for membrane binding. Observation in changes of the Ψ_s can be representative of different species interacting with the surface. If a large charged molecule binds to the surface, the net charge on the membrane surface will change,

hence affecting Ψ_s. Fluoresceinphosphatidylethanolamine (FPE) has been shown to be a versatile indicator of the electrostatic nature of the membrane [51, 128]. FPE consists of a fluorescent fluorescein group conjugated to a phosphatidylethanolamine lipid. The protonation state of the fluorescein moiety affects the fluorescence quantum yield, with the deprotonated state eliciting the greater fluorescence [142]. When incorporated into lipid bilayers FPE lies precisely at the water-lipid interface of the molecular surface (demonstrated in Figure 1.9.2), allowing it to detect changes in the charge distribution of the membrane in response to changes in Ψ_s.

To describe the FPE responsivity to the surface, the concentration of charged ions at the membrane surface must be assessed.

The Boltzmann equation describes the concentration of charged ions at the surface ($C_{i,s}$) and in bulk water ($C_{i,b}$). Z is the electrolyte valence of the ion in question, dependent on the properties of the surface (O'Shea, 2004).

$$C_{i,s} = C_{i,b} exp[-Z_i F \Psi_s / (RT)]$$

Equation 1.9.1.

When combined with the Henderson-Hasselbalch equation and rearranged, the equation gives:

$$log\left(\frac{C_F}{C_{HF}}\right) = pH - \left(pK - \frac{F\Psi_s}{RT\ln 10}\right) log\left(\frac{c_F}{c_{HF}}\right) = pH - \left(pK - \frac{F\Psi_s}{RT\ln 10}\right)$$

Equation 1.9.2.

pH = -log($C_{h,f}$), C_f and C_{hf} denote the concentration of the dissociated and pronated species of the acid-base pair respectively [82]. The function [pK − F Ψ_s /(RT ln 10)] denotes the relative pK for proton binding of the acid–base pair on the membrane surface. According to these equations, if the pH remains constant, changes to Ψ_s,

through charge interaction with the membrane will modify the protonation state of the FPE, which results in a change in the fluorescence yield. These effects can be simplified into an equation:

$$pK_S = pK_B + \Psi_s$$

Equation 1.9.3.

This equation highlights that changes in the electrostatic surface potential will promote a shift in the apparent pK of FPE. pK_S and pK_B represent the pK of FPE at the membrane surface (pK_S) and the pK of FPE in bulk solution (pK_B) [82]. This means that FPE in membranes offers a technique to measure the electrostatic potential directly.

Hence, FPE has been used in detecting charge interaction of a variety of proteins and peptides to membranes, such as cytochrome c oxidase signal sequence (p25) with PCPS phospholipid membrane vesicles, by virtue of a series of positive charges [51], the positive N-terminus of HIV fusion peptide gp41 with PC membrane vesicles and lymphocyte cells [143].

In this study, FPE is utilised to investigate the interactions of albumin, fibrinogen and a range of polypeptides in a variety of media and membrane compositions.

1.9.1.3 *The Membrane Dipole Potential (Ψ_d)*

The membrane potential arises from the contribution of electrical dipoles associated with the carbonyl group ($C^{\delta+}=O^{\delta-}$) and the oxygen-bounded phosphate ($O^{\delta-}$-$P^{\delta+}$) component of the phospholipids in the membrane. The water molecules in the Stern layer which have permanent molecular dipoles are also thought to contribute towards the dipole potential [88]. These dipolar groups are orientated in such that the hydrophobic interior of the membrane is positive with respect to the external aqueous

phase. The magnitude of Ψ_d is generally accepted to be of the order of hundreds of millivolts, with values ranging from 5 mV to 600 mV [88, 89, 138, 144], depending on the membrane composition. The factors that affect Ψ_d are generally mutually exclusive to those that affect Ψ_s; the only effect that has some cross-talk between the potentials is the indirect effects of ionic strength. Increased ions in the solution have been shown to affect the solvation of the ions in the Stern layer, thus affecting the dipoles of the associated water molecules known to contribute towards Ψ_d. The greatest effect on Ψ_d is the packing of the lipid molecules, phospholipid fatty acyl chains, not being polar, only make a minor contribution to Ψ_s [139]. The Ψ_d increases with the saturation of the lipid chains and are greatest in highly ordered saturated acyl chains and decreases as a function of disorder and introduction of unsaturated lipids [89, 145]. The presence of cholesterol (shown earlier) imparts more order into lipid membranes (Section 4.1), thus increasing Ψ_d. Recent work has shown that the structure of water molecules over different domains formations is marked different [146], which may contribute to more water in the Stern layer having dipoles orientated perpendicular to the membrane increasing the Ψ_d.

Quantifying these membrane dipoles is the cornerstone of lipid biophysics. The use of membrane probes have developed the understanding of these forces and the external influences that alter these potentials. It is not yet possible to directly measure Ψ_d as it would require a range of different measurements taken from the core of the bilayer to the surface. However, changes in Ψ_d have been accurately characterised by the use of an electrochromic probe Di-8-ANNEPS (4-[2-[6-(Dioctylamino)-2-naphthalenyl]ethenyl]-1-(3-sulfopropyl)-pyridinium). This dye uses a dual-wavelength ratiometric fluorescence value to measure the membrane dipole potential developed by Loew et al. [147]

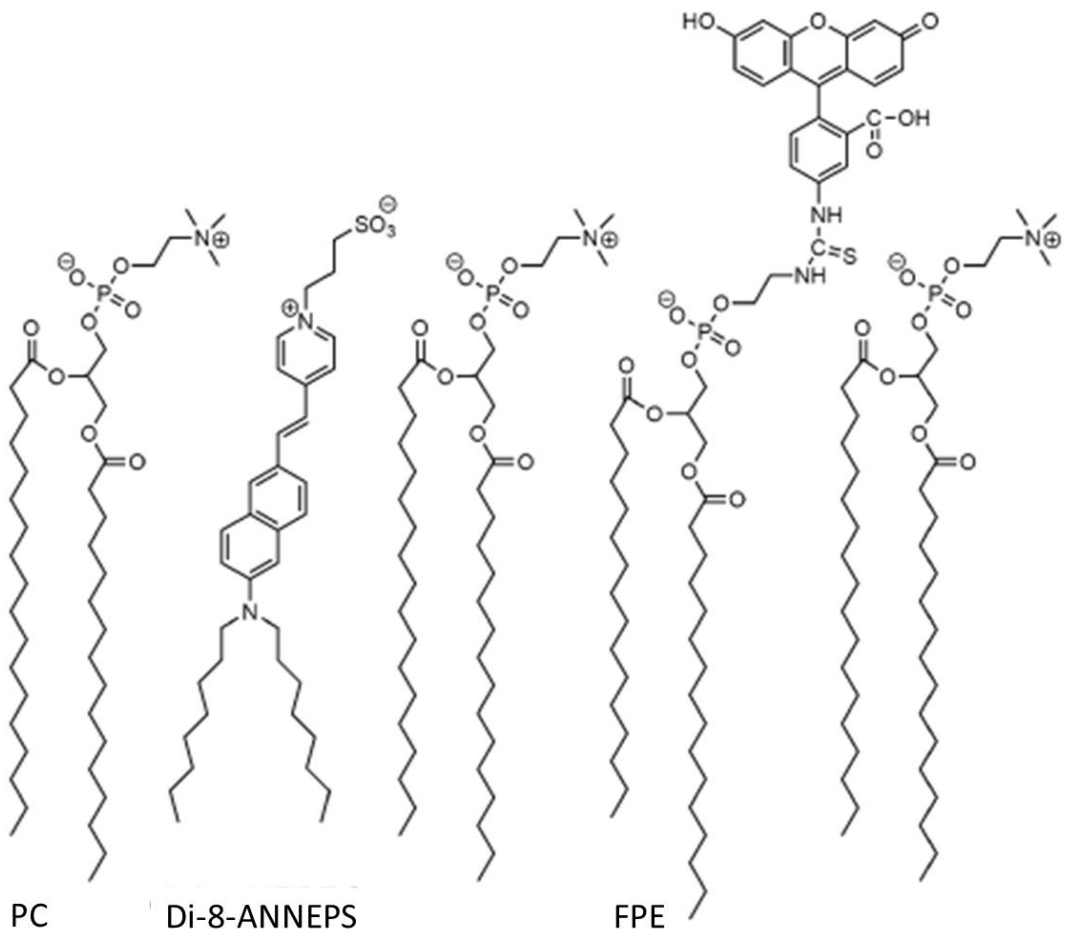


Figure 1.9.3. Structures of membrane potential probes: FPE and Di-8-ANEPPS, in a PC phospholipid membrane. Image constructed using ChemDraw.

The membrane probes employed clearly investigate different parts of the membrane bilayer (Figure 1.9.3). Di-8-ANEPPS incorporated into the membrane as such that the chromophore portion of the molecule lies beneath the head groups of the phospholipids and is subject to the influence of Ψ_d. The insertion of proteins and peptides into the membrane can be monitored using Di-8-ANEPPS. The insertion of macromolecules will perturb the balance of the resting $\Psi_{d,}$ by either increasing or decreasing the potential of the membrane, depending on the charge and orientation of the inserting molecule.

Monitoring the changes of fluorescence from these probes, allows us to examine changes in these potentials from the membrane. Interpretation of the fluorescence changes allow us to observe protein binding, insertion and conformational changes.

1.10 Aims and Objectives

The previous sections have outlined the field of intermolecular interactions that occur between protein species and both membranes. Although many of these processes are beginning to be understood in bespoke conditions, the ability to control sub-classes of intermolecular interactions remains elusive.

This study investigates the effect of various soluble reagents on the protein-surface interactions of abundant plasma proteins to both biological (membrane) and non-biological (metal) surfaces. The different combinations of the reagents are examined to see how the various proteins interact with the various surfaces, thus which intermolecular forces are disrupted in each condition. Combinations of these reagents are employed to investigate the nonspecific binding of the proteins to non-biological surfaces such as metals and beads, which are routinely used in detection machinery.

The presence of lipid domains in membranes, both model and cellular systems has been identified (see Section 1.8.3), with the formation of the domains dependent on the technique used and lipid composition. The reagents that modulate intermolecular interactions will be employed to investigate the organisation process of the lipid domains across various techniques.

Various proteins and peptides have been identified that co-localise to membrane microdomains and/or actively target the microdomains within a lipid bilayer. One of these proteins is the pathological protein Huntingtin, which has a characteristic polyglutamine expansion. This study will focus on potential processes that cause the microdomain formation that of the polypeptide expansions, with poly-lysine and polyglutamine peptides. The peptide-membrane interactions are studied in real-time in order to elucidate the mechanism and kinetics of the binding process with various

membrane compositions and various media. These interactions are followed by time-course investigations of the peptide-microdomain formation in the various media conditions.

The mains aims of this study are to:

- Elucidate the effects of various media reagents on the binding of exemplar plasma proteins to model membranes
- Establish conditions to allow the reduction of nonspecific binding of plasma proteins to non-biological surfaces used in detection instruments
- Characterise membrane microdomain formation in the presence of reagents that alter intermolecular interaction
- Elucidate a binding mechanism and kinetics for peptides that binding to microdomains in various membrane and media conditions
- Investigate how the binding of polypeptides alters membrane microdomain formation in supported lipid bilayers.

2 Materials and Methods

2.1 Lipid Compositions

Egg lecithin and phosphatidylserine (PS) were purchased from Lipid Products (UK). Egg lecithin is a naturally derived phosphatidylcholine (PC) mixture defined in Table 2.1.1 (DLPC (1,2-dilauroyl-sn-glycero-3-phosphocholine), DOPC (1,2-dioleoyl-sn-glycero-3-phosphocholine), DOPS (1,2-dioleoyl-sn-glycero-3-phospho-L-serine), DPPC (1,2-dipalmitoyl-sn-glycero-3-phosphocholine), DSPC (1,2-distearoyl-sn-glycero-3-phosphocholine)). Synthetic DOPC was purchased from Avanti Polar Lipids (Alabama, U.S.A). Sphingomyelin and cholesterol were purchased from Sigma Aldrich (UK).

Name	Description
	Mixed lipid
PC_{100}	32.1% 16:0 PC (DPPC), 2.1% 16:1 PC (Δ9 (cis/trans) PC), 11.7% 18:0 PC (DSPC), 36.2% 18:1 PC (DOPC), 12.5% 18:2 (DLPC), 5.5% 20:4 PC.
$PC_{70}Chol_{30}$	70% PC (as above), 30% Cholesterol
$PC_{55}Chol_{30}SM_{15}$	55% PC (as above), 30% Cholesterol, 15% Sphingomyelin
$PC_{70}PS_{30}$	55% PC (as above), 30% Phosphatidylserine
	Pure lipids
$DOPC_{55}Chol_{15}SM_{25}$	55% DOPC, 15% Cholesterol, 25% Sphingomyelin

Table 2.1.1: Lipid compositions used in this study.

2.2 Liquid Media Compositions

PBS containing 137mM NaCl, 2.7 mM KCl, 8.1 mM Na_2HPO_4, and 1.47 mM KH_2PO_4 was purchased as tablets from Dulbecco UK. Other electrolyte media were made with a phosphate base with a composition of 2.7 mM KCl, 8.1 mM Na_2HPO_4, and 1.47 mM KH_2PO_4. Reagents were brought from BDH (VWR). Electrolyte reagents NaSCN, Arg, Gly-Gly and Gly-Gly-Gly, were purchased from Sigma Aldrich. Electrolytes were osmotically balanced through the replacement of NaCl ions with reagents in Table 2.2.1. Some buffers were made at high ionic strength (HIS) at ~600 mM. All media compositions were made to pH7.4 unless indicated otherwise.

Media	NaCl (mM)	NaSCN (mM)	Arginine (mM)	Gly-Gly (mM)	Gly-Gly-Gly (mM)
PBS	137	0	0	0	0
Arg	87	0	100	0	0
Gly-Gly	87	0	0	100	0
Gly-Gly-Gly	87	0	0	0	100
NaSCN	50	87	0	0	0
Arg Gly-Gly	37	0	100	100	0
Arg NaSCN	0	87	100	0	0
Gly-Gly NaSCN	0	87	0	100	0
Gly-Gly-Gly NaSCN	0	87	0	0	100
Arg Gly-Gly NaSCN	0	50	74	100	0
Arg Gly-Gly NaSCN HIS	0	100	200	200	0
Arg Gly-Gly-Gly NaSCN HIS	0	100	200	0	200

Table 2.2.1: Media compositions used in this study.

2.3 Proteins and Peptide Species

Human serum albumin (HSA), fibrinogen and cell culture Poly-L-Lysine were purchased from Sigma Aldrich. Anti-IL-8 antibody (ab7747) and anti-fibrinogen antibody (ab58207) were purchased from Abcam plc. IgG control antibody (GTX 35009) was purchased from Gentex. Poly-L-lysine (10 residues) was supplied by Alamanda Polymers. All other chemicals were purchased from Sigma Aldrich.

$PolyQ_{28}$ was provided by Dr James Duggan, initially synthesised by Dr Erika Rosivatz and Dr Rudiger Woscholski (Imperial College London). The first 67 residues of exon 1 with 28 polyglutamine expansions (Q=28) were expressed through a modified DH5α *E.coli* [36].

2.4 Unilamellar Lipid Vesicle Formation

Membrane vesicles were prepared via the well-characterised pressure extrusion method [148]. Lipids dissolved in chloroform/methanol were mixed at the desired molar ratios (Table 2.1.1) and dried under an oxygen-free nitrogen stream in a round-bottom flask, rotating throughout to ensure a thin lipid film. The lipid film was rehydrated in the relevant media (Table 2.2.1). The resultant multi-lamellar vesicle solution was quickly frozen in liquid nitrogen and thawed in a hot water bath (above 45 °C) five times. Finally, the solution was extruded 10 times through a 25 mm diameter polycarbonate filter with 0.1 μm diameter pores (Nucleopore Corp.) using a pressure extruder (Lipex Biomembranes Inc.) In order for all lipids to be in a fluid phase, the lipids were heated to 45°C before and during extrusion. This process resulted in a monodisperse, unilamellar suspension of 100 nm phospholipid vesicles [149].

2.5 Membrane Vesicle Labelling With FPE

Fluoresceinphosphatidylethanolamine (FPE) was purchased from Life Technologies. PD-10 columns (Sephadex G-25 Medium) were purchased from GE Healthcare. The bomb extruder was supplied by Lipex Biomembrane Inc. A 2mg/ml FPE solution was dried from chloroform/methanol solution using oxygen-free nitrogen. FPE was hydrated in filtered ethanol. Ethanolic-FPE (never more than 0.1% ethanol (v/v)) was incubated with 13mM membrane vesicles at 37 °C for 1.5 h in the dark. Unincorporated FPE was removed via gel filtration using a media equilibrated (minimum 50ml wash) PD10 Sephadex column. This procedure leads to the incorporation of approximately 70% of the total FPE added, all of which is inserted into the outer membrane of the vesicles [128]. All steps were completed in minimal light to avoid photobleaching of FPE.

To determine whether membrane vesicles were successfully labelled with FPE, emission spectra (excitation 490 nm) of the FPE-labelled membrane vesicles were observed and compared to that of the fluorescent component of FPE (fluorescein sodium salt) as shown in Figure 2.5.1. The dielectric permittivity of the different environments results in a red-shift between the fluorescein in water (emission maximum 510 nm) and the FPE in the membrane (emission maximum 520 nm) [128].

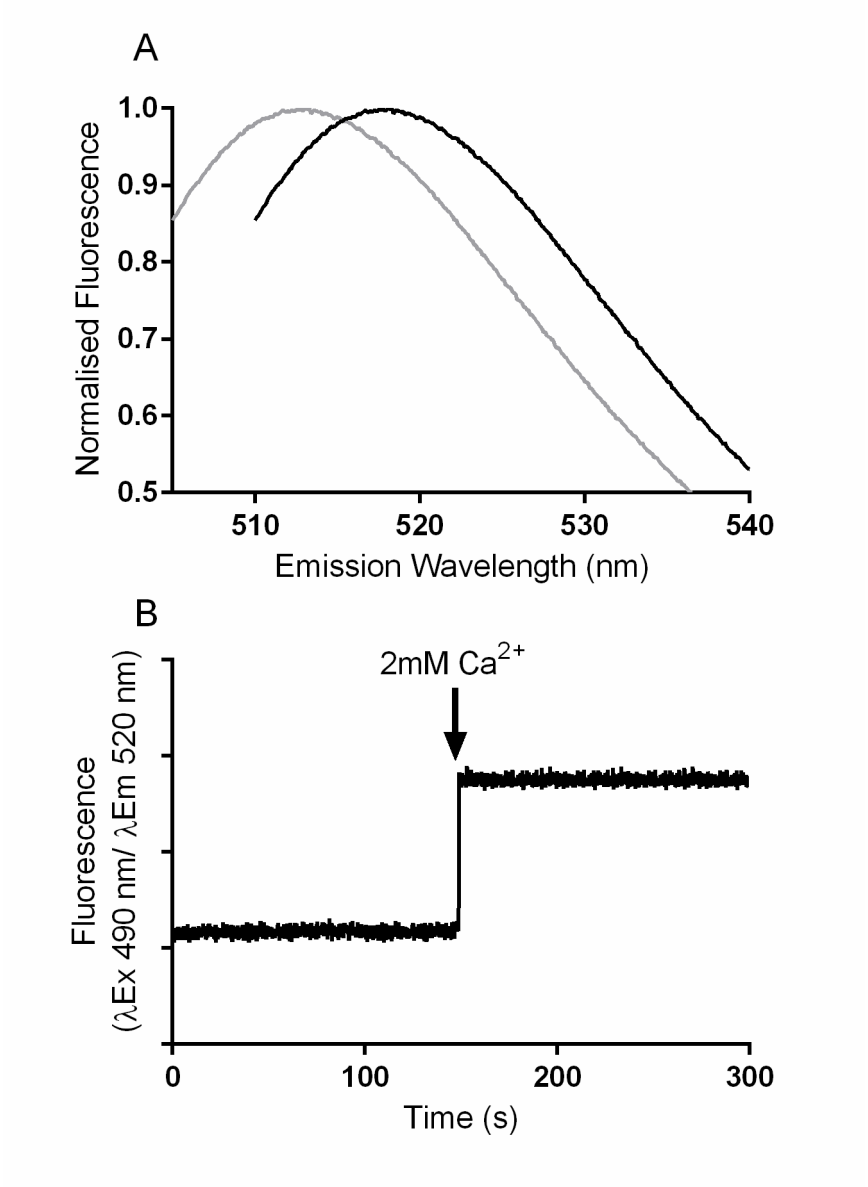


Figure 2.5.1 (A) The normalised emission spectra (excitation 490nm) of 400 µM FPE labelled PC_{100} membrane vesicles (black line) is red-shifted (peak emission 520 nm) in comparison to emission spectra of fluorescein sodium salt (peak emission 510 nm) at the same concentration in the absence of membrane vesicles (grey line). (B) Fluorescent intensity of FPE labelled 400 µM membrane vesicles in PBS, pH 7.4, was recorded at 520nm following excitation at 490 nm. An addition of 2 mM Ca^{2+} (in the form of $CaCl_2$) was added to the sample (denoted by the arrow).

The fluorescence intensity (*FI*) of membrane vesicles labelled with FPE was recorded at 520nm following excitation at 490nm. A 2 mM addition of Ca^{2+} (in the form of $CaCl_2$, 1M stock solution made up in the same media as the vesicles) was added to the membranes, which resulted in an increase of fluorescence, indicative of the FPE responding to the electrostatic potential of the membrane [128]. The addition

of Ca^{2+} to membranes labelled with FPE causes a reduction in the electrostatic surface potential, decreasing the magnitude of the surface potential. This results in an increase in the proportion of probe deprotonation and an increase in fluorescence intensity.

2.6 Spectroscopic Analysis of Membrane Probe FPE

Steady-state fluorescence spectroscopy was conducted with a Jobin Yvon Fluoromax 4 (HORIBA, Japan) or a Jobin Yvon Fluorolog 3 (HORIBA, Japan). Fluorescently labelled membrane vesicles (as described in Section 2.4) were diluted from 13mM stock to 400μM unless otherwise stated in appropriate media (Table 2.2.1). Spectra were collected (0.1 s integration time) and results were averaged over five repeats.

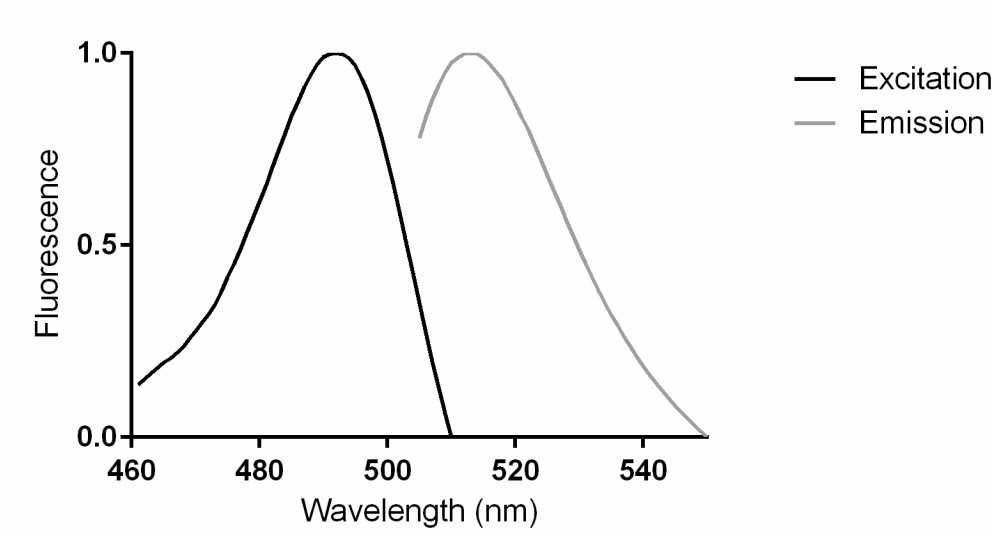


Figure 2.6.1 FPE excitation and emission spectra of 400 μM FPE labelled vesicles in PBS, pH 7.4. Excitation λ_{max} at 490 nm with emission λ_{max} at 520 nm. Changes to FPE emission were monitored in the presence of different media (Table 2.2.1)

Emission and excitation spectra were acquired before the various titration experiments to ensure the correct labelling of membrane vesicles (Section 2.5). In the presence of different media (Table 2.2.1), emission λ_{max} were observed for changes in the dielectric constant. The fluorescent responsivity of the probe is not affected by

the various media employed in the experiments (Section 2.7, Figure 1.9.1, Figure 5.1.1)

2.7 Fluorescence Analysis of FPE Probe

FPE labelled lipid vesicles were diluted in appropriate media to 400 μM. Protein/peptide samples were diluted in the same media as vesicles (unless otherwise stated in results). The fluorescence intensity of FPE labelled membranes vesicles was recorded over time by excitation at 490 nm and collecting the emission at 520 nm. The temperature was maintained at 25°C throughout all experiments. Once equilibrium was reached (*FI* is constant against time) proteins of interest were titrated into the solution and the Δ*FI* was recorded upon the establishment of a new equilibrium (averaged over 100 s).

Media dilution effects and photobleaching were corrected through the addition of equivalent volumes of media via titration over a comparable timeframe. Additions were deduced from protein Δ*FI*.

Graphs of Δ*FI* versus protein concentration (minimum of n=3 for all experiments of this type (such as Figure 3.1.2)) were plotted, and the resulting interaction curves were fitted to different nonlinear regression models using GraphPad Prism, with the preferred model chosen by comparison of R^2 values in collaboration with an F-test.

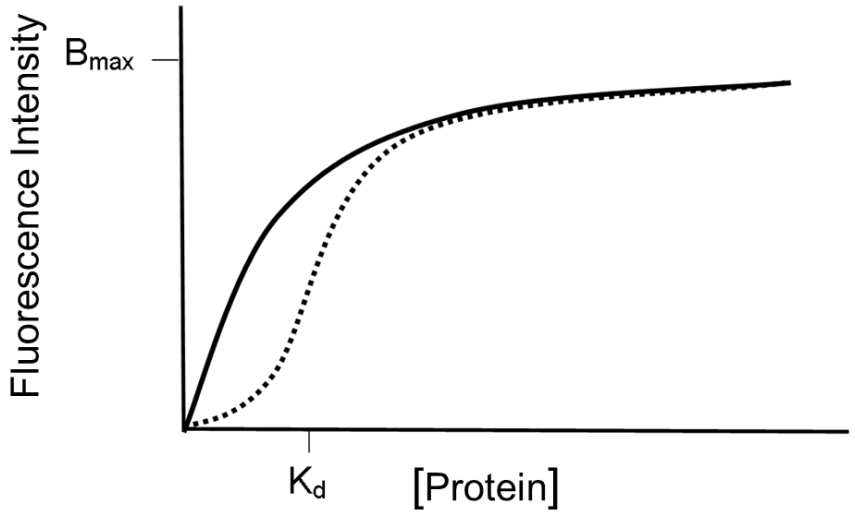


Figure 2.7.1. Binding model of protein concentration (x) and fluorescence intensity (y). Simple hyperbolic binding model (solid line). Single binding model with Hill coefficient (h) (dashed line); Hill coefficient represents an index of cooperativity.

$$y = \frac{B_{max}x}{K_d + x}$$

Equation 2.7.1 Simple hyperbolic binding model

$$y = \frac{B_{max}x^h}{K_d^h + x}$$

Equation 2.7.2. Simple cooperative binding model

The data is fitted to various binding models, which denote different reaction profiles; simple hyperbolic binding model (Equation 2.7.1), where y is the change is fluorescence (ΔFI), x denotes protein concentration, B_{max} is the binding capacity and K_d is the dissociation constant, the concentration at which half of the binding sites are occupied. Alternatively, a simple cooperative binding model is fitted, where h is the Hill coefficient, which represents an index of cooperativity (Equation 2.7.2).

An extra sum of squares F-Test was employed to determine which binding model best fit to the data (Equation 2.7.3).

$$F = \frac{(SS_1 - SS_2)/(DF_1 - DF_2)}{SS_2/DF_2}$$

Equation 2.7.3 Extra sum of squares F-test

This statistical test is required as increasing the degrees of freedom decreases the sum of squares. This results in an increase in the goodness of fit parameter, R^2. R^2 measures goodness of fit between 0 (no correlation) and 1 (perfect correlation), generally if $R^2 > 0.95$ the model is proposed to fit a data set well.

The F ratio quantifies the relationship between the relative increase in the sum of squares (SS) (the sum of vertical distances of the data points from the curve squared) and relative increases in the degrees of freedom (DF). If the simpler model is correct, the relative increase in the sum of squares (increasing in simplicity) is expected to equal the relative increase in degrees of freedom ($F \approx 1$). If a more complex model is correct the relative increase in the sum of squares is expected to be greater than the relative increase in degrees of freedom ($F >> 1$). If a simpler model is correct, the F ratio is approximately 1. If the ratio is much greater than 1.0 there are two further possibilities; the more complex model is correct, or random scatter in the dataset led to the better fit. If the *p*-value of an F-Test is low ($p \leq 0.05$) the more complex model is accepted.

Should the hyperbolic model with Hill coefficient fit better, there is implied cooperativity between molecules and the membrane such as [150].

B_{max} and K_d values were established from the fitting data, the differentiation between these parameters was defined by significant difference as calculated by a one-way ANOVA Fisher's LSD test between the different conditions.

2.8 Stopped-flow rapid mixing and analysis

Stopped-flow rapid mixing (SFRM) was utilised to observe binding interactions between proteins/peptides and membranes from ~1ms onwards. Experiments were performed at 25 °C, which was controlled using a water bath. Experiments were conducted on an SX20 Stopped-flow spectroscopy instrument (Applied Photophysics) equipped with a liquid handling unit at 25°C (Figure 2.8.1).

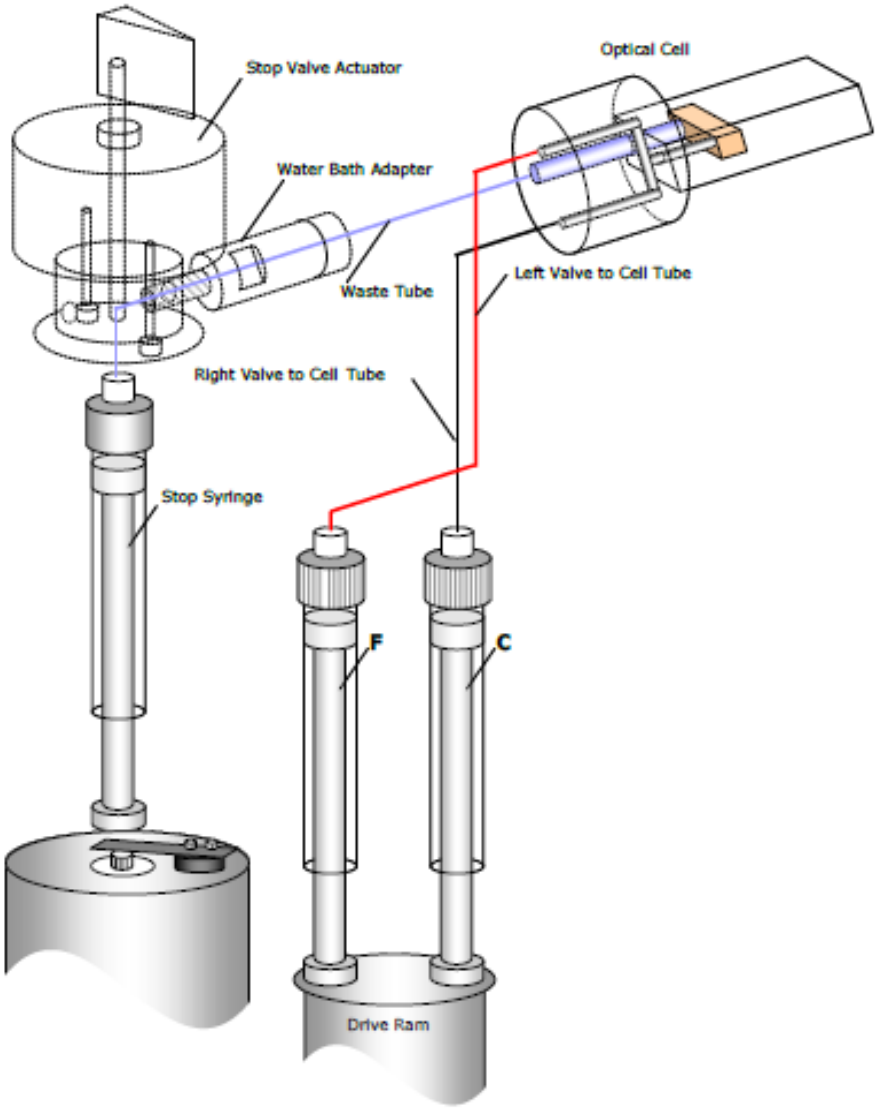


Figure 2.8.1. Stopped-flow circuit. Samples are loaded into respective syringes (F & C). Drive ram is powered by compressed nitrogen gas into the Optical Cell in a 1:1 ratio. Reagents are held in the Optical Cell during data collection, until is it ejected to waste. Adapted from [151].

Stopped-flow experiments were carried out with a 1:1 mixing ratio. Flow is initiated by a nitrogen-powered pneumatic drive ram, which drives the two syringes containing the samples (Figure 2.8.1. F & C). The samples are driven to the optical cell where the flow is stopped. Various parameters were recorded in the ProData viewer. Fluorescence intensity changes (ΔFI) were observed following excitation of the FPE probe at 490 nm.

2.8.1 Kinetic data analysis

The following software was used to analyse the data: i) ProData Viewer, Applied Optics Ltd SX20 stopped-flow fluorimeter software, ii) ProK-IV Kinetic Analysis and Data Simulation Software, iii) GraphPad Prism 6 and iv) Microsoft Excel 2013.

The binding capacity and rates were calculated from averaged time-resolved data (n=5 independent samples unless stated) obtained from stopped-flow rapid mixing (SFRM) experiments. Initially, the binding curves were dissected into binding ΔFI (increase with electropositive species) and a second phase interaction (insertion or dissociation of an electropositive species, etc. resulting in an *FI* decrease). The addition of an electronegative species results in a *FI* decrease upon binding and *FI* increase upon insertion. The binding phase was fitted to a single exponential with plateau values determined as the total *FI* increase/decrease (Equation 2.8.1).

$$Y = Y_0 + (Plateau - Y_0)^{*}(1 - exp(-K^{*}t))$$

Equation 2.8.1. Single exponential. Y is equal to the fluorescence signal at a time, t. Y_0 is *FI* when t=0. K is rate constant of exponential association and plateau of ΔFI when t= ∞

ΔFI plateau was plotted for each concentration in GraphPad prism and resulting curves were examined with the hyperbolic binding model (Equation 2.7.1) or hyperbolic with Hill coefficient binding model (Equation 2.7.2) as shown in Figure 2.7.1.

The SFRM traces were subjected to kinetic modelling using ProK-IV software, where the data was fitted to a varying numbers of mechanistic steps. Rate constants obtained from the model are more accurate than sums of the exponentials as they only represent the time points for which they are fitted. Several exponentials are extrapolated from zero and are therefore are influenced by one another.

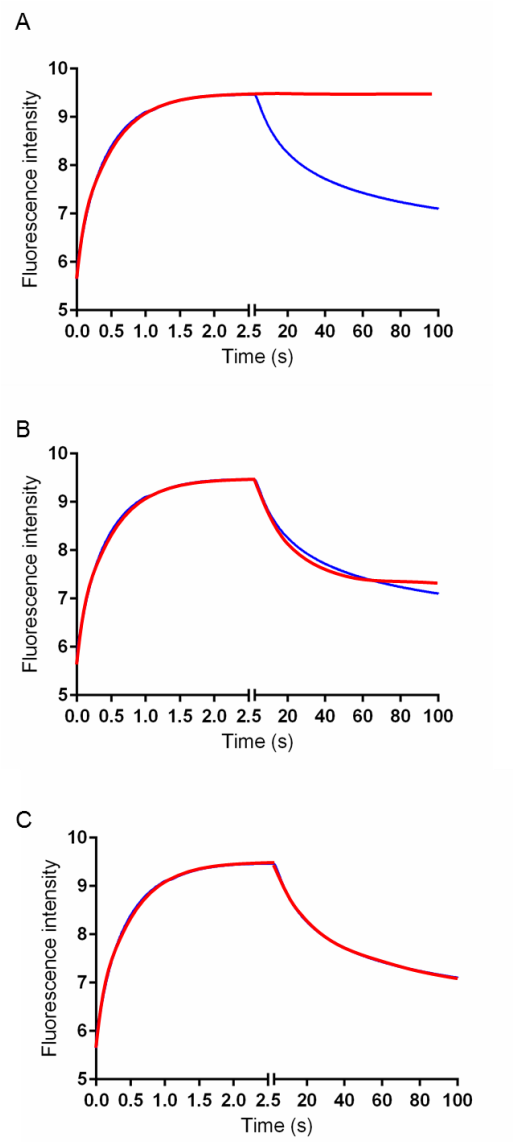


Figure 2.8.2. The blue line is an exemplary trace of a complex binding mechanism a peptide-membrane interaction. The red trace is the model fit of the trace, with varying mechanistic stems. (A) One step model A→B, (B) Two-step model A→B→C and (C) Three-step model A→B→C→D. A, B, C and D.

Kinetic model fit theoretical predictions of protein states	
A → B	A is free peptide, B is bound peptide
A→B→C	A is free peptide, B is bound peptide, C is inserted peptide
…	
A→B→C→D→E	A is free peptide, B is bound peptide, C-E are intermediates and inserted forms of the peptide

Figure 2.8.3. Kinetic model predictions of proteins state during a complex peptide-membrane interaction as depicted in Figure 2.8.2.

The SFRM traces obtained from polypeptide interactions with membranes are expected to have several different steps in the reaction. This enabled complex binding models to be established in a stepwise manner from the simplest binding reaction, where the fit is unsuitable (Figure 2.8.2A and Figure 2.8.3), to a more complex model which fits the data more reliably (Figure 2.8.2C and Figure 2.8.3). Increasing the complexity of the model decreases the sum of squares making the fit artificially better (described in Section 2.8.1), hence only clear improvements in the model are accepted. Association and dissociation may be multi-step increasing the model complexity further. The best model was determined by low variance, low standard errors, good fit by eye and linear residuals. If the residuals from the model were structured, it suggests there is a further parameter that is not represented by the model.

2.8.2 Protein Aggregation Studied by Thioflavin T

Aggregation during the polypeptide interaction with membranes was assessed by diluting 15 mM Thioflavin T (ThT) in media and monitoring changes in the fluorescence intensity following excitation at 442nm. The presence of hydrogen bonds produces rigid, highly ordered structures, such as β-sheets (indicative of aggregation). ThT binding these structures results in a change of the charge density of ThT, resulting in a red-shift in the excitation spectrum [152]. While monitoring

the fluorescence at 442nm, the excitation red-shift results in a pronounced increase in the ThT fluorescence intensity.

2.9 Supported Unilamellar Bilayers

Glass coverslips were cleaned by incubations with methanol, 1 M NaOH and 1 M HCl, washed thoroughly twice in distilled water and then incubated in a 10 mM $MgCl_2$ solution overnight at room temperature. Fluorescently-labelled vesicles (Section 2.5) were diluted to 1.3 mM in appropriate media and heated to 45 °C. Vesicles were added the slide and formed a bilayer via the vesicle rupture technique (Figure 2.9.1) overnight in the dark at room temperature. This resulted in the formation of a unilamellar bilayer on the glass surface as demonstrated by McConnell [153] which has been optimised for bilayer formation as shown in Figure 2.9.1.

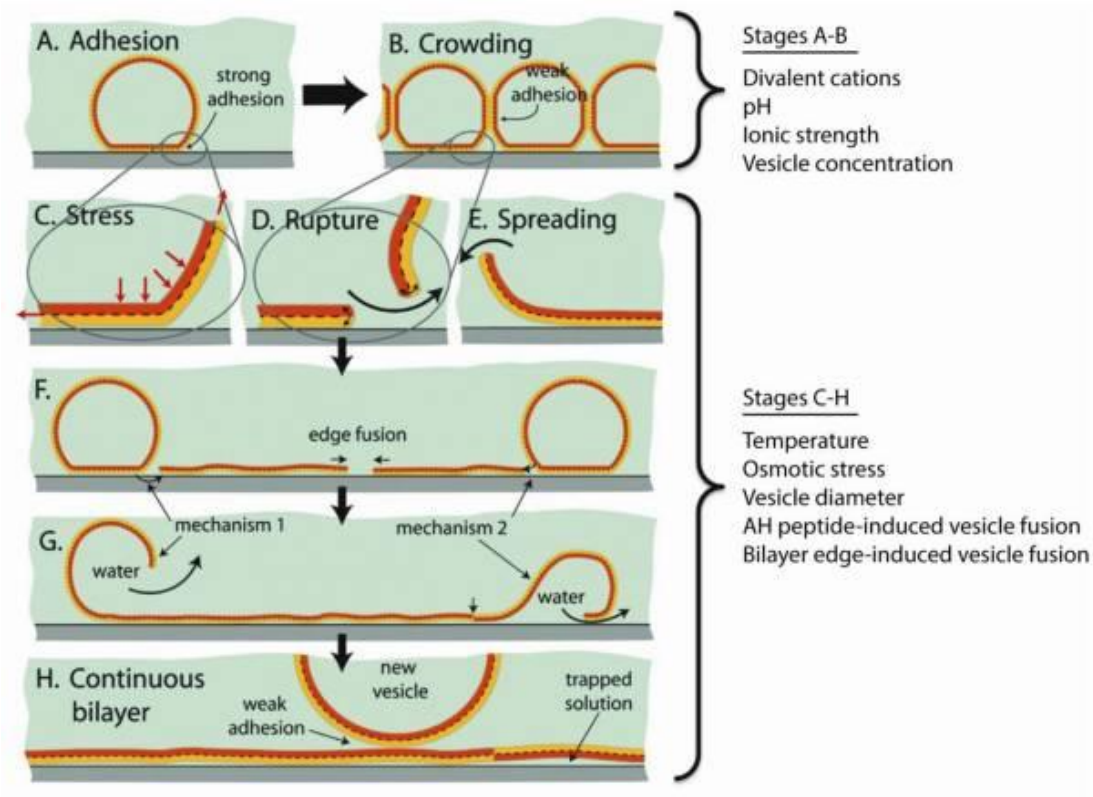


Figure 2.9.1. The mechanism for supported bilayer formation on solid support from lipid vesicles. Stages of SLB formation (A) adhesion, (B) crowding, (C-E) rupture and spreading of bilayer patches via mechanism 1 or 2, which can result in either leaflet exposed, (F, G). Coalescence of the bilayer edges forms a thermodynamically favourable bilayer, which releases excess water/lipid. (H) Once the continuous bilayer is formed, there are only weak adhesion forces to un-ruptured vesicles. Adapted from [15].

2.10 Optical analysis of membrane bilayers

2.10.1 Confocal microscopy of supported lipid bilayers

Single photon fluorescence microscopy was conducted on a Leica SP2 MP (Wetzlar, Germany), which utilises a laser scanning confocal optical arrangement. The microscope setup utilises a lens with a numerical aperture (NA) of 1.32 with a 63x oil immersion magnification. To increase sensitivity and prevent under-sampling 1024 x 1024 pixel (12-bit) images were taken. The maximum region of interest (ROI) possible was 238 μm with a lateral resolution of 222 nm (0.6λ/NA). Confocal microscopy was employed to decrease fluorescence background and decrease artefacts by specifically imaging the plane of the membrane. 300nm optical slices

were acquired over a 6 μm z-axis range and averaged three times. Laser excitation wavelength was chosen as close to FPE excitation as possible with a 488 nm laser, using the lowest laser power possible.

Parameters including offset, gain, photomultiplier voltage (PMT) and pinhole (in Airy units), were defined across a range of preliminary experiments. These remained constant for comparative validity and to negate photobleaching effects (Table 2.10.1). Each sample was imaged in three different locations and each condition studied in triplicate. All images captured were at room temperature in the dark.

	Laser Power	**PMT**	**Pinhole**	**ROI**
Image acquisition	25% 488 nm	900V	1 Airy	238 μm
Fluorescence Recovery After Photobleaching	75% 488 nm	900V	10 Airy	40 μm

Table 2.10.1 Microscope setting for imaging lipid bilayers. Values were defined in a range of preliminary experiments and held constant across different experiments.

2.10.2 Fluorescence Recovery After Photobleaching (FRAP)

FRAP denotes an optical technique that is able to quantify the lateral diffusion of a membrane bilayer. 2D diffusion coefficients are calculated through photobleaching a set area of a membrane (B, Figure 2.10.1). The lateral diffusion of non-bleached fluorescently labelled lipids restores the fluorescence (C, Figure 2.10.1). The difference in absolute levels between A and D (Figure 2.10.1) results from molecules that are immobilised at the bleached spot. These molecules are termed “the immobile fraction”.

FRAP was performed as a validity test of membrane integrity and fluidity between media conditions. Membranes elicited an average of ~2.5 $\mu m^2 s^{-1}$ for the 2D diffusion

coefficient. This correlates with literature defined measurements for a fluid bilayer [154]

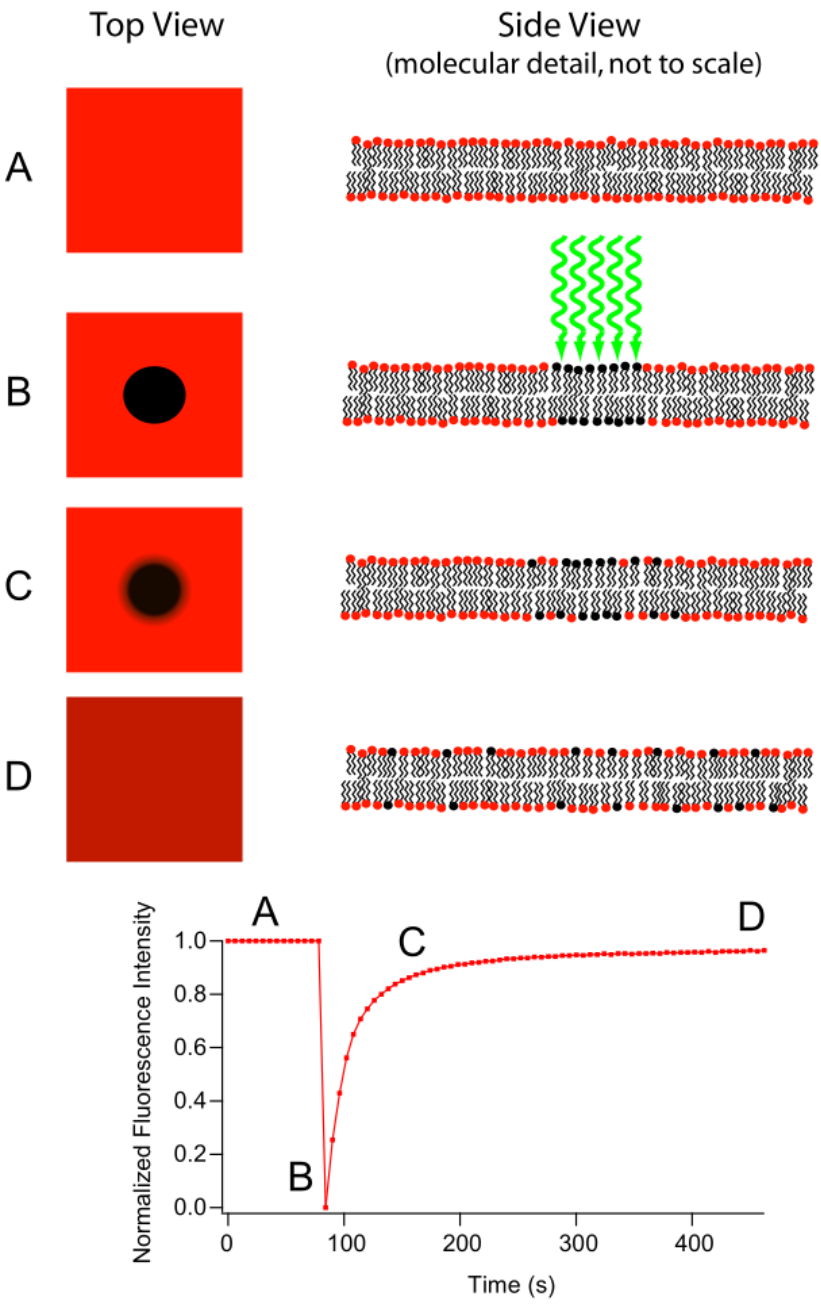


Figure 2.10.1 FRAP protocol. (A) Homogeneous membrane. (B) Fluorescence is bleached in a spot. (C) Lateral diffusion starts to establish fluorescence dependent on membrane fluidity. (D) Membrane fluorescence is re-established. The difference in level between A and D is defined as the immobile fraction. Adapted from [155]

The recovery of the fluorescence profile (B→C Figure 2.10.1) fits a single exponential function for determination of the half-recovery time $t_{1/2}$. The 2D

diffusion coefficients can be calculated using the Soumpasis equation (Equation 2.10.1) [154].

$$D_{r_n} = 0.224\ \frac{w^2}{t_{\frac{1}{2}}}$$

Equation 2.10.1. Soumpasis equation to calculate the 2D diffusion coefficient, where D is the fluorophore dissociation constant, w is the radius of the bleached area, and $t_{1/2}$ is the half-time of fluorescence recovery. [154].

2.10.3 Particle analysis quantification

Membrane microdomains were quantified using an automated image analysis tool, allowing quantitative analysis between different samples. The analysis routine was written in Java for Image J. Confocal microscopy image stacks (taken every 0.3 μm) were subject to an average z-projection to create a single image from each sample (Figure 2.10.2A). The images were filtered using a threshold value to remove speckle noise resulting in the removal of the background membrane phase (Figure 2.10.2B). Domains on the periphery of the image, which crossed the image boundary, were excluded, as their full size cannot be determined. The domain images were analysed using ImageJ's particle analysis tool and examined for a range of dimensions such as size, circularity, fluorescence density and aspect ratio (Figure 2.10.2C). The resulting datasets were compiled for further analysis with one-way ANOVA multiple-comparison or compiled in R for graphical representation.

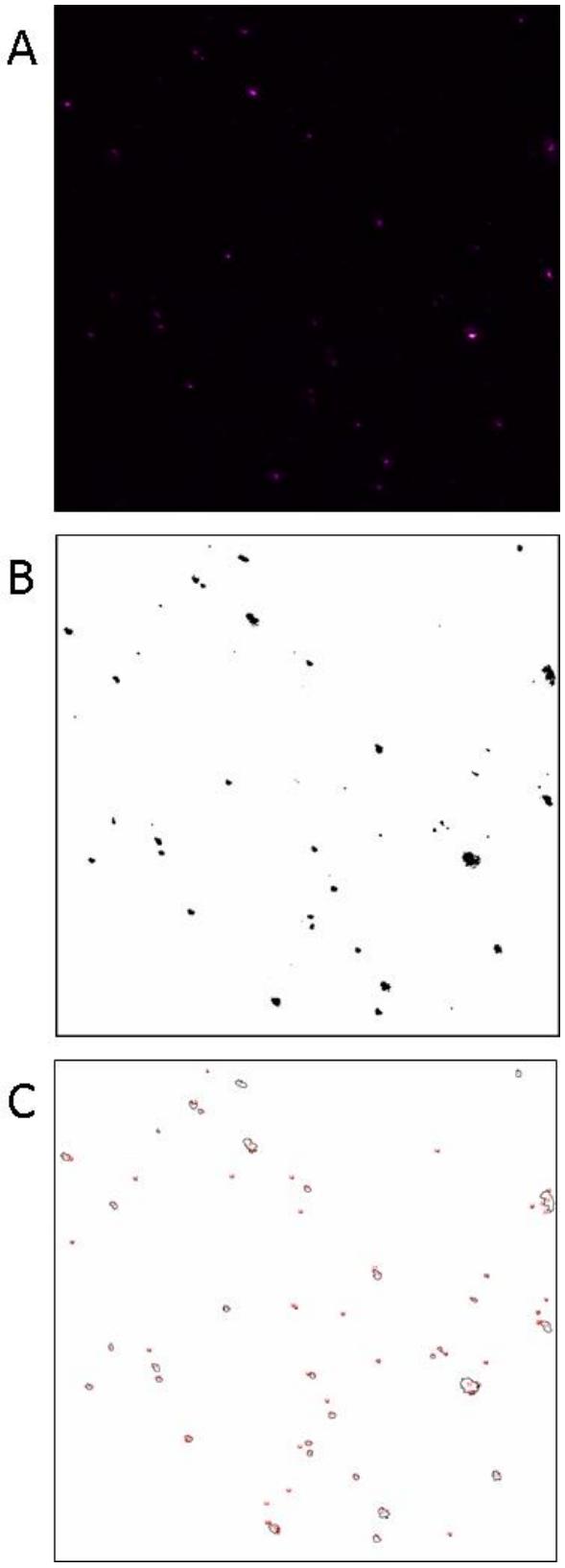


Figure 2.10.2. Confocal microscopy image processing. (A) An average confocal projection of a $PC_{70}Chol_{30}$ bilayer, bright regions are representative of FPE localisation into microdomains. (B) Image after thresholding to create a binary mask of each domain from (A). (C) The outlines of analysed particles are determined with ImageJ analyser tool from domains in (B). Size of each image is 238 μM x 238 μM.

2.11 Local spectroscopic analysis of supported lipid bilayer

Localised spectra of samples (FPE-labelled cells and bilayers) were recorded using a Leica SP2 MP confocal microscope, following excitation at 488 nm. Localised spectra were collected between 500-540nm for FPE labelled SLBs with 100 steps (0.4 nm steps). Spectra were further analysed in Graphpad Prism 6 for peak analysis and Savitzky-Golay spectral smoothing [156].

2.12 Atomic Force Microscopy

2.12.1 Bilayer preparation for AFM

Supported bilayers were formed with the aforementioned membrane vesicle fusion technique (Section 2.9). Synthetic lipids (Avanti, USA), were dried under a gentle oxygen-free nitrogen stream. Lipids were rehydrated in the appropriate media to form a lipid concentration of 0.5 mg/ml and tip-sonicated to clarity. The bilayer was formed on a freshly cleaved mica substrate. The mica was incubated with 10 mM $MgCl_2$ for approximately 30 minute, to maintain a reduced electronegative surface charge. 100 µl of lipid vesicle solution was added to the mica surface and heated to 50 °C for 1 h. The bilayer that was formed was washed 10 times with 100µl 37°C media to remove any adherent vesicles.

2.12.2 AFM image data capture and analysis

AFM images were captured using a Multimode 8 AFM on a Nanoscope V controller (Bruker) equipped with a fluid cell. Bruker DNP-C probes (k # 0.24 Nm^{-1}) were operated in peak force tapping mode. Different scanning ranges (between 10 and 150nm) were probed to obtain both fine and coarse structures. Images were taken at room temperature, which was stable between 25.5- 26 °C during imaging.

Image processing was carried out manually in Gwyddion [157]. Imaging processes included thresholding and removal of some imaging artefacts. To create images for data analysis, noise filtering and particle analysis were performed as previously described in ImageJ.

2.13 Surface Plasmon Resonance

2.13.1 Theory of SPR

A surface plasmon is constructed by a prism in the Kretschmann configuration, where a laser beam undergoes total internal reflection through the prism/ metal film interface. The angle (θ) at which the resonance occurs is very sensitive to changes in the refractive index of the medium adjacent to the metal surface [158].

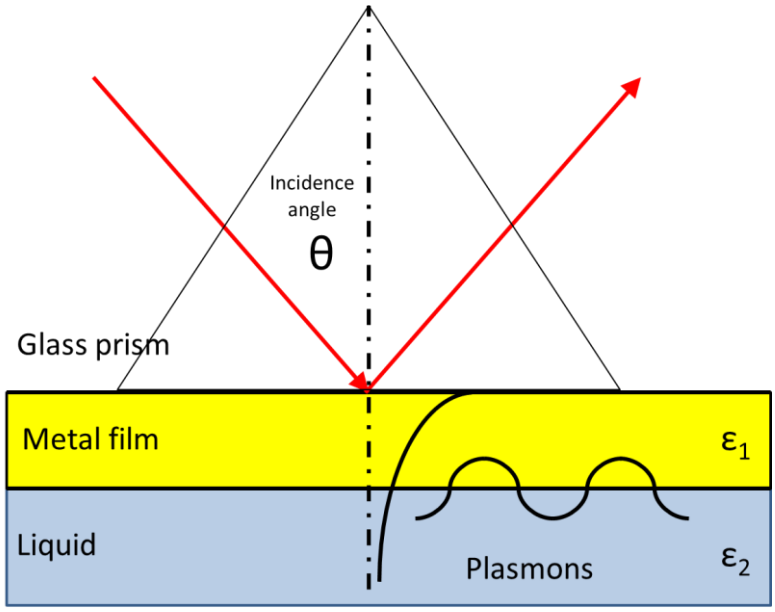


Figure 2.13.1. Kretschmann configuration of SPR. Laser in glass contacting metal interface at θ, creating the surface plasmon is sensitive to the refractive index of ε_2. Adapted from [158]

Surface plasmon resonance can be described by Maxwell's theory, in which free electrons in the metal exhibit density fluctuations.

The propagation of surface plasmons has a spectrum of natural resonant frequency (Eigen-frequencies (ω)) related to a wave vector (k). These are related to each other by dispersion relationship:

$$k_{sp} = \sqrt{\frac{\varepsilon_1 \varepsilon_2}{\varepsilon_1 + \varepsilon_2}}$$

Equation 2.13.1. The relationship between the Eigen frequency and the wave vector of surface plasmon k_{sp} is dependent of the dielectric constant of the metal film (ε_1) and liquid medium (ε_2).

The wave-vector is described by the frequency of light ω travelling through the medium ε1.

$$k_1 = \frac{\omega}{c}\sqrt{\varepsilon_1}$$

Equation 2.13.2. The wave function of the surface plasmon through the air, where c is the speed of light, ω is the Eigen frequency and ε_1 is the refractive index of the air.

In a vacuum, k_c, the dispersion relationship is a straight-line $k_1=\omega/c$, which never intersects the surface plasmon dispersion relationship. The adoption of the Kretschmann configuration shown in (Figure 2.13.1) negates the air-metal interface with the adoption of a glass prism, decreasing the dispersion relation and forming a plasmon at the metal-liquid interface [159]. The relationship between the plasmon and the dielectric constant of the different materials is evident (Equation 2.13.1).

2.13.2 SPR configuration

SPR analysis was conducted on a Reichert Life Sciences SR7000DC (Ametek Inc.) spectrometer, implemented with an SPR Autolink data acquisition programme. All experiments were undertaken at 25°C. The flow cell orientation of the instrument is illustrated in Figure 2.13.2, wherein the medium flows over the reference channel, followed by the binding channel coupled with microfluidics. This configurations allows investigation of specific and nonspecific interaction.

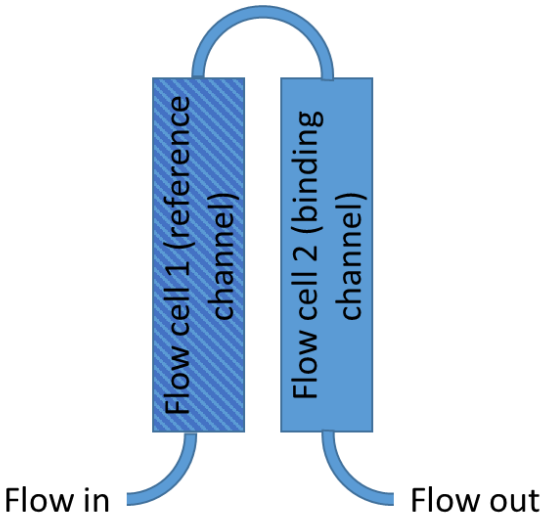


Figure 2.13.2. Flow cells of an SPR chip surface. Media flows in (left), over the first flow cell, used as a reference channel (to assess nonspecific binding to the chip surface) and then over the second flow cell, which is conjugated with a ligand of interest to form the binding channel.

2.13.3 Antibody Attachment Protocol

A baseline reading was established by allowing filtered degassed PBS-Tween (PBST) to flow over an SR7000 mixed self-assembled monolayer gold sensor slide composed of 10% COOH-$(PEG)_6$-C_{11}-SH, and 90% OH-$(PEG)_3$-C_{11}-SH, (Reichert Life Sciences, Ametek Inc.). The slide surface was activated with 1-ethyl-3-(3-(dimethylamino) propyl) carbodiimide (EDC, 0.2 M) and N-hydroxysuccinimide (NHS, 0.1 M) at 50 µl/min for 5 min. The appropriate antibody; either an anti-fibrinogen antibody (Abcam, ab10066), an anti-IL8 antibody (R&D Systems, MAB208), or an IgG isotype control antibody (Genetex. GTX35009) was then attached via amine coupling to the binding channel only (20 µl/ml, 5 min), during which, the reference channel was diverted. The remaining active sites in both channels were capped using ethanolamine (1 M) at 50 µl/min for 5 min to prevent sample immobilisation on the slide surface during subsequent binding reactions (Figure 2.13.3.). Correct antibody immobilisation on the surface is denoted by the

binding curve and the difference in equilibria of different channels at the end of the antibody attachment protocol (Figure 2.13.3)

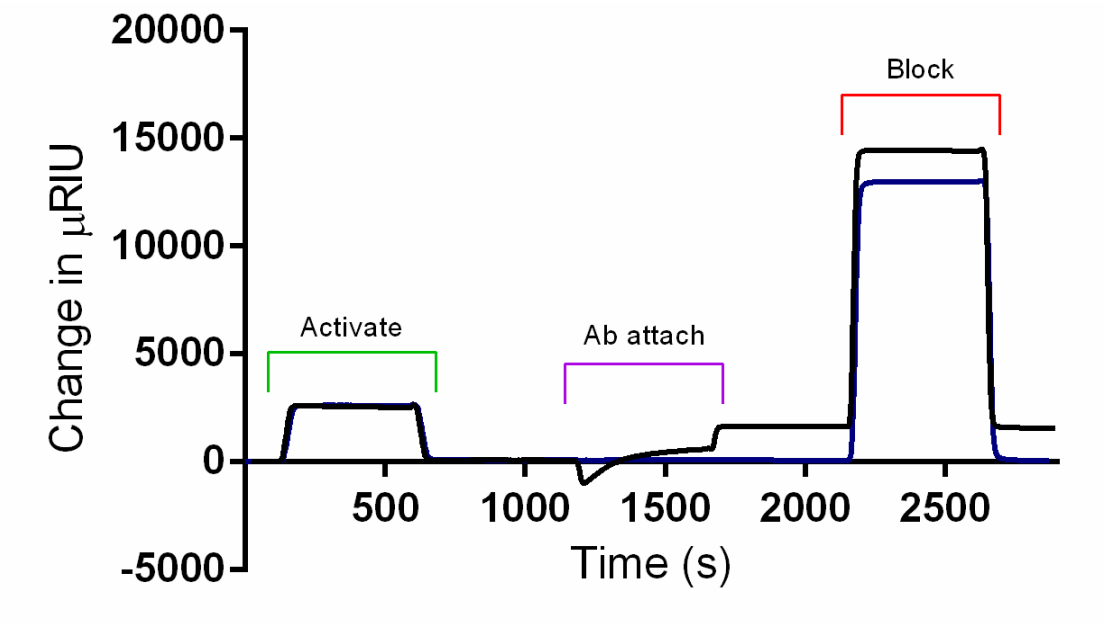


Figure 2.13.3 A sensogram illustrating an antibody attachment protocol for SPR experiments. The running buffer was PBST pH 7.4 at 25°C. The black trace denotes the binding channel, and the blue trace denotes the reference channel. (Green) The surface was activated with EDC 0.2M and NHS 0.1M (50 µl/min, 5 min) followed by 5 min buffer dissociation. (Purple) The reference channel was then diverted, and appropriate antibodies were attached to the binding channel at 20 µl/min for 5 min, followed by 5 min of buffer dissociation. (Red) both channels were then blocked with 1M ethanolamine (50 µl/min, 5 min). The difference between the binding and the reference channels at the end denotes immobilised antibodies on the surface in changes of Refractive index Units (RIU).

2.13.4 Protein Binding Reactions

Stable baselines were established with the appropriate filtered degassed media prior to binding reactions. Albumin stock was diluted in the appropriate media to 50mg/ml for nonspecific binding experiments. Fibrinogen (stock 10mg/ml) was diluted for specific binding (5µg/ml) and nonspecific binding (5-500µg/ml) in appropriate media. Protein solutions were flowed over the sensor slide for 5 minutes at a flow rate of 20 µl/min followed by a 5 min buffer dissociation (20 µl/min) period. The surface was regenerated with 5 mM HCl (100 µl/min for 2 min), and a baseline equilibrium was re-established in the running buffer between each binding reaction. Protein adsorption to the surfaces elicited changes in refractive index units (RIU).

2.14 Bio-Rad Bio-Plex Bead-Based Multi-Analyte Detection.

This work was experimentally carried out by industrial partners BioRad Bio-Plex R&D, D Jethwaney and W Tan.

The BioPlex 2200 (BioPlex) system [160] was used in accordance with the manufacturers guidelines. Different assay media; standard diluent, sample diluent, detection antibody diluent and assay buffer were supplied by Bio-Rad (CA, USA). Media were substituted in a stepwise manner described in Table 3.3.1 [161].

2.14.1 Detection of Analytes

All antibody pairs were directed against different noncompeting epitopes of their respective cytokines as supplied in the Human 27-plex cytokine assay kit.

Specific antibodies were conjugated onto pre-dyed beads. The detection beads have two distinct impregnated fluorophores of a unique concentration of infra-red and a unique concentration of red fluorophore that allows identification to specific x-y coordinates (Figure 2.14.1).

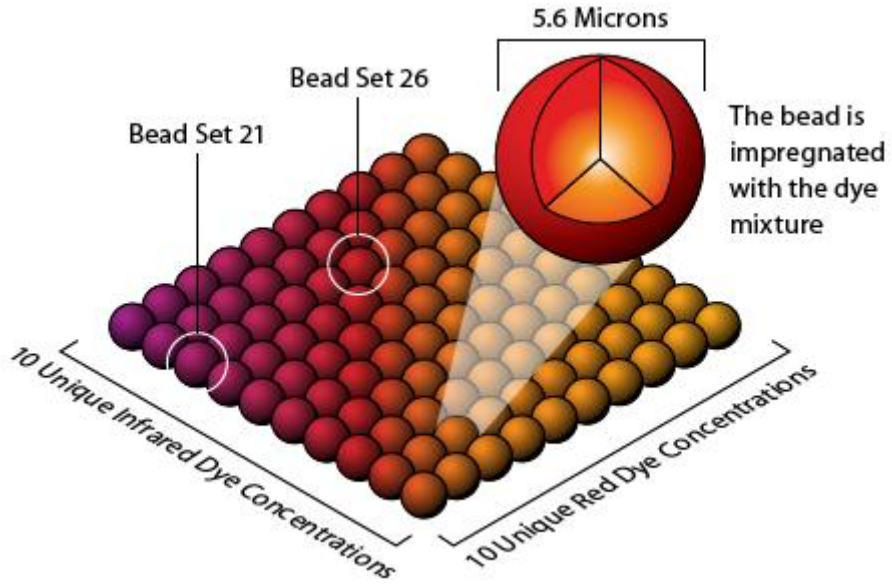


Figure 2.14.1. Standard Luminex bead profiling. The 5.6 µM beads are impregnated with a unique infra-red fluorophore and unique red fluorophore, this results in a matrix of beads with a set of beads that have a unique signature of red and infra-red dye. Adapted from [162]

The coupled beads are combined for multiple analysis and incubated with the protein sample for 60 min (Step 2 Figure 2.14.2). The samples were then incubated with biotinylated detection antibodies (30 min) and used to quantify the analytes present (Step 3 Figure 2.14.2). After washing away the unbound biotinylated antibodies, the beads were incubated with a reporter streptavidin-phycoerythrin (SA-PE) conjugate for 10 min. Excess SA.PE is then removed by further washes (Step four Figure 2.14.2). The beads were then passed through the Bio-Plex array reader to measure the fluorescence of bead and bound SA.PE. The assay detection uses two lasers first a 532nm green laser to excite the PE in the SA.PE, to quantify the amount of bound analyte. Secondly, a 635nm red laser to excite the dyes inside the beads, to identify the beads. Light scattering is used to differentiate single and double beads (Step five Figure 2.14.2). Assay incubations were performed at room temperature [163]. Data acquisition was performed using Bio-Plex manager^{TM} 6.0 at a low photomultiplier (PMT) setting [162] [163].

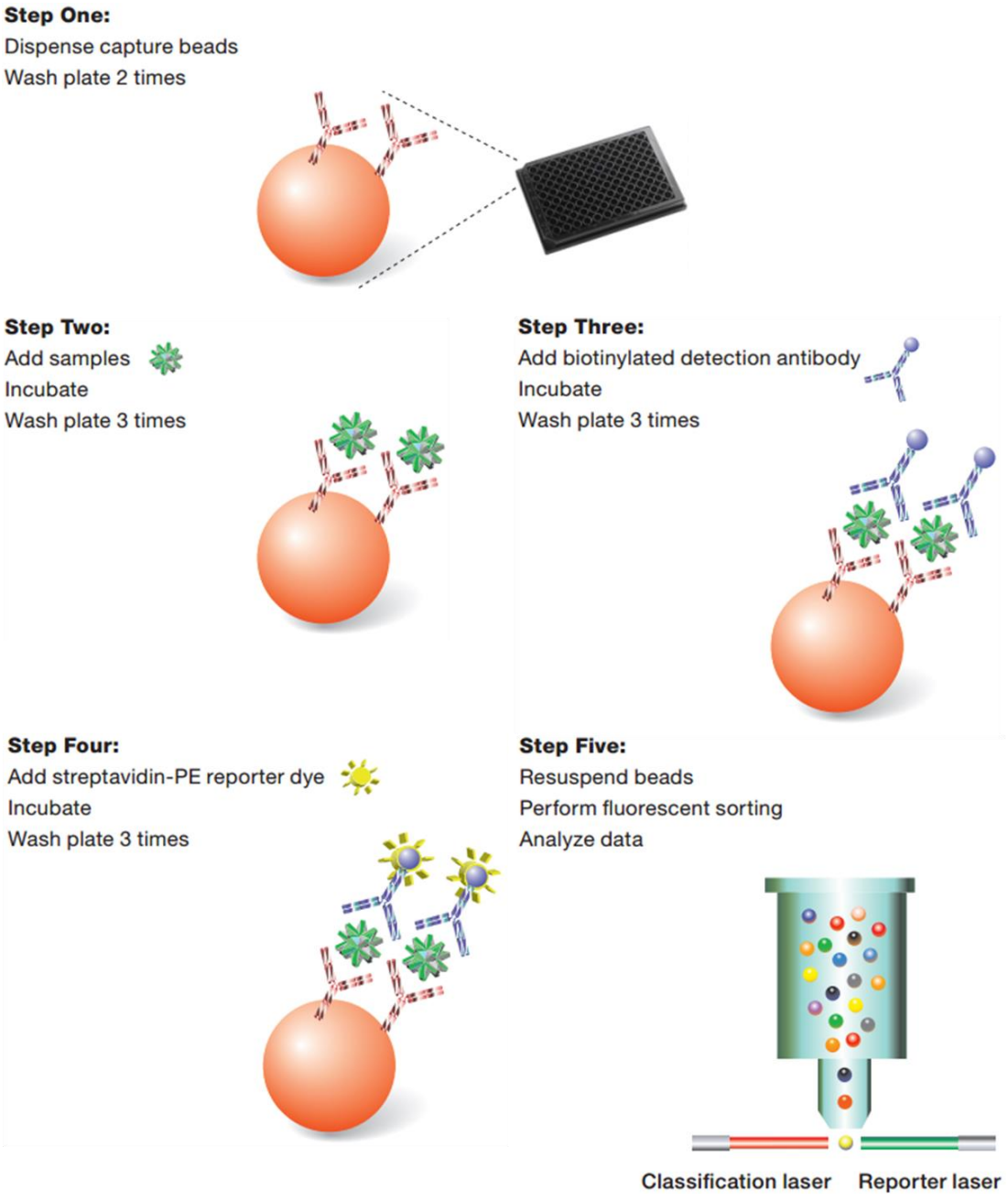


Figure 2.14.2. Schematic representation of BioPlex 2200 Luminex multiple analyte analysis. Beads are dispensed and washed twice. Protein in the sample are then captured by antibody conjugated beads. Biotinylated secondary antibody 'sandwiches' the sample. The streptavidin-PE reporter due binds to the biotin and is then quantified. Reproduced from [163].

2.14.2 Assay Performance Characteristics

Assay sensitivity, defined as the limit of detection (LOD), was evaluated by measurement of three replicates of the system with the zero standard value. These values represent the background median fluorescent intensity (bMFI) and subsequently fluorescence due to nonspecific binding [163, 164].

2.14.3 Assay Accuracy

Assay accuracy (or protein selectivity) is determined by a calculation of specific recovery; observed concentration value of a target antigen relative to the expected value of the protein binding in the sample [162, 163]. Specific recovery values <100% indicate that a target analyte does not elicit total selectively when binding to the antibody. Values >100% indicate that the antibody has decreased selectivity and elicits cross-reactivity to multiple proteins.

3 Rational Targeting of Sub-classes of Intermolecular Interactions

The nonspecific binding of proteins is a widespread across different technologies and plays a role in certain human diseases, such as prions disease [165] and Alzheimer's disease [166] . In this study, nonspecific binding is defined as the interactions between two molecules that, unlike antigen-antibody interactions, they do not elicit bio-recognition. (Section 1.4.6). In technologies, nonspecific binding can decrease the sensitivity of an instrument [159] or reduce the specificity of protein binding (in label-free techniques such as SPR) [167]. The aim of this section is to investigate the binding reactions between proteins and membranes (Section 3.1.1) and to then use different reagents to target and reduce these interactions. Two classes of reagents were used in this study; firstly the chaotropic ion sodium thiocyanate which has been previously characterised [54] (Section 1.6.1) and secondly, dielectric constant modifying reagents (DCMRs) which modify dielectric and electrostatic interactions as proposed in the mechanism outlined in (Section 1.6.2) and in work such as Richens et al. [42].

This analysis is carried out on a number of different model systems. Firstly, lipid vesicle membranes, followed up with specific and nonspecific interactions with SPR and Luminex systems. The modulation of these interactions in the model membranes will develop the basic understanding of how proteins and lipid interact, something that could later be exploited to develop increasingly complex model systems. Modulating the interactions that take place in detection instruments has the ability to increase the specificity of the interactions measured, resulting in more sensitive instruments. These effects could also be utilised to characterise the interaction that takes place, and be able to determine the dominant forces driving the interaction.

3.1 Assessing a Range of Soluble Reagents Effects on Nonspecific Binding

3.1.1 Protein-Membrane Binding Studies

The interaction of albumin and fibrinogen to a range of membrane compositions was investigated. Membrane vesicles were labelled with the membrane probe FPE as previously described (Section 2.6). Albumin and fibrinogen were chosen as examplars of globular and fibrous plasma proteins respectively due to their known association with nonspecific binding (as described further in Section 1.2.1 and 1.2.2). The spectral properties of FPE are known to respond to changes in the electrostatic surface potential of the membrane (Section 1.9.1.2.). The fluorescence intensity (*FI*) of FPE is responsive to the electrostatic surface potential of the membrane. The binding of positively or negatively charged molecules to the surface leads to changes in the ψ_s and can be quantified through measurements of the FPE fluorescence intensity (Figure 3.1.1.).

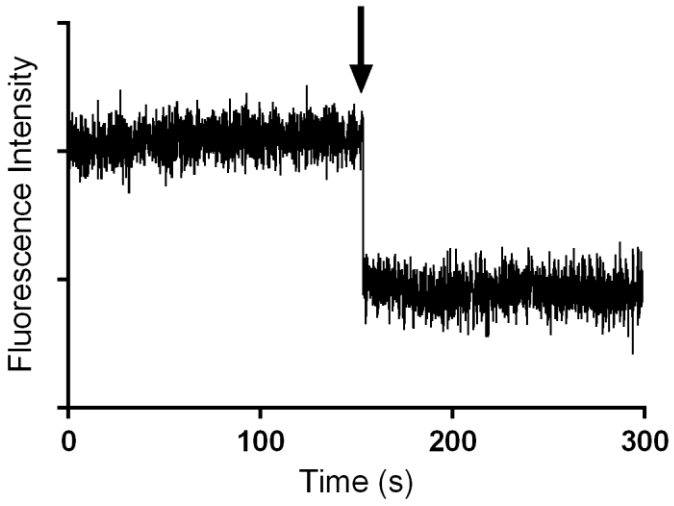


Figure 3.1.1. Changes in fluorescence intensity of FPE labelled PC_{100} vesicles with HSA addition. Fluorescence was recorded at 520 nm following excitation at 490 nm. Arrow denotes addition of 3 μM human serum albumin (HSA) to 400 μM vesicles in PBS pH 7.4 at 25°C

The interaction of proteins with a membrane causes a decrease in fluorescence until the membrane becomes saturated and a plateau are reached (Figure 3.1.2). These fluorescence plateaus established between protein titrations.

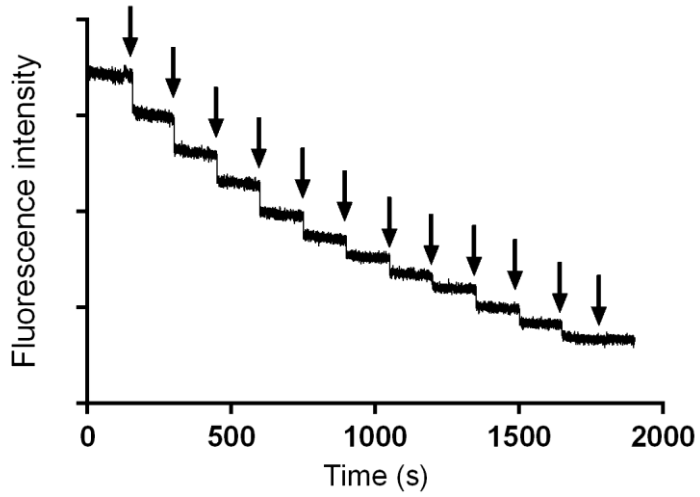


Figure 3.1.2 Changes in fluorescence intensity of FPE labelled PC_{100} vesicles with HSA addition. Fluorescence was recorded at 520 nm following excitation at 490 nm. Arrow denotes addition of 3 μM human serum albumin (HSA) to 400 μM vesicles in PBS pH 7.4 at 25°C until saturation.

With each addition of protein there is inherent addition of media which dilutes the cuvette and results in a small decrease of fluorescence. Therefore, the saturation point of the experiment can sometimes be obscured by the dilution factor. The plateau values between protein titrations (Figure 3.1.2) were averaged over time. An identical experiment with just buffer additions (in order to control for the dilution series) was subtracted from the protein binding curve (described in Section 2.7). The resultant media subtracted curve was plotted in Figure 3.1.3. Given the dilution of the vesicles with each addition and the sensitivity of the probe, we cannot state for certain that the binding has saturated, just that the probe responsivity has been saturated. Given the percentage increase of the PBS to ~25% at the concentrations

employed, the assay window is sufficient to demonstrate clear reduction in these signals.

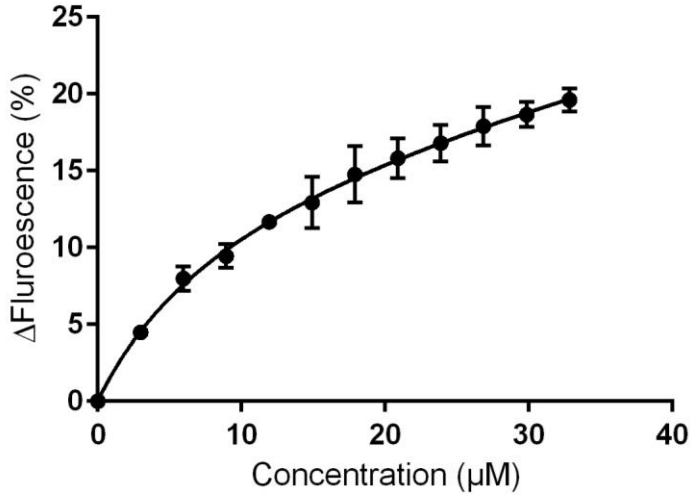


Figure 3.1.3. The average changes in fluorescent amplitudes from the binding of HSA to FPE labelled vesicles. 400 μM PC_{100} vesicles (n=3) in PBS (Table 2.2.1) at pH 7.4, 25°C. Data was fitted to a simple hyperbolic binding model.

Albumin and fibrinogen membrane interactions are deemed nonspecific in this context, as the binding reactions occur without specific molecular recognition events [19, 168]. Given the binding of albumin to the membrane does not involve any specific ligand-receptor binding, simple binding models are the most appropriate. Therefore, a hyperbolic binding curve was initially fitted to the data and compared with a more complex sigmoidal binding interaction (which would demonstrate cooperativity) the best fitting model was determined using an F-test (Section 2.7) . Figure 3.1.3 demonstrates a hyperbolic binding model. Therefore, modulation of this simple hyperbolic interaction can be investigated with media additions.

The reduction of the membrane binding affinity (K_d) and capacity (Bmax) is therefore classified as a reduction in nonspecific binding.

3.1.2 The Effect of Media Reagents on the Membrane Binding of Albumin and Fibrinogen

Reagents: Arg, Gly-Gly, Gly-Gly-Gly and NaSCN, chosen for their different biochemical properties, were screened for their independent effects on albumin and fibrinogen binding, (Section 1.2.1 and 1.2.2). Data shown in Figure 3.1.4 were fitted to the simple hyperbolic binding model (Figure 2.7.1, Equation 2.7.1) and the simple hyperbolic binding model with Hill coefficient (Figure 2.7.1 Equation 2.7.2). Following this analysis and the goodness of the fit (highest R^2 value), a simple hyperbolic binding isotherm was identified to be the most appropriate with B_{max} and K_d values tabulated for comparison (Table 3.1.3).

The binding of albumin and fibrinogen to membranes was initially investigated in PBS. NaCl ions were replaced with the reagents defined in Table 2.2.1 and examined for any reduction of B_{max} or increase in K_d when compared to PBS.

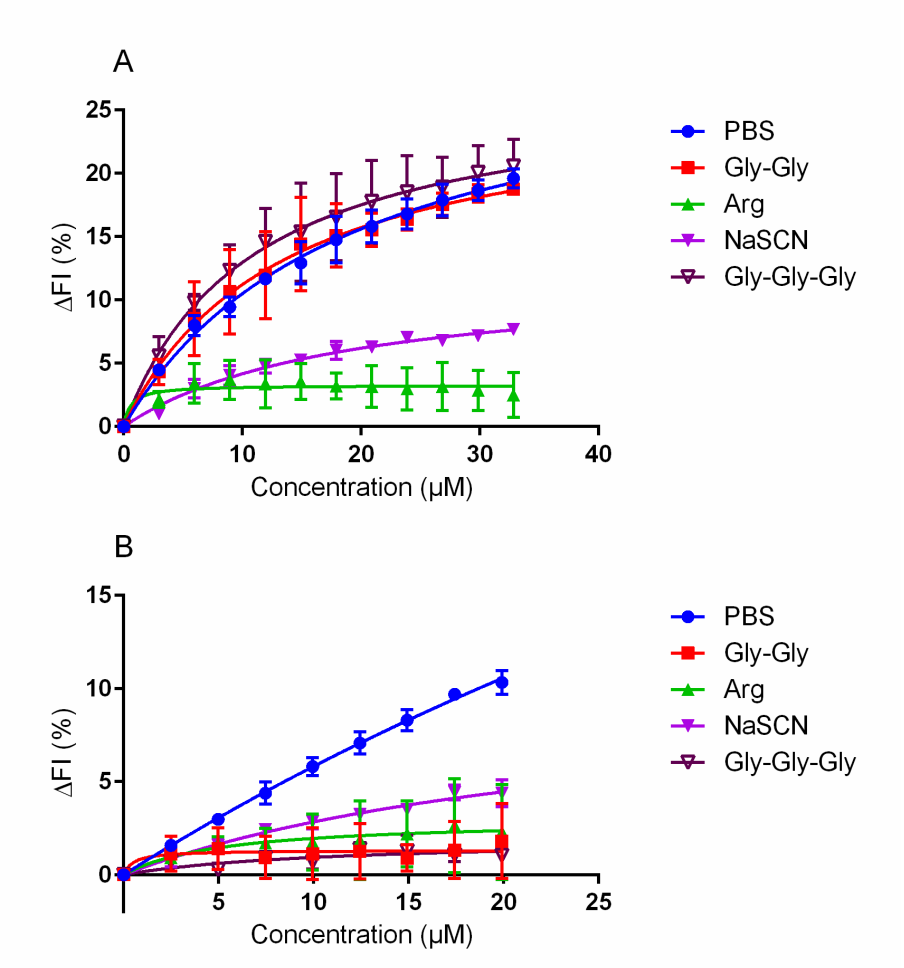


Figure 3.1.4 The changes in fluorescent amplitudes from the binding of (A) HSA and (B) fibrinogen to FPE labelled 400 μM PC_{100} vesicles in different media (Table 2.2.1) at pH 7.4, 25°C. The changes in fluorescence with protein concentration were fitted to the hyperbolic model. Table 3.1.1 shows the values obtained from the fit.

Media reagent	Albumin		Sig	Fibrinogen		Sig
	B_{max} (a.u.) ± SD	K_d (μM) ± SD		B_{max} (a.u.) ± SD	K_d (μM) ± SD	
PBS	30.45 ± 1.65	19.00 ± 2.09	N/A	58.1 ± 13.13	89.81 ± 23.98	N/A
Arg	3.26 ± 0.37	0.58 ± 1.29	****	2.591 ± 1.02	3.63 ± 5.32	***
Gly-Gly	26.24 ± 2.24	13.39 ± 2.79	Ns	1.518 ± 0.50	1.41 ± 3.15	****
Gly-Gly-Gly	26.98 ± 2.51	10.43 ± 2.84	Ns	0.88 ± 0.15	1.24 ± 0.41	****
NaSCN	8.96 ± 0.23	16.45 ± 10.25	**	10.36 ± 1.13	26.49 ± 0.46	**

Table 3.1.1. Effect of different media on the nonspecific binding of albumin and fibrinogen. HSA and albumin were added to PC_{100} vesicles in various electrolyte media (Table 2.2.1) at pH 7.4 conducted at 25°C. All binding profiles were fitted to single hyperbolic binding model with R^2 value ≥ 0.95, with variation reported as standard deviation (SD). Significant differences between treatments were statistically analysed using a one-way ANOVA in comparison to PBS, ** $p<0.01$, *** $p<0.005$, **** $p<0.001$.

The binding curves displayed in Figure 3.1.4 and B_{max} and K_d values shown in Table 3.1.1 demonstrate a marked reduction in membrane association in the presence of certain different reagents. Albumin-membrane interactions were significantly affected, only by the presence of Arg and NaSCN. Thiocyanate ions have been shown to decrease the nonspecific binding of albumin to membranes, which is in accordance to previous results [169]. The reduced albumin binding was attributed to the modulation of the water structure near to the macromolecular surfaces. The clustering of ions shields the charges and thus reduces charge-charge interactions (Section 1.6.1). The second class of reagents, DCMRs, modulate the ambient dielectric constant of the media. Gly-Gly and Gly-Gly-Gly have higher dielectric increments than arginine (Table 1.6.1) however, these were ineffective at reducing the binding of albumin to the membrane.

Previous studies have shown that arginine can suppress protein aggregation during folding and purification. Arginine has been shown to be dose-dependent and is most effective at higher concentrations (0.1-0.2 M) [74]. This work demonstrates that arginine is capable at reducing nonspecific binding, hence corroborating the hypothesis that arginine weakly interacts with proteins resulting in preferential solvation, which ultimately disrupts protein-protein interactions [42, 74]. It has been suggest that glycine-peptides suppress the attractive proximity energies by increasing the bulk dielectric constant (Section 1.6.2).

Thiocyanate reduced the binding capacity (B_{max}) of the fibrinogen-membrane interaction but was much less effective than the DCMRs. All DCMRs employed resulted in a dramatic reduction in both the B_{max} and K_d parameters; Gly-Gly resulted in B_{max} and K_d reduction from 58.1± 13.13 (a.u.) and 89.81 ± 23.98 (μM) in PBS to 1.518 ± 0.50 (a.u.) and 1.414 ± 3.15 (μM), respectively. The decrease in B_{max} can be interpreted as a reduction in binding sites; however, a reduction of K_d signifies an increased affinity. Gly-Gly-Gly further decreased the binding capacity of fibrinogen (B_{max}= 0.883 ± 0.15, K_d= 1.243 ± 0.41), suggesting the reduction in binding capacity is proportional to increased dielectric increment of the DCMR. As the surface area of the membrane vesicles remains constant, the reduction in the amount of binding sites is due to the decrease in attractive proximity energies between the proteins and the membrane.

The different effects of the chaotropic agent and DCMR on albumin and fibrinogen interactions with membranes in the presence of the different reagents suggests that the intermolecular forces that relate to the interactions of the proteins are different. When comparing the crystal structures of albumin and fibrinogen, the differences in

the interactions are perhaps less surprising due to the differences in the shape and charge distribution of the two protein surfaces (Section 1.2).

In the chosen conditions, the nonspecific binding of the proteins examined was reduced, but not eliminated (Table 3.1.1) (determined when B_{max} is not significantly different to 0).

3.1.3 The Synergistic Effect of Multiple Reagents on Membrane Binding

Due to the reagents having different mode of actions. They were tested in combination to see if the effects are additive/synergistic or antagonistic.

A combination of two active reagents in the media resulted in the binding profiles shown in Figure 3.1.5. During the experiment, no precipitation was observed. This suggests that the reagents neither form aggregates with one another, nor form insoluble reagent-protein complexes. B_{max} and K_d values were derived as before (Section 2.6) and shown in Table 3.1.2

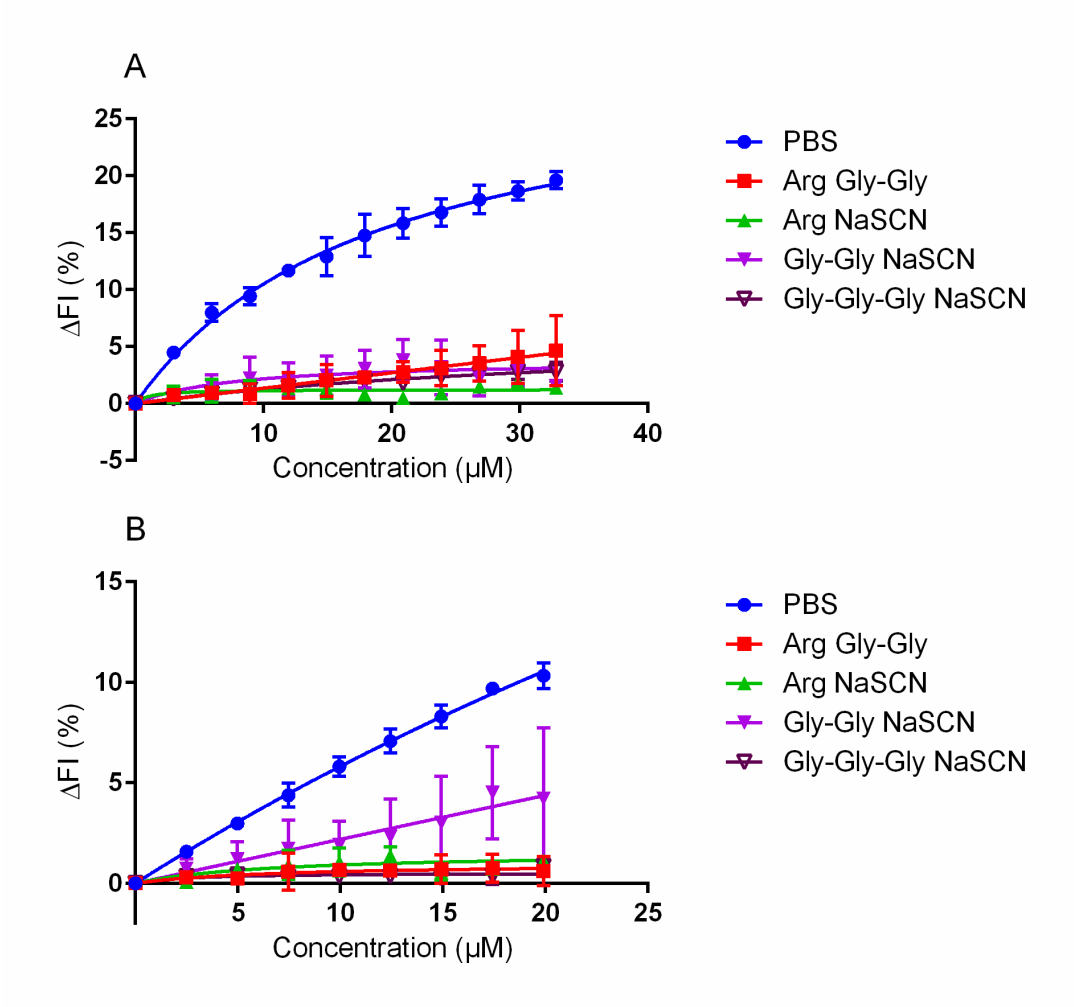


Figure 3.1.5. The changes in fluorescent amplitudes from the binding of (A) HSA and (B) fibrinogen to FPE labelled 400 μM PC_{100} vesicles in different media (Table 2.2.1) at pH 7.4, 25°C. The changes in fluorescence with protein concentration were fitted to the hyperbolic model. Table 3.1.2 shows the values obtained from the fit.

Media ID	Albumin			Fibrinogen		
	B_{max} (a.u.) ± SD	K_d (μM) ± SD	Sig	B_{max} (a.u.) ± SD	K_d (μM) ± SD	Sig
PBS	30.45 ± 1.65	19.00 ± 2.09	N/A	58.1 ± 13.13	89.81 ± 23.98	N/A
Arg Gly-Gly	12.02 ± 1.17	18.75 ± 1.77	****	10.36 ± 1.12	26.49 ± 4.62	****
Arg NaSCN	1.24 ± 0.23	1.00 ± 1.77	****	1.74 ± 0.75	8.71 ± 4.49	****
Gly-Gly NaSCN	3.86 ± 1.17	7.76 ± 3.17	****	3.53 ± 1.64	19.41 ± 3.43	***
Gly-Gly-Gly NaSCN	2.55 ± 0.64	2.63 ± 0.44	****	1.58 ± 0.22	1.17 ± 0.31	****

Table 3.1.2. A summary of the values obtained from albumin or fibrinogen binding profiles. PC_{100} vesicles in various electrolyte media (Table 2.2.1) at pH 7.4, conducted at 25°C. All binding profiles were fitted to single hyperbolic binding model with R^2 value ≥ 0.95, with variations reported as standard deviation (SD). Significant differences (Sig) between treatments were statistically analysed using a one-way ANOVA multiple comparison to PBS, p>0.05, * defines p>0.05, ** p>0.01, *** p>0.005, **** p>0.001.

The combination of two DCMRs did not lead to a decrease the measured parameters that define the protein-membrane interactions any more than the independent reagents (Arg, Gly-Gly Table 3.1.2). These observations suggest that the reagents have the same mode of action, hence affecting the same intermolecular interactions. Chaotrope-DCMR combinations resulted in a marked decrease in the binding of both proteins species. This suggests that each have a distinct mode of action; Gly-Gly-Gly NaSCN decreases both the B_{max} and K_d of albumin and fibrinogen (B_{max}= 2.55 ± 0.64, K_d= 2.63 ± 0.44 and B_{max}= 1.58 ± 0.22, K_d= 1.17 ± 0.31 respectively). The reduction in both parameters suggests a decrease in the number of binding sites yet an increased binding affinity (see discussion). Experimentally, the ΔFI of protein binding was indistinguishable by eye to that of media dilution (Figure 3.1.6) however, data analysis highlighted that the binding is virtually eliminated (Figure 3.1.5).

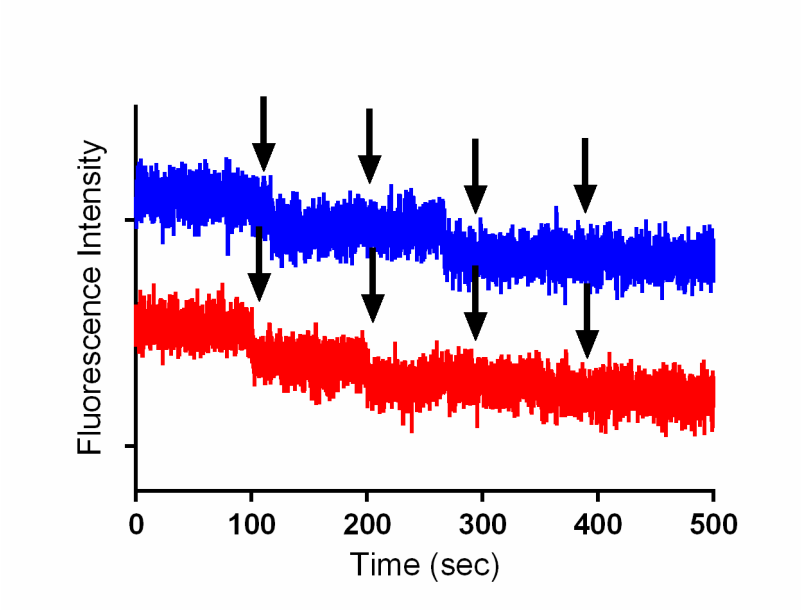


Figure 3.1.6. Changes in fluorescence intensity of FPE labelled 400 µM PC_{100} vesicles in Gly-Gly-Gly NaSCN (Table 2.2.1). All experiments were conducted at pH7.4, conducted at 25°C were recorded at 520nm following excitation at 490 nm. Blue trace arrows denote additions of 3 µM HSA until saturation. Red trace arrows denote addition of 0.5% (v/v) media representing a control for the media addition.

Given that the probe responsivity is not affected by the reagent media (shown in Figure 1.9.1) the reduction in the binding below the sensitivity of the probe can be regarded as an elimination of the nonspecific binding. Other factors were still considered in order to categorise the mode of action and further synergistic effects.

3.1.4 Further Synergistic Effect of Multiple Reagents on Membrane Binding

The reagent complexes used in the previous section were further modified in order to further investigate additive/synergistic effects. With the most effective medium tested, the impact of increasing the number of reagent as well as reagent concentration and subsequent ionic strength.

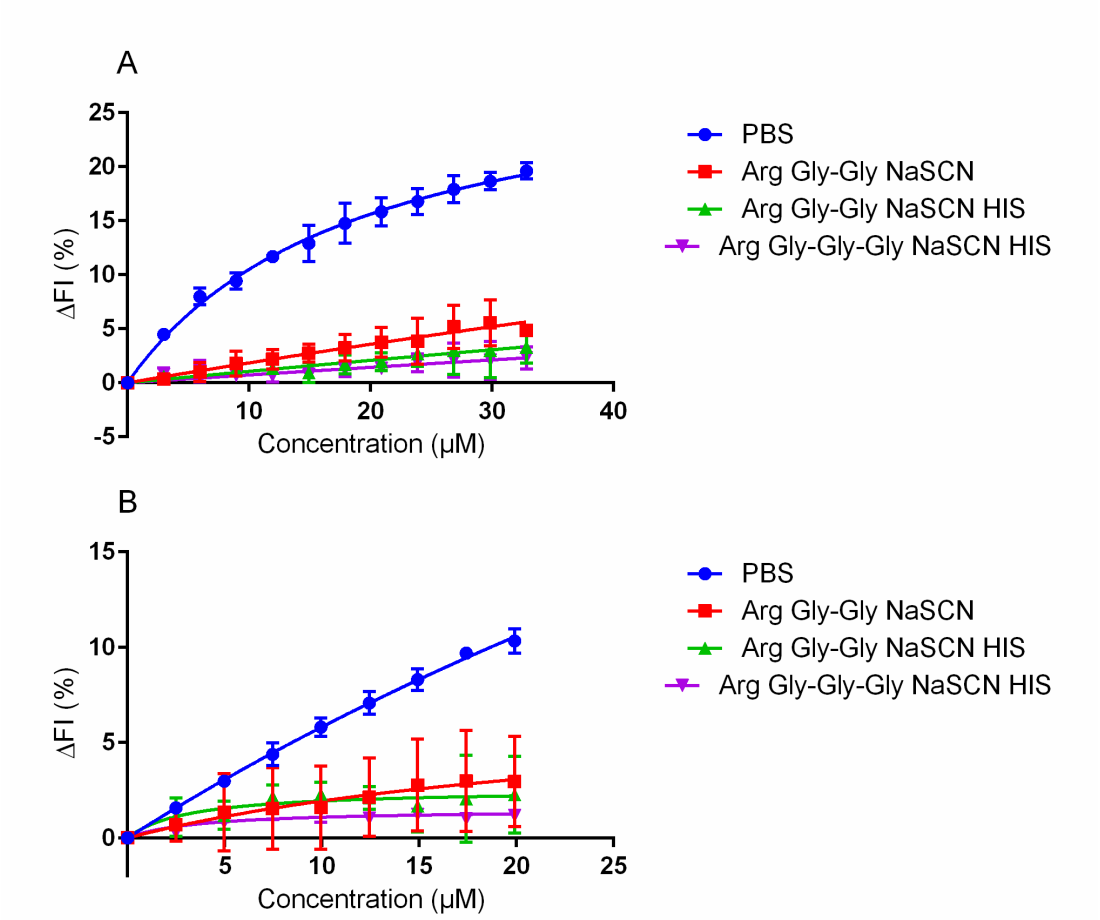


Figure 3.1.7. The changes in fluorescent amplitudes from the binding of (A) HSA and (B) fibrinogen to FPE labelled vesicles. 400 μM PC_{100} vesicles in different media (Table 2.2.1) at pH 7.4, 25°C. The changes in fluorescence with protein concentration were fitted to the hyperbolic model. Table 3.1.3 shows the values obtained from the fit.

Within these mixtures, the effects of ionic strength on the binding reactions were also assessed. Ionic strength has a direct effect on charge-charge interactions, due to the reduction of electrostatic interactions. The effect of the other reagents employed are expected to show concentration dependence, hence increasing concentration may further reduce the intermolecular forces.

To quantify the effects of the reagents, the B_{max} and K_d were calculated and tabulated for comparison (Table 3.1.3).

Media Reagent	Albumin			Fibrinogen		
	B_{max} (a.u.) ± SD	**K_d (µM) ± SD**	**Sig**	**B_{max} (a.u.) ± SD**	**K_d (µM) ± SD**	**Sig**
PBS	30.45 ± 1.65	19.00 ± 2.09	N/A	58.1 ± 13.13	89.81 ± 23.98	N/A
Arg Gly-Gly NaSCN	5.32 ± 1.13	23.52 ± 3.65	****	8.97 ± 1.44	36.7 ± 8.39	***
Arg Gly-Gly NaSCN HIS	1.63 ± 0.54	6.83 ± 0.49	****	2.55 ± 0.68	3.19 ± 3.29	***
Arg Gly-Gly-Gly NaSCN HIS	2.13 ± 0.42	3.27 ± 0.50	****	1.14 ± 0.68	1.97 ± 0.32	****

Table 3.1.3. A summary of the values obtained from albumin or fibrinogen binding to PC_{100} vesicles in electrolyte media (Table 2.2.1). Experiments were conducted at pH 7.4, 25°C. All binding profiles were fitted to single hyperbolic binding model with R^2 value ≥ 0.95, with various reported as standard deviation (SD). Significant differences (Sig) between treatments were statistically analysed using a one-way ANOVA multiple comparison to PBS, p>0.05, * defines p>0.05, ** p>0.01, *** p>0.005, **** p>0.001.

The more complex media compositions, and compositions with higher ionic strength, did not suffer any chemical issues such as; precipitation or absorbance of the reagent to the sides of the cuvette, lipid aggregation or solubility issues with the protein species.

Figure 3.1.7 shows that the use of three reagents prepared to the same ionic strength as PBS (Table 3.1.3, Arg Gly-Gly NaSCN) did not further reduce the B_{max} compared to the two reagent mixture of Gly-Gly NaSCN or Gly-Gly-Gly NaSCN (Table 3.1.2). Increasing the ionic strength of the media and hence further decreasing any charge-charge interactions did show a minor further reduction of the binding albumin and fibrinogen to the membrane. In Table 3.1.3, Arg Gly-Gly-Gly NaSCN HIS reduced binding in the same trend as with the other reagent media B_{max}= 2.31 ± 0.42, K_d= 3.27 ± 0.50 and B_{max}= 1.14 ± 0.68, K_d= 1.97 ± 0.32 for albumin and fibrinogen respectively.

3.1.5 Summary of Membrane Binding Effect by Different Media

Molecule employed	Effect on B_{max} or K_d			
	Albumin		Fibrinogen	
	B_{max}	K_d	B_{max}	K_d
Arg	↓↓↓	-	↓↓	↓
Gly-Gly	-	-	↓↓	↓
Gly-Gly-Gly	-	-	↓↓↓	↓
NaSCN	↓↓↓	-	↓	↓
Arg NaSCN	↓↓	↓↓↓	↓↓↓	↓↓
Gly-Gly-Gly NaSCN	↓↓↓↓	↓	↓↓↓	↓
Arg Gly-Gly-Gly NaSCN HIS	↓↓↓	↓↓	↓↓	↓↓↓

Table 3.1.4 The relative effect of reagents on B_{max} and K_d in relation to control PBS. One-way ANOVA analysis was carried out followed by a Fisher's LSD test and grouped by the statistical power to determine relative effects. (-) not significantly different (↓) corresponds to 99% confidence, (↓↓) 99.5%, (↓↓↓) 99.9% and (↓↓↓↓) 99.99%.

The relative effects of the different media is summarised in Table 3.1.4. These values along with the K_d and B_{max} values shown in Table 3.1.1, Table 3.1.2 and Table 3.1.3 indicate that Arg NaSCN, Gly-Gly-Gly NaSCN and Arg Gly-Gly-Gly NaSCN HIS are the three most effective media combinations. All reductions are denoted in B_{max} and K_d values however, which promotes further discussion.

The use of membrane binding to represent nonspecific binding has both advantages and disadvantages. The advantages are that with simple membrane compositions, the methods are highly reliable and replicable. This allows an understanding of the binding interactions that take place, which can be then attributed to the modulation of different intermolecular forces (see discussion). The disadvantages however are that the fluorescent method employed is not as sensitive as other detection instruments and the results require confirmation in another sytem to ensure it is not a lipid-specific effect.

3.2 The Investigation of Nonspecific Binding between Proteins and Surfaces

The combinations of reagents described in the previous section were shown to be effective in membrane binding systems. In these systems, the 'nonspecific' interactions, such as the long-range charge-charge and dipole interactions, between the protein and the membrane were eliminated. The knowledge gained from the membrane system was then applied to non-biological surfaces compromised by nonspecific binding, such as biosensor detection instruments including SPR [159, 167, 170], to see if the intermolecular interactions affected are general or specific to lipid systems. The label-free nature of the SPR detection, lacks the secondary detection step to identify the specificity of the interaction such as antibody-based detection (i.e. the 'sandwich' techniques of ELISA and Luminex). The use of SPR to examine nonspecific binding allows a more sensitive technique to quantify the molecular binding events, as well as examine effects on specific interactions.

SPR signal changes are dependent on the optical-related changes on the surface of the gold chip (Figure 2.13.1). The surface of the SPR chip is conjugated with a specific antibody (Section 2.13.3). Figure 3.2.1 shows a representative specific binding curve of fibrinogen to an anti-fibrinogen antibody (described in Figure 2.13.3).

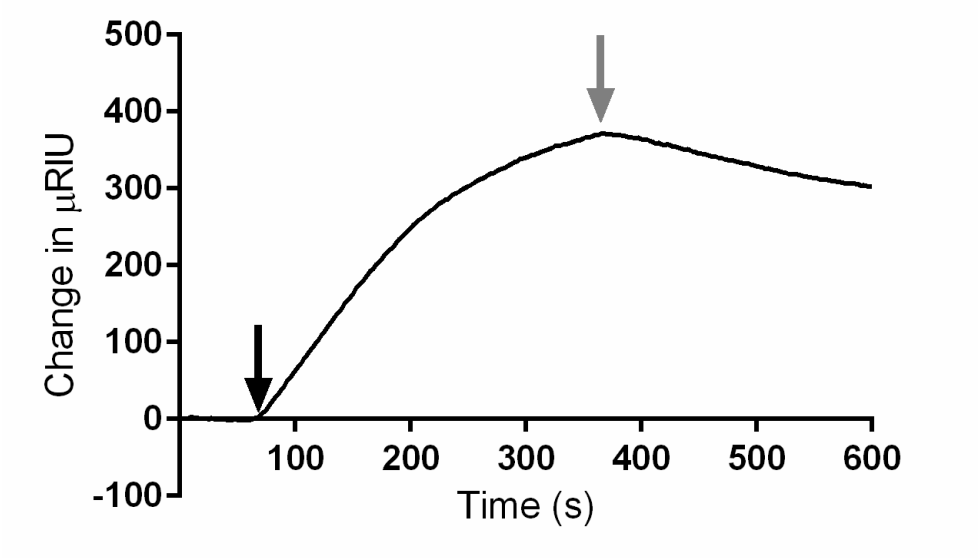


Figure 3.2.1 A sensogram of the fibrinogen interaction with an anti-fibrinogen antibody. Changes denoted in refractive index units (µRIU) in PBS (pH7.4), conducted at 25°C. The equilibrium baseline was established. Black arrow indicates the start of fibrinogen association (5µg/ml, flow rate 20 µl/min, 5 min). Grey arrow indicates buffer dissociation (20 µl/min, 5 min).

Binding reactions are categorised into four stages: the baseline, the association phase, a steady-state phase, and the dissociation phase. Baselines are established by the equilibrium of signal over time (Figure 3.2.1, 0 s to the black arrow). The protein then flows over the surface during the association phase where mass adsorption to the surface occurs (black arrow Figure 3.2.1). This results in a positive change in the refractive index. The steady state phase is established if a binding reaction reaches saturation during the association phase, where any additional protein association is in equilibrium with its dissociation. The dissociation phase (grey arrow Figure 3.2.1) is recorded following protein association. The buffer is flowed across the slide, washing away both bound and unbound proteins relative to the affinity of the initial interaction. The association and dissociation curves are typically fitted to single exponentials however, the shape of the total binding curve is based on several parameters. These include the affinity of ligand, protein concentration, refractive index contribution from the interacting protein, stoichiometry or the presence of various ligands. The weak dissociation phase shown in Figure 3.2.1 indicates a high-

affinity interaction, which is attributed to the specific interaction of fibrinogen to the anti-fibrinogen antibody.

In order to validate the reduction of nonspecific binding, the interaction needs to be tested with increasingly complex models. Therefore, instead of simple bimolecular interactions, both specific antibody:antigen interactions and nonspecific protein:antibody interactions are assessed.

The nonspecific binding properties of albumin were investigated in PBS across a range of different antibodies. In order to reproduce the current detection capabilities, the slide and the protocol used were in accordance with the latest techniques (Section 2.13), which have previously been optimised to minimise nonspecific binding. These optimisation techniques are centred on the development of the sensor chip, specifically PEGylation, which forms a layer of neutrally charged, random coils. This shields the interactions of proteins to the slide surface [171-174].

Initially, the nonspecific binding of albumin to an SPR chip conjugated with an IgG isotype control antibody and the chip surface was investigated. The configuration of the SPR flow cells, illustrated in Figure 2.13.2, is such that the protein will initially flow over the reference (blank) flow cell then to the antibody-bound flow cell. Isotype control antibodies have the same core domains as specific antibodies, yet lack any specificity for any of the proteins being examined in the study. When used in this context, it allows for the interrogation of proteins that bind directly to the core domains of the antibody and by extension, an array of different antibodies. The effect of nonspecific binding was also established with an anti-IL-8 antibody.

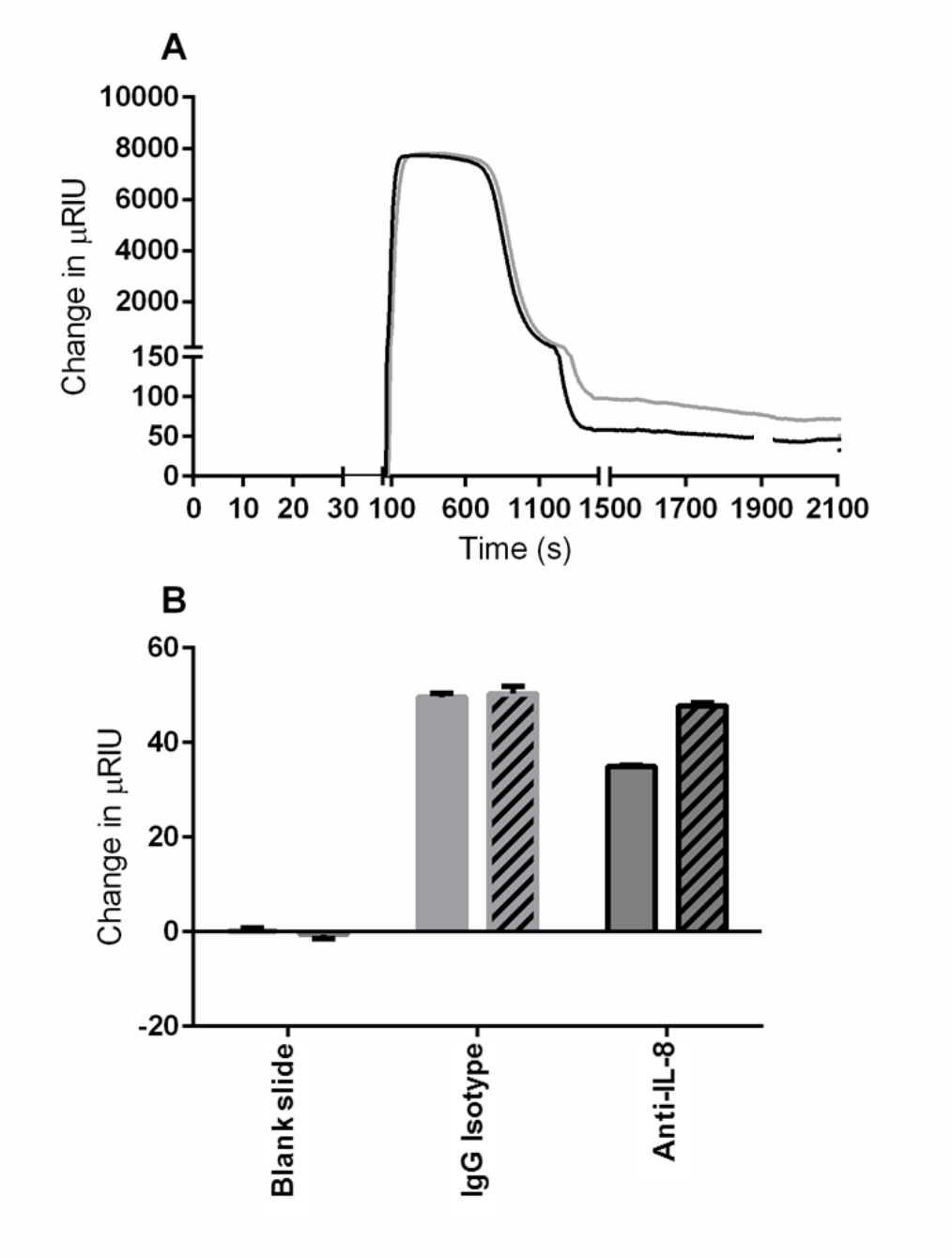


Figure 3.2.2. Nonspecific binding of albumin to the SPR surface and non-related antibodies. Protein association between 100-900s at 20µl/min, buffer dissociation 900-1500s at 20µl/min (A) Sensogram of nonspecific binding of albumin (50 mg/ml) in PBS pH7.4 at 25°C to an anti-IL-8 bound SPR surface (black trace) and reference surface (grey trace). A nonlinear axis was used to highlight binding after high refractive index change (B) Albumin interacts nonspecifically with both the antibody-conjugated (solid) and reference (dashed) channels of an SPR sensor chip with different antibodies present. PBS buffer control shows no change in refractive index.

The interaction of albumin to an isotype IgG control antibody conjugated surface elicits different association and dissociation kinetics than the specific fibrinogen binding shown (Figure 3.2.1). Albumin binding seems to elicit a much greater

surface response than specific fibrinogen binding, however, the binding profile of albumin interaction has very quick association and dissociation phases. Due to the protein concentration in the albumin solutions, there is an observed changed in the refractive index however, it is unknown if there is a direct surface interaction during the protein incubation period. The DCMRs employed in this study are also shown to increase the refractive index (Figure 3.2.3A). This was expected due to changes in the dielectric constant which affects the refractive index in the relationship shown in Equation 2.13.2 (Section 2.13). Subsequently, these refractive-index changes obscure the observation of direct surface interactions during the protein incubation. In the associated sensograms (Figure 3.2.2A, Figure 3.2.4B etc.) nonlinear axes were used to visualise baseline differences before and after incubation. It is noteworthy that when DCMRs are employed in the background-running buffer, these changes were negated, such as those shown in Figure 3.2.6.

After the protein incubation, the baseline following dissociation was greater than the initial baseline (Figure 3.2.2), this suggests binding to the surface. The antibody does not have any specific recognition therefore, the binding was deemed nonspecific. These differences were quantified by the ΔRIU from baselines prior to and after protein incubation. Results in Figure 3.2.2 A were replicated in the same fashion over an anti-IL-8 antibody with results shown in Figure 3.2.2 B.

Figure 3.2.2B shows that albumin binds nonspecifically to both the antibody-conjugated (solid) channels and the reference (dashed) channels of both antibody species. ΔRIU is typically higher in the reference channel than the antibody conjugated channel (Figure 3.2.2B and Figure 3.2.3A) which suggests that albumin preferentially binds to the surface. During initial antibody attachment, the surface is saturated with antibodies (Figure 2.13.3), hence any interaction with the antibody-

conjugated surface suggest that the protein binds to the core antibody domains. This is in agreement with previous observations [54].

A selection of the nonspecific binding reagents was used to eliminate the nonspecific binding to the IgG isotype control antibody (Figure 3.2.3).

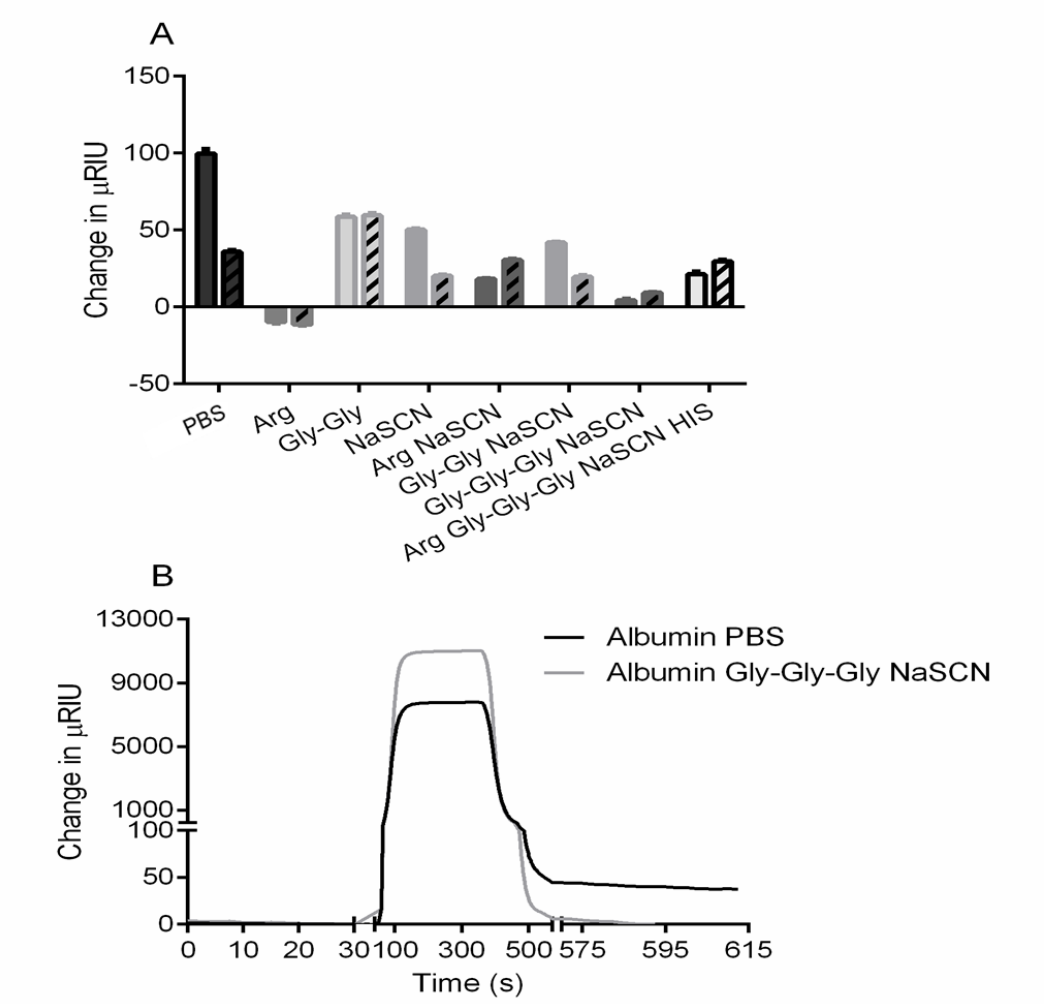


Figure 3.2.3. Nonspecific binding of albumin in various media. (A) Nonspecific binding of albumin (50 mg/ml) to IgG isotype control antibody conjugated sensor chip in different electrolyte media (Table 2.1.1) at pH 7.4, experiments were conducted at 25°C. Nonspecific binding of albumin in both antibody conjugated (solid) and reference (dashed) channels. (B) Protein association between 100-400 s at 20 µl/min, buffer dissociation 400-600 s at 20 µl/min. Nonspecific binding of albumin in PBS media (black) and elimination in Gly-Gly-Gly NaSCN (grey).

Nonspecific binding was decreased in the presence of different reagents. Arg media resulted in a negative ΔRIU, meaning that the post-incubation baseline is lower than the initial baseline. Any reduction from the initial baseline suggests a removal of

mass from the surface. There was a similar change in both the antibody-conjugated and reference channels, which suggests that the PEG monolayer is compromised by Arg interaction.

NaSCN is the best single reagent to reduce nonspecific albumin binding however, does not eliminate the binding. The combination of Gly-Gly-Gly NaSCN virtually eliminates nonspecific binding (Figure 3.2.3). These results exhibit the same trends as those shown in the membrane binding results (Table 3.1.4). This suggests that the intermolecular forces that resonate from the protein surface, i.e. electrostatic and hydrophobic forces (discussed in Section 1.2) are being affected, instead of a lipid specific force.

To efficacy of the media was tested further by out using fibrinogen at different concentrations, 5 μg/ml and 500 μg/ml (Figure 3.2.4).

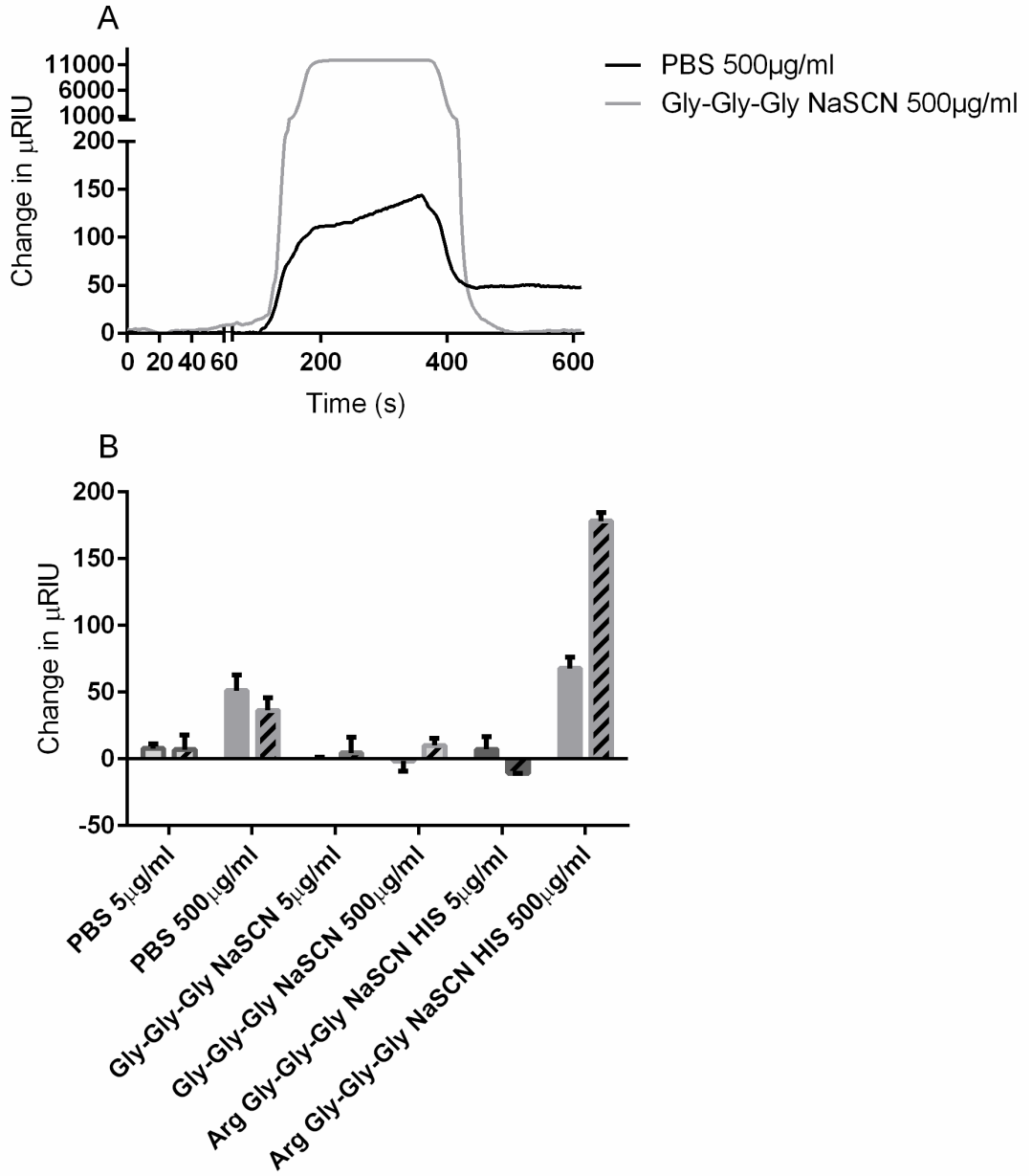


Figure 3.2.4 Nonspecific binding of fibrinogen to SPR surface. (A) Nonspecific binding of fibrinogen (500µg/ml) to an isotype IgG control antibody conjugated sensor chip in PBS and Gly-Gly-Gly NaSCN. Protein association between 100-350 s at 20 µl/min, buffer dissociation 350-600 s at 20 µl/min. (B) Nonspecific binding of fibrinogen to an IgG isotype control antibody over a range of concentrations (5-500 µg/ml) with boundary values shown in different electrolyte media (Table 2.2.1) at pH 7.4, experiments were conducted at 25°C antibody-conjugated (solid) and reference (dashed) channels.

Fibrinogen exhibited nonspecific binding similar to that of albumin (Figure 3.2.2). At the concentrations employed fibrinogen does not alter the refractive index like albumin, and a binding curve can be visualised (Figure 3.2.4). Fibrinogen nonspecific binding to an antibody-conjugated surface has a quick association phase

(100-200s) followed by a slower association phase as the nonspecific binding saturates (200-350s) dissociation phase (decrease from peak ΔRIU at 350 s). This suggests that the interaction is weaker than the specific interactions shown to an anti-fibrinogen antibody (Figure 3.2.1). After the dissociation phase is complete (after 450 s) there is a clear deviation from the initial baseline, indicating nonspecific binding.

Nonspecific binding was evaluated as in Figure 3.2.2A, with the binding of fibrinogen in the antibody conjugated (solid) channel and reference (dashed) channel. In the standard running buffer, PBST, fibrinogen is shown to bind nonspecifically in both channels, although the ΔRIU is higher to the antibody-conjugated surface, suggesting that fibrinogen preferentially binds the core antibody domains.

The two most effective media combinations showed previously (Figure 3.1.6 and Figure 3.1.5) (Gly-Gly-Gly NaSCN and Arg Gly-Gly-Gly NaSCN HIS) were employed against the nonspecific binding established. Gly-Gly-Gly NaSCN eliminated fibrinogen binding across the concentrations employed. At the higher fibrinogen concentration, Arg Gly-Gly-Gly NaSCN HIS resulted in an apparent increase of nonspecific binding instead of the reduction of nonspecific binding as previously shown with albumin-surface interactions (Figure 3.2.3) and fibrinogen-membrane interactions (Figure 3.1.7). Without further investigation this result is difficult to elucidate however, it could be due to high concentrations of Arg interacting directly with the surface.

Using the reagents outlined, the protein-binding albumin (Figure 3.2.3) or fibrinogen (Figure 3.2.4) to the SPR sensor surface or to an isotype antibody control surface can be effectively eliminated. A reduction in nonspecific binding events increases the

selectivity of a binding reaction; only specific interactions would result in response. This may also increase the sensitivity of a given reaction, provided that sufficient validations experiments are carried out to ensure that the specific interactions are not diminished.

3.2.1 Effects of Anti-nonspecific Binding Reagents on Specific Binding Reactions

As previously stated (Section 1.4.6), the physical parameters affected by the presence of these reagents are not able to distinguish between specific and nonspecific interactions resulting in the difference being specified by the user. As a result of this, the conditions established here have the potential to compromise some of the specific interactions discussed and must be addressed in their practical settings.

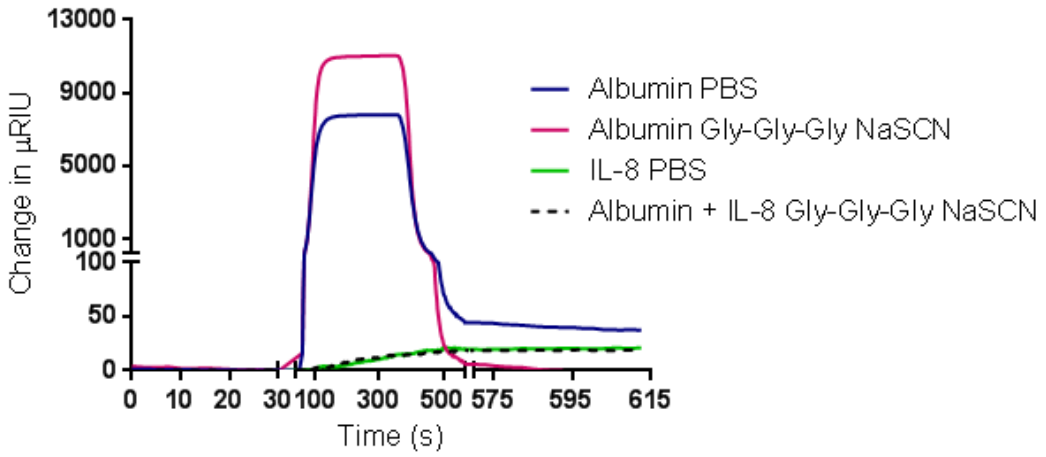


Figure 3.2.5. The impact of Gly-Gly-Gly NaSCN on the nonspecific binding of albumin and the specific binding of IL-8. The nonspecific binding of albumin (50 mg/ml) in PBS (blue) is eliminated in the presence of Gly-Gly-Gly NaSCN (mauve). The specific binding of IL-8 to the anti-IL-8 antibody in PBS was estabilished at a low, yet detectable level (green). To test whether the specific interactions can take place at the same time as the reduction in nonspecific binding, the running buffer was changed to albumin in Gly-Gly-Gly NaSCN. Specific binding of IL-8 to the anti-IL-8 antibody in the presence of albumin in Gly-Gly-Gly NaSCN is maintained (dashed black line). Protein association between 100-400 s at 20 µl/min, buffer dissociation 400-600 s at 20 µl/min. Non-linear y axis were used to negate the refractive index changes by the buffer alone (albumin PBS, albumin Gly-Gly-Gly NaSCN). Non-linear axis were used in the x-axis to . All reactions were repeated in triplicate pH 7.4 at 25°C.

The specific binding of IL-8 to an anti-IL-8 antibody was conducted as in Figure 3.2.1. IL-8 binding at 10 ng/ml in PBS is at the lower end of the Reichert, detectable range. The signal recovered is at a low, but detectable level. In complex solutions such as blood, the concentration of albumin (50mg/ml) exceeds that of cytokines (10ng/ml). At the concentrations employed here the nonspecific binding of albumin is higher (51 ± 0.97 μRIU (Figure 3.2.5)) than the specific binding of IL-8 (35 ± 0.56 μRIU (Figure 3.2.5)) illustrating that the system was unable to detect the analyte.

It has been shown in the control experiments that albumin binding can be eliminated by media alterations (Figure 3.2.3). A specific binding reaction of IL-8 to the anti-IL8 antibody was established in the presence of albumin in the anti-nonspecific binding media (used as a running buffer). The specific interaction of IL-8 was indistinguishable from an identical reaction in PBS where no albumin was present (Figure 3.2.5). This leads us to believe that the specificity of the instrument would be greatly improved, through the antibody interacting only with its specific analyte, without nonspecific binding of other proteins (Section 3.3).

The effects of the regents on specific interactions were further investigated with specific binding of fibrinogen (5 μg/ml) to an anti-fibrinogen antibody as in Figure 3.2.1. Specific interactions were examined in control PBS media, as well as reagent combinations that were previously shown to be effective in the nonspecific binding experiments (Figure 3.2.4). In these experiments, the reagent media were used as the running buffer to negate gross refractive index differences seen with previous DCMRs (Figure 3.2.4).

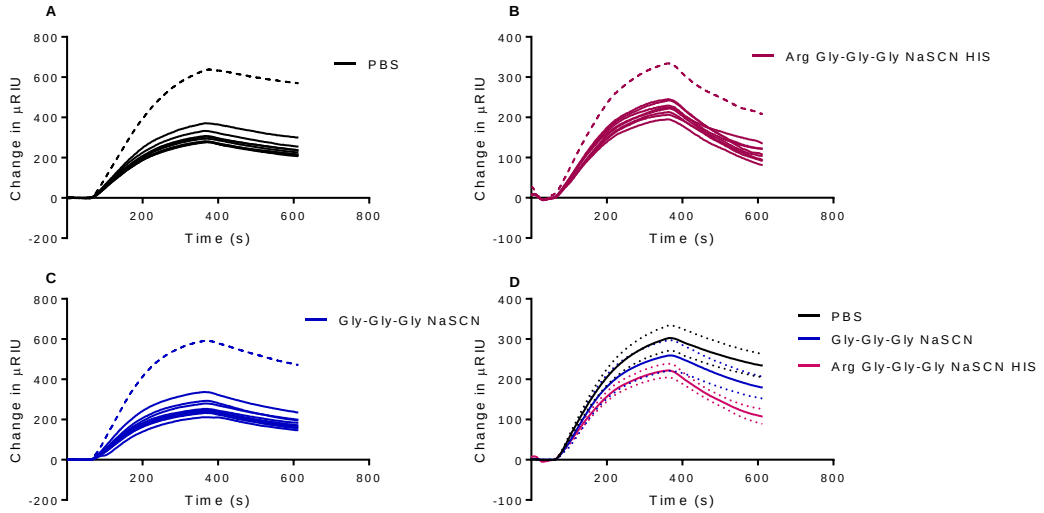


Figure 3.2.6. The specific binding of fibrinogen (5 µg/ml) to an anti-fibrinogen antibody in different media. Protein association was between 100-400s at a flow-rate of 20µl/min, buffer dissociation was between 400-600s at a flow rate of 20µl/min. The running buffer and protein diluent for each experiment were (A) PBS, (B) Arg Gly-Gly-Gly NaSCN HIS, (C) Gly-Gly-Gly NaSCN (Table 2.1.1) pH7.4 at 25°C. Binding experiments were repeated 8 times per sample. Between binding experiments, the antibody was regenerated with 5mM HCl (100 µl/min for 2 min) (Section 2.13.4.). Experiments were performed in triplicate. (D) Comparison of the average binding curve (initial reaction excluded in accordance with manufacturer guidelines) in the presence of different media. Dashed lines represent ± standard deviation. The first binding curve of each condition contains loosely associated antibodies that are lost under initial regeneration, as such the data (dotted) is excluded from the average.

Changes in the running buffer alter either the kinetic profile or binding yield (Figure 3.2.1) (Figure 3.2.6). Gly-Gly-Gly NaSCN media does not affect the kinetic profile of binding, however, it is associated with a slight decrease in the binding capacity (Figure 3.2.6C). This is attributed to the elimination of the nonspecific binding. The reduction in specific binding was 53 ± 3 µRIU, whereas the nonspecific fibrinogen binding to the surface or antibody core was shown to be approximately the same (Figure 3.2.4A (49 ± 2 µRIU)). Removal of the nonspecific contribution increases the specificity of the binding reaction (Figure 3.2.6A). Arg Gly-Gly-Gly NaSCN HIS media reduced the binding capacity of fibrinogen further, with related changes in the kinetic profile. The association and dissociation phases of fibrinogen binding in

Figure 3.2.6B are more pronounced, suggesting that the protein-antibody affinity is reduced by the presence of the reagents.

3.2.2 Effect of Detergent Molecules on Binding Reactions

Once satisfied that the different reagents were capable of eliminating nonspecific interactions and not affecting specific interactions, other components of the media were investigated. As discussed previously (Section 3.1) several common detergents have been characterised for various applications, such as protein solubilisation, stabilisation and reduction of nonspecific binding [78, 79, 175, 176]. Two detergent species with similar properties were employed (Section 3.1) to investigate whether the intermolecular forces can be reduced further. If the detergent interacts with the non-polar patches of the protein surface, the dispersion forces will be negated [79].

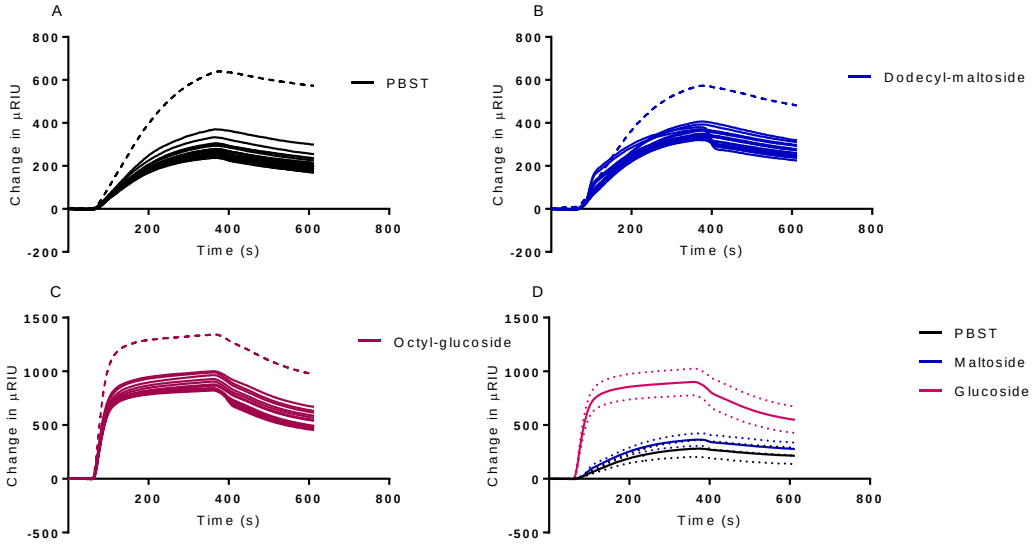


Figure 3.2.7. The specific binding of fibrinogen (5 µg/ml) to an anti-fibrinogen antibody conjugated surface, with various detergents. Protein associates with the surface between 100-400s at a flow rate of 20µl/min. The protein dissociates between 400-600s at a flow rate of 20µl/min. Between binding experiments, the antibodies were regenerated with 5mM HCl (100 µl/min, 2 min) for ≥ 10 times. Running buffer of PBS at pH7.4, experiments were conducted at 25°C with different detergents (A) Tween 20 (B) Dodecyl-maltoside (C) Octyl-glucoside. Experiments were performed in triplicate. (D) The average binding curves of fibrinogen in the different media, dashed lines represent ± SD. The first binding curve of each condition contains loosely associated antibodies that are lost under initial regeneration, as such the data (dotted) is excluded from the average.

Figure 3.2.7A demonstrates a fibrinogen anti-fibrinogen antibody interaction in PBS with Tween 20 as a detergent (as previously seen in Figure 3.2.1). The detergent was replaced with either the dodecyl-maltoside (Figure 3.2.7B) or octyl-glucoside detergent (Figure 3.2.7C). The presence of dodecyl-maltoside does not significantly affect the binding capacity of the protein. The initial association and dissociation kinetics of the dodecyl-maltoside binding curves suggest that the dodecyl-maltoside may interact with the protein/surface prior to the protein-antibody interaction. The octyl-glucoside detergent was shown to be inappropriate as a possible replacement detergent as Figure 3.2.7C illustrates that there is a two-fold increase in binding as well as faster association kinetics. These results suggest that the octyl-glucoside detergent is either binding directly to the surface, or is altering the fibrinogen protein causing enhanced protein binding.

Detergents are employed to disrupt dispersion forces however, as previously discussed (Section 1.6.2), these forces are weaker than the electrostatic interactions disrupted by the other soluble reagents previously employed. Figure 3.2.7 demonstrates that the alternative detergents are unable to attenuate nonspecific binding independently (see discussion) therefore, in order for them to increase the efficacy of the media, they must work collaboratively with NaSCN, which has shown efficacy previously.

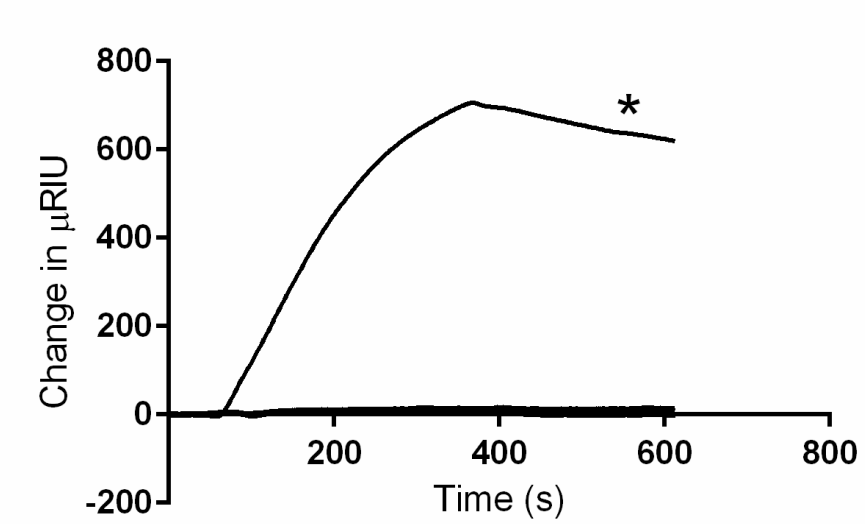


Figure 3.2.8. Specific binding of fibrinogen (5 μg/ml) to an anti-fibrinogen antibody surface. Protein association is between 100-400s at a flow rate of 20μl/min, buffer dissociation is between 400-600s at a flow rate of 20μl/min. Between binding experiments, antibodies were regenerated with 5mM HCl (100 μl/min, 2 min) ≥ 10 times. Experiments were conducted in Gly-Gly-Gly NaSCN dodecyl-maltoside media (Table 2.2.1) pH7.4 at 25°C. Experiments were performed in triplicate with representative data shown. Asterisk denotes the first binding reaction.

The dodecyl-maltoside detergent in the presence of the other reagents (Figure 3.2.8) disrupted fibrinogen interactions with an anti-fibrinogen antibody. The initial binding curve (denoted with an asterisk Figure 3.2.8 (~600 μRIU) correlates with previously recorded levels of binding (Figure 3.2.7 (~600 μRIU). After the first binding reaction and surface regeneration, no more binding is detected. This suggests that there are adverse effects on the protein-antibody complex in the presence of all anti-nonspecific binding reagents and the dodecyl-maltoside detergent. A possible explanation is that the protein-antibody interaction is stabilised by the combination of reagents and detergent and is therefore unable to be regenerated by HCl. This would result in further protein being unable to bind to occupied antibodies.

As both detergent species affected the specific interactions that the detection instrument relies on, neither were considered as a media reagent for the reduction of nonspecific binding.

3.3 Validation of Anti-Nonspecific Media in Multiplex Immunoassays

This work was done in collaboration with industrial partners BioRad Bio-Plex R&D, D Jethwaney and W Tan.

The use of soluble reagents in the medium has been shown to eliminate nonspecific binding whilst maintaining specific binding in both model membrane systems (Section 3.1.1) and surface plasmon resonance (Section 3.2). However; the question remains: 'can nonspecific binding be eliminated in the presence of multiple analytes, where issues such as molecular crowding and cross-reactivity may play a role?' (e.g. [42, 177, 178]. To answer these questions, a multiple analyte bead-based detection instrument was employed (Luminex BioPlex 2200). Within multi-analyte detection, nonspecific binding may arise from electrostatically driven nonspecific binding (as described above), or cross-reactivity of the different antibodies in the array. Cross-reactivity interactions further complicate the definition of specific bio-recognition events, and nonspecific electrostatic events. Different antibodies elicit different antigen specificity; the higher the specificity, the lower the number of binding partners the antibody has. This study was conducted on a pre-validated, commercially available panel of antibodies, therefore, it is assumed that the target antigen has a higher affinity for the antibody than a cross-reacting partner, and hence cross-reactivity is categorised as a nonspecific binding event. A Bio-Plex 27-plex human cytokine assay determines the analyte-antibody interaction of 27 proteins simultaneously (explained in detail in Section 2.14). This assay is designed to measure levels of: Fibroblast growth factor (FGF) basic, Eotaxin, Granulocyte-colony stimulating factor (G-CSF), Granulocyte-macrophage-colony-stimulating factor (GM-CSF), Interferon gamma (IFN-γ), Interleukin 1-beta (IL-1β), Interleukin 1-receptor antagonist (IL-1ra), Interleukin-2 (IL-2), Interleukin 4 (IL-4), Interleukin

5 (IL-5), Interleukin 6 (IL-6), Interleukin 7 (IL-7), Interleukin 8 (IL-8), Interleukin 9 (IL-9), Interleukin 10 (IL-10), Interleukin 12 (IL-12 (p70)), Interleukin 13 (IL-13), Interleukin 15 (IL-15), Interleukin 17 (IL-17), Interferon gamma-induced protein 10 (IP-10), Monocyte Chemoattractant Protein-1 (MCP-1 (MCAF)), Macrophage inflammatory protein 1-alpha (MIP-1α), Macrophage inflammatory protein 1-beta (MIP-1β), Platelet-derived growth factor-BB (PDGF-BB), Regulated on activation normal T cell expressed and secreted (RANTES), Tumour necrosis factor alpha (TNF-α) and Vascular endothelial growth factor (VEGF).

3.3.1 Experimental design

Historically, complex detection assays, such as Bio-Plex, have used bespoke media for each component of the instrument such as; the standard diluent, sample diluent, detection antibody diluent (DAD) and assay running buffer. The experimental design outlined in Table 3.3.1 allows elucidation of the best media available in any/all of these components.

	Standard diluent	Sample diluent	Detection antibody diluent (DAD)	Assay running buffer
Control	Control	Control	Control	Control
Test 1A	Gly-Gly-Gly NaSCN	Gly-Gly-Gly NaSCN	Gly-Gly-Gly NaSCN	Gly-Gly-Gly NaSCN
Test 1B	Gly-Gly-Gly NaSCN	Control	Control	Control
Test 1C	Gly-Gly-Gly NaSCN	Gly-Gly-Gly NaSCN	Control	Control
Test 1D	Gly-Gly-Gly NaSCN	Gly-Gly-Gly NaSCN	Control	Gly-Gly-Gly NaSCN
Test 1E	Gly-Gly-Gly NaSCN	Gly-Gly-Gly NaSCN	Gly-Gly-Gly NaSCN	Control
Test 2A	Arg Gly-Gly-Gly NaSCN	Arg Gly-Gly-Gly NaSCN HIS	Arg Gly-Gly-Gly NaSCN HIS	Arg Gly-Gly-Gly NaSCN
Test 2B	Arg Gly-Gly-Gly NaSCN	Control	Control	Control
Test 2C	Arg Gly-Gly-Gly NaSCN	Arg Gly-Gly-Gly NaSCN HIS	Control	Control
Test 2D	Arg Gly-Gly-Gly NaSCN	Arg Gly-Gly-Gly NaSCN HIS	Control	Arg Gly-Gly-Gly NaSCN
Test 2E	Arg Gly-Gly-Gly NaSCN	Arg Gly-Gly-Gly NaSCN HIS	Arg Gly-Gly-Gly NaSCN HIS	Control

Table 3.3.1. Experimental design of nonspecific reagent usage in the Bio-Plex 27 human cytokine assay. Control media were the most up-to-date Bio-Rad formulations (as of September 2014) compared against Gly-Gly-Gly NaSCN and Arg Gly-Gly-Gly NaSCN HIS (Table 2.1.1) at pH7.4, experiments were conducted at 25°C.

3.3.2 Investigation of bead detection and separation

During the antibody detection step, the different antibody beads are sorted in order to quantify the different antibodies present in the multiplex kit. The antibodies are detected by the unique properties of two dyes impregnated into the beads (as discussed in Section 2.14). The Bio-Plex bead maps were visualised to investigate whether the beads segregated correctly in the presence of the different media. Figure

3.3.1A denotes the bead map under Bio-Rad conditions; each protein in the panel has a distinct x-y representative of the dyes impregnated in the bead (Figure 3.3.1A, Blue circle). The green circle in Figure 3.3.1B shows that in the presence of Gly-Gly-Gly NaSCN, the bead map is maintained. Arg Gly-Gly-Gly NaSCN HIS media alters the bead map as illustrated in Figure 3.3.1 by the red circle.

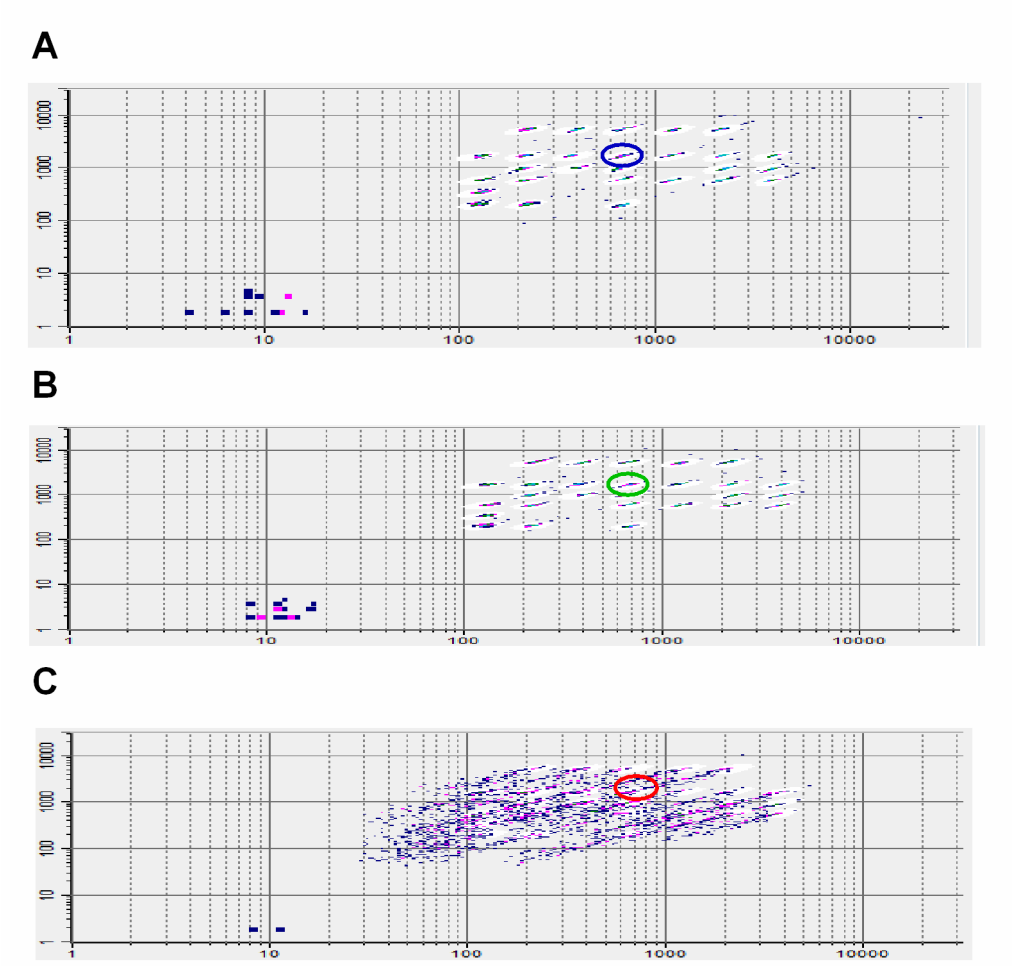


Figure 3.3.1. A bead map of Bio-Plex. The x-y coordinates are based on the unique combination of impregnated dyes on the bead (Figure 2.14.1). (A) Control Bio-Rad media, where bead separation is denoted by the blue circle. (B) Gly-Gly-Gly NaSCN media, where bead separation is denoted by the green circle (C) Arg Gly-Gly-Gly HIS media, where the bead separation is denoted by the red circle.

The bead map may be influenced by the high ionic strength of the media; the increased ionic-shielding of the medium may have caused by the beads interact with one another resulting in reduced segregation and mischaracterisation.

The bead fluorescence quantification in the segregation region is still assigned to the protein in which they are expected to segregate. As such, the area may contain some beads that are segregated correctly and others incorrectly. This medium is ultimately incompatible with specific bead-based detection in its current formulation, however the other metrics from the study, such as nonspecific binding can still be inferred with this caveat.

3.3.3 Identification of nonspecific binding

The amount of nonspecific binding was determined by through observation of the background median fluorescence intensity (bMFI) (Section 2.14.2.). bMFI values are representative of ΔFI when no analyte is present, i.e. the interaction of reagents in the media and the cross-reactivity of antibodies to one another. These values determine the limit of detection (LOD) for each antibody-conjugated bead. BioRad laboratories define the values as the concentration of analyte corresponding to the MFI of the background (or zero standards) plus two standard deviations [163].

Figure 3.3.2 illustrates the effects of different reagent mixtures on nonspecific binding as average values of all 27 proteins (Table 3.3.1). The use of media reagents (Table 2.2.1) instead of control Bio-Rad media resulted in a marked decrease in bMFI values (Figure 3.3.2). The reductions shown are most pronounced in Tests: 1A, 1D, 1E and 2A. Test 1A and 2A represent tests in which all media components of the instrument have been replaced (Table 3.3.1). Test 1D has all components besides the DAD replaced, whereas Test 1E has all components replaced besides the assay running buffer. These values are averaged across all antibody panels and are therefore representative of all the antibody beads shown in the bead map in Figure 3.3.1.

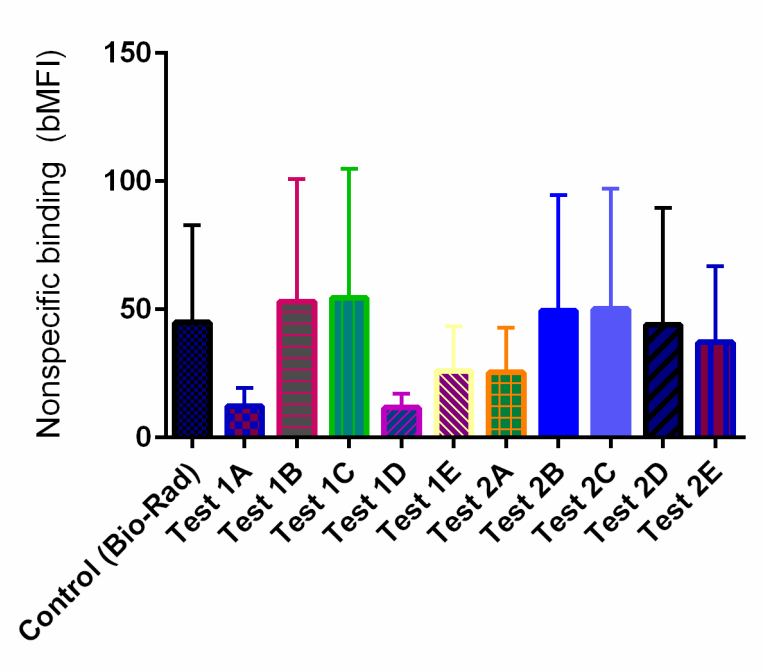


Figure 3.3.2. The background Median Fluorescence Intensity (bMFI) reading nonspecific binding of all 27 proteins in the panel. Binding was observed in the presence of control (Bio-Rad), Gly-Gly-Gly NaSCN (Test 1) and Arg Gly-Gly-Gly NaSCN HIS media (Test 2), experiments were conducted at pH7.4 and 25°C. Experiments repeated four times. The experimental differences between the conditions are outlined in Table 3.3.1.

The results in Figure 3.3.2 show that replacing the running buffer (Test 1A, 1D and 2A) has the largest effect on nonspecific binding. When the media is used solely for the protein (standard and sample) diluents (test species B & C), the levels of nonspecific binding are not markedly affected. These results suggest that any nonspecific binding occurs during the sample incubation step (Section 2.14.1), potentially as a result of nonspecific binding of analytes to the different antibody species. The running buffer represents the largest volume of liquid used during the assay therefore, if only the diluents were replaced, the reagents present would become diluted to ineffective concentrations.

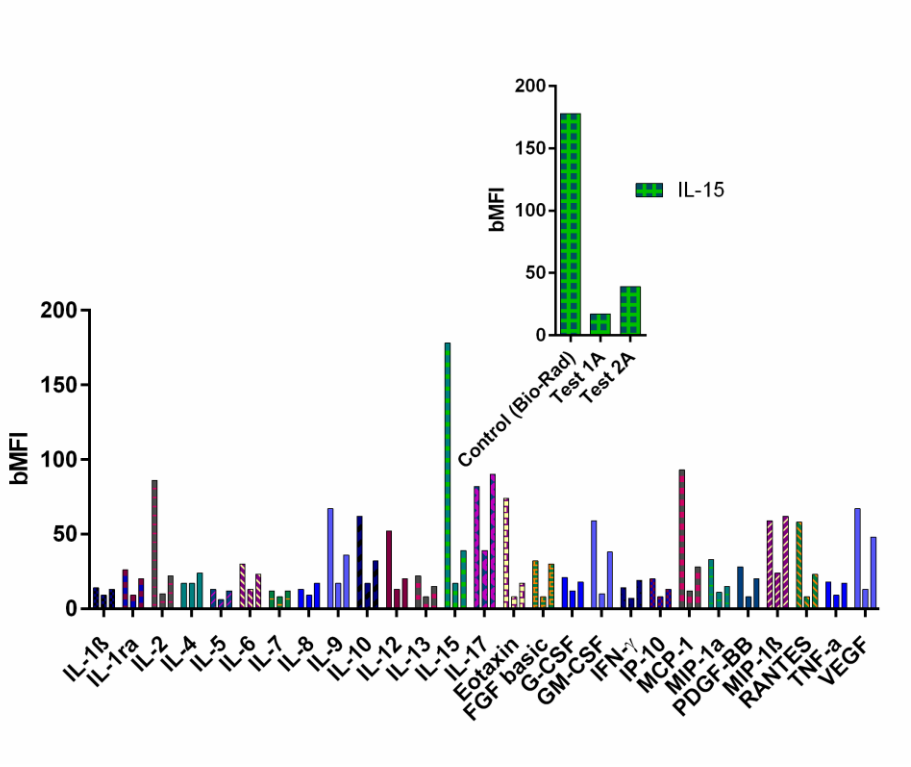


Figure 3.3.3. Nonspecific binding to specific antibody beads in Bio-Plex analysis. Values are background median fluorescence intensity (bMFI) values. Each protein has associated three bars (see insert): Control: Bio-Rad buffer, Test 1A: Gly-Gly-Gly NaSCN used as all buffers and Test 2A: Arg Gly-Gly-Gly NaSCN HIS.

After the most effective combinations for the media replacement had been established (Test 1A, Table 3.3.1, Figure 3.3.2), differences between antibodies in the panel were observed. Figure 3.3.3 illustrates the differences between the antibodies nonspecific binding capacities. The variation results from the sensitivity and specificity of the antibody where sensitivity refers to the detection of low analyte concentration in a solution. This is directly proportional to the affinity of the interaction. Specificity refers to the antibodies' interaction with protein antigens; an antibody with perfect specificity would only exclusively bind its related protein. Many antibodies have been shown to bind other proteins nonspecifically. These interactions have been shown to be driven by hydrophobic interactions [179]. In this study there is variation between the different antibodies in the panel, highlighting the differences in selectivity (e.g. IL-15 has a bMFI of 175 and IL-7 has a bMFI of 13).

The lower the fluorescence intensity, the lower the nonspecific binding and the higher the selectivity.

Treatment with Gly-Gly-Gly NaSCN and Arg Gly-Gly-Gly NaSCN HIS decreased the nonspecific binding in the majority of protein in the panel (Figure 3.3.3). This, in turn, decreases the LOD and hence increases the sensitivity of the instrument.

The experiments shown in Figure 3.3.3 were also carried out in different combinations shown in Table 3.3.1. In tests 2B-E, some proteins such as VEGF, G-CSF and GM-CSF exhibited increased nonspecific binding that contributes to the increase shown in Figure 3.3.2. This may have been due to the segregation issues highlighted in Figure 3.3.1. These effects were not present in Tests 1A or 2A, suggesting that it may result from cross-reactivity between the media reagents, the existing BioRad buffers and these specific antibodies (Figure 3.3.2).

In order to test the efficacy of the media in a functional form, the specific interactions were observed in the presence of the media.

3.3.4 Specific binding of analytes

Specific binding of the analytes to their respective antibody bead was observed. This was to confirm that the reduction in nonspecific binding was a function of the media reagents and is not a reduction in total binding capacity.

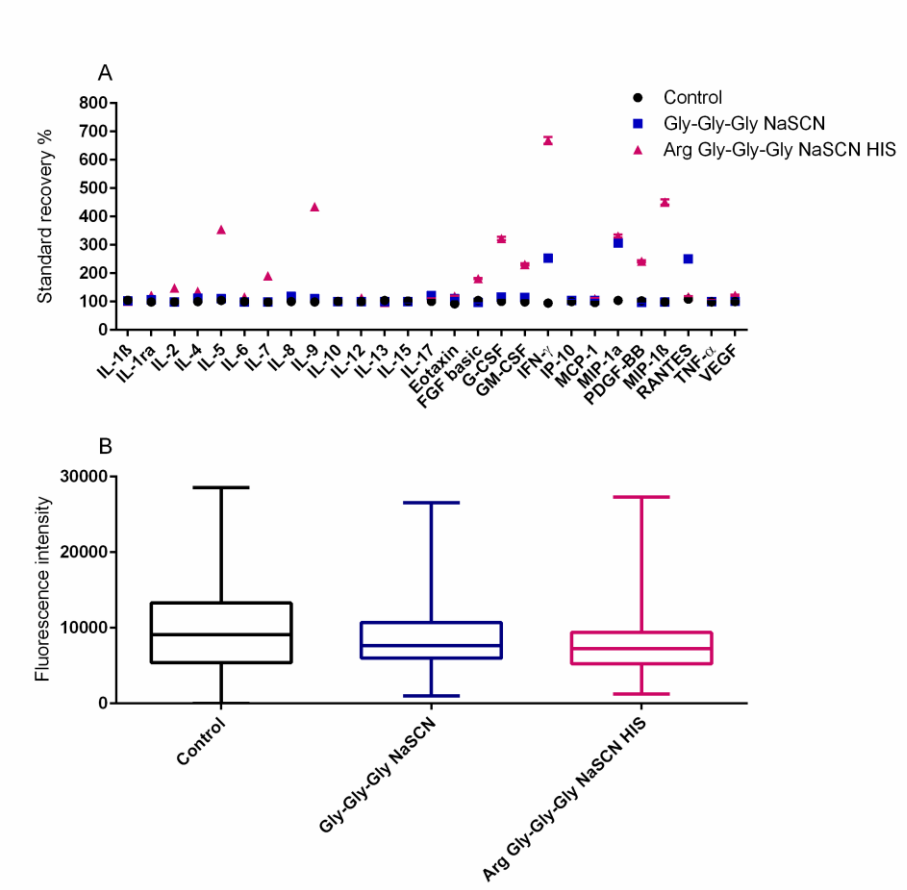


Figure 3.3.4. Specific recovery % of the protein in different media in Bio-Plex. (A) Each point represents the specific recovery of one of the cytokines in the panel. All specific recovery values of Bio-Rad control exhibit ~100%, Gly-Gly-Gly NaSCN has three proteins with >100% recovery and Arg Gly-Gly-Gly NaSCN HIS 10 proteins with >100% recovery, with no recovery responses below 95% across all media conditions. (B) Total fluorescence values of specific binding. Box plots show that there is no significant difference between the different media treatments.

Specific interactions can be observed through specific recovery and total fluorescence (Figure 3.3.3). A known concentration of the protein standard (in the linear detection range of the instrument) is added to the assay, and then the amount

of protein detected in the sample (observed concentration) gives a % recovery of the protein added [161].

$$\text{Specific Recovery} = \frac{[\text{Observed concentration}]}{[\text{Expected concentration}]} \times 100$$

Equation 3.3.1. Specific recovery is the ratio of observed concentration and expected concentration.

With a known protein concentration in the standard, recovery percentage is used to examine the specific binding of a protein to the antibody. In Bio-Rad defined situations [163], specific recovery is referenced to 100% (Figure 3.3.4A). The proteins in Bio-Rad control media demonstrated specific recovery between, 95-109% (Figure 3.3.4A). Gly-Gly-Gly NaSCN elicited a similar trend (97-116%) with three results eliciting a much greater response (MIP-1α (307%), IFN-γ (253%) and RANTES (251%); Figure 3.3.4). The high ionic strength media had 11/27 proteins above 120% recovery (IL-2 (148%), IL-5 (355%), IL-7 (191%), IL-9 (435%), FGF basic (181%), G-CSF (322%), GM-CSM (231%), IFN-γ (668%), MIP-1α (331%), PDGF-BB (242%) and MIP-1β (451%)) with 16 other proteins in the accepted range (97-120%). Values recorded above 100% protein recovery suggest that either more protein is binding than in the sample, or that the mischaracterisation of the beads leads to false levels of protein binding. Given the complexity of the panel, these results suggest that of the proteins in the panel are adversely reacting with the reagents in the medium, such as some of the proteins being salted out due to the increased ionic strength, resulting in aggregation and nonspecific binding.

Another parameter of specific binding that was examined was the mean total fluorescence intensity. Figure 3.3.4B illustrates that there was no significant difference between each treatment. These results in unison suggest that the specific

interactions are not disrupted by Gly-Gly-Gly NaSCN in a multi-ligand system, as previously established in single-ligand systems (Sections 3.2.1). The Arg Gly-Gly-Gly NaSCN HIS media may negatively affect the interaction of the proteins with the antibodies.

The Gly-Gly-Gly NaSCN media has been found to be suitable in all test parameters, with clear segregation of beads. The elimination of nonspecific binding offers an increased LOD for all the proteins examined thus developing the assay further, and allowing for detection of previously undetectable protein concentrations.

3.4 Discussion

The ability to target the different intermolecular forces that occur between molecules is of great interest. This study has shown that it is now possible to have a measure of control in reducing undesirable interactions in analyte detection systems, whilst maintaining the specific interactions that these instruments rely on. The results shown will be discussed to propose the mechanism of action for the reagents and their benefit of the wider scientific community.

3.4.1 The Interaction of Albumin with Model Membranes

The interaction of albumin with model membranes was employed as an example of a nonspecific binding interaction. These interactions were then modulated with two classes of reagents that theoretically affect intermolecular interactions in different ways. The first reagent, sodium thiocyanate, is known to be effective in reducing intermolecular interactions [54]. The second class of reagents consisted of a range of DCMRs, which have predicted and measured effects on the dielectric constant (Section 1.6.2). These reagents were initially employed in protein-membrane systems as defined by Wall et al., [128].

Human serum albumin was employed as the most abundant protein in biological fluids in the body such as blood and cerebrospinal fluid [16]. Albumin has been shown to be bind due to nonpolar patches on the protein surface [16]. The protein carries a net electronegative charge which is detected by electrostatic potential changes by FPE in the membrane [128] (Figure 3.4.1)

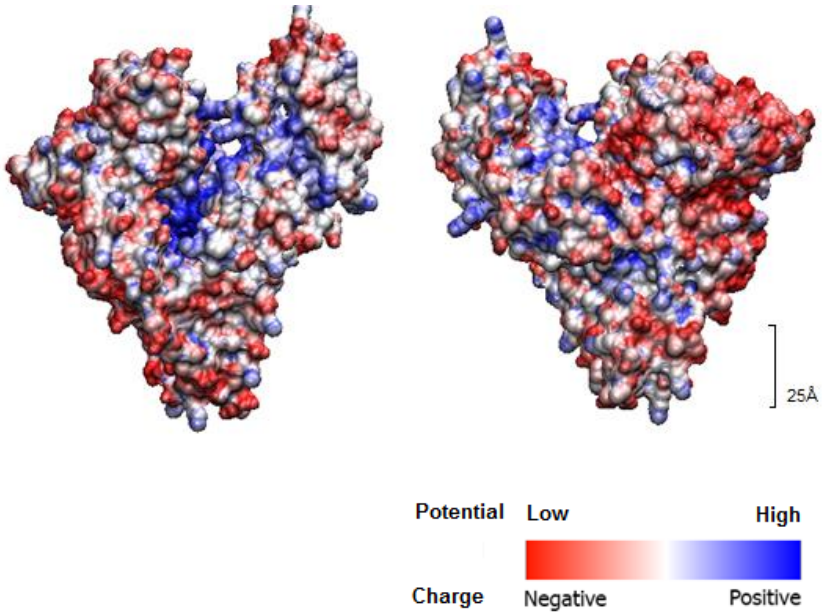


Figure 3.4.1. Electrostatic map of human serum albumin. Blue zones are positively charged regions; red zones are negatively charged. Projections are 180° y-axis rotation from one another.

Specific interactions (such as those discussed in Section 1.4.6) rely on several close membrane interactions. These interactions are exemplified by antibody interactions such as those illustrated in Figure 3.4.2. The specific antibodies are raised against purified samples of albumin or long peptides that then result in interactions with nanomolar affinity. These interactions rely on several site-specific interactions in three-dimensions such as, electrostatic interactions between positive and negative amino acid side chains and hydrogen bonding between peptide backbones or polar side chains, hydrophobic interactions etc. These forces may be across the surface, or access solvent-free pockets that are inaccessible from bulk media. These 'specific' interactions are orientation dependent, although none of these interactions alone are different from the 'non-specific' interactions targeting by the reagents in this study, the culmination of the forces makes them specific.

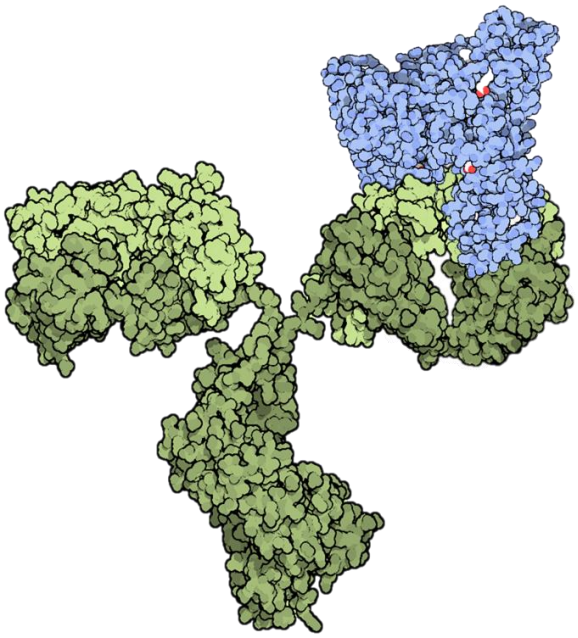


Figure 3.4.2. Anti-albumin antibody interaction with albumin. Protein structures from protein database.

NaSCN caused a reduction in protein-membrane interactions (Figure 3.1.4). This observation is in agreement with the conclusions drawn by Richens et al. [54] in addition to Rees and Lilley [29], who found that NaSCN is effective at decreasing protein-protein interactions in some other protein species.

As discussed in Section 1.6.1, thiocyanate ions have a high entropy of hydration. Considering that ions have been shown to localise to the protein surface [180], the SCN^- ions will orientate the water molecules towards the ion surface and away from the protein surface [181, 182]. The surface of albumin (shown in Figure 3.4.1) is charged (denoted by red and blue patches) and the protein carries a net -17 negative charge. The ordering of water across the protein surface slows the rotational coefficient, or lifetime of the water molecules, thus creating a solvation zone on the protein surface. Solvation zones have unique local dielectric constants. As the water molecules are no longer free to move as they are in the bulk water, the dielectric

constant is increased [57] (Section 1.6.2). Figure 3.4.3 proposes how NaSCN may orientate across the albumin surface.

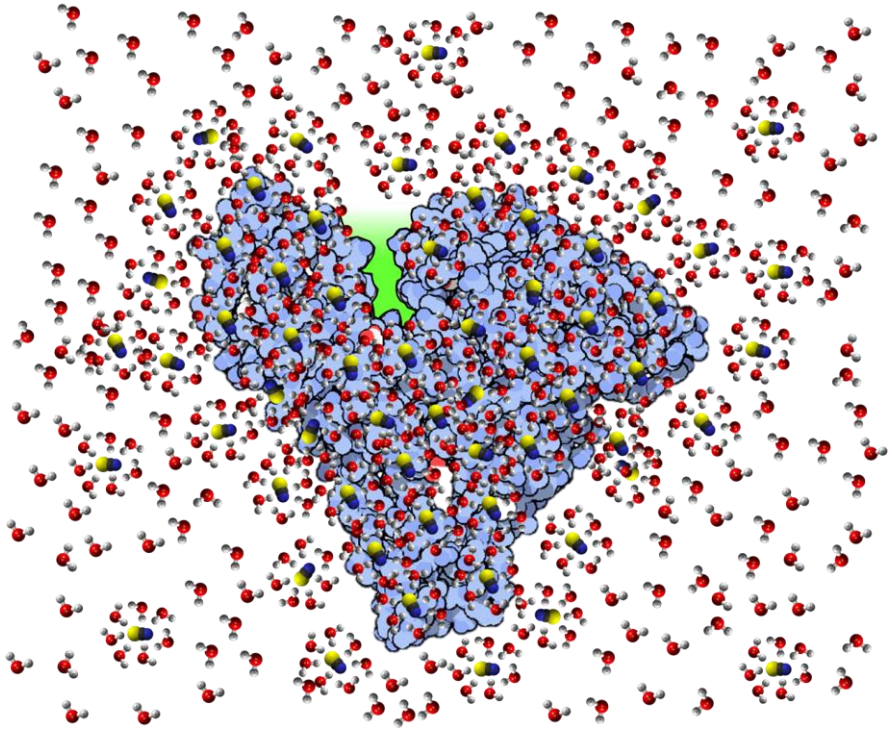


Figure 3.4.3. Possible mode of action for reducing nonspecific binding of albumin. PDB model of HSA with SCN^- (yellow, black and blue) localised to the surface. SCN^- ions then order the local water structure surrounding them (H_2O, white and red). The ions that localise at the protein surface changes the type and magnitude of interactions present. Solvent-free pockets are illustrated in green.

This increase in local dielectric constant would decrease the short-range Coulomb interactions in accordance with Coulomb's law. By utilising these properties, the binding of albumin with NaSCN was greatly diminished, suggesting that the interaction profile of albumin is able to be modified in this way. The reduction of these parameters has pronounced effects in reducing nonspecific binding of several proteins [54]. Rees and Lilley *et al* used NaSCN as a potential method to minimise nonspecific binding when characterising affinity resins. This study highlighted that several proteins were not affected by NaSCN (including fibrinogen used in this study), and therefore have different forces that drive their propensity to nonspecifically bind [29], (Figure 3.1.4).

3.4.2 The Interaction of Fibrinogen with Model Membranes

Thiocyanate was effective in reducing the protein-membrane binding of fibrinogen at the concentrations previously employed (Section 3.1.1 Figure 3.1.4) however, the binding was not eliminated. This result is in agreement with Rees and Lilley [29] and we expect that this is due to the different surface properties of the proteins employed [16, 25, 183, 184]. Fibrinogen contains tightly clustered negative domains, modelled as negatively charged 'beads', which are associated with strong Coulomb forces produced from the negatively charged amino acid residues. [183]. The proposed method of surface solvation by thiocyanate ions was insufficient to deal with such concentrated point charges. Charge-charge interactions are the longest range intermolecular force (Section 1.4.1) and extend beyond the protein surface, where NaSCN may be less effective.

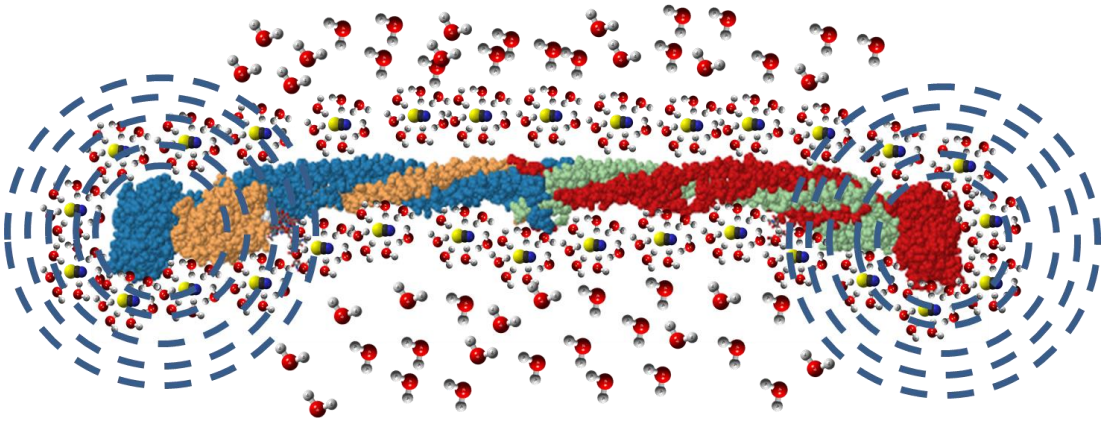


Figure 3.4.4 Fibrinogen crystal structure (PDB 3GHG) shows subunits wrap around each other in a coiled-coil structure; thus reducing the hydrophobic surfaces available. Thiocyanate ions are placed around the surface in the proposed fashion. Bead structures at the end of the protein contain groups of negative charges. Coulomb forces that radiate from point charges may be affected by NaSCN but not efficiently negated.

DCMRs were employed in order to eliminate the nonspecific binding. The dielectric constant has been theoretically predicted to affect nonspecific binding in the past [42] but it has never been functionally tested to eliminate binding. Considering this, Arg, Gly-Gly and Gly-Gly-Gly were chosen.

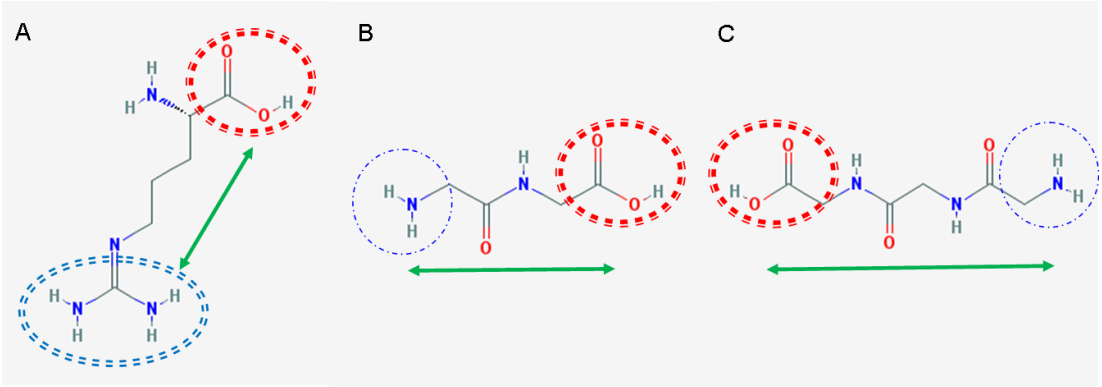


Figure 3.4.5. The structure of different dielectric molecules; negative dipole contribution circled in the red circle, positive contribution circled in blue, length of dipole shown with green arrow (A) Arginine, positive charge imparted from two NH_2 chains, dipole length relatively long (B) Gly-Gly, standard amino acid dipole, dipole length relatively short. (C) Gly-Gly-Gly, standard amino acid dipole with longest dipole length employed.

Arg is zwitterionic, has a large dipole moment (+62 D) and has been shown to interact directly with proteins [74]. Gly-Gly is an uncharged dipolar molecule (+71 D) however, the dielectric increment increases with dipole length (Gly-Gly-Gly (+128 D)). The increasing dielectric increment of glycyl-peptides correlates to an increase in the dipole length (Gly-Gly-Gly-Gly, Gly-Gly-Gly-Gly-Gly, etc. (Figure 3.4.5)). Gly-Gly and Gly-Gly-Gly were chosen due to their sufficient dielectric increment/ residue ratios in addition to practical considerations such as cost.

Increasing the dielectric constant has a direct effect on both charge-charge and dipole interactions. As seen in 1.4.1 and 1.4.2, all of the charge-charge, charge-dipole and dipole-dipole interactions are dependent on the solution's dielectric constant of the solution. Increasing the ambient dielectric environment decreases the proximity energies; this leads to a reduction in electrostatic interaction and subsequently reduces nonspecific binding.

Historically, these qualities may have been (perhaps unwittingly) employed with a negative dielectric increment of sugars (sucrose= -7.6D) and freeze-drying of proteins. [70, 185, 186]. As water is drawn from the sample, both the sucrose and

protein are concentrated. This causes a decrease in the dielectric constant whilst increasing the charge-charge repulsion between adjacent protein molecules and preventing ice formation, thus acting as a cryoprotectant [187]. We have shown that a positive dielectric increment is effective in decreasing intermolecular interactions, hence molecules with a positive increment, as shown in Table 1.6.1, can be used as nonspecific binding reagents.

3.4.3 Interaction of Albumin and Fibrinogen to Antibodies and Surfaces

Protein-membrane interactions have acted as a reliable model for the elimination of nonspecific binding however, specific interaction and molecular recognition, such as those between antigens and antibodies, cannot be tested. Plasmonic-based biosensors were employed to test the reduction of nonspecific interactions, whilst retaining the specific interactions that the instrument is focussed on. Historically, these technologies have been shown to suffer from nonspecific binding, which decreases the sensitivity of the instrument [188]. Efforts have been made to reduce nonspecific binding using SPR most commonly through the development of more and more sophisticated sensor chips [171-174]. PEGylation is frequently used to reduce nonspecific interactions however it is susceptible to thermal and oxidative degradation over time [189-191], which results in a decreased performance in nonspecific adsorption [25]. Different protein targets require different affinity tags on the chip to immobilise the proteins. These specialised chips frequently avoid using PEGylation in order to accommodate smaller reactive sites, such as those used for amine coupling, and hence suffer a trade-off of nonspecific fouling.

This study has shown that with careful implementation of the different reagents, media can be created to target nonspecific interactions of both albumin and fibrinogen without compromising specific interactions, (specifically a combination of

Gly-Gly-Gly and NaSCN Figure 3.1.5, Table 3.1.4). Certain reagents (Arg) resulted in increased nonspecific binding to the surface (Figure 3.2.3), hence any formulations must be further validated before use. The specific interactions, such as the interaction between fibrinogen and an anti-fibrinogen antibody demonstrated here (Figure 3.2.5 and Figure 3.2.6) are orders of magnitude stronger than nonspecific interactions, and are not affected. This is due to the well-characterised model of antibody binding taking place in solvent-free pockets [192, 193]. These binding pockets have several different molecular recognition mechanisms such as lock and key and induced fit binding [194] (discussed in Section 1.4.6).

The only intermolecular force not modulated by changes in the dielectric constant are that of dispersion forces. Dispersion forces are between two non-polar molecules and resultant from spontaneous dipole creation. Given the spontaneous nature of their inception, there is no defined mechanism, which can be targeted by specific reagents. As a result, detergent molecules were added to interact with the protein surface via hydrophobic attraction of the hydrocarbon tail. This changes the protein surface and in turn changes related forces dependent on the detergent head group [79]. Several detergents have been created to solubilise proteins [175] however, in this study, a dodecyl-maltoside (n-dodecyl-β-D-maltoside) and a octyl-glucoside (octyl-β-D-glucopyranoside) are employed to impart similar properties of a positive dielectric increment species [175]. In this study, the detergents had adverse effects on protein-antibody specific interactions.

Using the media reagents to reduce nonspecific interactions offers a range of benefits over currently available methods. Many current detection instruments demand expensive pre-treatment steps or sample treatments such as albumin or plasma reduction kits that may introduce additional variation between samples and other

unwanted side-effects [24, 195]. These side-effects may include the removal of proteins associated with albumin, which has shown to be numerous [16]. Removing these proteins would decrease the bioavailability of potential targets and increase the number of false-negatives. The nonspecific media also has unique benefits of being ubiquitous in the detection instrument, instead of local effects such as the development of sensor chips in SPR. The media used in this study could also be used in combination with other sensor chips and negate any nonspecific binding trade-off.

3.4.4 Interaction of Multiple Analytes with Media Reagents

Within complex media, molecular crowding has been shown to be important in the theory that underpins molecular interactions [42]. In Section 3.1 and 3.2.1 such considerations were investigated for the ability to block nonspecific binding in multi-ligand systems. These results have demonstrated however, that the modulation of ionic strength must be controlled for each technique. High ionic strength conditions in protein-membrane systems have been shown to be effective (Figure 3.1.7). In the bead-based multiple analysis assays employed, it is suspected that the high concentration of reagents resulted in detrimental effects to the bead-map (Figure 3.3.1) therefore is less unsuitable for this detection method.

As previously stated, simple salts do not directly affect the ambient dielectric constant of water (Oncley 1943). Ionic strength however, has been well characterised to decrease electrostatic interactions that take place between molecules. Charge-charge interactions present the strongest interaction with the largest distance dependence (1/r) (Figure 1.4.1). Ions in the solution (either of salts or the different active reagents employed here) decrease these reactions by shielding the charges. A positive or negatively charged ion will have an electric field decay 1/r however, if

there are other charged ions in close proximity, they will have their own ion cloud of attraction and repulsion and hence electrostatic attractions will be decreased.

The ability to co-incubate albumin (characterised for nonspecific binding) and IL-8 to an anti-IL-8 antibody (characterised for specific binding) resulted in no reduction of the specific binding. The PBS-equivalent Gly-Gly-Gly NaSCN media was also shown to be highly efficacious against the majority of a 27-plex cytokine panel. These results suggest that the mechanism of the media reagents is independent of molecular crowding events when employed at these physiological concentrations.

3.4.5 Summary of intermolecular forces

Within the media reagents employed here, we propose that potentially three main effects are working synergistically. Firstly the thiocyanate ions localise to protein surfaces and increase the local dielectric constant through solvation mediation of the water molecules. Secondly, the ambient dielectric constant of the solvent was increased through the addition of dielectric molecules such as Gly-Gly-Gly, and finally, an increase in ionic strength by virtue of the reagents being present, decreasing charge-charge interactions via ionic shielding (especially in HIS media). These reagents have been shown to elicit their effects independently of one another and to work in collaboration, reducing nonspecific binding, without perturbing specific interactions.

3.4.6 Future Work of Nonspecific Binding Reagents

A rationally designed and tested media system offers an exciting step forward in the utilisation of modern tools by effectively targeting and modulating specific intermolecular forces. These forces have been augmented successfully in both model lipid membrane and commercially available detection systems. Similarly, the

molecules allow identification of the dominant molecular interactions and evolution into different fields, such as protein-protein interactions for folding-pathways, or lipid-lipid interactions in membrane associations. These may include Alzheimer's disease [31, 196], Huntington's disease [197, 198] and prion diseases [165, 199, 200]. The ability to understand the forces that govern these protein-folding interactions may help develop therapeutics to target the protein folding. These could aim to increase the efficacy, or may provide environments in which the proteins can refold. These processes have been targeted previously in Alzheimer's disease [166, 201, 202] and reviewed in [203], however none provide a therapy yet that has significance in the modulation of the disease.

The proposed mode of action, wherein the reagents alter the hydration of the protein and/or surface is of great interest. The water network at the water-lipid interface of membrane bilayers has recently been shown [131, 204]. This work suggests that each membrane architecture has a distinct water network, however the formation and impact of the water has not been fully assessed. Using these reagents, a functional method to characterise the impact of the water network on membrane microdomains can be established.

4 Results

Regulation of membrane microdomain formation: Modulation of lipid head group interactions by targeting specific non-covalent molecular forces

The existence of membrane microdomains (rafts) has been validated through several different experimental techniques, such as fluorescence microscopy [15], AFM [119], sum-frequency generation [97] in model membranes [124] and living membranes [126] (Section 1.8.3) as well as computational modelling [205],. The existence of these domains correlates with specialised localised membrane functions [206]. Some factors that control the assembly and disassembly of microdomains have been observed and characterised, including the lipid acyl chain length and temperature (see Section 1.8.2).

In this chapter, the interactions between the media and the membrane surface are assessed. As discussed previously in Section 1.8.3, interfacial water molecules have been highlighted as a potential causative effect of membrane raft formation [207]. Therefore, the media surrounding the microdomain may affect the raft formation. This analysis is overdue and pivotal to accurate *in vitro* analysis and modelling of biological systems (or biological membranes).

Raft formation has been characterised by using naturally derived lipids, and analysed using fluorescent confocal microscopy to image supported lipid bilayers (SLB) [107]. Orthogonal techniques were then employed, such as AFM and spectral examination of membrane probes in the membrane microdomains in order to understand the physical properties of the membranes.

These studies identify the factors that affect membrane microdomain formation. This will allow us to more faithfully represent aspects of the complex cellular environment and understand the interactions that take place.

The ability to affect the membrane patterning of *in vitro* membranes post-formation, offers scope to increase the complexity of model systems and make interaction studies of membrane proteins or protein: membrane interactions more informative.

4.1 Assessing the Membrane Organisation of Microdomains in the Presence of Soluble Reagents

4.1.1 Spatial Localisation of Membrane Microdomains with Various Lipid Compositions

Fluorescently labelled membrane bilayers can be visualised with laser scanning confocal microscopy through an incorporation of a fluorescent membrane probe FPE. In this study, FPE was employed to examine the effect of reagents on membrane organisation, see Figure 4.1.1 for examples of the images obtained.

Varying the membrane compositions results in different membrane organisations (Section 1.8.2). FPE labelled PC_{100} bilayers form a homogenous bilayer (Section 1.8.2), which results in uniform fluorescence over the membrane surface [124].

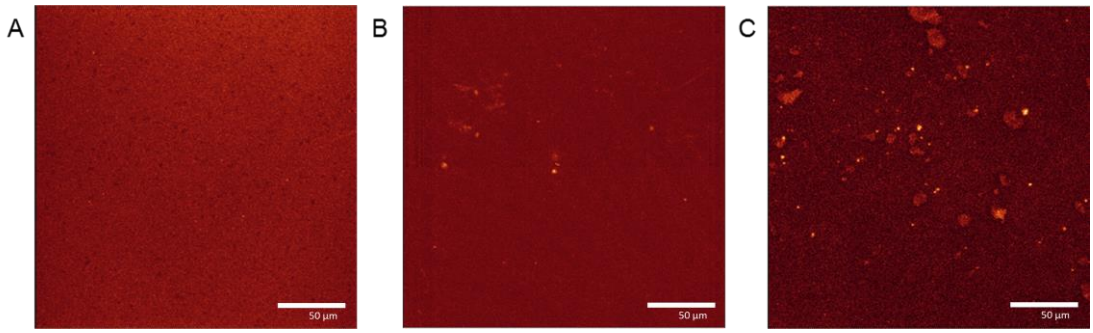


Figure 4.1.1 Fluorescence microscopy of an FPE labelled membrane bilayer in different membrane compositions. (A) A homogeneous bilayer of PC_{100} membranes, (B) A heterogeneous bilayer of $PC_{70}Chol_{30}$ membranes and (C) A heterogeneous bilayer of $PC_{55}Chol_{30}SM_{15}$ membranes. All experiments were conducted in PBS media at pH7.4 at 25°C. Bilayer formation is outlined in Section 2.9 and imaging in Section 2.10.1.

Cholesterol localises with an array of lipids to form more complex structures, leading to the development of microdomains. Increasing concentrations of cholesterol has been shown to result in phase transitions, i.e. the formation of different lipid phases within a bilayer (see Section 1.8.2). Historically, work has been carried out to

characterise different lipid phases by varying the lipid compositions and concentrations of each to form phase diagrams (Figure 1.8.6) [14, 103, 124, 208, 209]. The fluorescent probe employed in the present study is FPE, a fluorescent phospholipid that possesses acyl chains identical to those of DPPE [128]. Therefore FPE is a high Tm lipid that prefers to co-localise with cholesterol, this means that if able, FPE will localise into more ordered L_o domains. The brighter regions shown in Figure 4.1.1B result from tighter packing of the FPE molecules in membrane microdomains, making the domains brighter than the background membrane. Figure 4.1.1C domains are expected to contain different combinations of cholesterol, sphingomyelin and FPE domains. These assumptions arise from previously characterised systems and phase diagrams constructed with the same lipid compositions [124, 208].

Imaging the bilayers over time results in a loss of fluorescence during image capture due to photobleaching. Although these factors have to be monitored and controlled for during image capture, the phenomenon can be used to our advantage in order to investigate certain membrane properties, such as membrane fluidity.

Fluorescence Recovery After Photobleaching (FRAP) experiments (Section 2.10.2) were used to examine the membrane fluidity (Section 2.10.2) and the 2D diffusion coefficients of the fluorophore. This approach also allowed the determination of the photobleaching properties of FPE. The laser power used to photobleach the fluorophore was three-fold greater than the power used for imaging hence photobleaching effects during imaging are less pronounced. To generate statistically viable domain frequencies, each sampled was imaged three times. The position of image acquisition was randomly selected for each sample.

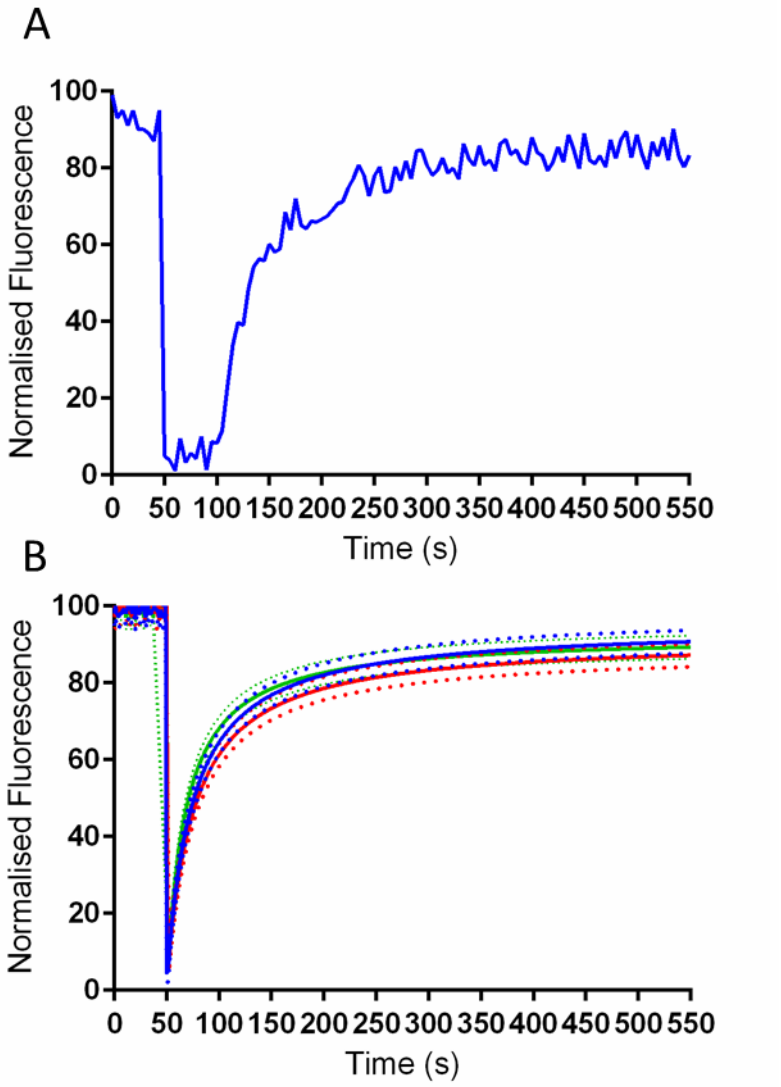


Figure 4.1.2 Fluorescence recovery after photobleaching (FRAP) of lipid vesicles (A) A normalised experimental trace of FRAP of PC_{100} bilayers in PBS (pH7.4) at 25°C. An ROI of 20 µm radius, was photobleached at 75% laser power for 50 s, and fluorescent recovery was observed for 500 s. (B) Analysis of FRAP data from PC_{100} bilayers in different media; PBS (blue), NaSCN (Green) and Gly-Gly-Gly (Red) media (Table 2.2.1) at pH 7.4, experiments were at 25°C. For statistical analysis, the bleach time 50-100 s was removed and the curves were fitted to an exponential curve (solid line). Dotted lines represent ± SD.

Media	Bleach radius (μm)	Fluorescence recovery (%)	Half-time ($t_{½}$) (s)	D ($\mu m^2/s$)
PBS	20	90.2 ± 4.1	34.21 ± 1.91	2.62 ± 0.16
NaSCN	20	89.5 ± 3.3	41.28 ± 2.95	2.17 ± 0.18
Gly-Gly-Gly	20	87.9 ± 5.3	34.01 ± 2.01	2.64 ± 0.16

Table 4.1.1. Membrane fluidity calculated using FRAP. The 2D diffusion coefficient was calculated from the FRAP data using the Soumpasis equation (Equation 2.10.1).

Membrane fluidity is denoted by the diffusion coefficient (D), calculated by the Soumpasis equation (Equation 2.10.1) (Section 2.10.2). Half-time recovery ($t_{½}$) values were calculated by fitting a single exponential to the fluorescence recovery (>50 s). FRAP of the PC_{100} membranes (Table 4.1.1) showed a recovery time in agreement with the values defined in the literature for membranes of the same composition [102]. Following a one-way ANOVA, the different lipid compositions or media employed throughout the experiments did not significantly ($p<0.05$) affect the fluidity of the fluorescence microscopy SLBs.

4.1.2 Assessing factors that affect membrane microdomain formation with FPE-labelled SLBs

Following this, the membrane organisations of various lipid compositions were examined with different soluble reagents in the media. These reagents have previously been used to affect the intermolecular forces that govern protein interactions by potentially affecting the water network on the membrane surface (Section 3.1). It has recently been proposed that the water structure of different

membrane microdomains varies extensively [131, 146] hence, changes in the media may affect the lipid organisation observed.

Two different media compositions (Table 2.2.1) were substituted for PBS, NaSCN containing media and Gly-Gly-Gly containing media. Media were replaced during membrane vesicle creation and all subsequent steps to ensure that the media reagents were equally dispersed on both sides of the membrane bilayer. Changes in the media mid-SLB formation may affect the formation efficacy of the membrane (Section 2.9). Images were taken over three different areas of a sample replicated in three membrane batches in order to ensure that the effects are representative.

4.1.2.1 *PC_{100} Membranes*

The probe incorporation and dispersity into the membrane and microdomains was validated by the addition of 2mM Ca^{2+} in the form of $CaCl_2$ (Figure 4.1.3). The addition of calcium ions to the bilayer resulted in a uniform increase in fluorescence. These results demonstrate that the FPE probe is responding to the electrostatic membrane surface potential. The positive charges of the calcium ions adsorbing to the membrane causes an electropositive change in Ψs; this results in the FPE probe deprotonation and subsequently an observed increase in fluorescence is observed [51] (Section 1.9.1.2). These effects were similar across all the media employed, with a representative PBS image shown in Figure 4.1.3.

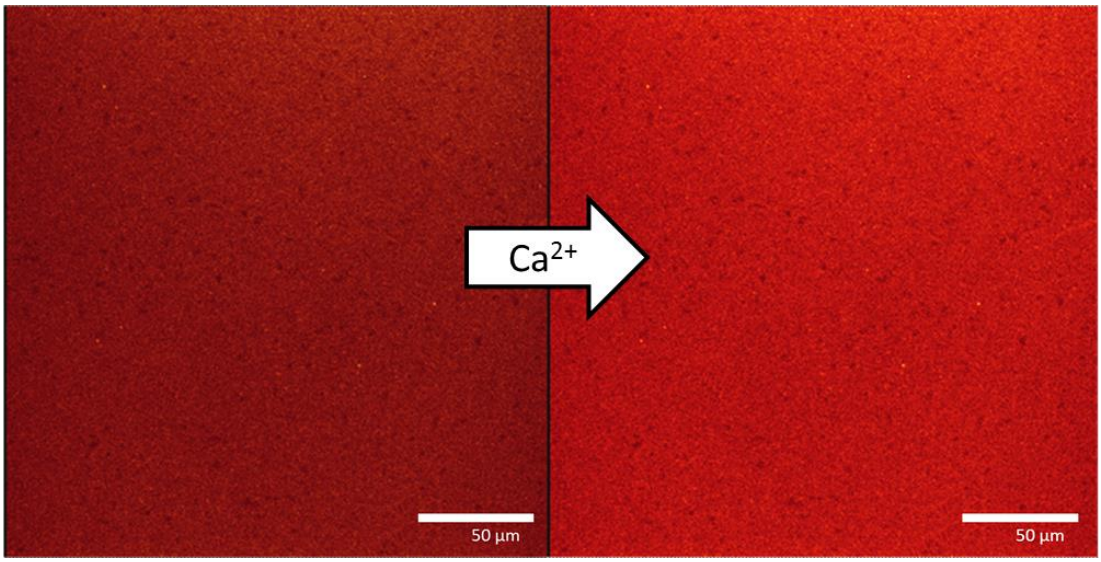


Figure 4.1.3. Confocal microscopy image of an FPE labelled PC_{100} bilayer before and after the addition of 2mM Ca^{2+} in the form of 1M $CaCl_2$. Experiments were conducted in PBS at pH7.4, at 25°C.

Membrane images were quantified as described in Section 2.10.3, with histograms shown in Figure 4.1.5.

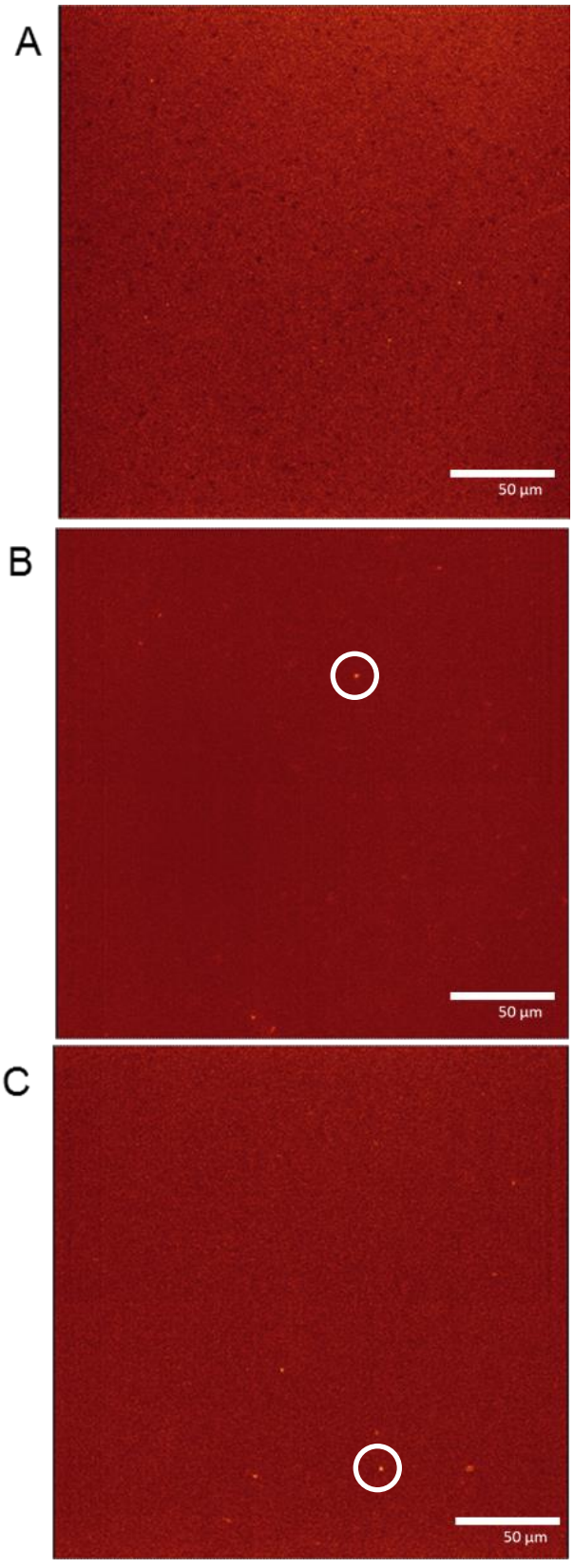
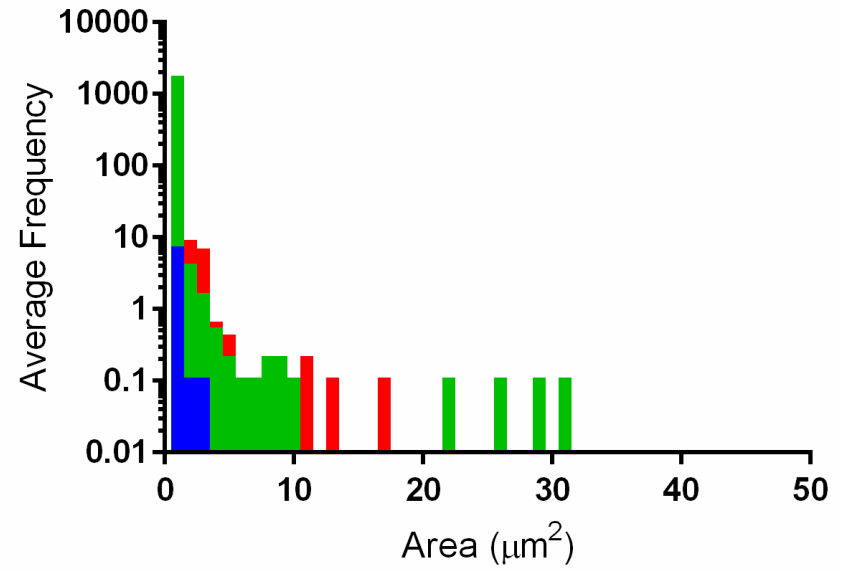


Figure 4.1.4. Average z-projection of confocal image stacks with FPE labelled PC_{100} membranes. (A) PBS, (B) NaSCN and (C) Gly-Gly-Gly media (Table 2.2.1) at pH7.4. Experiments were conducted at 25°C. Images are representative of membrane condition, n=9. Images 238 x 238 µm, scale bar shown 50 µm. White circles in (B) and (C) highlight membrane microdomains.



Media	Total Number of Regions	Total Micro-domain Area (μm²)	Total Membrane Area (μm²)	Average Micro-domain Size (μm²)	% Coverage
PBS	2039	5098	509796	2.5	0.01
NaSCN	64590	285486	509796	4.42	0.56
Gly-Gly-Gly	148833	443523	509796	2.98	0.87

Figure 4.1.5 Distribution of membrane microdomains in FPE labelled PC_{100} supported lipid bilayer (SLB). The histogram shows the size of microdomains shown in Figure 4.1.4, in different media. Blue = PBS, Green = NaSCN, Red = Gly-Gly-Gly, (Table 2.1.1) at pH7.4, experiments were conducted at 25°C. Images from 238 x 238 μm, each sample imaged three times and repeated in three samples (n=9). Table of statistics obtained from image analysis.

PBS PC_{100} membranes are homogeneous across the majority of samples imaged, denoted by 0.01% microdomain coverage (Figure 4.1.4, Figure 4.1.5). These results are consistent with the current literature [123, 124]. The phase diagram of ^{12}BrPC/DPPC/cholesterol systems at 25°C, (see Figure 1.8.6) gives an approximation of the phases present in the PC bilayers used. Binary mixtures of PC with different acyl chains are able to have two separate phases, liquid disordered, l_d and gel phase P_{β}'. These phases only occur when saturated lipids (such as DPPC) represent > 80% of the membrane composition resulting in the formation of small gel phases (Figure 1.8.6) [208]. The PC_{100} composition employed here only has ~55% of lipid with saturated acyl chains (32.1% DPPC, Table 2.1.1). Hence, any domains visualised are

not formed by the properties of the lipid acyl chains, which is illustrated in Figure 4.1.4, where the PC_{100} membranes are homogenous in PBS.

The substitution of media with NaSCN or Gly-Gly-Gly resulted in the observation of a small population of microdomains (Figure 4.1.4). These microdomains covered ~0.56% and 0.87% of the bilayer for NaSCN and Gly-Gly-Gly respectively (highlighted by white circles in Figure 4.1.4). The microdomain formation may be explained by an altered headgroup interaction between the PC lipids in order to pack more tightly. This may result in the formation of a gel phase microdomain consisting of DPPC and DSPC present in the lipid mixture (Table 2.1.1) preferentially associating with the DPPE acyl-chain analogue of FPE. Alternatively, it may be the FPE, which upon sensing the electrostatic surface potential of the membrane (see Section 1.9.1.2, Figure 1.9.3) may have augmented the local interaction with nearby lipids causing it to increase in fluorescence intensity.

4.1.2.2 *$PC_{70}Chol_{30}$ Membranes*

$PC_{70}Chol_{30}$ membranes were shown to form heterogeneous membranes with distinct microdomains in PBS media (Figure 4.1.8A), as reported previously [4, 124, 208]. The membranes have been shown to be fluid by FRAP experiments (Figure 4.1.2), where lipids are expected to associate and dissociate into longer lived microdomain structures. The FPE in both the lipid background and the membrane microdomains was shown to respond to the electrostatic membrane potential. This was characterised by an increase in fluorescence following the addition of calcium ions (Figure 4.1.6).

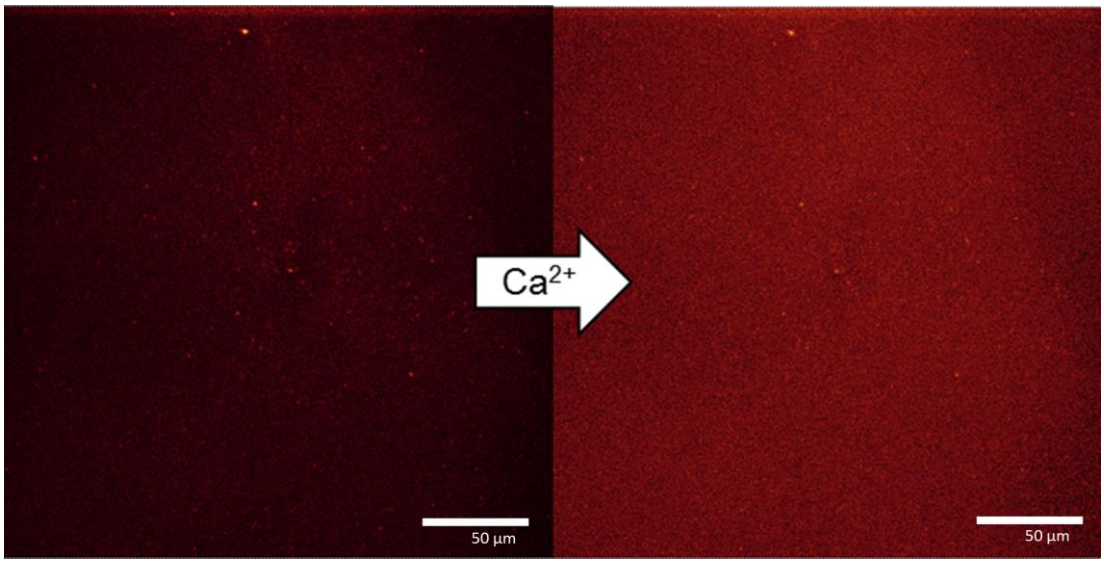


Figure 4.1.6. Confocal microscopy of an FPE labelled $PC_{70}Chol_{30}$ bilayer before and after the addition of 2mM Ca^{2+} in the form of 1M $CaCl_2$. Experiments were conducted in PBS pH7.4 at 25°C.

The phase diagram of ^{12}BrPC/DPPC/cholesterol systems at 25°C, see Figure 1.8.6, give an approximation of phases present in the $PC_{70}Chol_{30}$ bilayers used. With approximate ratios of unsaturated PC (45%): saturated PC (55%) in the naturally derived PC (Table 2.1.1), and 30% cholesterol, the membrane should exhibit two phases, the liquid disordered phase, l_d and the liquid ordered phase, l_o. Decreasing the proportion of cholesterol, or increasing the proportion of saturated lipids has been characterised to exhibit three phases, l_o, l_d and P_β'. Figure 4.1.8 denotes a representative fluorescence microscopy image of $PC_{70}Chol_{30}$ membranes in different electrolyte media. In all three media conditions, the membrane is heterogeneous with microdomains of the same intensity. This is demonstrated by the histogram of domain brightness depicted in Figure 4.1.7.

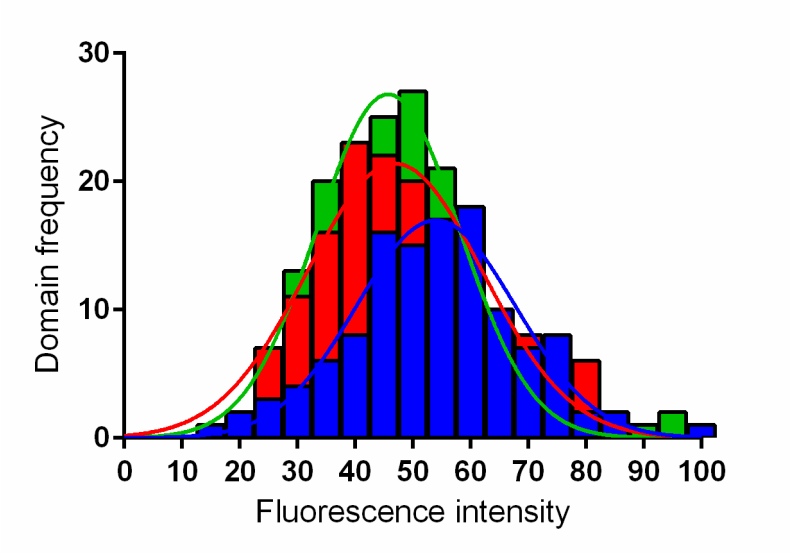


Figure 4.1.7. A histogram of $PC_{70}Chol_{30}$ microdomain fluorescence intensity in different media. Blue= PBS, red= NaSCN and green= Gly-Gly-Gly) at pH7.4. Fluorescence intensity is normalised between each membrane. Gaussian distribution fits shown as fitted line.

Figure 4.1.7 demonstrates that the $PC_{70}Chol_{30}$ membranes in all media conditions have a unimodal distribution of fluorescence. An F-test was carried out to compare a single Gaussian to a sum of two Gaussians where the data was best fitted to a single Gaussian (all $R^2 > 0.95$, $p<0.05$). This suggests that two phases are present, l_o microdomains on a background of l_d. Due to the tighter packing of gel phase, P_β', and the preference of FPE to form these domains, they are expected to be brighter than l_o domains, if present.

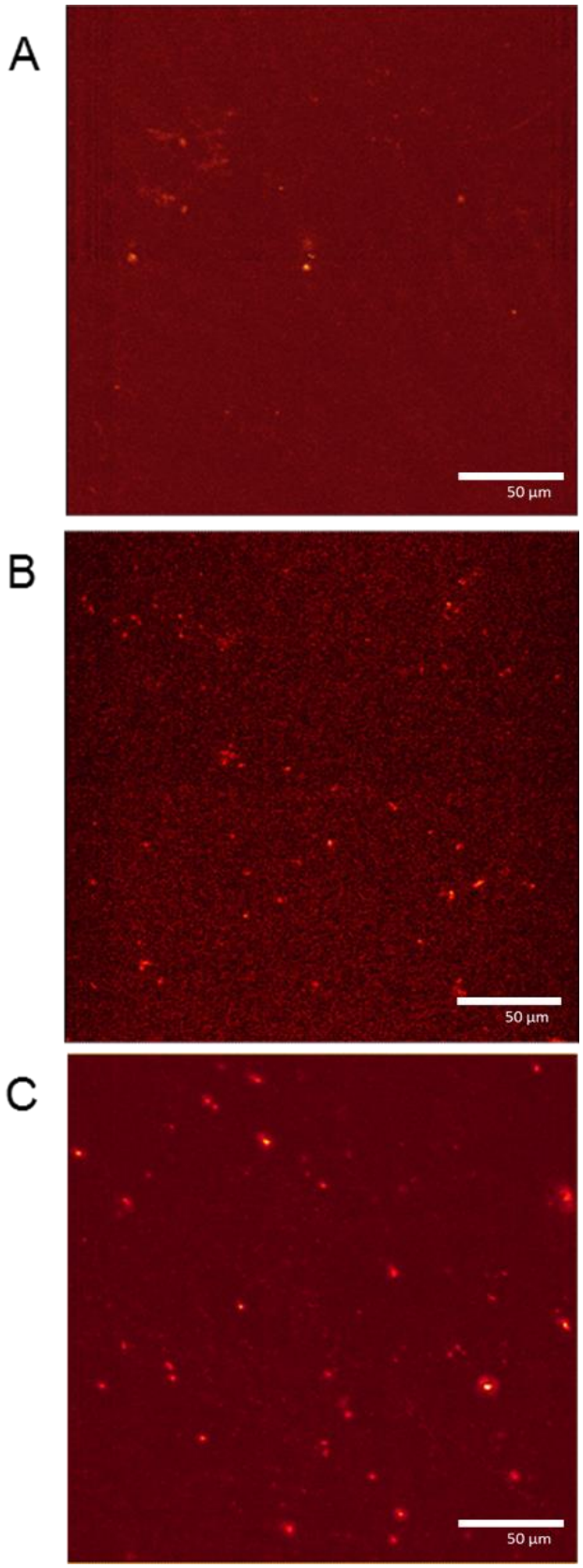
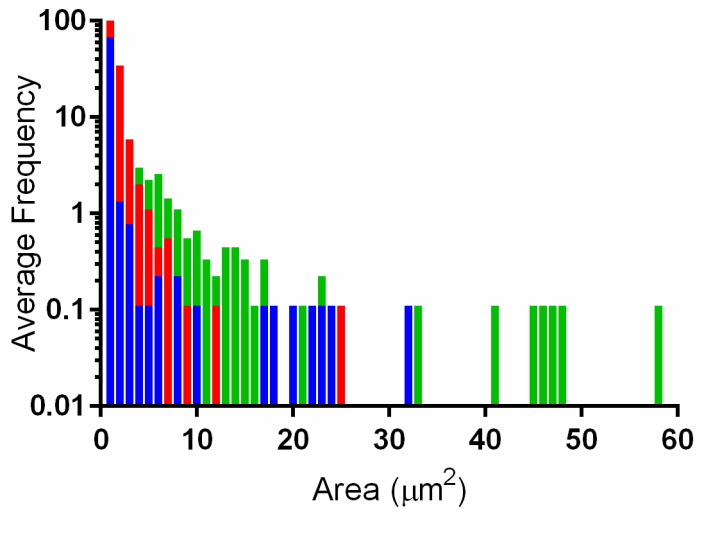


Figure 4.1.8. Average z-projection of confocal image stacks with FPE labelled $PC_{70}Chol_{30}$ membranes. (A) PBS, (B) NaSCN and (C) Gly-Gly-Gly media at pH7.4. Experiments were conducted at 25°C. (Table 2.2.1) Images are representative of membrane condition, n=9. Images 238 x 238 µm, the scale bar is 50 µm.



Media	Total Number of Regions	Total Micro-domain Area (μm^2)	Total Membrane Area (μm^2)	Average Micro-domain Size (μm^2)	% Coverage
PBS	29828	224310	509796	7.52	0.44
NaSCN	2626370	1610955	509796	6.14	3.16
Gly-Gly-Gly	509796	953319	509796	2.59	1.87

Figure 4.1.9 Distribution of membrane microdomains in FPE labelled $PC_{70}Chol_{30}$ supported lipid bilayer (SLB). The histogram shows the size of microdomains shown in Figure 4.1.4 in different media. Blue = PBS, Green = NaSCN, Red = Gly-Gly-Gly, (Table 2.1.1) at pH7.4. Experiments were conducted at 25°C. Images from 238 x 238 μm, each sample was imaged three times and repeated in three samples (n=9). Table of statistics obtained from image analysis.

The images obtained from the heterogeneous membranes shown in Figure 4.1.8 can be quantified for the domain formation in different media (Figure 4.1.9). NaSCN promotes the formation of more domains than Gly-Gly-Gly, with a six-fold and four-fold increase in domain coverage with the two different treatments respectively (Figure 4.1.9). Although NaSCN slightly decreases the mean domain size (7.25 μm^2 to 6.14 μm^2), Figure 4.1.9 demonstrates that both large and small populations of domains are greatly increased. Gly-Gly-Gly leads to an increase in the population of smaller domains only; this suggests that the increase in domain size may be through different mechanisms (discussed later).

An increase in the total membrane coverage suggests that both reagents are altering the lipid interactions, such as to have an effect on the aggregation of the lipids. Given that there is no evidence for the formation of a third distinct phase, the reagents are likely to alter the head-group interaction between the PC and cholesterol lipids. Cholesterol has been demonstrated to associate with lipids with a variety of stoichiometry and geometries, where cholesterol has been shown to associate with PC phospholipids in a tight 1:1 ratio, or loosely associate with two lipids in a 1:2 ratio [47, 119, 210]. These stoichiometries are dependent on the hydrogen bonding of the α or β-face of the cholesterol molecule (Figure 1.8.2). Employing reagents that alter these interactions may shift the bonding to favour 1:1 interactions, which would result in a tighter packing of cholesterol to saturated lipids to form smaller microdomains or favour 1:2 interactions, which may allow binding of more saturated or unsaturated PC lipids with cholesterol to form larger domains. Without molecular simulations of the different possible scenarios, nor the experimental analysis of a range of pure lipid systems, the biophysical answer is difficult to elucidate, this study provides the first evidence that these headgroup interactions may drive the formation of new, larger, or previously unfavourable domains.

4.1.2.3 $PC_{55}Chol_{30}SM_{15}$ Membranes

Cell membranes have a complex make up of several different lipids (Section 1.8). To model this *in vitro* membranes of increasing complexity were examined. Sphingomyelin has different properties to the phospholipids and cholesterol that have been employed so far, thus increasing the chemical complexity of the SLB and modelling more cell-like conditions in which a variety of lipids are present [211].

The FPE-labelled $PC_{55}Chol_{30}SM_{15}$ membranes are heterogeneous, with the larger numbers of fluorescent patches indicating the presence of microdomains see Figure

4.1.10. The addition of calcium ions, in the form of calcium chloride resulted in a uniform increase in fluorescence across the membrane. Thus, the FPE present in the different membrane architecture responded equally to the more electropositive membrane surface in all media conditions tested.

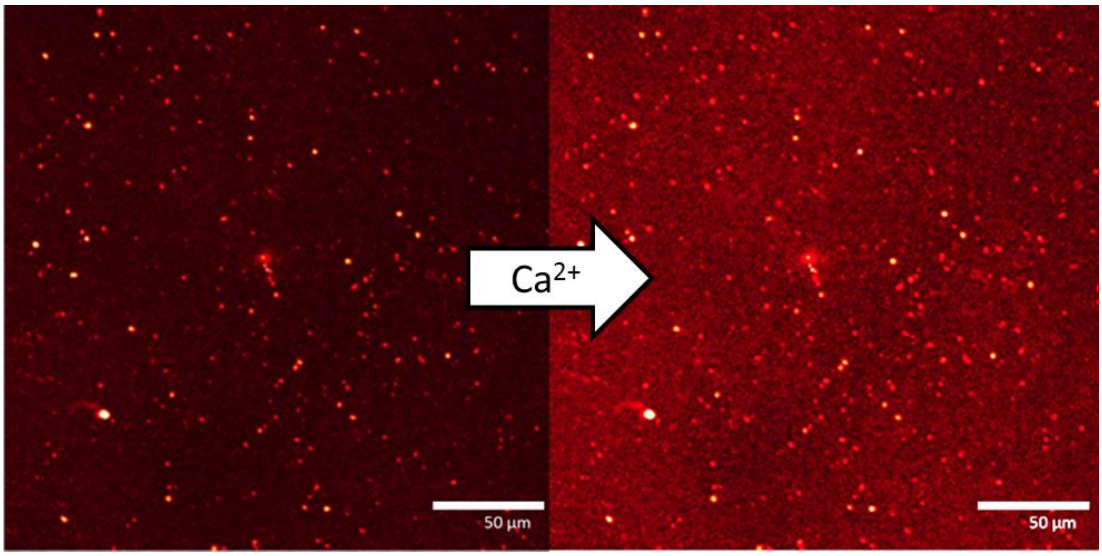


Figure 4.1.10. Confocal microscopy of an FPE labelled $PC_{55}Chol_{30}SM_{15}$ bilayer. The addition of 2mM Ca^{2+} in the form of 1M $CaCl_2$. Media contained Gly-Gly-Gly (Table 2.2.1) at pH7.4. Experiments were conducted at 25°C.

The presence of sphingomyelin in the bilayer has previously been shown to form microdomains in the absence of cholesterol therefore, the FPE is likely to accumulate in microdomains with cholesterol and sphingomyelin simultaneously and independently [106]. Phase diagrams have been established with POPC as a representative low-melting point lipid, cholesterol and SM as a high melting point lipid, see Figure 1.8.7 [106, 107]. These classical phase diagrams, unfortunately, do not accurately model the complexity needed for the naturally derived lipids used in these systems. The naturally derived PC contains a variety of high T_m and low T_m lipids (Table 2.1.1). When combined with sphingomylein, the lipid compositions are too complex to characterise into phase diagrams or be computationally model.

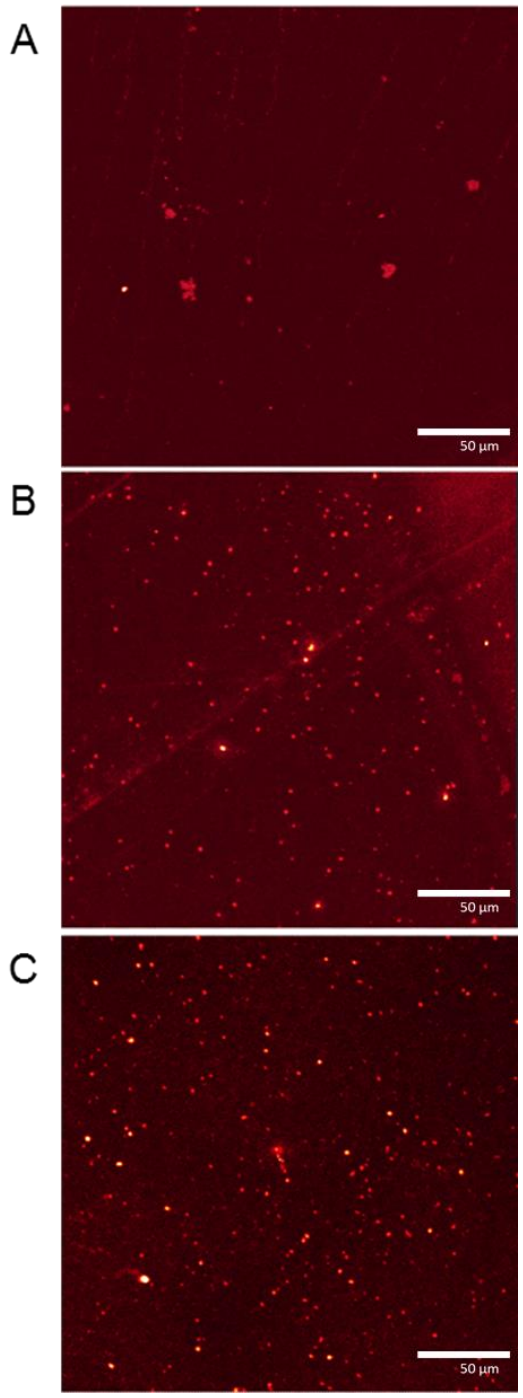


Figure 4.1.11. Average z-projection of confocal image stacks with FPE labelled $PC_{55}Chol_{30}SM_{15}$ membranes. (A) PBS, (B) NaSCN and (C) Gly-Gly-Gly media at pH7.4. Experiments were conducted at 25°C. (Table 2.2.1) Images representative of membrane condition, n=9. Images 238 x 238 µm, scale bar shown in (A) 47.62 µm.

The membrane formation shown in PBS suggests that there are three phases with two distinct microdomains 'floating' on a background of the third lipid phase. The different fluorescence intensity between different microdomains, donated in Figure

4.1.11A, demonstrates that there are two clear microdomains. The different media conditions appear to maintain the two different domain types. The fluorescent intensity of the domains was fitted to the Gaussian distribution function, where the data was best shown to fit to a sum of two Gaussians ($P<0.05$, $R^2>0.9$) (Figure 4.1.12).

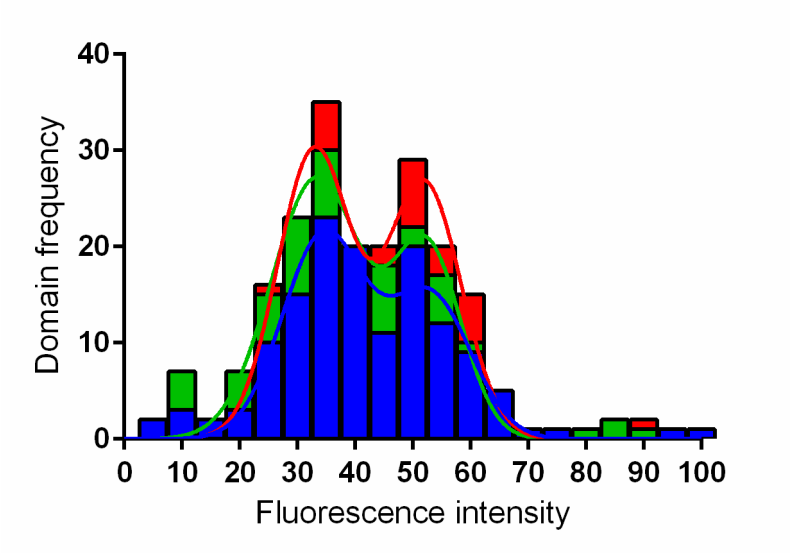
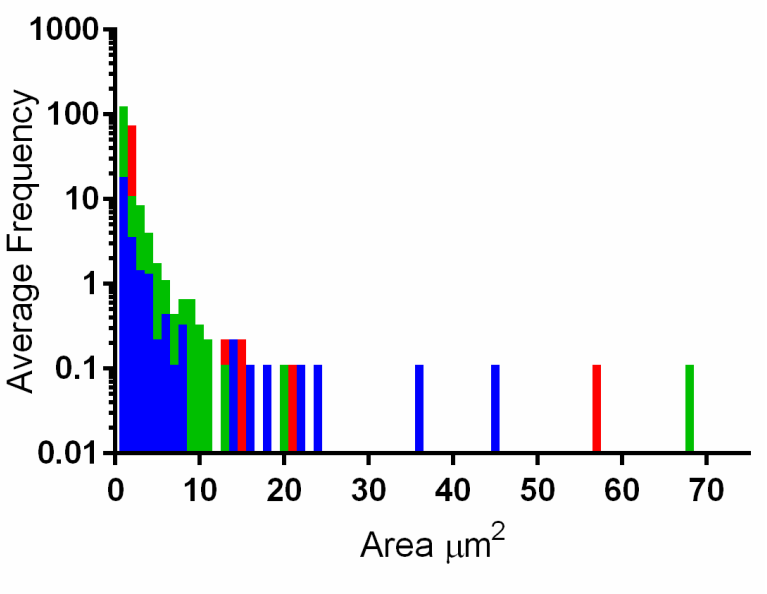


Figure 4.1.12. A histogram a $PC_{55}Chol_{30}SM_{15}$ membrane microdomain fluorescence intensity in different media. Blue= PBS, red= NaSCN and green= Gly-Gly-Gly at pH7.4. Fluorescence intensity is normalised between each membrane. Gaussian distribution fitted shown as fitted line.

The differences in intensities suggest that the FPE is packed tighter into some microdomains than others. Given the saturated acyl-chains present in sphingomyelin (Figure 1.8.2), the lipids preferentially form gel-phase microdomains with other saturated lipids such as DPPC, DSPC and the DPPE acyl-chain analogue of FPE.



Media	Total Number of Regions	Total Micro-domain Area (μm²)	Total Membrane Area (μm²)	Average Micro-domain Size (μm²)	% Coverage
PBS	67028	361955	509796	5.4	0.71
NaSCN	225501	876849	509796	3.88	1.72
Gly-Gly-Gly	726197	1835266	509796	2.52	3.60

Figure 4.1.13 Distribution of membrane microdomains in the FPE labelled $PC_{55}Chol_{30}SM_{15}$ supported lipid bilayer (SLB). The histogram shows the size of microdomains shown in Figure 4.1.4, in different media. Blue = PBS, Green = NaSCN, Red = Gly-Gly-Gly, (Table 2.1.1) pH7.4 at 25°C. Images from 238 x 238 μm, each sample imaged three times and repeated in three samples (n=9). Table of statistics obtained from image analysis.

In the different media employed, the microdomains domain coverage was increased in both NaSCN and Gly-Gly-Gly containing medium compared to PBS (Figure 4.1.13). Proportionally, the PBS membranes have a higher mean microdomain size than microdomains formed in NaSCN media, although there is a clear increase in the population of large domains in the presence of NaSCN (Figure 4.1.13). It can be assumed that the decrease in average size is attributed to an increase in the smaller domains compared to larger domains (Figure 4.1.13). Gly-Gly-Gly resulted in the largest microdomain coverage increase in sphingomyelin-containing membranes however, domains in Gly-Gly-Gly medium were approximately half the size of

domains in PBS. This effect of Gly-Gly-Gly is the same as in $PC_{70}Chol_{30}$ membranes; where there was an increase in the population of smaller domains only (illustrated in Figure 4.1.13).

Recently, simulation studies have shown the importance of electrostatic interactions of SM to related lipids and sterols [211-213]. It has been suggested by Bjorkbom *et al.*, that an increase in head group size resulted in a decrease of the main transition temperature [212], deduced by atom-scale molecular dynamic simulations and fluorescence anisotropy experiments. These results also showed that increasing the size of the head group (with associated increase in hydrogen bonds with water and close lipids) resulted in the formation of ordered-cholesterol containing microdomains. These simulations expand on the initial work of Pandit *et al.* [214] who demonstrated that interfacial electrostatic interactions are important for stabilising cholesterol interactions with SMs. Based on the observations reported in the literature it can be inferred that in the system employed here, that the media reagents potentially alter the headgroup interactions between the lipids, subsequently affecting their packing.

4.1.3 Assessing factors that affect membrane microdomain formation with Di-8-ANEPPS labelled SLBs

Differential packing of the FPE probe with lipids in the bilayer forms the fluorescent microdomains. The excitation spectra of Di-8-ANEPPS is altered when it orientates with the dipoles of phospholipids and/or sterols in the bilayer; this leads to electronic redistribution within the probe resulting in a red/blue shift in the excitation spectra [141]. At the spectral range used here, only the excited (membrane incorporated) fluorescence is detectable. The different lipids employed in this study have been shown to alter the dipole potential of the membrane [205, 215]. In a lipid vesicle

system, a ratio of dual-fluorescence is monitored. The ratio of the λ_{ex} maximum and λ_{ex} minimum allows for monitoring of the dipole potential, and controls for variations in light scattering or variations n the dye concentration [72, 145, 216]. Utilising SLBs negates any light-scattering artefacts. The dye concentration is controlled between experiments, and the absolute fluorescence intensity is not compared between samples. Therefore, the distribution of fluorescence intensity can be monitored for changes in dipole potential resulting from changes in membrane composition and medium composition.

4.1.3.1 *PC_{100} membranes*

The Di-8-ANEPPS labelled PC_{100} bilayer exhibit a homogenous layer of fluorescence in the same fashion as FPE-labelled PC_{100} membranes. Therefore, the presence of any fluorescence is validation that the probe is incorporated into the membrane (Figure 4.1.14).

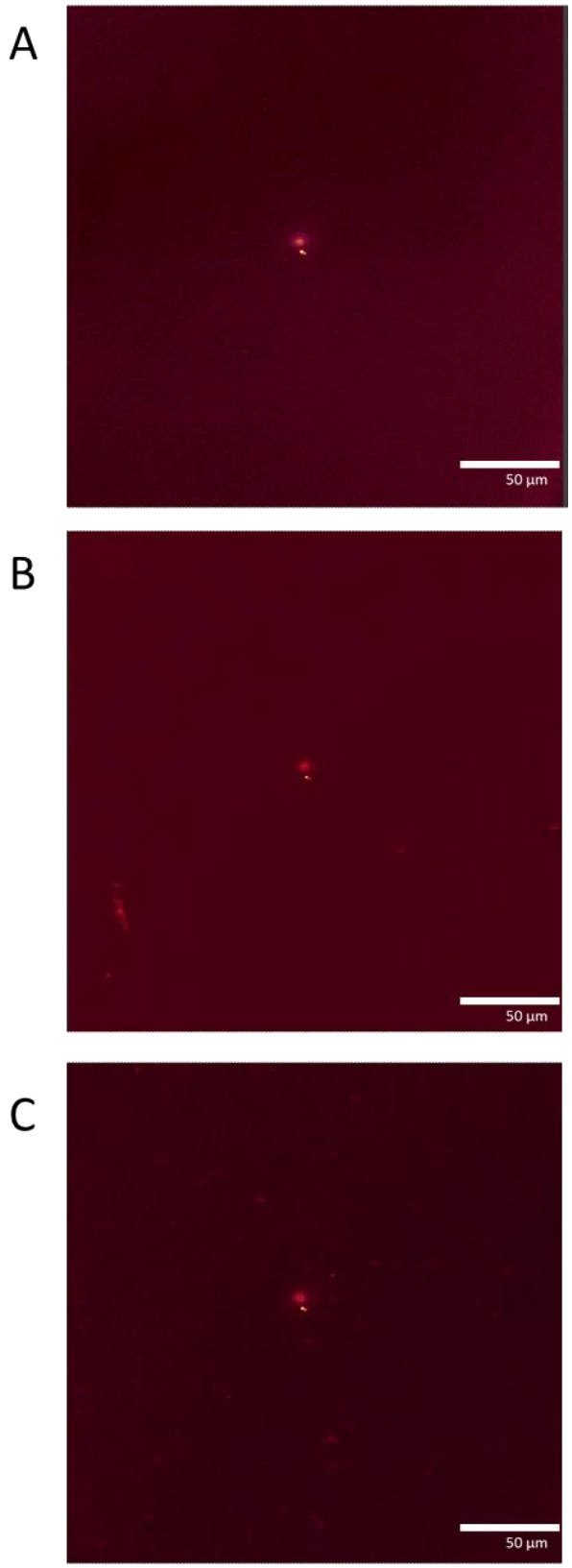
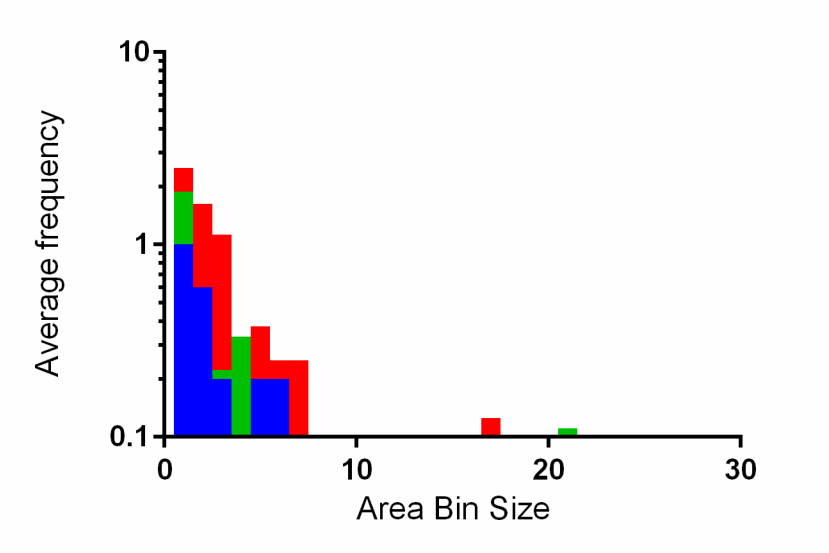


Figure 4.1.14. Average z-projection of confocal image stacks with Di-8-ANEPPS labelled PC_{100} membranes. (A) PBS, (B) NaSCN and (C) Gly-Gly-Gly media (Table 2.2.1) at pH7.4. Experiments were conducted at 25°C. Images are representative of membrane condition, n=9. Images 238 x 238 µm, scale bar shown 50 µm. An optical aberration is present in all images using Di-8-ANEPPS, which is subsequently removed from the analysis

The large central spot, illustrated in Figure 4.1.14, is conserved in all images using Di-8-ANEPPS as the fluorescent probe. This is an optical aberration from the fluorescent microscope settings used to capture the image. During image analysis, an exclusion mask was placed around the aberration to remove it from quantification.



Media	Total Number of Regions	Total Micro-domain Area (µm²)	Total Membrane Area (µm²)	Average Micro-domain Size (µm²)	% Coverage
PBS	11	36	509796	3.27	7.0E-05
NaSCN	23	43	509796	1.87	8.0E-05
Gly-Gly-Gly	52	192	509796	3.69	4.0E-04

Figure 4.1.15. Distribution of membrane microdomains in Di-8-ANEPPS labelled PC_{100} supported lipid bilayer (SLB). The histogram shows the size of microdomains shown in Figure 4.1.4, in different media. Blue = PBS, Green = NaSCN, Red = Gly-Gly-Gly, (Table 2.1.1) at pH7.4, experiments were conducted at 25°C. Images from 238 x 238 µm, each sample imaged three times and repeated in three samples (n=9). Table of statistics obtained from image analysis.

The PC_{100} membranes in PBS were homogenous. In the different media (Gly-Gly-Gly and NaSCN), the incidence of microdomain was not substantially different (Figure 4.1.5). The distributions of the domain sizes were similar to FPE-labelled microdomains (Figure 4.1.5). The mean microdomain sizes was 3.27 µm^2 for PBS media, 1.87 µm^2 for NaSCN media and 3.69 µm^2 for Gly-Gly-Gly media. The

structure of Di-8-ANEPPS and its incorporation into the membrane beneath the phospholipid head groups (Figure 1.9.3), means that the probe is unlikely to segregate into microdomains, like the FPE probe, but Di-8-ANNEPS will sense local dipole changes of nearby microdomains [72, 217, 218].

Figure 4.1.15 demonstrates the coverage of domains using the Di-8-ANEPPS probe is (0.000063%) and effectively zero, in all conditions, therefore the membranes are viewed as homogenous. Any differences in domain percentage are noise within the assay.

4.1.3.2 *$PC_{70}Chol_{30}$ membranes*

The Di-8-ANEPPS labelled $PC_{70}Chol_{30}$ membranes had a heterogeneous distribution of fluorescence similar to FPE-labelled $PC_{70}Chol_{30}$ membranes (Figure 4.1.8). Figure 4.1.16 illustrates the $PC_{70}Chol_{30}$ membranes were heterogeneous in all the media employed. At the wavelengths examined, the presence of fluorescence in the bilayer validates the insertion of the Di-8-ANEPPS dye into the membrane. The heterogeneity of the membrane arises from the Di-8-ANEPPS probe responding to areas of different magnitude of membrane Ψ_d than in the bilayer. Cholesterol has been shown to increase the magnitude of Ψd, which suggests that the brighter patches of the membrane are representative of cholesterol-containing microdomains [205, 215].

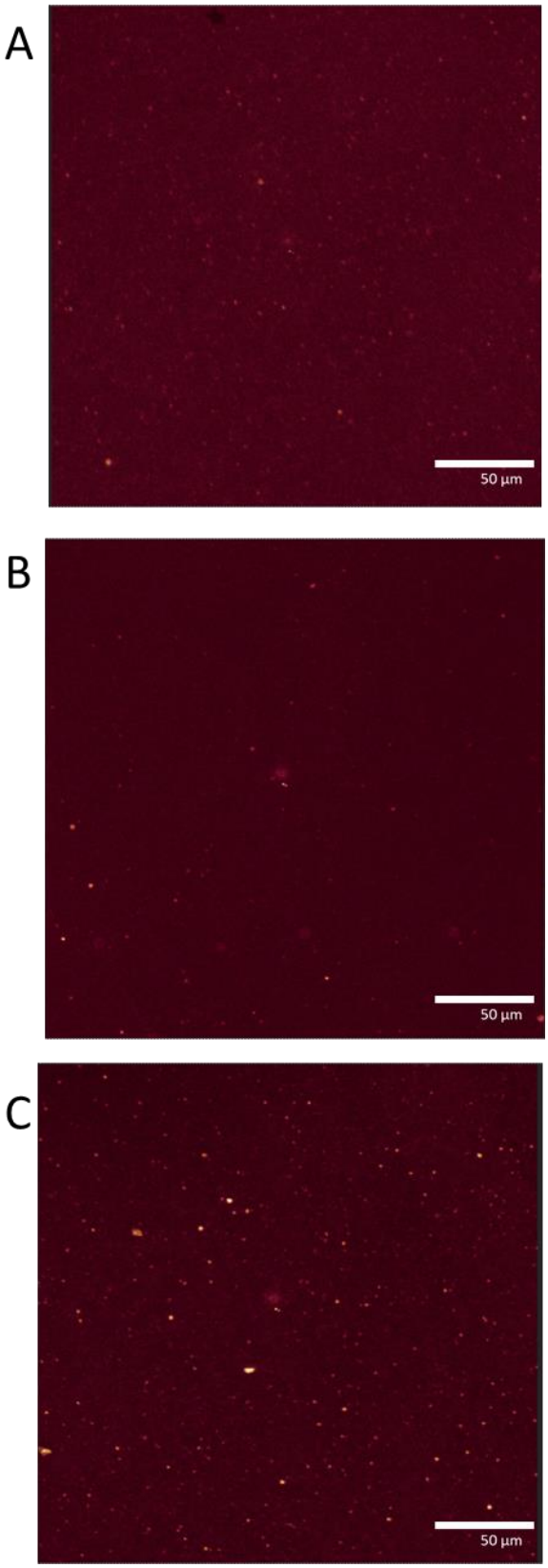
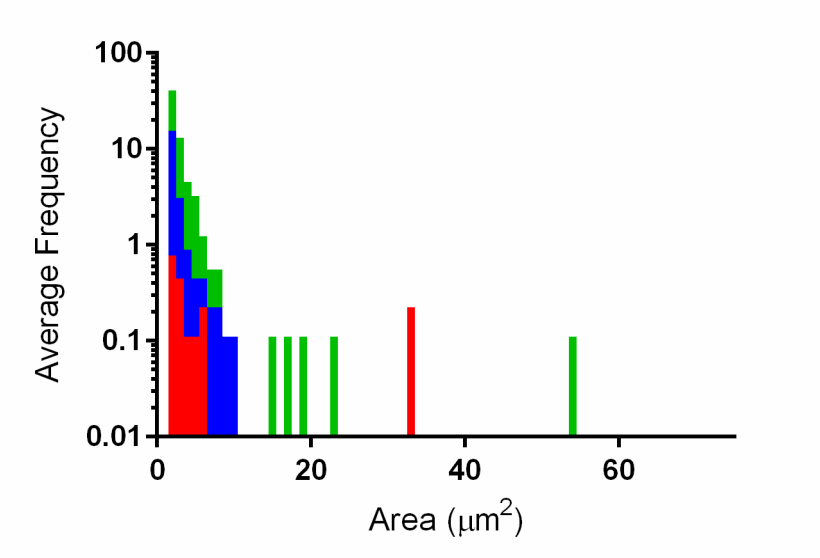


Figure 4.1.16. Average z-projection of confocal image stacks with Di-8-ANEPPS labelled $PC_{70}Chol_{30}$ membranes. (A) PBS, (B) NaSCN and (C) Gly-Gly-Gly media at pH7.4. Experiments were conducted at 25°C. (Table 2.2.1) Images are representative of membrane condition, n=9. Images 238 x 238 µm, the scale bar is 50 µm.



Media	Total Number of Regions	Total Micro-domain Area (μm^2)	Total Membrane Area (μm^2)	Average Micro-domain Size (μm^2)	% Coverage
PBS	826	4919	509796	4.79	0.96
NaSCN	341	541	509796	1.58	0.11
Gly-Gly-Gly	3314	16928	509796	5.11	3.32

Figure 4.1.17. Distribution of membrane microdomains in Di-8-ANEPPS labelled $PC_{70}Chol_{30}$ supported lipid bilayer (SLB). The histogram shows the size of microdomains shown in Figure 4.1.4 in different media. Blue = PBS, Green = NaSCN, Red = Gly-Gly-Gly, (Table 2.1.1) at pH7.4, experiments were conducted at 25°C. Images from 238 x 238 μm, each sample imaged three times and repeated in three samples (n=9). Table of statistics obtained from image analysis.

The number of domains present in PBS $PC_{70}Chol_{30}$ membrane as detected by Di-8-ANEPPS and FPE is similar, with comparable microdomain size and coverage of the membrane (Figure 4.1.9 and Figure 4.1.17). This suggests that both probes are detecting the presence of tightly packed cholesterol microdomains. FPE detects the microdomains by preferential inclusion into the domain whereas; Di-8-ANEPPS detects microdomains by the increase in dipole potential in the presence of cholesterol [215, 219]. Figure 4.1.18 demonstrates the fluorescence intensity of the microdomain was shown to fit to a unimodal Gaussian distribution, demonstrating that two phases are present in the membrane; a background l_d phase and l_o

microdomains. The different media used did not significantly alter the fluorescent intensity distribution of the microdomains (Figure 4.1.18 ($p>0.05$)).

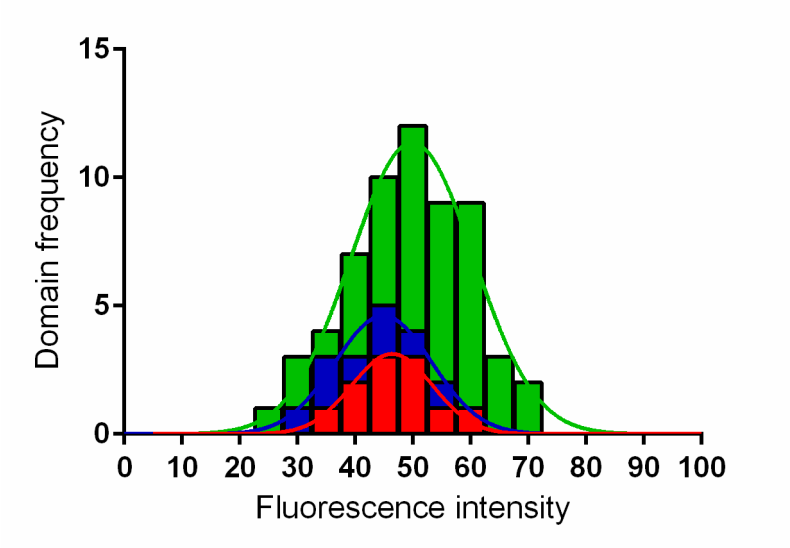


Figure 4.1.18. A histogram a $PC_{70}Chol_{30}$ membrane microdomain fluorescence intensity in different media. Blue= PBS, red= NaSCN and green= Gly-Gly-Gly at pH7.4. Fluorescence intensity is normalised between each membrane. Gaussian distribution fitted shown as fitted line.

The number of domains increases in the presence of Gly-Gly-Gly (as shown with the FPE probe (Figure 4.1.9)) and the domain coverage increases approximately three-fold (Figure 4.1.17). The average microdomain size between the conditions remained similar, which suggests that the increase in microdomain coverage is dependent on the domain frequency, instead of increased domain size. Interestingly, the number of domains decreases in the presence of NaSCN when detected by Di-8-ANEPPS (Figure 4.1.17) and the domain coverage in the presence of NaSCN decreases approximately 10-fold (Figure 4.1.17).

4.1.3.3 ***$PC_{55}Chol_{30}SM_{15}$ membranes***

The Di-8-ANEPPS labelled $PC_{55}Chol_{30}SM_{15}$ membranes had a heterogeneous distribution of fluorescence comparable to that of the $PC_{70}Chol_{30}$ Di-8-ANEPPS labelled membranes and the $PC_{55}Chol_{30}SM_{15}$ FPE-labelled membranes. Figure 4.1.19 illustrates that the intensity of fluorescence between the microdomains was not the same suggesting that multiple dipole moments are present in the same bilayer in distinct domains.

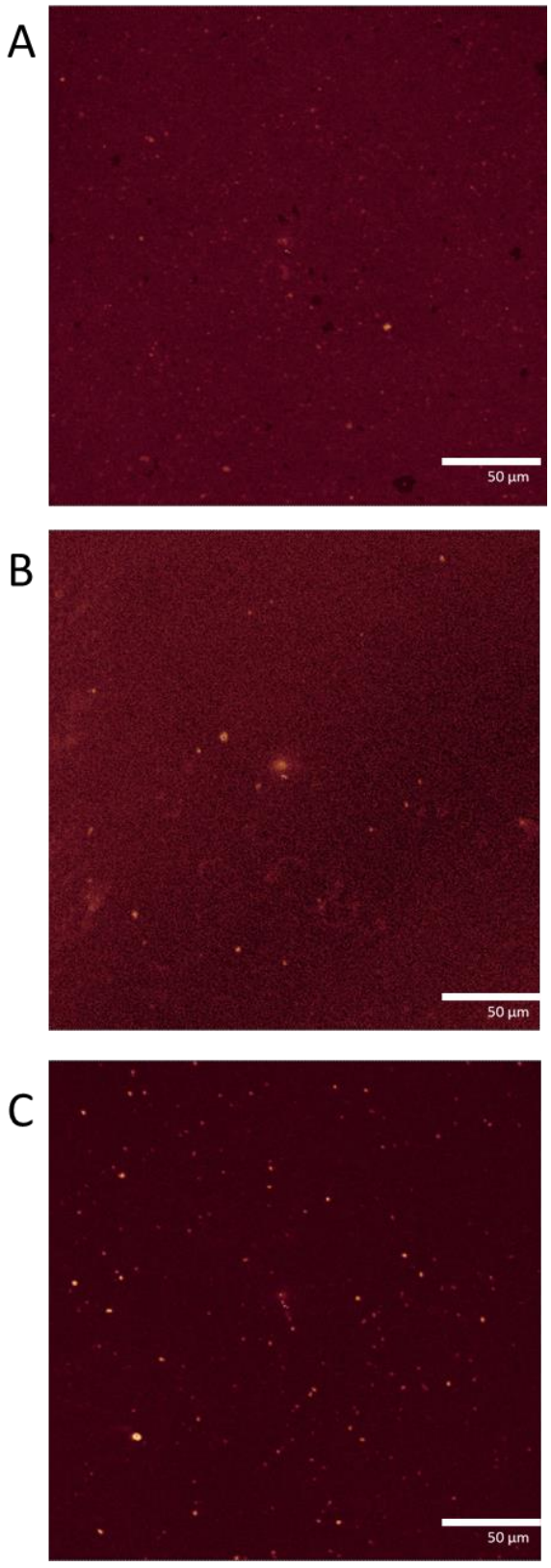
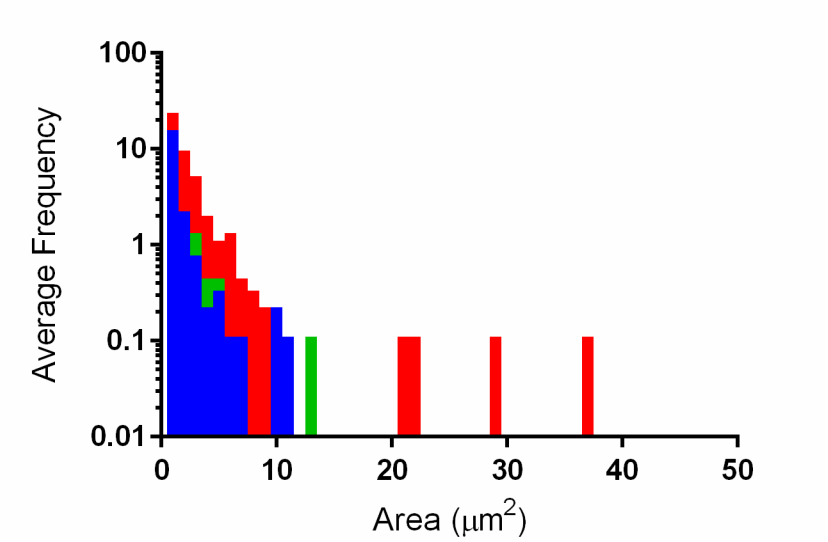


Figure 4.1.19 Average z-projection of confocal image stacks with Di-8-ANEPPS labelled $PC_{55}Chol_{30}SM_{15}$ membranes. (A) PBS, (B) NaSCN and (C) Gly-Gly-Gly media at pH7.4. Experiments were conducted at 25°C. (Table 2.2.1) Images representative of membrane condition, n=9. Images 238 x 238 µm, scale bar shown in (A) 47.62 µm.



Media	Total Number of Regions	Total Micro-domain Area (μm²)	Total Membrane Area (μm²)	Average Micro-domain Size (μm²)	% Coverage
PBS	74594	452601	509796	6.07	0.89
NaSCN	255140	975240	509796	3.82	1.91
Gly-Gly-Gly	408227	1742710	509796	4.27	3.42

Figure 4.1.20 Distribution of membrane microdomains in Di-8-ANEPPS labelled PC-$_{55}$Chol$_{30}$SM$_{15}$ supported lipid bilayer (SLB). The histogram shows the size of microdomains shown in Figure 4.1.4, in different media. Blue = PBS, Green = NaSCN, Red = Gly-Gly-Gly, (Table 2.1.1) pH7.4 at 25°C. Images from 238 x 238 μm, each sample imaged three times and repeated in three samples (n=9). Table of statistics obtained from image analysis.

The number of domains present in the Di-8-ANEPPS labelled SLBs is similar to those with $PC_{55}Chol_{30}SM_{15}$ FPE-labelled SLBs. The microdomain coverage increased in both NaSCN and Gly-Gly-Gly significantly ($p>0.1$ and $p>0.05$ respectively (Figure 4.1.20)).

Figure 4.1.19 illustrates that the $PC_{55}Chol_{30}SM_{15}$ membranes have microdomains with different dipole magnitudes. This is evident by the domains having different fluorescent intensities. Following analysis, the domain intensities were shown to exhibit a bimodal distribution and was fitted best to a sum of two Gaussians (Figure 4.1.21 ($P<0.05$, $R^2>0.9$)).

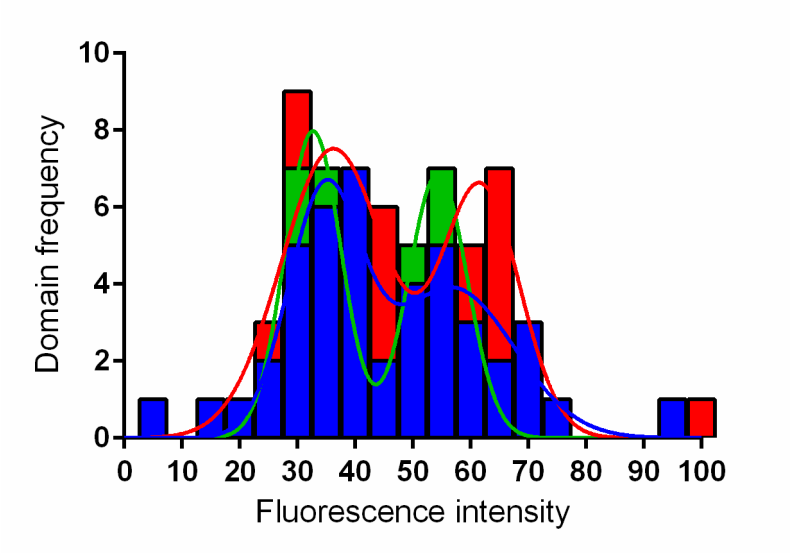


Figure 4.1.21. A histogram of $PC_{55}Chol_{30}SM_{15}$ membrane microdomain fluorescence intensity in different media. Blue= PBS, red= NaSCN and green= Gly-Gly-Gly at pH7.4. Fluorescence intensity is normalised between each membrane. Gaussian distribution fitted shown as fitted line.

The FPE-labelled $PC_{55}Chol_{30}SM_{15}$ membrane also demonstrated microdomains with two different intensities (Figure 4.1.12). The molecular simulations of the sphingomyelin with the FPE domains suggested that three phase membranes are possible with the formation of P_{β}' and l_o microdomains on a l_d background. Ψ_d has been shown to increase with increasing order of the membrane. As previously discussed, the formation of liquid ordered or gel phase microdomains are more by definition, more ordered than the lipid background. The ability for the probe to accurately measure these changes, allow us to observe the membrane in the presence of various reagents.

The media reagents employed here alter the electrostatic interactions of the lipid head groups, this then alters the molecular packing of the lipids and subsequently increases the dipole potential of the local lipid organisation.

4.2 Quantification of Microdomain Formation in Supported Lipid Bilayers Assessed Using AFM

Fluorescence microscopy has been shown to be a reliable method for the detection of membrane microdomains. These results rely on the fluorescent probe inclusion/exclusion from microdomains (see Section 4.1.2) or the fluorescent probe increasing fluorescent intensity in a different environment (see Section 4.1.3) [124, 128]. The detection of microdomains through fluorescence microscopy has limitations. The microscope arrangement employed (see Section 2.10.1) is diffraction limited. Using the Nyquist theorem microdomains below ~0.2 μm^2 are observed by representative values being averaged over a larger area. This may alter the results shown by under-representing domains of 0.2 μm^2 and below. These effects were investigated using AFM, as well as quantifying the effects of the various reagent media with AFM.

4.2.1 PC_{100} membranes

The topography of a PC_{100} bilayer in PBS was initially examined using AFM. The bilayer was virtually homogeneous, with some small defects where the bilayer had not fused correctly. The presence of the defects in the membrane can be used to our benefit as they permit the bilayer height to be measured. Figure 4.2.1 demonstrates that the distance from the top of the bilayer to the surface of the mica support, this distance was resolved at ~4 nm, which is consistent with the known value of the thickness of a membrane bilayer [84].

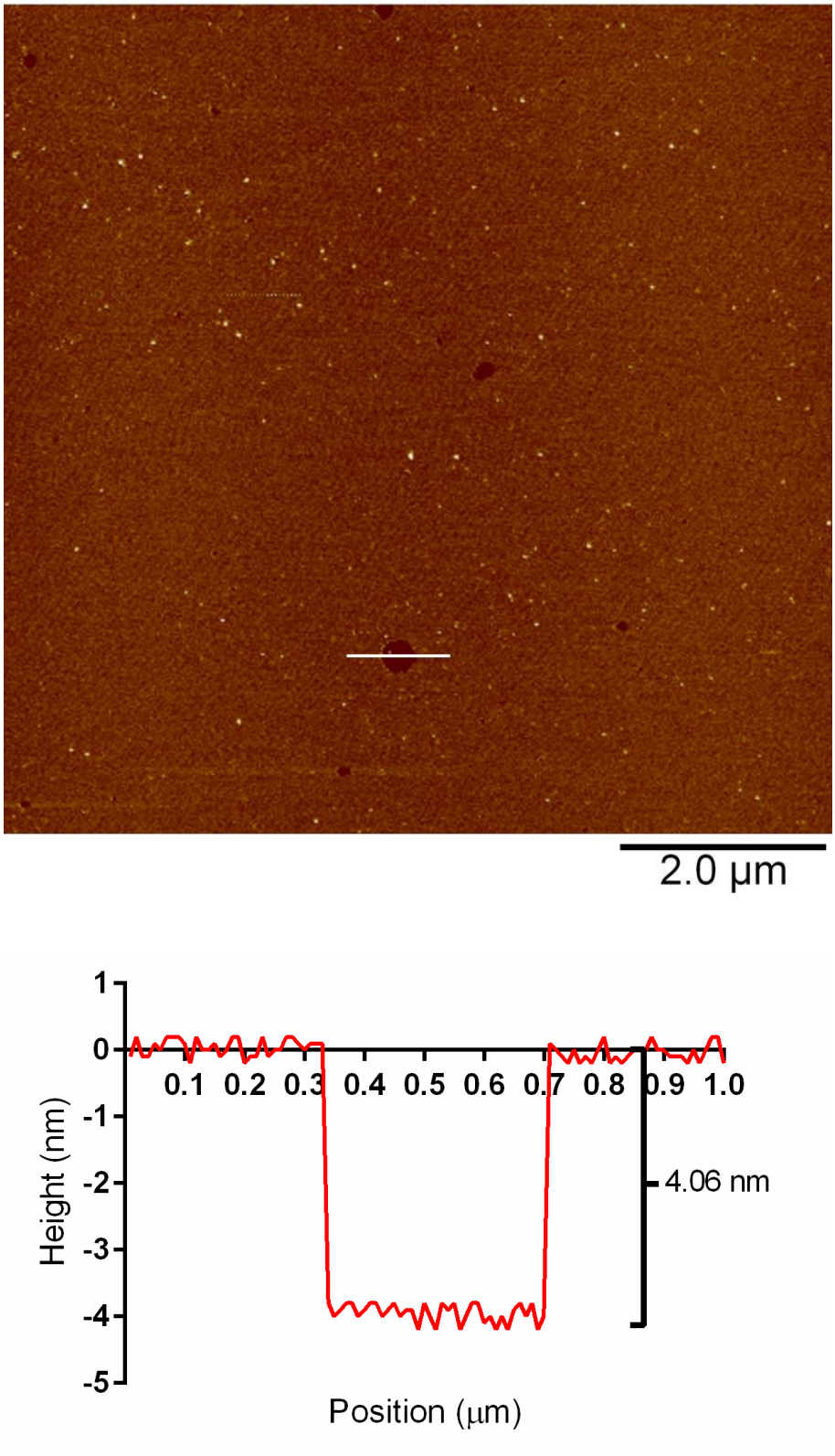


Figure 4.2.1. Atomic force microscopy of a SLB. (Upper panel) AFM image of PC_{100} bilayer in PBS media, at pH7.4, the experiment was conducted at 25°C. (Lower panel) A z-profile of the bilayer across a defect (white line, upper panel) in the membrane. The AFM tip scans across the membrane surface (0 nm) and then drops to the bilayer-free mica surface (-4 nm), upon returning to the bilayer.

The PC_{100} membranes were shown to be homogenous in PBS media (Figure 4.2.1A). The media in which the membranes were formed was substituted for the same media used in the fluorescence microscopy studies (Sections 4.1.2.1 and 4.1.3.1). The resultant membranes formed were shown also to be homogenous (Figure 4.2.2).

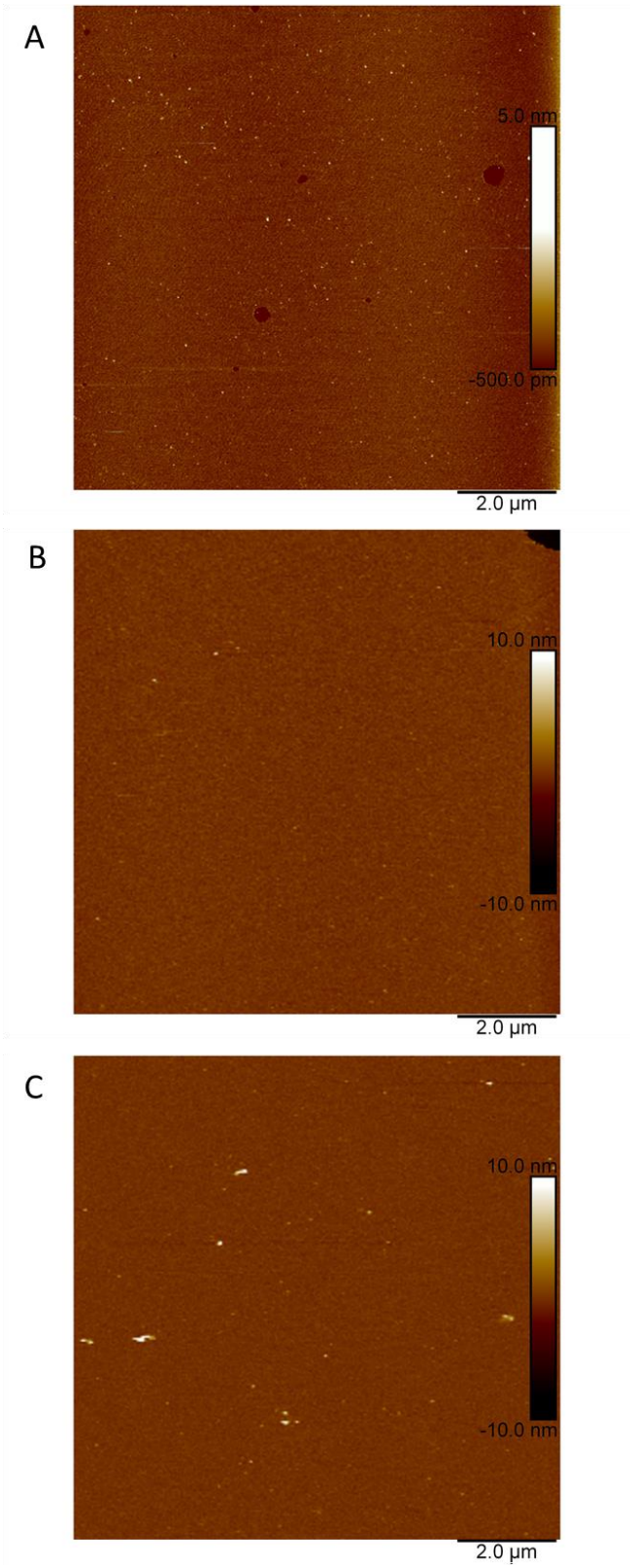


Figure 4.2.2. AFM image of PC_{100}. (A) PBS, (B) NaSCN and (C) Gly-Gly-Gly media (Table 2.2.1) at pH7.5, the experiment, was conducted at 25°C. Images taken were 10 x 10 µm.

The microdomains observed using fluorescence (Section 4.1.2.1), in the presence of NaSCN and Gly-Gly-Gly only accounted for ~1% of the membranes imaged. Given the scanning range of the AFM employed was between 10 x 10 and 50 x 50 μm, depending on possible resolution and each fluorescent image was 238 x 238 μm, an area ~23-fold greater was imaged with the fluorescent technique. Therefore, it is less likely to observe microdomains with AFM (such as Figure 4.2.2).

Considering the differences in the physical properties between mica and glass coverslips, such as net surface charge, the formation of the membranes is different (Sections 2.12.1). This resulted in difficulties forming the $PC_{70}Chol_{30}$ and $PC_{55}Chol_{30}SM_{15}$ used in the fluorescent techniques. In order to quantify the effects of microdomain formation, a pure lipid mixture $DOPC_{60}Chol_{15}SM_{25}$ (Table 2.1.1) was utilised with the membrane phase behaviour previously characterised using AFM [220].

4.2.2 $DOPC_{60}Chol_{15}SM_{25}$

Initially, the bilayer phases were examined in MilliQ water, as has been used in previous studies [15, 131, 132, 220]. MilliQ water allows imaging of the bilayer devoid of any ions. Although these conditions are frequently used to categorise lipid behaviour, it must be noted that this condition is highly unrepresentative of a biological bilayer.

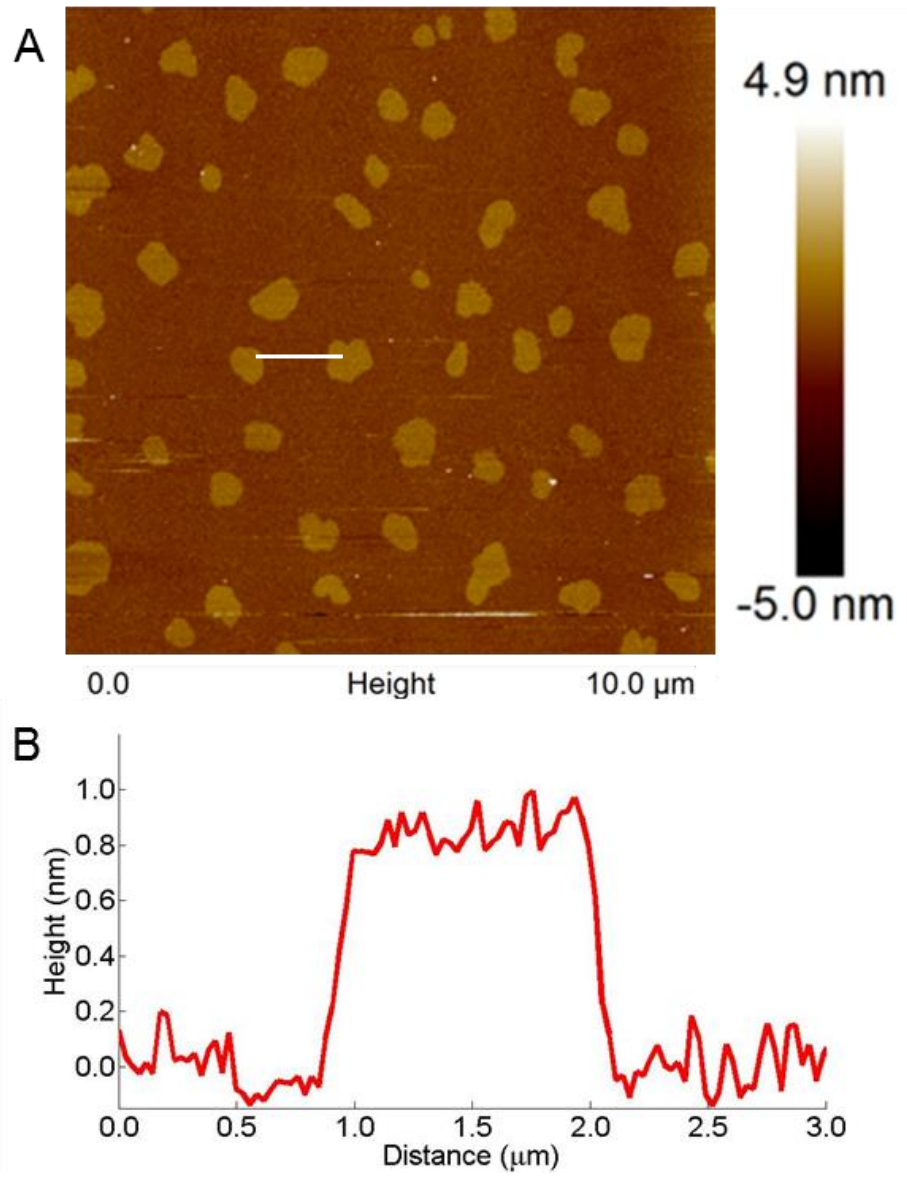


Figure 4.2.3. AFM of $DOPC_{60}Chol_{15}SM_{25}$ (A) AFM image of a $DOPC_{60}Chol_{15}SM_{25}$ membrane in MilliQ water, at pH 7.4, conducted at 25°C, scanning range of 10 x 10 µm. (B) Z-profile of bilayer across microdomain (white line) from darker brown to light brown.

AFM is reliant on height variation between microdomains and the background lipid, which is representative of increased lipid ordering in the microdomains. The membrane has been shown to be 4nm high, which was examined by the distance from the surface of the bilayer to the mica support (Figure 4.2.1). The z-profile, illustrated in Figure 4.2.3B, shows that the microdomain is raised 0.8-1 nm above the lipid background. $DOPC_{60}Chol_{15}SM_{25}$ membranes have previously been characterised in a phase diagram in MilliQ water ([132], Section 1.4.61.8.2), where l_o

microdomains are present on a l_d background. The ordering of saturated chains and cholesterol in the microdomains, results in tightly packed lipids in l_o phases, which raises the domains above the disordered unsaturated chains of l_d phases (Section 1.8.2).

The structure of a $DOPC_{60}Chol_{30}SM_{15}$ bilayer, known to be heterogeneous (Figure 4.2.3), was interrogated below the diffraction limit of the fluorescent microscope employed (<200nm). Figure 4.2.4 demonstrates that at <200nm the membrane was homogenous and did not exhibit any smaller microdomains that would not be visible by fluorescent techniques.

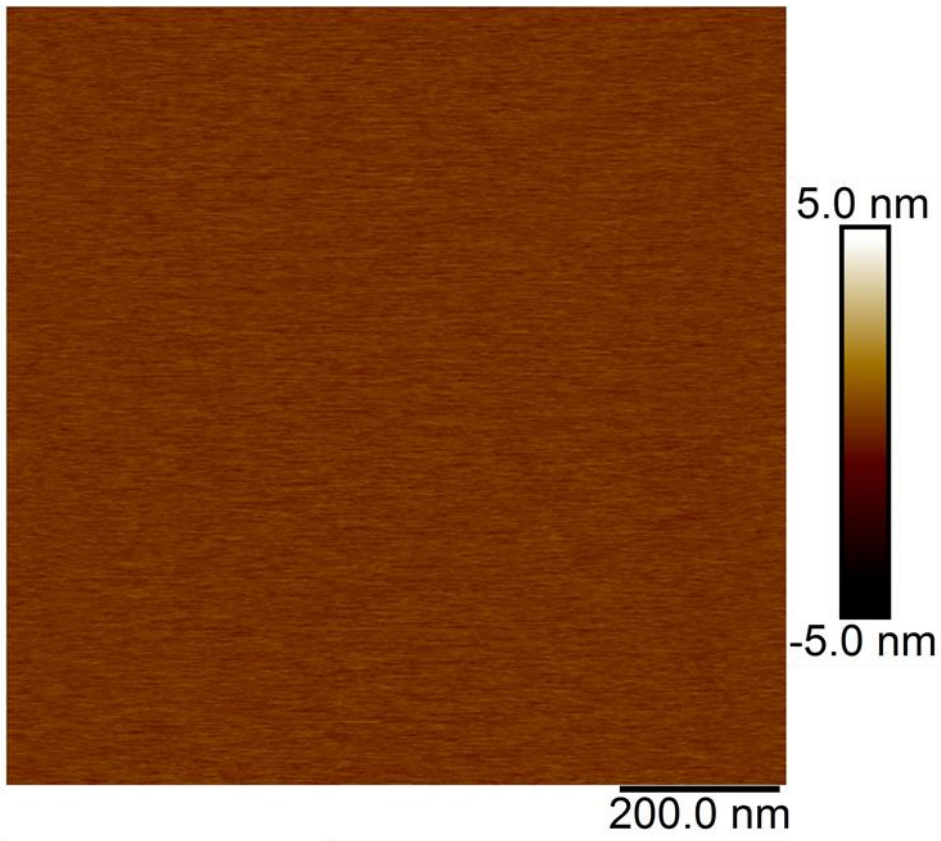


Figure 4.2.4. AFM image of $DOPC_{60}Chol_{15}SM_{25}$ in PBS media at pH7.5. The experiment was conducted at 25°C. The image was taken at the highest possible spatial resolution.

To achieve spatial resolution below 200nm, the scanning range (image size) is low which, decreases the likelihood of detecting domains (Figure 4.2.4). Therefore, when

further imaging bilayers, the scanning range was increased to the maximum of 50 x 50 µm.

Due to the inability to reproduce all of the membranes used in the fluorescence microscopy study, the membrane microdomains established here are used to try and interpret the forces that underpin microdomain assembly/disassembly (Section 1.8.2). The membrane compositions used in the AFM were then corroborated using the FPE-labelled fluorescent technique later (see Section 4.2.3.)

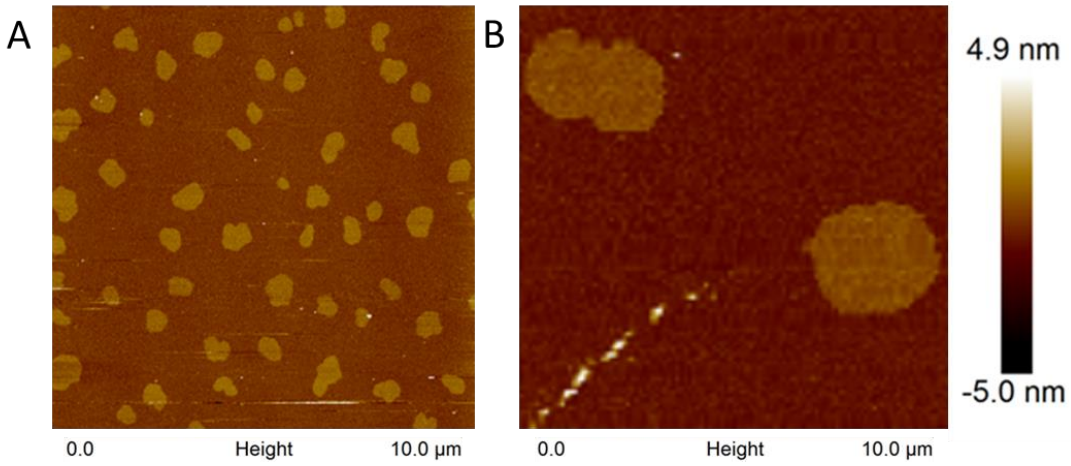
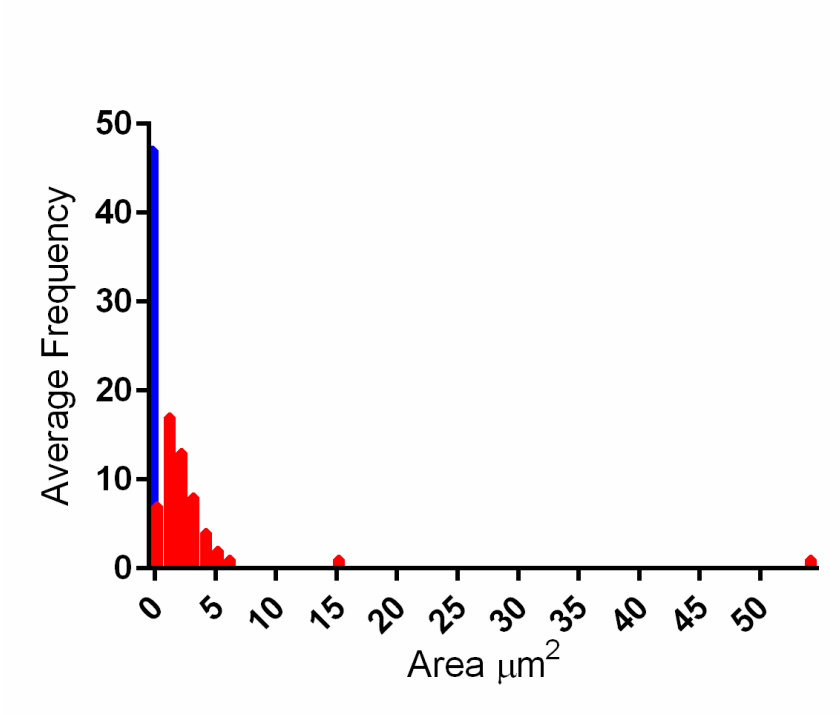


Figure 4.2.5 AFM image of $DOPC_{60}Chol_{15}SM_{25}$ membranes. (A) MilliQ water and (B) PBS, at pH 7.4, experiments were conducted at 25°C, the scanning range of images is 10 x 10 µm.



Media	Total Number of regions	Total Microdomain area (μm^2)	Average Microdomain size (μm^2)	Total Membrane Area (μm^2)	% Coverage
Water	47	9.4	0.2	300	3.13
PBS	95	341	3.59	5900	5.78

Figure 4.2.6. Distribution of membrane microdomains. (Upper panel) The histogram shows the size of microdomains shown in Figure 4.2.5, in different media. Blue = MilliQ water, Red = PBS, (Table 2.1.1) at pH7.4 conducted at 25°C. Images were assessed from a range of scanning ranges, with each sample imaged as many times as possible, replicated three times. (Lower panel) Table of values obtained from image analysis.

AFM is a more unstable technique than fluorescence microscopy; hence the frequency in which AFM images are obtained is variable and is much more experiment specific. The average domain size and microdomain percentage coverage were used in the analysis to make comparisons between each condition. The microdomains present in MilliQ water (0.2 μm^2) are much smaller than both AFM-derived PBS images and fluorescence microscopy derived microdomain sizes (AFM; 3.6 μm^2 (Figure 4.2.5), fluorescence microscopy; 5.4-7.5 μm^2 (Figure 4.1.13 and Figure 4.1.9 respectively)). The increased the salt concentration between MilliQ and PBS resulted in an 18-fold increase in domain size and an increase in microdomain

coverage (Figure 4.2.6). This change is very pronounced and serves as a perfect example of how characterisation of lipid phases in pure water, is highly unrepresentative of physiological conditions. The ionic screening of Na^+ Cl^- in the PBS, changes the interaction of the head group charges, a phenomena which has been demonstrated previously [2].

The media reagents used in the fluorescence microscopy study (Section 4.1) were examined and compared to PBS media; AFM was used to quantify the effects of the different media.

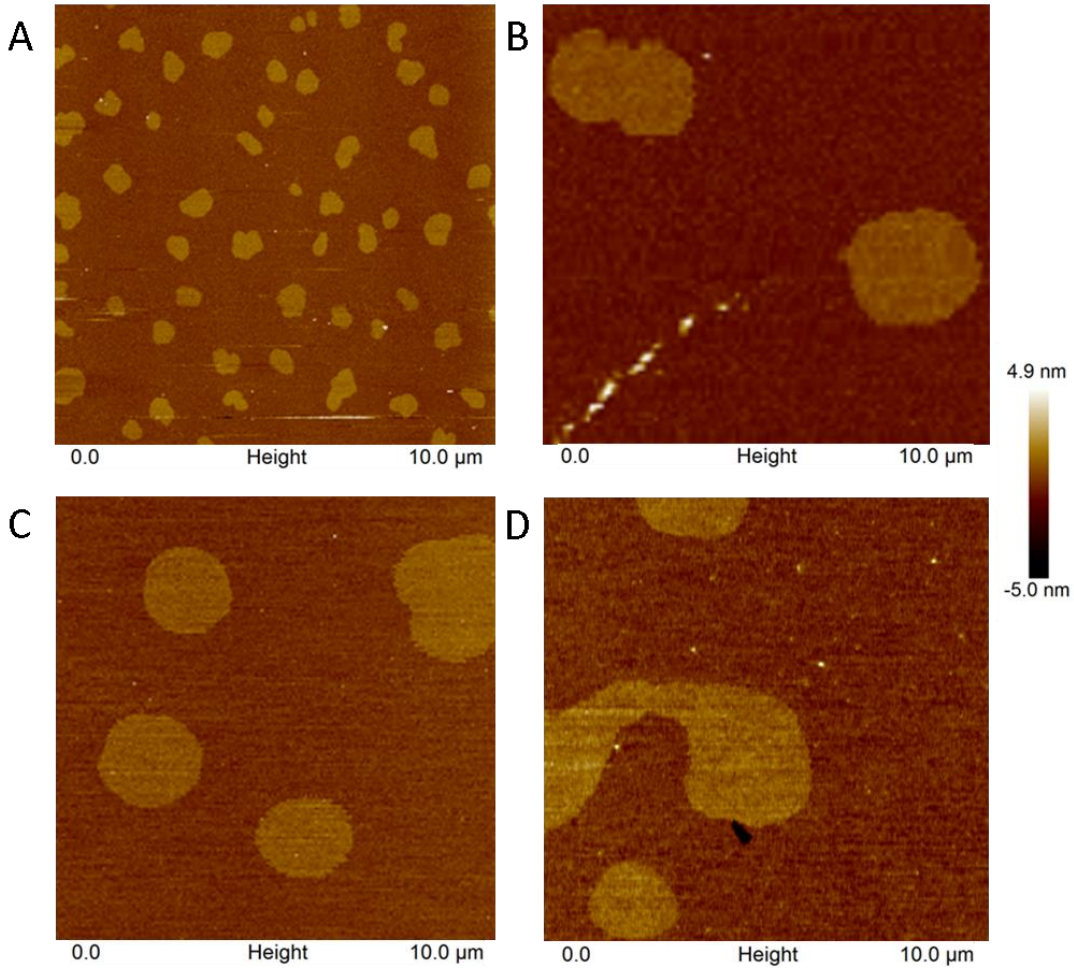


Figure 4.2.7 AFM images of $DOPC_{60}Chol_{15}SM_{25}$ membranes. (A) MilliQ water, (B) PBS, (C) NaSCN and (D) Gly-Gly-Gly. All media (Table 2.1.1) were used at pH 7.4 and experiments conducted at 25°C, images are 10 x 10 µm.

Images observed in Figure 4.2.7 were collected at 10 x 10 μm for comparison between media treatments. Microdomains were also observed at a larger scanning range of 50 x 50 μm to increase the frequency of microdomains analysed. The images were processed via the method described in (Section 2.12.2), with domain masks illustrated in Figure 4.2.8 to display the qualitative and quantitative difference between media reagents.

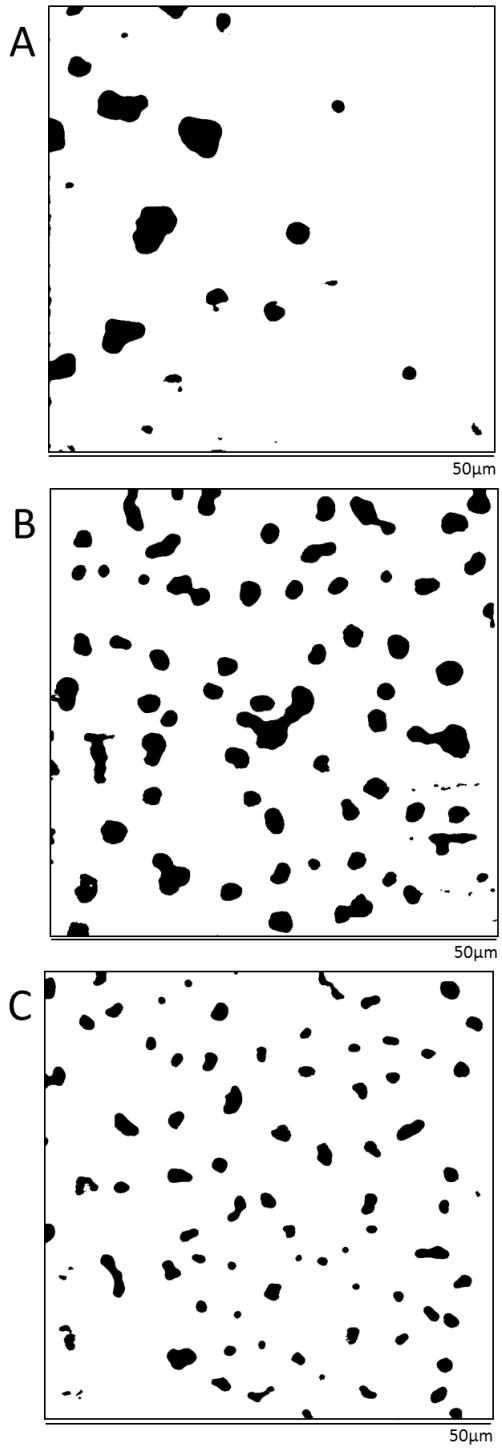
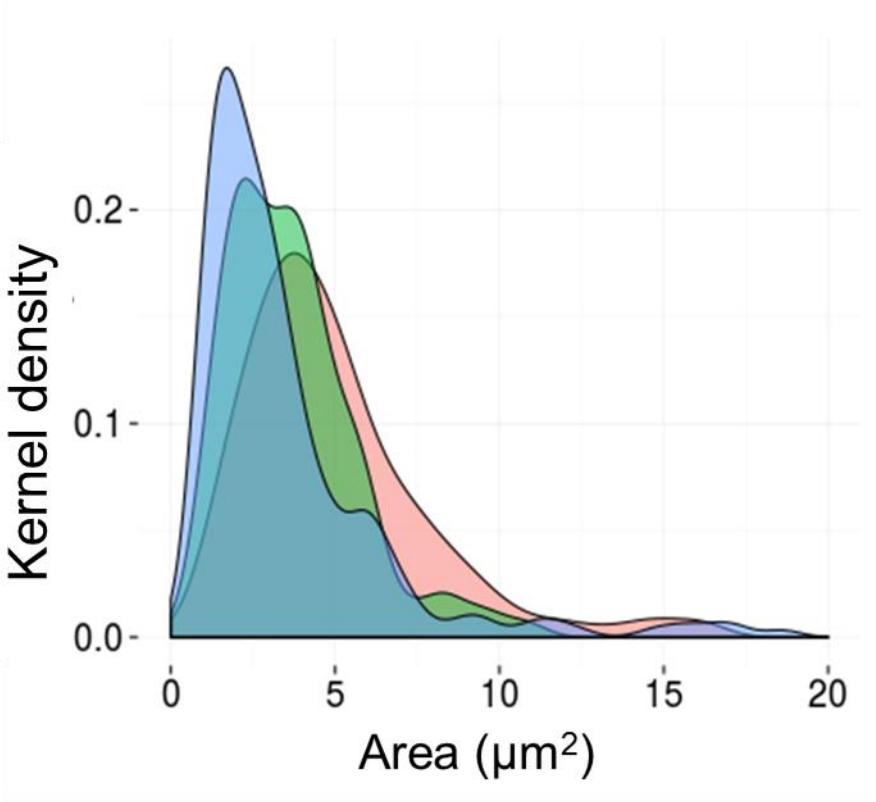


Figure 4.2.8 AFM images of $DOPC_{55}Chol_{15}SM_{25}$ membrane bilayers, corrected for the membrane background. Domain masks are shown for ease of qualification between species. Each image is representative of 50 x 50 µm bilayers in (A) PBS (B) NaSCN and (C) Gly-Gly-Gly media (Table 2.2.1) at pH7.4, experiments were conducted at 25°C.



Media	Total Number of Regions	Micro-domain Area (µm²)	Total Membrane Area (µm²)	Average Microdomain Size (µm²)	% Coverage
PBS	95	341	5900	3.59	5.78
NaSCN	380	848	10900	2.23	7.78
Gly-Gly-Gly	136	535	5000	3.93	10.7

Figure 4.2.9 Histogram of microdomains from images with scanning ranges between 10-50 µm. (Upper panel) Histogram shows the size of microdomains shown in Figure 4.2.8, in different media. Blue = PBS, Green = NaSCN, Red = Gly-Gly-Gly, (Table 2.1.1) at pH7.4, conducted at 25°C. (Lower panel) The values obtained from image analysis with microdomain coverage and average microdomain size used to quantitate between samples. Results were plotted as a kernel density estimate to compare between samples.

NaSCN and Gly-Gly-Gly promote the formation of domains as illustrated in Figure 4.2.8. These increases correlate with the results shown using the confocal microscopy technique (see Section 4.1.2 and Figure 4.1.11).

4.2.3 Comparison of AFM and fluorescence microscopy techniques

It was not possible to investigate all the different membrane conditions with both AFM and fluorescence microscopy, this was due to technical issues of not being able to form membranes on the mica surface. therefore, following the AFM analysis of $DOPC_{60}Chol_{15}SM_{25}$ membranes, these membranes have been studied using fluorescence microscopy to compare the different techniques. The use of an orthogonal technique was used to assess the confidence of the conclusions drawn from the utilization of either technique.

The presence of the FPE probe was validated by the addition of Ca^{2+} ions; the probe was shown to respond equally to the increase in membrane electrostatic surface potential.

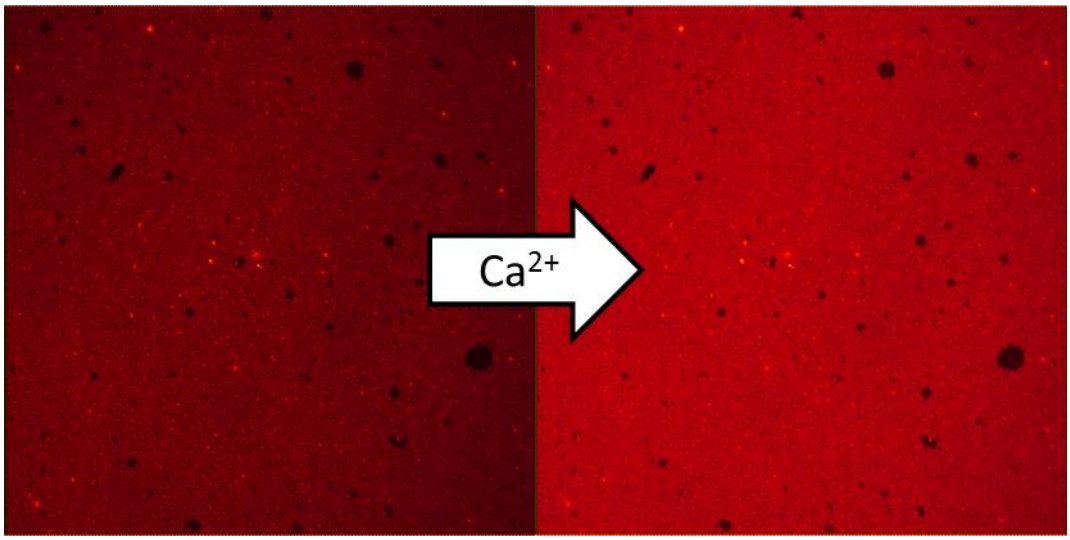


Figure 4.2.10. Confocal microscopy of an FPE labelled $DOPC_{60}Chol_{15}SM_{25}$ bilayer. The addition of 2mM Ca^{2+} in the form of 1M $CaCl_2$ PBS at pH7.4, experiments were conducted at 25°C.

The $DOPC_{60}Chol_{15}SM_{25}$ membranes were shown to be heterogeneous, like those demonstrated with AFM (Figure 4.2.8) and the $PC_{55}Chol_{30}SM_{15}$ membranes, investigated using fluorescence microscopy (Section 4.1.2). The membranes were made in the media previously employed and imaged using the fluorescence microscopy system as previously described.

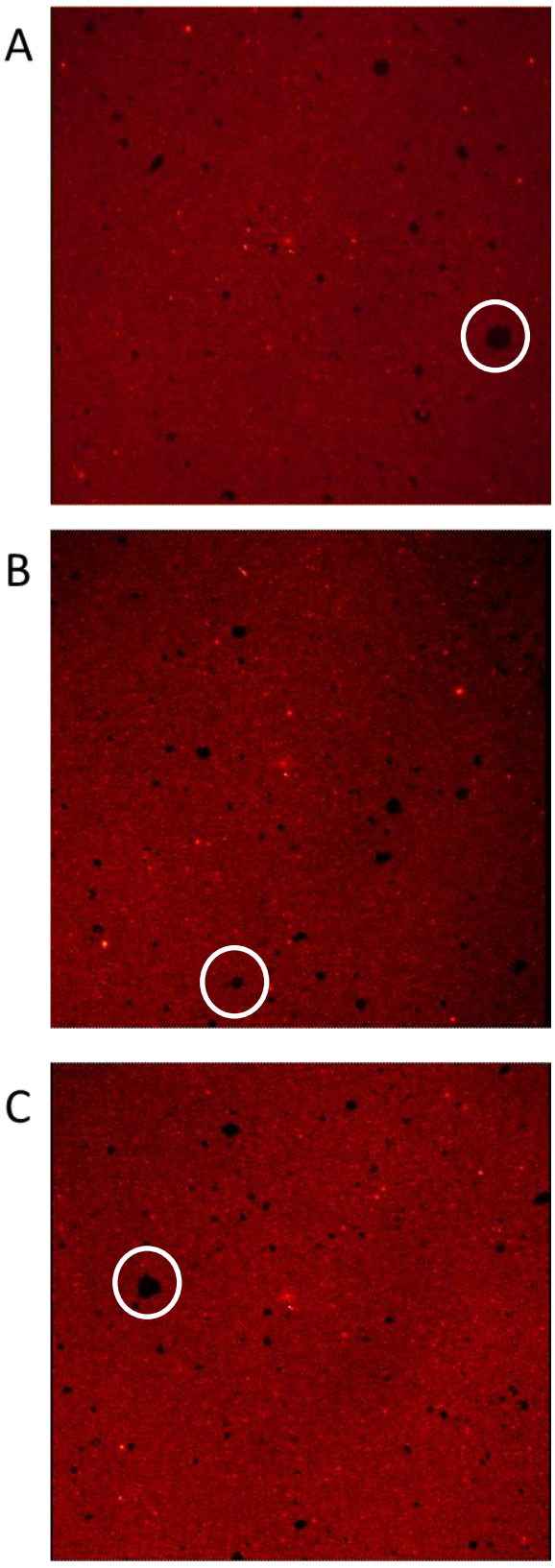
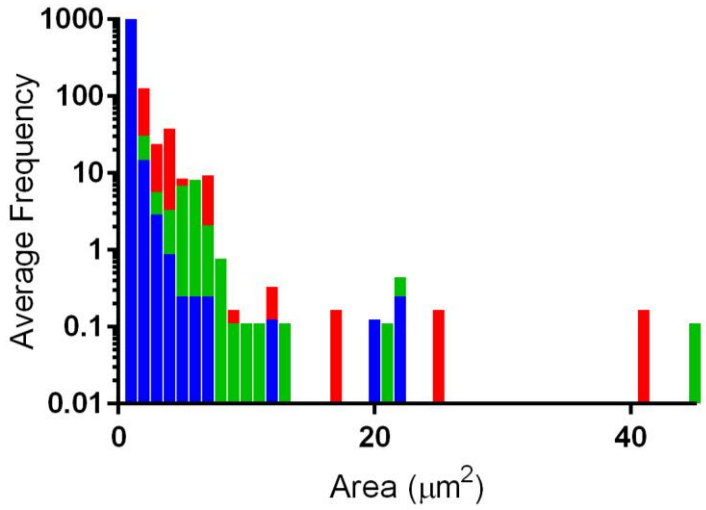


Figure 4.2.11. Average z-projection of confocal image stacks with FPE labelled $DOPC_{60}Chol_{15}SM_{25}$ membranes. (A) PBS, (B) NaSCN and (C) Gly-Gly-Gly media (Table 2.2.1) at pH7.4, experiments were conducted at 25°C. Images are representative of membrane condition, n=9. Images 238 x 238 μm, scale bar shown 50 μm. White circles highlight fluorescent free patches, which are defects in the membrane

Figure 4.2.11 illustrates the formation of the $DOPC_{60}Chol_{15}SM_{25}$, where membranes were shown to have an increased number of non-fluorescent patches (highlighted with white circles). The identity of these domains was investigated by monitoring the addition of Ca^{2+} (Figure 4.2.10), upon Ca^{2+} addition, there was no increase in fluorescence. This suggests that the FPE probe is entirely excluded from the microdomain, or, more likely is that there is a defect in the membrane formation and there is no membrane present. Due to the lack of fluorescence these spots are below the threshold limit and therefore do not count as false-positive domains. The number of defects in the membranes were greater than those in the same lipid composition formed by AFM, possibly due to the differences between the bilayer formation processes (Section 2.12) (Figure 4.2.8) as well as all of the other lipid compositions using fluorescence microscopy (see Figure 4.1.3, Figure 4.1.6 and Figure 4.1.10). One explanation for this is due to the increased proportion of sphingomyelin. In the membranes the lateral mobility of the bilayer is decreased resulting in a more fragile bilayer with more defects [93].



Media	Total Number of Regions	Total Micro-domain Area (μm^2)	Total Membrane Area (μm^2)	Average Micro-domain Size (μm^2)	% Coverage
PBS	4124	16619	509796	4.03	3.26
NaSCN	7365	28651	509796	3.89	5.62
Gly-Gly-Gly	5774	29619	509796	5.13	5.81

Figure 4.2.12. Distribution of membrane microdomains in FPE labelled $DOPC_{55}Chol_{15}SM_{25}$ supported lipid bilayer (SLB). The histogram shows the size of microdomains illustrated in figure 4.1.4, in different media. Blue = PBS, Green = NaSCN, Red = Gly-Gly-Gly, (Table 2.1.1) pH7.4 at 25°C. Images from 238 x 238 μm, each sample imaged three times and repeated in three samples (n=9). Table of statistics obtained from image analysis.

The different electrolyte media resulted in the same increase in domain size and frequency as with those shown with the AFM technique (see Figure 4.2.9). This change is consistent with the other lipid compositions containing naturally derived lipids: PC_{100}, $PC_{70}Chol_{30}$, $PC_{55}Chol_{30}SM_{15}$. The domain coverage of the membrane was less when using fluorescence microscopy, instead of AFM. This is suggested to be due to the differences between the detection efficiency of the techniques. The detection of membrane microdomains using AFM is absolute, i.e. the domains are detected based on the height of changes between the lipid phases whereas, the domains detected by fluorescence microscopy require the incorporation of FPE into microdomains.

4.2.4 Spectroscopic Analysis of FPE in Membrane Vesicles

The forces outlined in Section 1.4, which were previously attenuated to reduce protein-binding interactions (Section 3.1), also affect membrane systems. To quantify the underlying mechanisms of how these forces affect the microdomain assembly, the environment of the fluorescent probe in the bilayer was examined. This generated spectral information about the differences between the media treatments. The data obtained was used in combination with the data shown previously to try to elucidate a mechanism that governs microdomain control in these instances.

A change in the water network on the membrane surface is a possible causative factor that governs the assembly of membrane microdomains. In this study, the behaviour of the water at the bilayer surface was inferred through spectroscopic analysis of FPE (as fluorescence emission spectra, Figure 2.6.1). FPE spectra were observed by fluorescence spectroscopy in both membrane vesicles and SLBs. Emission maxima (λ_{emiss}) were tabulated in comparison in Table 4.2.1.

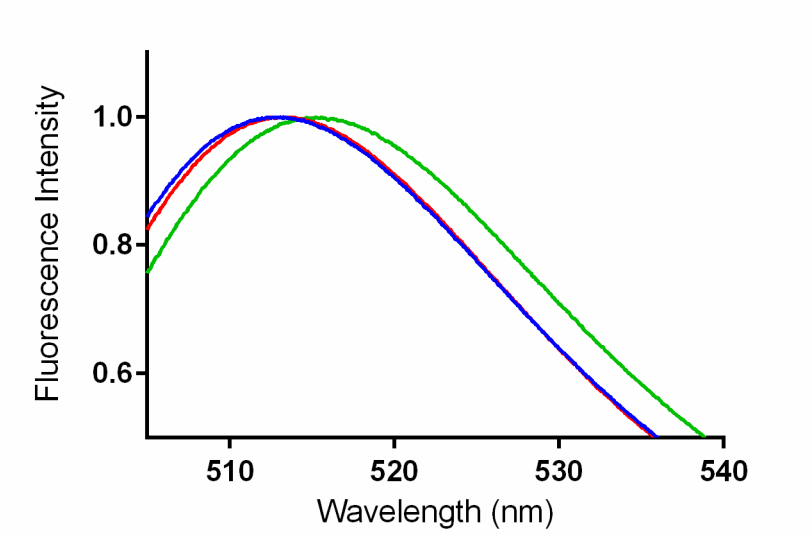


Figure 4.2.13. The normalised emission spectra (excitation 490nm) of 400 µM FPE labelled $PC_{70}Chol_{30}$ membranes in the presence of different media. PBS = blue, NaSCN = green and Gly-Gly-Gly= red pH7.4 at 25°C. λ_{emiss} values are tabulated in Table 4.2.1.

Spectroscopic analysis of FPE was conducted in the various media using $PC_{70}Chol_{30}$ membranes. Within a membrane bilayer, the FPE probe is positioned in the Stern layer of the membrane and is responsive to the electrostatic membrane potential (Section 1.9.1.2). NaSCN media led to a λ_{emiss} red-shift of 2.6 ± 0.25 nm (Table 4.2.1). Conversely, Gly-Gly-Gly did not result in a λ_{emiss} change. These λ_{emiss} changes are directly related to the dielectric constant change from bulk-phase water (~80) to a membrane surface (~20) (Section 2.6). NaSCN elicits a further red-shift which suggests that the dielectric constant on the surface is different in the presence of NaSCN. Charged ions localise to the membrane surface [66], the chaotropic nature of NaSCN is theorised to slow the rotational coefficient of the water molecules, and in turn, increases the dielectric constant at the Stern layer. This was previously suggested to reduce the electrostatic interactions between the membrane and the protein. In this study, the alteration of the dielectric constant may explain the differences in microdomain formation shown in the presence of NaSCN. Gly-Gly-Gly has a positive dielectric increment, as such, is it hypothesised to increase the dielectric constant and order the water molecules around the peptide (Section 1.6.2). The presence of Gly-Gly-Gly did not affect the λ_{emiss} of the probe; this suggests that the dielectric constant detected by the probe is unchanged. Gly-Gly-Gly is uncharged at neutral pH and is, therefore, unlikely to bind directly to the membrane. Considering this, the presence of Gly-Gly-Gly may affect intermolecular forces further from the membrane surface, undetectable by the probe. This theorem may explain the observed reduction in longer ranged electrostatic interactions such as those seen with fibrinogen binding interactions (see Section 3.1.1).

4.2.5 Spectroscopic Analysis of FPE in Supported Lipid Bilayers

Media	Vesicle λ_{emiss}	Background SLB λ_{emiss}	Microdomain SLB λ_{emiss}
PBS	513.1 ± 0.15	512.9 ± 0.09	514.7 ± 0.11
NaSCN	515.7 ± 0.19	514.7 ± 0.13	515.6 ± 0.19
Gly-Gly-Gly	513.3 ± 0.20	510.5 ± 0.10	510.7 ± 0.15

Table 4.2.1. Summary of λ_{emiss} values determined from FPE spectra in different membrane systems; vesicles and $PC_{70}Chol_{30}$ SLBs. Media PBS, NaSCN and Gly-Gly-Gly (Table 2.2.1) pH7.4 at 25°C.

In control PBS media, the emission spectra maxima varied between the membrane phases, with a blue shift between l_d background to l_o domains by 1.8 ± 0.2 nm (Table 4.2.1). The documented behaviour of the probe [128], as shown in Figure 2.5.1, indicates that the λ_{emiss} of the probe blue-shifts when moveing from the solution (dielectric constant ~80) to the membrane (dielectric constant ~20). Therefore, the blue-shift observed between the membrane background, and the microdomain (Figure 4.2.14) suggests that the probe is sensing an increase in dielectric constant, moving closer to the emission in solution. Figure 4.2.3 and previous AFM characterisation (Figure 4.2.4), shows that the probe-containing microdomains are raised above the background membrane. This novel environment clearly effects the emission of the probe, inferring that the dielectric constant, and therefore the water network, is different. These results correlate with reported experimental and simulation studies (such as [47, 131]) that suggest that water molecules adjacent to l_o domains are more ordered than those on the surface of l_d domains. The spectra of the probe in these different environments therefore allows the study of the aqueous environment adjacent to membrane domains, as seen previously in studies such as Disalvo et al. [221].

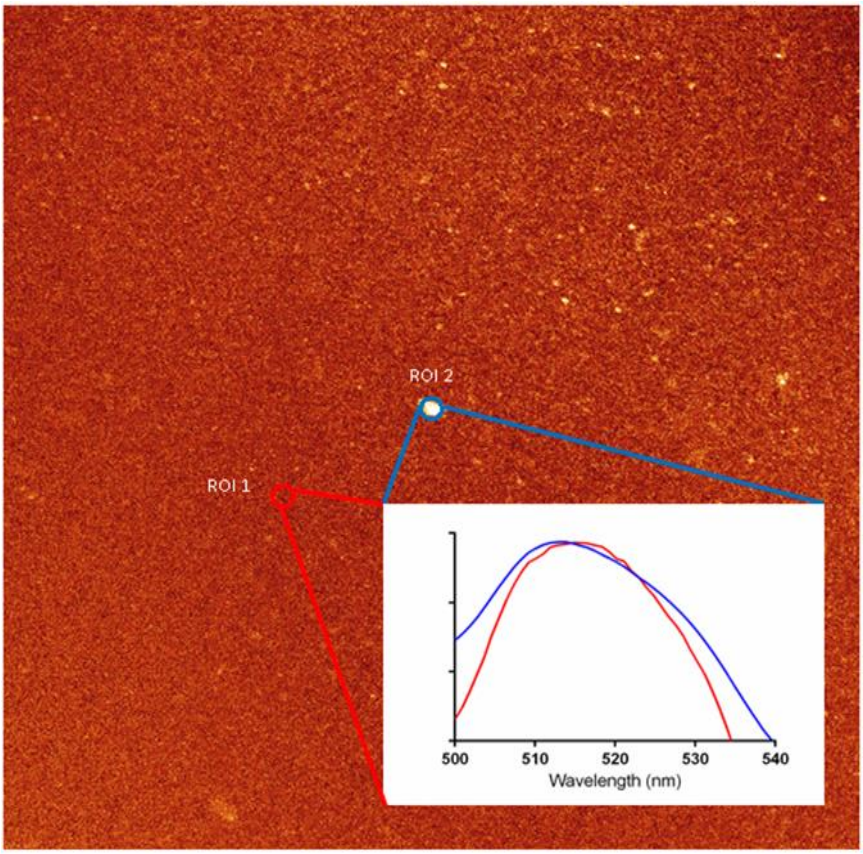


Figure 4.2.14. $PC_{70}Chol_{30}$ SLB with phase separation, in PBS at pH7.4, conducted at 25°C. (Inset) Excitation spectra were collected at 490nm. ROI 1 represents the membrane background; ROI 2 represents a membrane microdomain. λ_{emiss}. Values were tabulated Table 4.2.1

The λ_{emiss} differences between media are denoted in Figure 4.2.14, with results shown in Table 4.2.1. The λ_{emiss} of the FPE spectra in Gly-Gly-Gly media did not change between microdomain and background membrane conditions. NaSCN media exhibited a ~2nm λ_{emiss} blue shift of the FPE spectra between membrane formations. This shift of 2nm is the same difference as seen between microdomain and background membrane conditions in PBS media. The 2 nm blue shift, however, was in the context of a 4.6 nm red shift between the different media. These observations result in the PBS microdomain λ_{emiss} being the same as NaSCN background λ_{emiss} values. This suggests that the SCN^- ions order water molecules adjacent to the L_d phase making them indistinguishable to water molecules adjacent to the L_o phase in PBS (Table 4.2.1).

Together, these results imply that differences in the structure of the membrane-associated water may be important in controlling the membrane organisation.

4.3 Discussion

The aim of this study was to examine the factors that alter membrane microdomain (raft) formation. The question remains how previously categorised factors, such as acyl-chain length [208], temperature [208], head group interaction [211, 222] and ionic strength are linked, and which of these may dominate the formation of these domains in different lipid environments. The data obtained in this section highlights another potential causative factor in the microdomain assembly. It is thought that the assembly of microdomains is dependent on specific non-covalent molecular interactions between the aqueous environment and the membrane headgroup regions. This, in turn, may affect the headgroup interactions and microdomain formation [102, 223]. The media reagents employed here were used in Chapter 3 to attenuate the forces that affect binding of proteins to membranes and proteins to surfaces. Here, the hydrogen bonds between the head groups of different lipid species, or between the lipid head groups and the water molecules, are altered. These forces have been demonstrated in studies such as Slotte *et al.* [210, 213], which have shown that the size of sphingomyelins head group changes the amount of hydrogen bonds it forms and subsequently, the number of lipids it interacts with.

Previous studies indicate that the nature of water changes when interfaced with a membrane bilayer. Water associated with membrane microdomains is not the same as water associated with the background lipid bilayer, both of which are distinctly different to bulk water [131]. These studies have included both experimental work [131, 132, 221, 224], and computational analysis [125, 205]. These studies highlight that the membrane lipids associate with water in a number of ways, dependent on the

nature of the lipid head group. On average, each lipid associates with 11-14 interfacial water molecules; ≤1 confined in hydrophobic tails, 6-7 around phosphate head, 4-6 around the acyl chains (Figure 4.3.1)[204]. These water molecules exhibit distinct properties and have been shown to modify the packing and density of lipids via hydration expansion [204] or hydrogen bonding modifications [224].

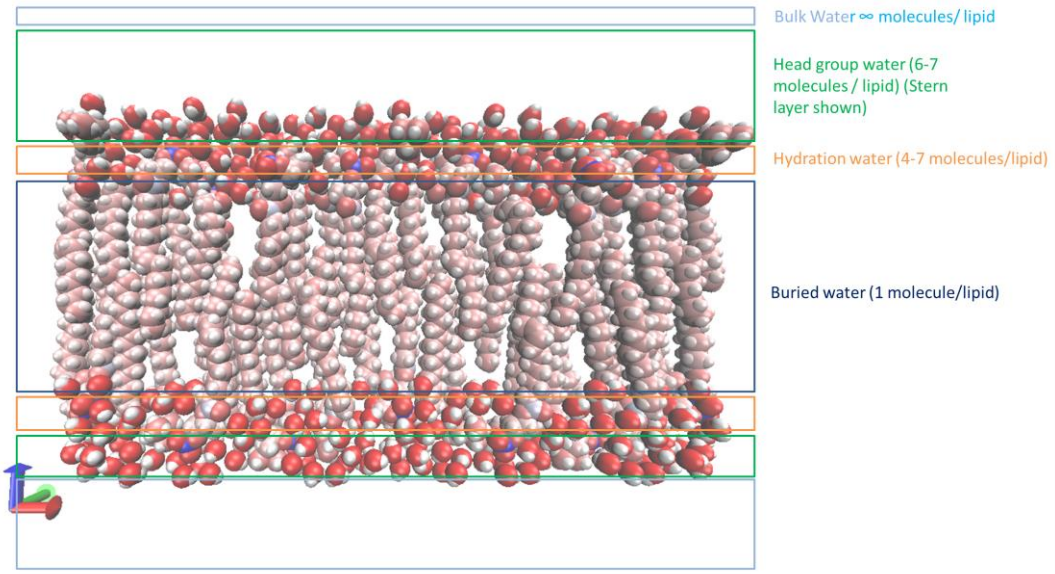


Figure 4.3.1. A DPPC bilayer with associated water molecules. Water molecules are present in four distinct layers: (1) Buried water in acyl chains, which are highly unfavourable (dark blue), (2) hydration water around the phosphate group of phospholipids (orange), (3) water associated with the head group, with water in the Stern layer shown, with the boxed area representing the diffuse layer (green) and (4) water not associated with the membrane i.e. bulk phase water. Created using Visual Molecular Dynamics.

This chapter has sought to alter the interactions between lipid head groups and water molecules, by the use of soluble reagents. The data presented in this section of results suggests that the presence of NaSCN and Gly-Gly-Gly can increase the microdomain frequency in all the membrane compositions studied. These effects were shown to be evident across a variety of different lipid compositions. The was demonstrated with two different fluorescent probes and various techniques, including atomic force microscopy (Figure 4.1.6- Figure 4.2.7).

The modulation of membrane microdomains using different media reagents has been shown to be different to previously characterised effects, such as increasing ionic strength. This was demonstrated by the difference between pure water and PBS (Figure 4.2.7) [101, 222], where microdomains were eighteen-fold larger, but the overall domain coverage increased less than two-fold. This suggests that in the higher ionic strength conditions, single larger domains form preferentially over multiple smaller domains. Increasing ionic strength decreases electrostatic interactions between the lipid head groups. The increased salt concentration could therefore, reduce repulsive forces between domains, resulting in domain clustering. The media employed were ionically balanced with PBS therefore, the ubiquitous increase in the percentage of domains present in the SLBs suggests that the further effect seen with the media reagents are not ionically driven, and microdomain assembly is promoted through different interactions.

The use of both the Di-8-ANEPPS probe and the FPE probe, offered insight into the various aspects of the membrane. The Di-8-ANEPPs probe assesses the dipole potential of the membrane and as such, whether the microdomains contain cholesterol or whether the tight-packing is sufficient to raise the dipole potential. The FPE probe allows investigation of the electrostatic surface potential whilst also aggregating into microdomains due to its DPPE acyl chains. In PC_{100} membranes, the Di-8-ANEPPS fluorescence did not change in the presence of the different reagents however, FPE reported an increase in small microdomains, suggested to be pseudo-gel phase lipids due to the PC-only lipid composition. The Di-8-ANEPPS probe is located further into the membrane (Figure 1.8.2) hence; the probe relies on orientation with large membrane dipoles in order to increase fluorescence. Given that cholesterol is the greatest contributor to changes in the membrane dipole, the

formation of PC only gel-like domains may not have been sufficient to promote fluorescence. Another possibility is that the domains are a result of an increase in fluorescence by the FPE probe instead of clustering into gel-like domains. $PC_{70}Chol_{30}$ membranes were shown to be heterogeneous when utilising both FPE and Di-8-ANEPPS probes in PBS. Both experiments also reported an increase in the frequency and size of microdomains in the presence of Gly-Gly-Gly. Di-8-ANEPPS labelled $PC_{70}Chol_{30}$ membranes in the presence of NaSCN resulted in a decrease in detected domains. This may be caused by the same mechanism proposed for the PC_{100} membranes, i.e. NaSCN promotes the formation of PC-only domains, which would result in the cholesterol becoming more evenly distributed across the microdomains. This would result in the increase in domains detected by the FPE probe, however with lower cholesterol percentage in the microdomains, hence the Di-8-ANEPPS probe may underestimate the domain frequency.

The membrane conditions containing sphingomyelin resulted in the detection of microdomains of different intensities with both FPE and Di-8-ANEPPS. This, alongside the approximate phase diagrams previously discussed, suggests that there are three clear lipid phases in all the different media conditions. The presence of NaSCN and Gly-Gly-Gly both increase the frequency of domains, suggesting that once the lipid reorganisation is complete, there is adequate cholesterol or sphingomyelin to aggregate into new microdomains, which are subsequently detected by both the Di-8-ANEPPS and FPE probe.

The observed results on microdomain formation can be investigated further via computational modelling to elucidate a mechanism for each reagent employed. Sodium thiocyanate, as previously discussed (Section 1.6.1), has been proposed to order the water molecules on the surface due to its relatively high entropy of

hydration [169, 225]. When water molecules solvate SCN^- ions, the hydrogen bonding between the water molecules is disrupted, and the water is drawn to the SCN^- ions. This then increases the local dielectric constant around the ions as the rotation correlation time of the water molecules is decreased [226]. Ions have been shown to associate with to the membrane surface [59, 64, 181] therefore; the dielectric constant of the membrane surface will be increased in relation to the membrane surface.

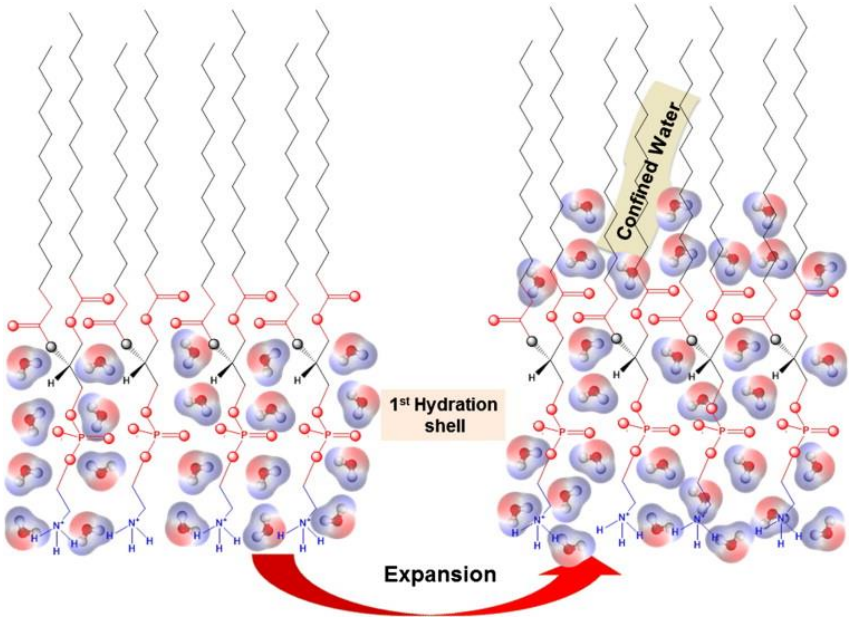


Figure 4.3.2. Hydration of lipid head groups in lipid molecules following the expansion and preferential hydration of lipids [204].

The local ordering of water molecules across microdomains causes more water to be localised to the surface of the membrane [131]. The fluorescent moiety of FPE is located in the Stern layer of the membrane bilayer (interfacial water area (Figure 4.3.1)), and is able to report the water structure by proxy. There is a ~5nm red-shift in the λ_{emiss} when in the presence of NaSCN, compared to FPE in PBS membrane vesicles. A blue-shift in the λ_{emiss} has also been observed between different membrane organisations in an SLB such as those shown between L_o and L_d domains

in Figure 4.2.14. In the presence of NaSCN in the SLB's system. The blue shift is maintained between the membrane organisations, as well as the observed blue shift between NaSCN and PBS media. These observations show that the FPE spectra is the same between L_o domains in PBS and L_d domains in NaSCN. This may suggest that NaSCN is modulating the water structure across the membrane background, potentially creating an environment that is more like that observed in microdomains. The different water structure may result in tighter lipid packing and hence the increase in observed microdomain formation (Figure 4.3.3).

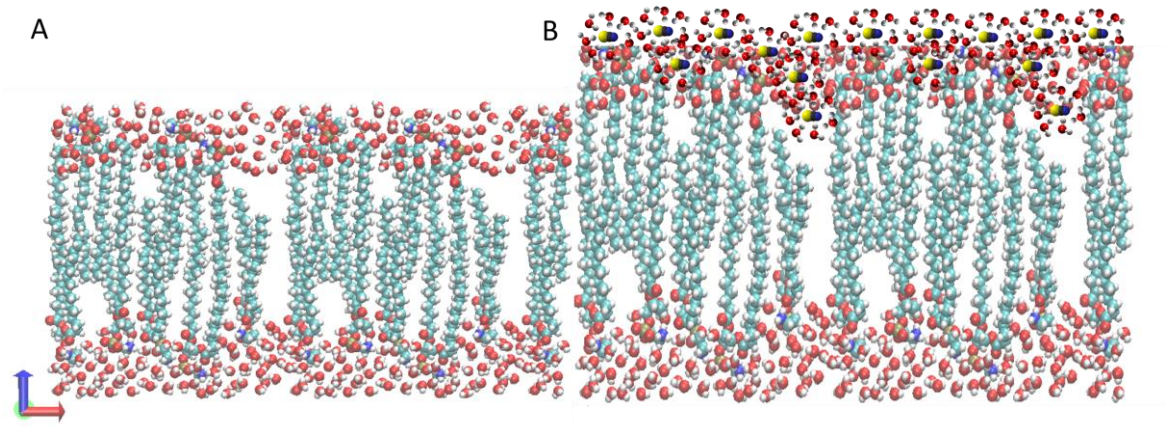


Figure 4.3.3. Proposed mechanism for NaSCN derived microdomain formation through preferential hydration of bilayer similar to the mechanism shown in Figure 4.3.2. (A) POPC bilayer (blue and white) with associated water molecules (red and white). (B) POPC expanded bilayer with NaSCN (yellow, black and blue). Created by Visual Molecular Dynamics.

Gly-Gly-Gly has been theorised to increase the ambient dielectric constant of a solution [42]. In contrast to the effect of NaSCN, Gly-Gly-Gly media does not lead to any discernible shifts in λ_{emiss} from PBS media and does not exhibit λ_{emiss} changes between L_o and L_d formations in SLBs. Although the different reagents have shown to affect a similar phenomenon of increasing domain formation, it is apparent that the mechanisms that underlie this process are different. The modulation of the microdomains by NaSCN can be discussed in a molecular context, strengthened by

the effect on the probe, leading to the suggestion that the interactions are short ranged.

Charge-charge and dipole interactions have been previously shown to control some formations of microdomains dependent on the electrostatic repulsion of lipid head groups [227]. The DCMRs employed here, have been examined to decrease the strength of charge-charge and dipole interactions of protein binding. It is well established that proteins and small peptides associate with the membrane and elicit specific activities that are microdomain dependent (discussed in Section 1.8.2). This association of small peptides has been shown to result in a direct electrostatic attraction of peptides to the surface [72, 228]. Gly-Gly-Gly does not bind directly to membranes as seen through both fluorescent vesicle interactions (Section 3.1.1), and does not change the spectra of FPE (Figure 4.2.13). It is hypothesised that the effects of Gly-Gly-Gly (when in solution), are delivered through longer-ranged water structure effects to the membrane (Figure 4.3.4). Studies investigating depolarised light scattering and dielectric spectroscopy [229, 230] highlighted that the addition of a dielectric peptide to membranes could alter the water structure dynamics up to 5 hydration layers from the surface. This is achieved by orientating the hydrogen bonding of water. The orientation of water reduces the charge-charge attraction and dipole forces in relation to Coulomb's law (by reducing ε, Section 1.4) The presence of the Gly-Gly-Gly in the diffuse layer of the membrane may also increase the zeta potential of the membrane. Here it is proposed that as the water structure on the membrane surface changes, environments are created in which microdomains are favourably assembled.

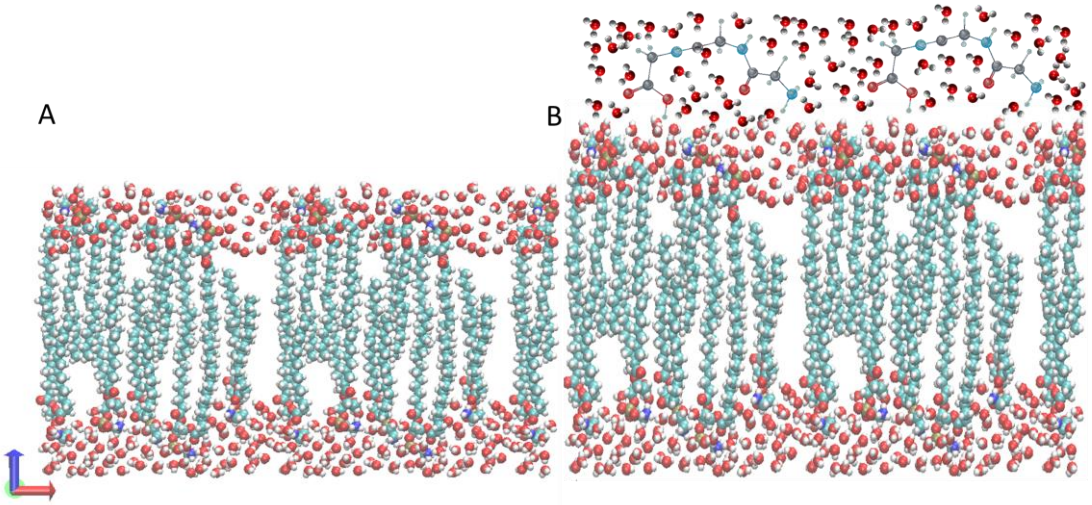


Figure 4.3.4. Proposed mechanism for Gly-Gly-Gly derived microdomain formation through preferential hydration of bilayer similar to the mechanism shown in Figure 4.3.2. (A) POPC bilayer (blue and white) with associated water molecules (red and white). (B) POPC expanded bilayer with Gly-Gly-Gly (blue, black and red). Created by Visual Molecular Dynamics.

The different membranes employed have been characterised by their relative position in phase-diagrams created through various mixtures in acyl chain lengths, typically in pure MilliQ water [208]. These lipid compositions are altered by temperature as defined in Figure 1.8.7. In summary, increasing the temperature provides the lipid molecules with higher entropy thus reducing the potential to form stable domains. With other external factors kept constant such as temperature and pH an increase of domain size would only occur if the cholesterol was physically removed to change the ratio of lipid and enter a different lipid phase (such as the three phase organisations suggested by $PC_{70}Chol_{20}$ membranes (Figure 1.8.6B)). With the various media employed, domain coverage ubiquitously increased. The proposed mechanisms above would suggest that the background L_d domains are more ordered, due to a different water structure on the surface modulated by the presence of NaSCN ions, or Gly-Gly-Gly. The water structure may then force the dispersion of cholesterol into a pseudo-L_o phase where it could form new domains of lipid and cholesterol that were previously dispersed throughout the lipid background.

The membranes' fluidity was examined to see whether it was affected by the reagents. FRAP of the various membrane compositions in PBS were shown to have membrane mobility within the literature defined values [102]. The membrane fluidity was unchanged in the presence of either NaSCN or Gly-Gly-Gly (Figure 4.1.2). In the fluorescence microscopy studies above, the domains were long-lived and were stable over tens of minutes. During AFM detection, the membrane fluidity was more variable between samples, with some images 'blurring' due to domains flickering during interrogation with the tip. The observations suggest that the membrane fluidity may be different in the presence of NaSCN and Gly-Gly-Gly, hence, there would be keen interest in further fluidity studies in the presence of the various reagents to observe conditions that may affect domain coalescence.

Understanding these parameters is essential for the understanding of the forces that drive microdomain formation in biological systems. Within cells, microdomain formations have been examined, such as the immune synapse [231]. However, the complex combination of protein-lipid rafts and lipid-only rafts await a full molecular description [232]. It is, therefore, likely that at least some of the physical phenomena described for these model systems may be applicable to the complex nature of the cell membrane.

4.3.1 Future Work for Membrane Microdomain Formation Processes

The ability to control and understand microdomain formation via different intermolecular forces relies on an understanding of microdomains at the molecular level. Here, the variety of the various techniques offers a novel insight into water modulation by bulk phase media changes. The recent development of ultra-fine AFM offers the potential to investigate the water structure of membrane microdomains directly. This approach would help to corroborate the proposed mechanism in this

study, which would deepen the understanding of the current mechanisms for microdomain formation. Another technique, vibration sum frequency generation (SFG), has been used to interrogate the interactions between lipid head-groups, specifically hydrogen bonding between charged and uncharged lipids [97]. This study has highlighted that PS molecules may form hydrogen bonds with PC in the membrane and effect the lateral organisation of the membrane. SFG, in the presence of the various media reagents, may identify further headgroup interactions being modified by the presence of the medium.

5 Polypeptide Control of the Assembly/Disassembly of Membrane Microdomains

Chapter 4 assessed the study of membrane microdomain assembly with regards to media interactions. Several factors have been shown to affect the assembly of membrane microdomains.

Interactions of macromolecules with membranes have been of considerable interest, with interactions being categorised between of a host of proteins, peptides and polymers [120]. These interactions are of interest to many surface chemistry, biochemistry and biophysics disciplines [233]. Peptide-membrane interactions specifically, have been linked to a host of disease pathologies including Alzheimer's disease [31, 196], Huntington's disease [197, 198] and prion diseases [165, 199, 200].

Polypeptide association with membranes has been previously described, with characterisation of the association and insertion kinetics of different polypeptides [30, 234]. This study extends these previous investigations by assessing the binding characteristics of the interaction, as well as investigating the affect of the interactions on the membrane architecture.

Here the binding properties of polypeptides to different membrane compositions are measured in the presence of various media reagents. The membrane compositions employed in this section are PC_{100} membranes, to investigate simple phosphatidylcholine binding interactions, $PC_{70}Chol_{30}$ membranes, to investigate the effect of a lipid fluidity modulating sterol, and $PC_{70}PS_{30}$ membranes, to investigate the effect of an anionic lipid.

The binding profiles and kinetics are investigated to elucidate any processes that may affect membrane microdomain assembly or disassembly. This utilises fluorescent probes FPE and thioflavin T (ThT), which detect the electrostatic surface potential and formation of any polypeptide secondary structure respectively [128, 152]. The polypeptide membrane interactions were also visualised using confocal microscopy to observe microdomain formation over time. The results of this study will help to characterise polypeptide interactions with membranes and to gain insight into factors that govern the assembly and disassembly of membrane microdomains in every day experiments, as well as disease pathologies such as Huntington's disease.

5.1 Results

5.1.1 Membrane Interaction of Polypeptides

Stopped-flow rapid mixing (SFRM) was used to study the interaction of the polypeptides to various FPE labelled membrane vesicles. SFRM allows interrogation of protein-membrane interactions after ~ 1 ms.

Poly-l-lysine was employed as a representative string of positive charges at two different lengths; cell-culture poly-l-lysine ($PolyK_{cc}$) ranging between 500-1000 residues and 10-residue poly-l-lysine ($PolyK_{10}$). The first exon of Huntingtin protein (14 residues) with a 28-residue polyglutamine expansion, termed $PolyQ_{28}$, was then employed to elucidate any association of Huntingtin peptides to the membrane (see Section 1.2.4) (Table 5.1.1).

Species	Sequence	Peptide isoelectric point	Net Charge at pH 7.4
$PolyK_{10}$	KKKKKKKKKK	11.5	10
$PolyK_{cc}$	500-1000 K	11.5	500-1000

PolyQ$_{28}$	MATLEKLMKAFESLKSFQQQQQQ QQQQQQQQQQQQQQQQQQQQQQ	9.8	1

Table 5.1.1. Summary of polypeptide properties calculated using a peptide calculator [235].

The interactions of the polypeptides were tested across various membrane compositions: PC_{100}, $PC_{70}Chol_{30}$ and $PC_{70}PS_{30}$ and in four different media: Tris, PBS, NaSCN and Gly-Gly-Gly (Table 5.1.2).

Poly K$_{10}$											
PC$_{100}$				**PC$_{70}$Chol$_{30}$**				**PC$_{70}$PS$_{30}$**			
Tris	PBS	NaSCN	Gly-Gly-Gly	Tris	PBS	NaSCN	Gly-Gly-Gly	Tris	PBS	NaSCN	Gly-Gly-Gly
Poly K$_{CC}$											
PC$_{100}$				**PC$_{70}$Chol$_{30}$**				**PC$_{70}$PS$_{30}$**			
Tris	PBS	NaSCN	Gly-Gly-Gly	Tris	PBS	NaSCN	Gly-Gly-Gly	Tris	PBS	NaSCN	Gly-Gly-Gly
Poly Q$_{28}$											
PC$_{100}$				**PC$_{70}$Chol$_{30}$**				**PC$_{70}$PS$_{30}$**			
Tris	PBS	NaSCN	Gly-Gly-Gly	Tris	PBS	NaSCN	Gly-Gly-Gly	Tris	PBS	NaSCN	Gly-Gly-Gly

Table 5.1.2. Experimental design of polypeptide interactions with various membranes, in different media. All experiments were carried out at pH7.4 at 25°C. Each membrane preparation was created in triplicate with five repeats of each concentration examined.

5.1.2 PolyK$_{10}$ Interaction with Various Membranes in Different Media

Initially, PolyK$_{10}$ was investigated with PC_{100}, $PC_{70}Chol_{30}$ and $PC_{70}PS_{30}$ membranes in four different media: a low ionic strength media, (10mM Tris) and three higher ionic strength media PBS, NaSCN and Gly-Gly-Gly (Table 2.2.1).

FPE labelling of membrane vesicles, in various media and membrane compositions, was confirmed by SFRM of the membrane and calcium ions (in the form of $CaCl_2$ as previously demonstrated in Figure 2.5.1). Ca^{2+} adsorption to the membrane results in an increase of fluorescence (Figure 5.1.1). ,

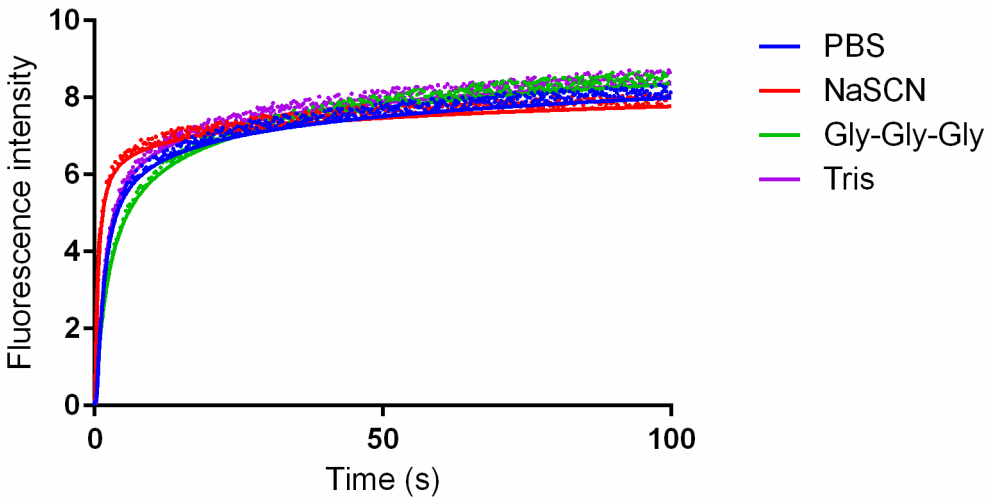


Figure 5.1.1. FPE responsivity to Ca^{2+}. Average trace (n=3, ± SD) of the interaction between PC_{100} membranes and 2mM $CaCl_2$ in PBS (blue), NaSCN (red), Gly-Gly-Gly (green) and Tris (purple) pH7.4, experiments were conducted at 25°C measured by SFRM.

The increase in fluorescence demonstrated in Figure 5.1.1 indicates that the FPE is present in the bilayer and is responsive to the electrostatic potential of the membrane. Given that are now large differences in rate or maximum capacity, the interactions can be measured easily managed by FPE fluorimetry.

5.1.2.1 *PC_{100} membranes*

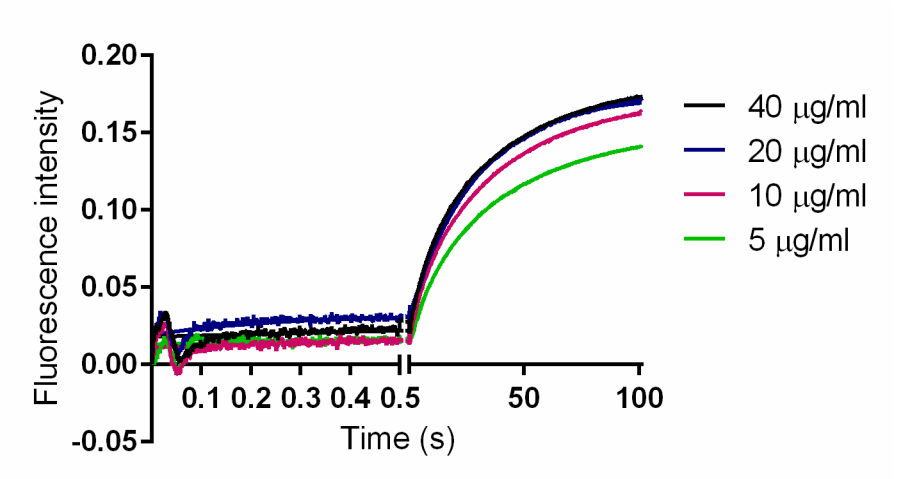


Figure 5.1.2. Binding of $PolyK_{10}$ to PC_{100} membrane in PBS at pH7.4, experiments were carried out at 25°C. Each trace is an average of five binding experiments (n=3).

Addition of $PolyK_{10}$ to PC_{100} membranes (Figure 5.1.2) resulted in a dose-dependent increase in the intensity, although above 40 μg/ml, the peptide started to saturate the

probe. Blank controls (media only additions to the membranes) were performed and deducted from protein-binding traces to control for any dilution or photobleaching effects.

The results from Figure 5.1.2 were fitted to a single exponential to obtain ΔFI plateau values, i.e. the maximum increase in fluorescence. The values obtained for different concentrations of polyK$_{10}$ were analysed in a secondary graph by plotting the ΔFI plateau vs. peptide concentration (see Figure 5.1.3). The binding graph was fitted to both a single binding isotherm (hyperbolic) and a cooperative sigmoidal (hyperbolic with Hill coefficient) binding curve as described in Section 2.8.1. Following F-test analysis, it was observed that the data was best fitted to a hyperbolic equation. The derived B_{max} and K_d values (Table 5.1.3) allow quantitative analysis between membrane types and media conditions.

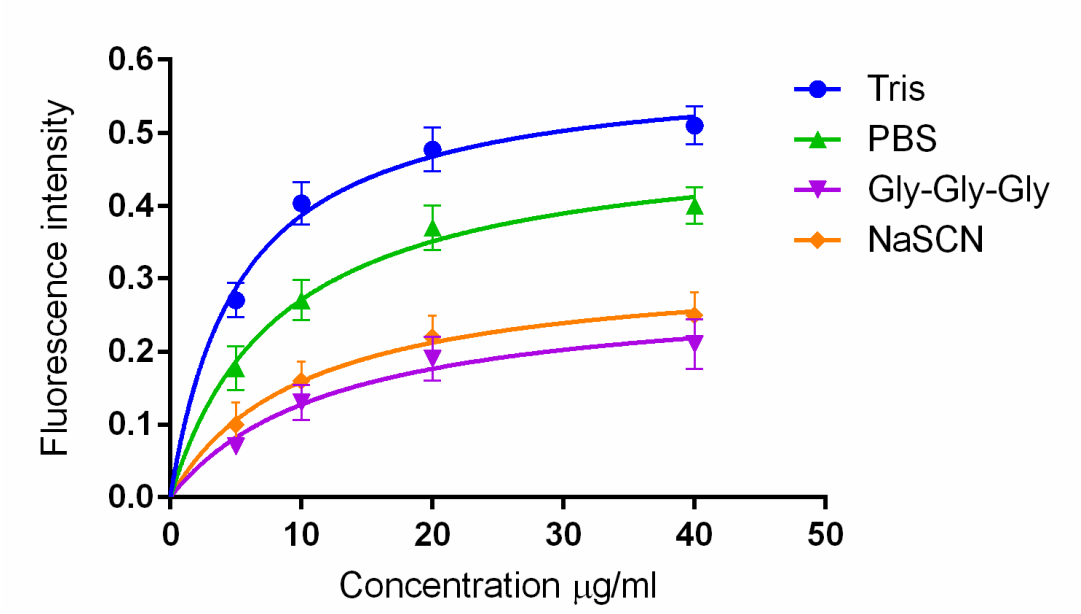


Figure 5.1.3. Binding of PolyK$_{10}$ to PC$_{100}$ membranes. Plateau ΔFI values from SFRM analysis of PolyK$_{10}$ binding to PC$_{100}$ membranes were fitted to a single hyperbolic binding model. Different media, Tris (blue), PBS (green), Gly-Gly-Gly (purple) and NaSCN (orange), were at pH7.4 (Table 2.2.1), with experiments conducted at 25°C.

	PC_{100}			
	B_{max} (a.u.)	**sd ±**	**K_d (µg/ml)**	**sd ±**
Tris	0.59	0.08	7.34	0.21
PBS	0.43	0.05	11.37	0.20
Gly-Gly-Gly	0.23	0.08	26.22	0.47
NaSCN	0.31	0.07	21.13	0.40

Table 5.1.3. B_{max} and K_d values $PolyK_{10}$ binding to PC_{100} membranes. SFRM Δ*FI* values were fitted to a hyperbolic binding curve and hyperbolic binding curve with Hill coefficient, the best fit was determined by an F-test. All media pH7.4 (Table 2.2.1), with experiments conducted at 25°C.

$PolyK_{10}$ has an isoelectric point above the pH of 7.4, hence carried a net positive charged in these experiments. PC_{100} vesicles lipids are net neutral however, due to the zwitterionic properties of the choline head group; therefore the binding is expected to be electrostatically driven. Comparison of the data from low ionic strength (10mM Tris) and the high ionic strength (PBS) conditions provides support for this expectation. The apparent binding affinity of $PolyK_{10}$ binding was 1.37 ± 0.20 µg/ml in PBS and 0.74 ± 0.21 µg/ml in Tris, suggesting that buffer ions shield the charges between the electrolyte and the membrane (Section 1.9.1.2) thus reducing the electrostatic interaction [41].

The presence of NaSCN and Gly-Gly-Gly decreased not only the apparent affinity of the $PolyK_{10}$ to the membrane but also the binding capacity when compared to PBS media; the B_{max} was reduced from 0.43 ± 0.05 in PBS to 0.23 ± 0.08 and 0.31 ± 0.07 for NaSCN and Gly-Gly-Gly respectively (Table 5.1.3). The affinity of the interaction is significantly decreased (one-way ANOVA, $p<0.05$) as demonstrated by an approximately two-fold increase in the K_d (PBS K_d; 11.37 ± 0.20, NaSCN; 26.22 ± 0.47, Gly-Gly-Gly; 21.13 ± 0.40 (Table 5.1.3)). NaSCN and Gly-Gly-Gly have been shown to affect intermolecular interactions of proteins in different ways. NaSCN is effective at reducing nonpolar interactions and broad surface charges, decreasing the electrostatic attraction between the polypeptide and the membrane.

Gly-Gly-Gly increases the ambient dielectric constant and decreases attraction forces (Chapter 3).

As well as reporting on the equilibrium measurements of peptide:membrane interaction the SFRM technique allows for kinetic modelling of the interaction. Kinetic modelling is advantageous as it enables the entire reaction to be fitted to either a simple model (i.e. a single exponential) or more complex model (including 2 or more steps), providing rate constants for each step that are independent of the step that has preceded it. Increasing the number of steps in the mechanism (i.e. A→B→C→D in a 3-step linear model) tends to result in improved goodness of fit between the observed and modelled data, but of course increases the complexity needed to describe the reaction. For the current SFRM data the best kinetic model for each trace was determined by comparing the variance, the standard deviation, the goodness of fit by eye, and by ensuring that the plotted residuals were close to zero across the whole data set (see e.g. inset to Figure 5.14A).

For all four buffer conditions, PolyK_{10} interaction with PC_{100} vesicles was best fitted to a two-step mechanism, i.e. A → B → C (Figure 5.1.14) with rate constants K_1 and K_2 (table 5.1.4). In this two step mechanism conformation "A" represents the unbound polypeptide whose concentration decreases over time until depleted (Figure 5.14.Aii, blue curve). Conformation "C" represents the reaction end-point of a membrane bound polypeptide (Figure 5.14.Aii, green curve). Conformation B represents an intermediate that is formed during the process and could have several different possibilities such as: the polypeptide partitioning into the water-bilayer interface, a clear intermediate complex with the polypeptide and lipid or a conformational change on the surface. Given the relative magnitude of B (maximum

of 10% of polypeptide configuration at any given time) the intermediate is not a rate limiting step.

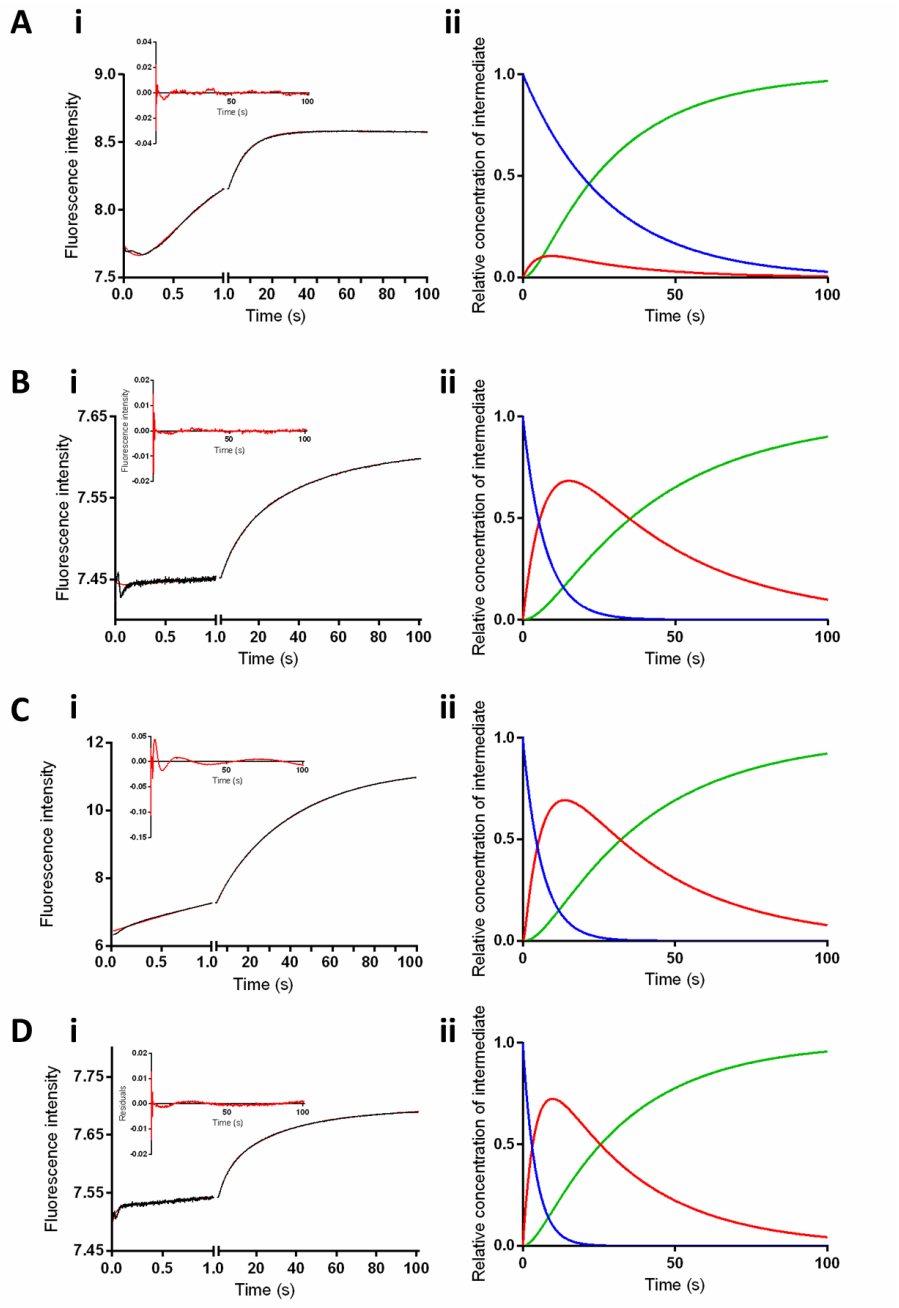


Figure 5.1.4. Kinetic modelling of 40 µg/ml PolyK$_{10}$ interacting with FPE labelled PC$_{100}$ vesicles. (A) Tris, (B) PBS, (C) NaSCN and (D) Gly-Gly-Gly. (i) An averaged trace of PolyK$_{10}$ interaction to PC$_{100}$ (black). This interaction is modelled (red) with the residuals of the kinetic model shown in the insert. (ii) The relative concentration of intermediate species suggested by the binding model, each colour represents a different intermediate in the reaction A→B→C. At any time point A+B+C= 1. All experiments were conducted at pH 7.4 at 25°C.

	PC_{100}			
	K_1 ($\mu gml^{-1}s^{-1}$)	**sd ±**	**K_2 ($\mu gml^{-1}s^{-1}$)**	**sd ±**
Tris	0.036	0.003	11.72	0.02
PBS	0.42	0.002	1.37	0.003
Gly-Gly-Gly	0.16	0.0003	2.25	0.002
NaSCN	0.23	0.004	29.96	0.62

Table 5.1.4. Kinetic rates of 40 µg/ml $PolyK_{10}$ interaction with FPE labelled PC_{100} vesicles in media. Experiments were conducted at pH 7.4, 25°C. K_1 represents the rate between A→B and K_2 represent the rate between B→C in binding intermediates such as Figure 5.1.4.

In PBS media (Figure 5.1.4B) a two-step binding model is also preferred. The intermediate conformer is much greater than in Tris (Figure 5.1.4A), with a faster A→B conversion, yet slower B→C conversion with approximately 5-10% unbound polypeptide still present at the end of the time observed. This suggests that the intermediate is partitioning into the water-bilayer interface, which is slower in PBS. This is attributed to the ionic shielding of the charges on the polypeptide, which decreases the attraction to the membrane [236].

The different rates shown for the $PolyK_{10}$ interaction in the various media correlate with the membrane capacity and binding affinities shown in Table 5.1.3. In Tris (low ionic strength) media, the conversion of A→B is slow (0.036 ± 0.003 $\mu gml^{-1}s^{-1}$) however, this is compensated by a fast B→C rate (11.72 ± 0.02 $\mu gml^{-1}s^{-1}$). PBS has a much faster A→B (0.42 ± 0.002 $\mu gml^{-1}s^{-1}$) transition rate which results in more intermediate (B) formation; however the B→C rate is approximately ten-fold slower (1.37 ± 0.003 $\mu gml^{-1}s^{-1}$) than in Tris (11.72 ± 0.02 $\mu gml^{-1}s^{-1}$). The A→B transition in Gly-Gly-Gly and NaSCN is faster than in Tris media, yet lower than PBS values suggesting that the energy needed to partition to the membrane surface is slightly decreased (Table 5.1.4).

5.1.2.2 *$PC_{70}Chol_{30}$ membranes*

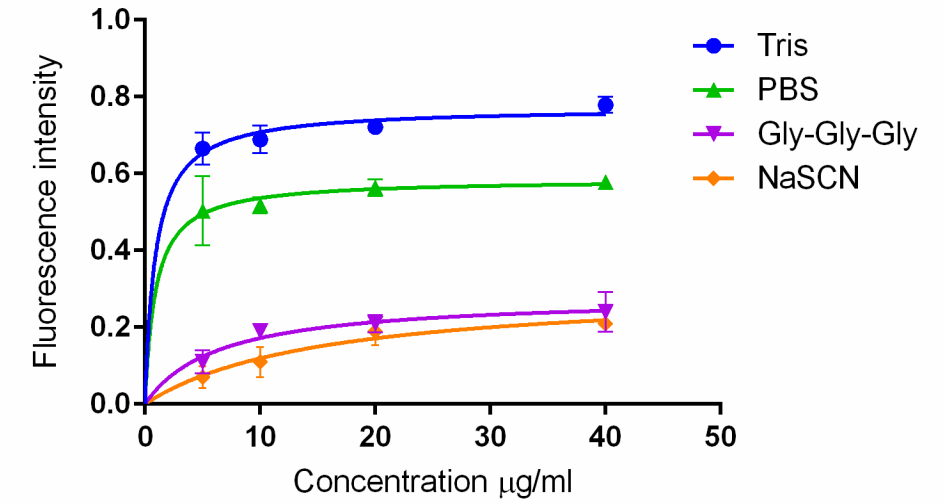


Figure 5.1.5. Plateau Δ*FI* values from SFRM analysis of PolyK$_{10}$ binding to PC$_{70}$Chol$_{30}$. The binding interactions were fitted to a single hyperbolic binding model. Different media, Tris (blue), PBS (green), Gly-Gly-Gly (purple) and NaSCN (orange), were at pH7.4 (Table 2.2.1), with experiments conducted at 25°C.

	PC$_{70}$Chol$_{30}$			
	B_{max} (a.u.)	**sd ±**	**K_d (μg/ml)**	**sd ±**
Tris	0.77	0.02	6.13	0.14
PBS	0.59	0.01	9.26	0.16
Gly-Gly-Gly	0.24	0.04	24.16	0.29
NaSCN	0.21	0.23	14.85	0.21

Table 5.1.5. B_{max} and K_d values PolyK$_{10}$ binding to PC$_{70}$Chol$_{30}$ membranes. SFRM Δ*FI* values were fitted to a hyperbolic binding curve and hyperbolic binding curve will Hill coefficient, the best fit was determined by an F-test. All media used were at pH7.4 (Table 2.2.1), with experiments conducted at 25°C.

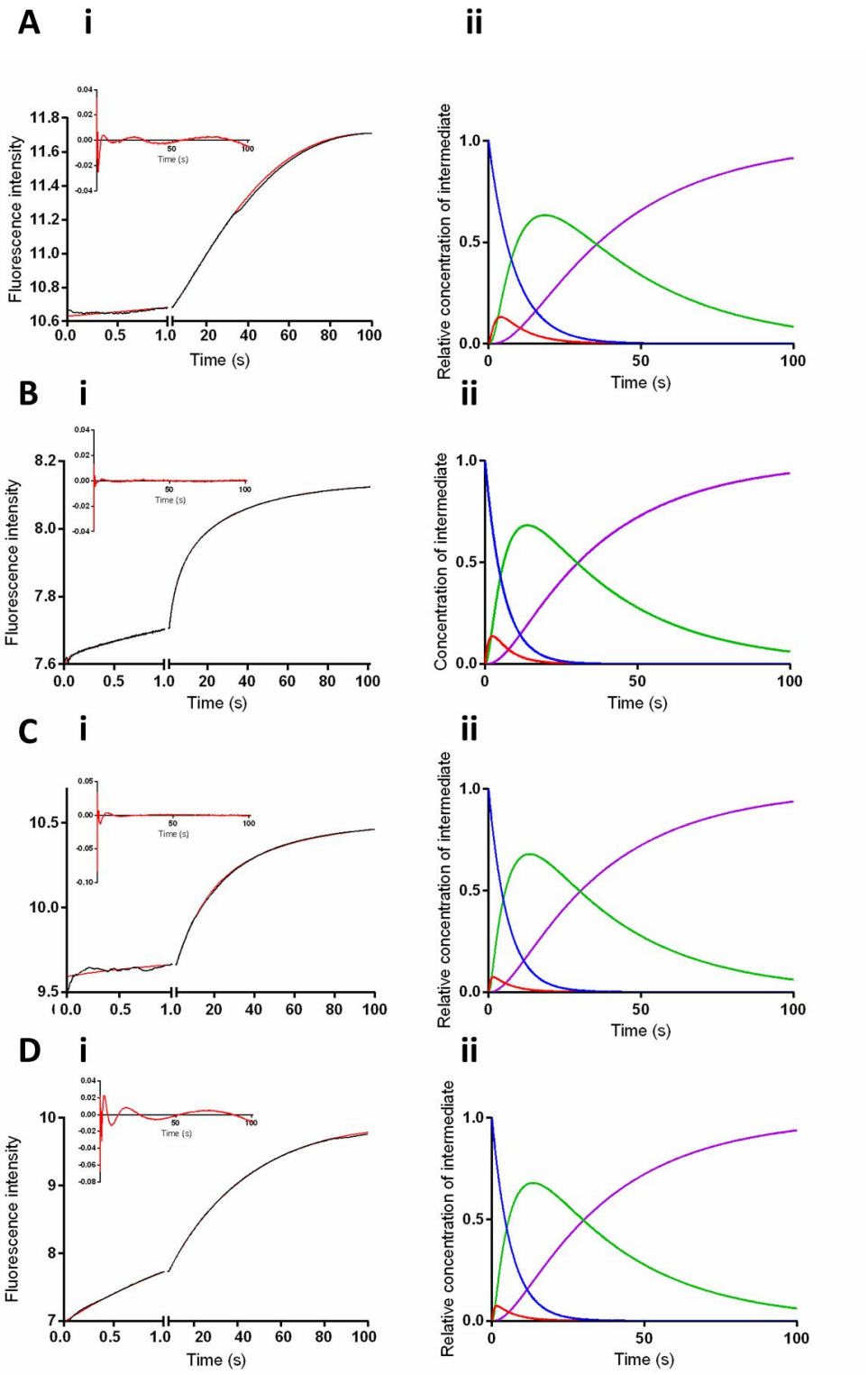


Figure 5.1.6. Kinetic modelling of 40 µg/ml PolyK$_{10}$ interacting with FPE labelled PC$_{70}$Chol$_{30}$ vesicles. (A) Tris, (B) PBS, (C) NaSCN and (D) Gly-Gly-Gly. (i) An averaged trace of PolyK$_{10}$ interaction to PC$_{70}$Chol$_{30}$ (black). This interaction is modelled (red) with the residuals of the kinetic model shown in the insert. (ii) The relative concentration of intermediate species suggested by the binding model, each colour represents a different intermediate in the reaction A→B→C→D. At any time point A+B+C+D= 1. All experiments were conducted at pH 7.4 at 25°C.

	$PC_{70}Chol_{30}$					
	K_1 ($\mu gml^{-1}s^{-1}$)	**sd ±**	**K_2 ($\mu gml^{-1}s^{-1}$)**	**sd ±**	**K_3 ($\mu gml^{-1}s^{-1}$)**	**sd ±**
Tris	0.16	0.0013	5.26	0.004	0.68	0.003
PBS	0.117	0.0004	2.02	0.022	0.59	0.003
Gly-Gly-Gly	0.228	0.0031	21.2	0.45	0.76	0.011
NaSCN	0.162	0.0003	12.96	0.09	1.71	0.002

Table 5.1.6. Kinetic rates of 40 µg/ml $PolyK_{10}$ interacting with FPE labelled $PC_{70}Chol_{30}$ vesicles in various media. Experiments were conducted at pH 7.4, 25°C. K_1 represents the rate between A→B; K_2 represents the rate between B→C and K_3 represent the rate between C→D in binding concentration intermediates such as Figure 5.1.6.

The kinetic modelling of the $PolyK_{10}$ $PC_{70}Chol_{30}$ interaction was shown fit a three-step mechanism in all media conditions, unlike that found with PC_{100} interactions (Figure 5.1.4), which elicited a two-step mechanism. This suggests that there is an undefined further mechanistic step. The additional reaction step could occur at any point in the reaction i.e. a new A→B, B→C or C→D step, with the previous three steps explained by the PC_{100} interaction. In comparison to the PC_{100} interactions, the new step is observed in the first 20s of peptide association with the membrane (Figure 5.1.4, Figure 5.1.6). This suggests that this step occurs upon initial interaction with the membrane. The intermediate formation of B is not rate limiting; this is demonstrated as a maximum of ~10% of the unbound peptide (A) is converted to the new intermediate (B). The intermediate C increases almost simultaneously with B, suggesting the step is very quick. The presence of cholesterol in the membrane results in a phase change creating ordered lipid microdomains (L_o) (shown in Section 4.1.2.2). Given the increased binding capacity and affinity of the $PolyK_{10}$ to cholesterol-containing membranes (Table 5.1.5), the step could be the microdomains/cholesterol attracting more $PolyK_{10}$ during binding.

The first rate (K_1), in which A is converted to B, is the slowest reaction step (Table 5.1.6). Considering that the overall binding reaction is similar to PC_{100}, this suggests that the polypeptide binds to both the PC and cholesterol in the membrane.

Gly-Gly-Gly and NaSCN both reduced the binding rate and affinity of $PolyK_{10}$ to the membrane. Interestingly the B_{max} values were reduced in comparison to PC_{100} membranes (Table 5.1.3 and Table 5.1.7) in the same media, suggesting that the cholesterol-mediated preferential binding is abolished and that there is a decrease the binding sites in the membrane.

5.1.2.3 *$PC_{70}PS_{30}$ membranes*

The binding concentration curves of $PolyK_{10}$ in all the different media were shown to fit to a hyperbolic binding model binding similar to the other membrane compositions.

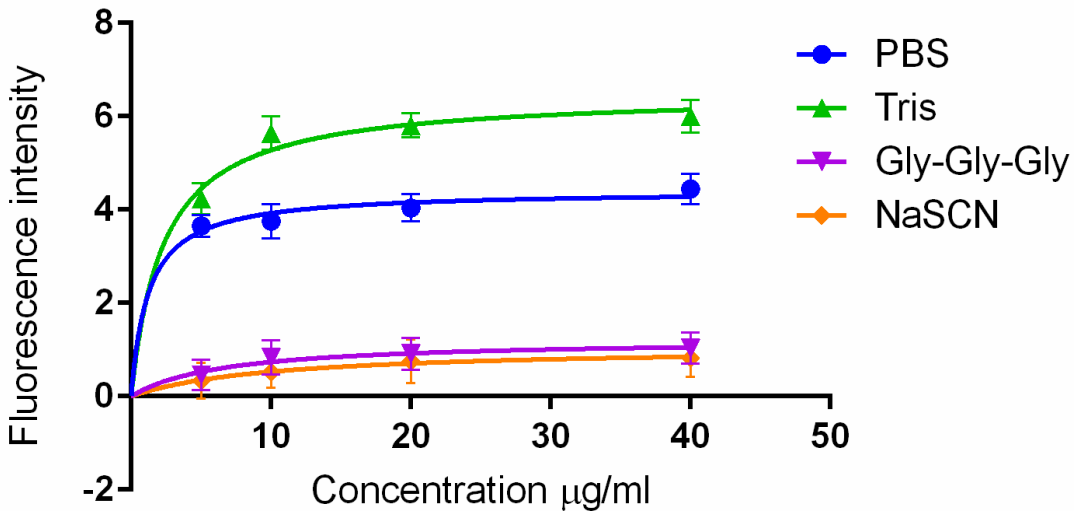


Figure 5.1.7. Plateau Δ*FI* values from SFRM analysis of $PolyK_{10}$ binding to $PC_{70}PS_{30}$. Binding interactions were fitted to a single hyperbolic binding model. Different media, Tris (blue), PBS (green), Gly-Gly-Gly (purple) and NaSCN (orange), were at pH7.4 (Table 2.2.1), with experiments conducted at 25°C.

	$PC_{70}PS_{30}$			
	B_{max} (a.u.)	**sd ±**	**K_d (μg/ml)**	**sd ±**
Tris	6.04	0.24	1.06	0.01
PBS	4.56	0.18	1.82	0.02
Gly-Gly-Gly	1.06	0.11	6.38	0.05
NaSCN	0.82	0.01	7.86	0.07

Table 5.1.7. B_{max} and K_d values $PolyK_{10}$ binding to $PC_{70}PS_{30}$ membranes. SFRM Δ*FI* values were fitted to a hyperbolic binding curve and hyperbolic binding curve will Hill coefficient, the best fit was determined by an F-test. All media used were at pH7.4 (Table 2.2.1), with experiments conducted at 25°C.

The interaction of $PolyK_{10}$ with $PC_{70}PS_{30}$ membrane had an approximately four-fold greater binding capacity and affinity than both PC_{100} and $PC_{70}Chol_{30}$ membranes (PC_{100} Tris B_{max} = 0.59 ± 0.08, $PC_{70}Chol_{30}$ Tris B_{max} = 0.77 ± 0.02, $PC_{70}PS_{30}$ Tris B_{max} = 2.61 ± 0.01) (Table 5.1.7). These results are somewhat unsurprising given the electrostatic attraction between the positive charges of the lysine residues and negatively charged phosphatidylserine lipids. NaSCN and Gly-Gly-Gly media resulted in a marked decrease in binding capacity of approximately four-fold when compared to PBS media and six-fold when compared to Tris media. The attenuation of binding in the NaSCN and Gly-Gly-Gly media is thought to be due to a reduction in electrostatic forces as shown in Chapter 3.

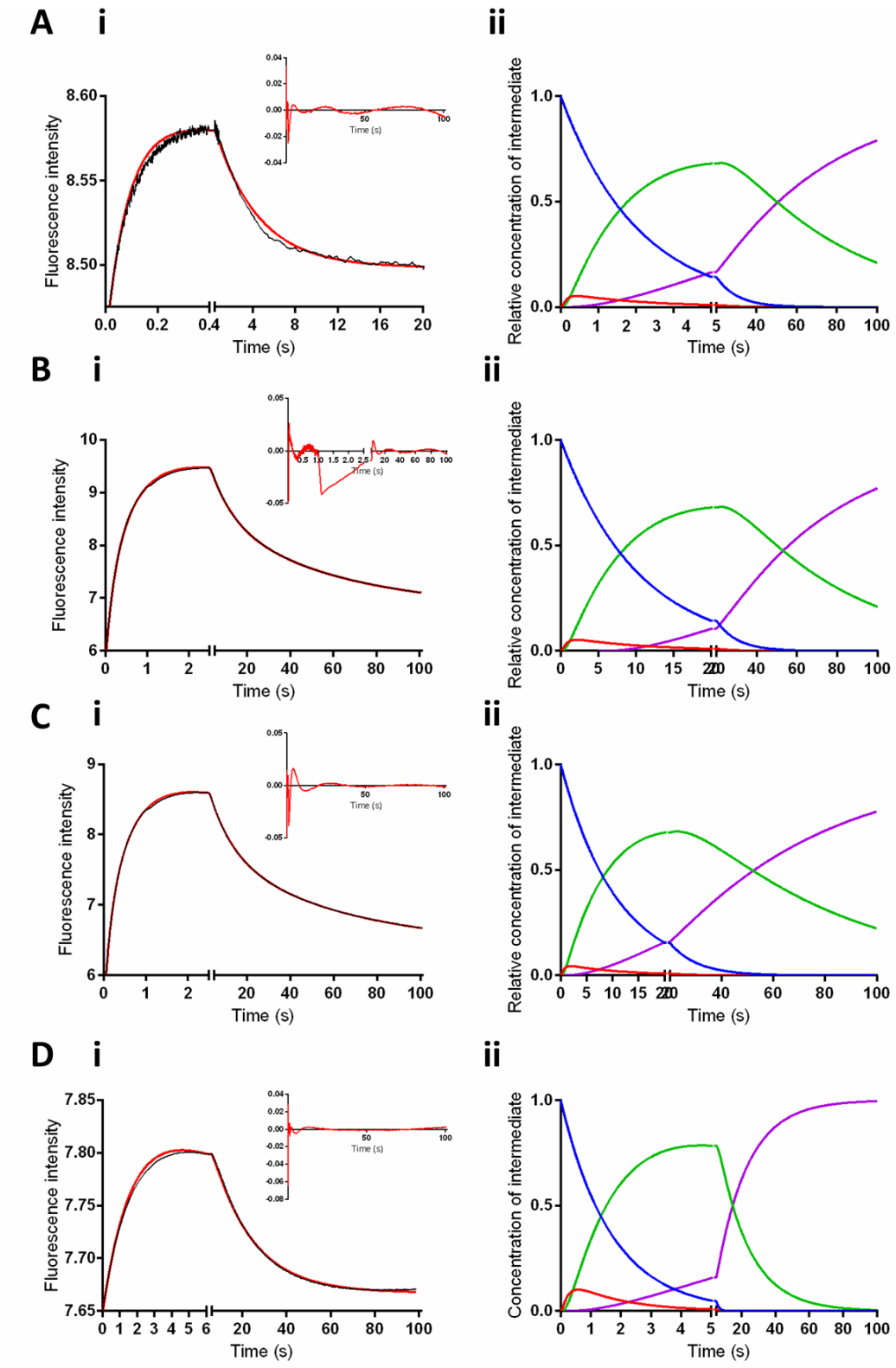


Figure 5.1.8. Kinetic modelling of 40 µg/ml PolyK$_{10}$ interacting with FPE labelled PC$_{70}$PS$_{30}$ vesicles. (A) Tris, (B) PBS, (C) NaSCN and (D) Gly-Gly-Gly. (i) An averaged trace of PolyK$_{10}$ interaction to PC$_{70}$PS$_{30}$ (black). This interaction is modelled (red) with the residuals of the kinetic model shown in the insert. (ii) The relative concentration of intermediate species suggested by the binding model, each colour represents a different intermediate in the reaction A→B→C→D. At any time point A+B+C+D= 1. All experiments were conducted at pH 7.4 at 25°C.

	$PC_{70}PS_{30}$					
	K_1 ($\mu gml^{-1}s^{-1}$)	**sd ±**	**K_2 ($\mu gml^{-1}s^{-1}$)**	**sd ±**	**K_3 ($\mu gml^{-1}s^{-1}$)**	**sd ±**
Tris	1.53	0.004	5.34	0.025	0.097	0.0006
PBS	1.90	0.003	6.53	0.036	0.23	0.007
Gly-Gly-Gly	0.60	0.002	23.96	0.12	4.26	0.03
NaSCN	0.09	0.0005	7.86	0.03	1.79	0.003

Table 5.1.8 Kinetic rates of 40 µg/ml $PolyK_{10}$ interacting with FPE labelled $PC_{70}PS_{30}$ vesicles in various media. Experiments were conducted at pH7.4, 25°C. K_1 represents the rate between A→B, K_2 represents the rate between B→C and K_3 represent the rate between C→D in binding concentration intermediates as shown in Figure 5.1.8.

The kinetic modelling of $PolyK_{10}$ interaction with $PC_{70}PS_{30}$ membranes is more complex than the PC_{100} membrane interactions, however somewhat surprisingly, no more complex than the binding observed to $PC_{70}Chol_{30}$ membranes. Figure 5.1.8 demonstrates that the kinetic model accurately models the decrease in fluorescence. The residuals shown in (Figure 5.1.8B (i) insert) denote a drop at 1 s due to a pressure aberration in the SFRM trace. The initial A→B rate (K_1 Table 5.1.8) and concentration of the intermediates highlights the increased association of the peptide in the first 2.5 s of the SFRM trace. After the peak in *FI*, the concentration of the intermediates is similar to those shown after 100s of association in the other membrane types (Figure 5.1.4) After 5s, the only intermediates present are D and E. This would suggest that the initial association is being fitted to a two-step mechanism as previously seen with PC_{100} membranes. The third reaction step is therefore proposed to be C→D represents the mechanistic step when compared to PC_{100} interactions.

The kinetic rate profiles of $PolyK_{10}$ interactions with $PC_{70}PS_{30}$ membranes were distinctly different to those seen in other membranes. The rates of K_2 are comparable to PC_{100} membranes although, K_1 are faster in $PC_{70}PS_{30}$ membranes related to the increased binding rate. The K_3 rate representing bound polypeptide to a further

configuration is much slower than the association rates in Tris and PBS; these rates are dramatically increased in the presence of Gly-Gly-Gly and NaSCN, suggesting that the media are actively contributing to the formation of the new intermediate.

5.1.2.4 *Thioflavin T Interaction with PolyK$_{10}$ in the Presence of Membrane Vesicles*

An intermediate protein conformation was seen across all three membrane types (green line in concentration determinants). The origin of the intermediate was expected to be the partitioning of the polypeptide into the water-bilayer interface, or a conformational change of the polypeptide on the surface. The possibility of a conformational change occurring on the membrane surface was monitored using ThT. ThT increases the fluorescence yield in the presence of hydrogen bond formation and has been characterised in a variety of different polypeptide and amyloid species [31] .

SFRM of ThT in solution and PolyK$_{10}$ resulted in a small, insignificant fluorescent changes demonstrating that the polypeptide was not, and does not, aggregate upon rapid mixing in all media tested (Figure 5.1.9 black). SFRM of ThT in solution and the various membranes vesicles did not result in any fluorescence change thus demonstrating that the membranes are not aggregated (Figure 5.1.9 red).

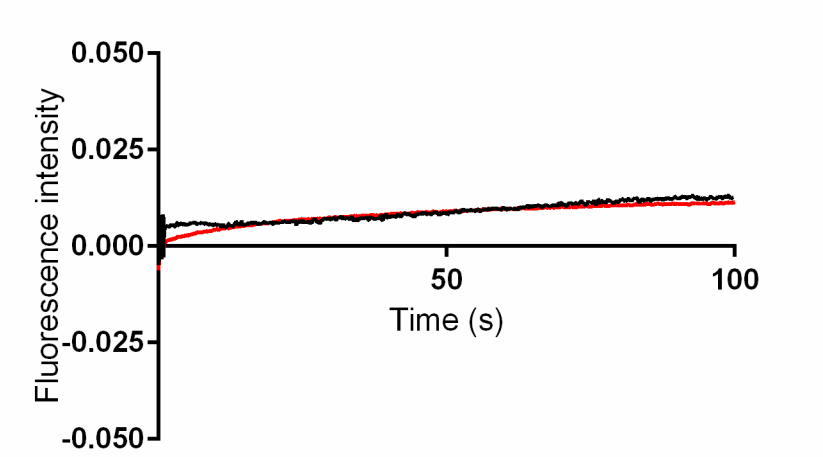


Figure 5.1.9. SFRM trace of Δ*FI* of ThT following excitation at 482nm. Interaction between ThT in solution and $PolyK_{10}$ 40μg/ml (black) or 400 μM unlabelled PC_{100} membranes (red). Experiments were conducted in PBS at pH7.4 at 25°C.

Figure 5.1.10 demonstrates fluorescent changes of that the $PolyK_{10}$ interactions with the membranes in the presence of ThT resulted in Δ*FI* that are comparable to the Δ*FI* using FPE as a probe.

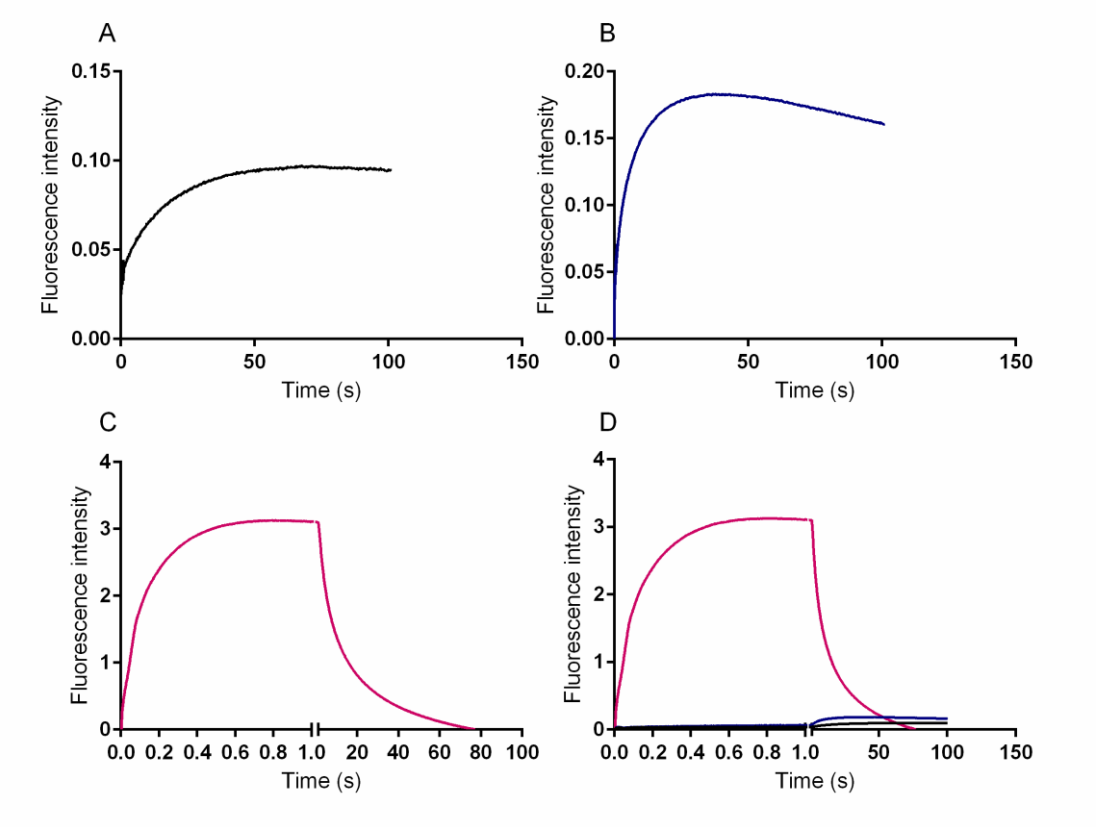


Figure 5.1.10. SFRM trace of Δ*FI* of membranes labelled ThT following excitation at 482nm interacting with PolyK$_{10}$ 40µg/ml. (A) PC_{100} membranes (B) $PC_{70}Chol_{30}$ and (C) $PC_{70}PS_{30}$. Relative effects of fluorescence changes in different membranes in (D).

Hydrogen-bonded PolyK$_{10}$ only forms in the presence of membrane vesicles, which accounts for the binding intermediate previously shown in Figure 5.1.4. The PolyK$_{10}$ interaction with $PC_{70}PS_{30}$ membranes resulted in hydrogen bond formation and decay within the same time-frame of the FPE fluorescence increase and decay. These results suggest that the final mechanistic step is beyond simple membrane interactions and warrants further investigation.

5.1.2.5 *Summary of PolyK$_{10}$ interactions*

	PC_{100}				$PC_{70}Chol_{30}$				$PC_{70}PS_{30}$			
	Tris	PBS	NaSCN	Gly-Gly-Gly	Tris	PBS	NaSCN	Gly-Gly-Gly	Tris	PBS	NaSCN	Gly-Gly-Gly
Number of kinetic steps	2	2	2	2	3	3	3	3	3	3	3	3
Apparent K_D (μM)	7.3	11.4	26.2	21.1	6.1	9.3	24.2	14.9	1.1	1.8	6.4	7.9
Binding mode	H	H	H	H	H	H	H	H	H	H	H	H

Table 5.1.9. Summary of interactions between PolyK$_{10}$ and membranes. Kinetic steps and binding affinities are summarised from tables above. Binding mode denoted as either hyperbolic (H) or cooperative (C).

PolyK$_{10}$ interactions are the most basic interactions observed in this chapter. All interactions exhibit simple, hyperbolic binding interactions. As previously demonstrated in Chapter 3, NaSCN and Gly-Gly-Gly decrease the binding interactions of PolyK$_{10}$ to the various membranes. The interactions are expected to be primarily driven through electrostatic interactions between the positive charge of the polypeptide and the negative charge of the phosphatidylserine.

5.1.3 PolyK$_{cc}$ Interaction with Various Membranes in Different Media

The interaction and binding intermediates of short-chain poly-lysine to various membranes have been examined. Long-chain poly-lysine interactions were also characterised in order to characterise the interaction further. To account for the differences between residue lengths, μg/ml quantities remained the same between the different species used. PolyKcc is termed ‘cc’ due to its common use in cell culture. The binding characteristics of both PolyK species highlights the affinity of and potential binding modes of various membranes. This work has impact in a host of fields that use PolyK$_{cc}$ in cell culture. PolyK$_{cc}$ binding to cell membranes may have unexpected consequences on the cells being studied.

5.1.3.1 *PC_{100} membranes*

Long-chain poly-lysine exhibited different binding profiles to its short-chain variant in PC_{100} membranes. The binding capacity is increased in Tris membranes, but not in PBS, Gly-Gly-Gly or NaSCN media (Table 5.1.10).

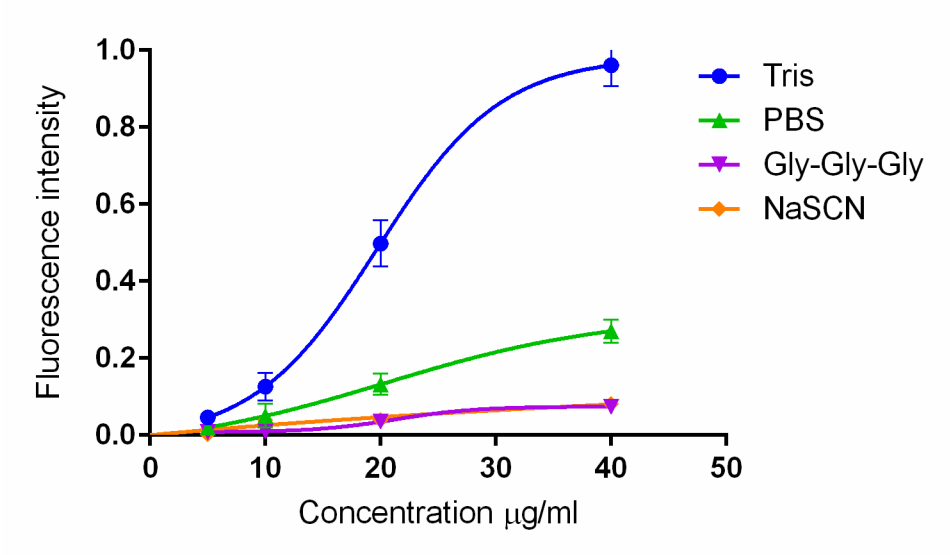


Figure 5.1.11. Plateau Δ*FI* values from SFRM of $PolyK_{cc}$ binding to PC_{100} membranes in different media. Tris (blue), PBS (green), Gly-Gly-Gly (purple) and NaSCN (orange), were at pH7.4 (Table 2.2.1), with experiments conducted at 25°C.

	PC_{100}					
	B_{max} (a.u.)	**sd ±**	**K_d (μg/ml)**	**sd ±**	**h**	**sd ±**
Tris	1.021	0.045	12.15	0.35	2.347	0.36
PBS	0.27	0.04	13.29	3.137	2.092	0.22
Gly-Gly-Gly	0.074	0.012	21.25	0.95	0.36	0.052
NaSCN	0.081	0.0035	1.909	0.56	-	-

Table 5.1.10. B_{max} and K_d values of $PolyK_{cc}$ binding to PC_{100} membranes. SFRM Δ*FI* values were fitted to a hyperbolic binding curve, and hyperbolic binding curve will hill coefficient. The best fit was determined by an F-test. All media were used at pH7.4 (Table 2.2.1), and the experiments were conducted at 25°C.

The changes in the fluorescent amplitudes were fitted to both simple binding (hyperbolic) cooperative binding models (sigmoidal or hyperbolic with Hill coefficient) (shown in $PolyK_{10}$). Following analysis via an F-test, it was clear that the data best fit to a cooperative binding model. The binding in Tris and PBS denoted Hill coefficients of ~2 (Table 5.1.10) where the Hill coefficient quantifies the

cooperativity of polypeptide binding. A Hill coefficient of 2 denotes either a preference for dimeric binding to the PC_{100} membrane vesicles or, the first molecule binding promotes binding of further polypeptides however, given the large size of the polypeptide species employed, the latter explanation is more likely. Binding in the presence of Gly-Gly-Gly suggests negative cooperativity (Hill coefficient of 0.356) where the binding of one polypeptide decreases the affinity for another to bind. The binding in the presence of NaSCN fits better to a simple binding model. These effects may be explained by the decreased binding capacity, or the reagents solubilising the polypeptide thus keeping it monomeric. It is noteworthy that the Hill coefficient is always a minimum approximation of the cooperativity of the molecules, if the first binding step is sigmoidal, it will lead to an underestimation in cooperativity for the rest of the binding reaction.

The kinetic profiles were modelled in the same way as for $PolyK_{10}$ with the results shown in Figure 5.1.12. $PolyK_{cc}$ interaction to PC_{100} membranes was best fitted to a three-step mechanism, A→B→C→D, suggesting a more complex binding reaction than that seen in Figure 5.1.4 with $PolyK_{10}$.

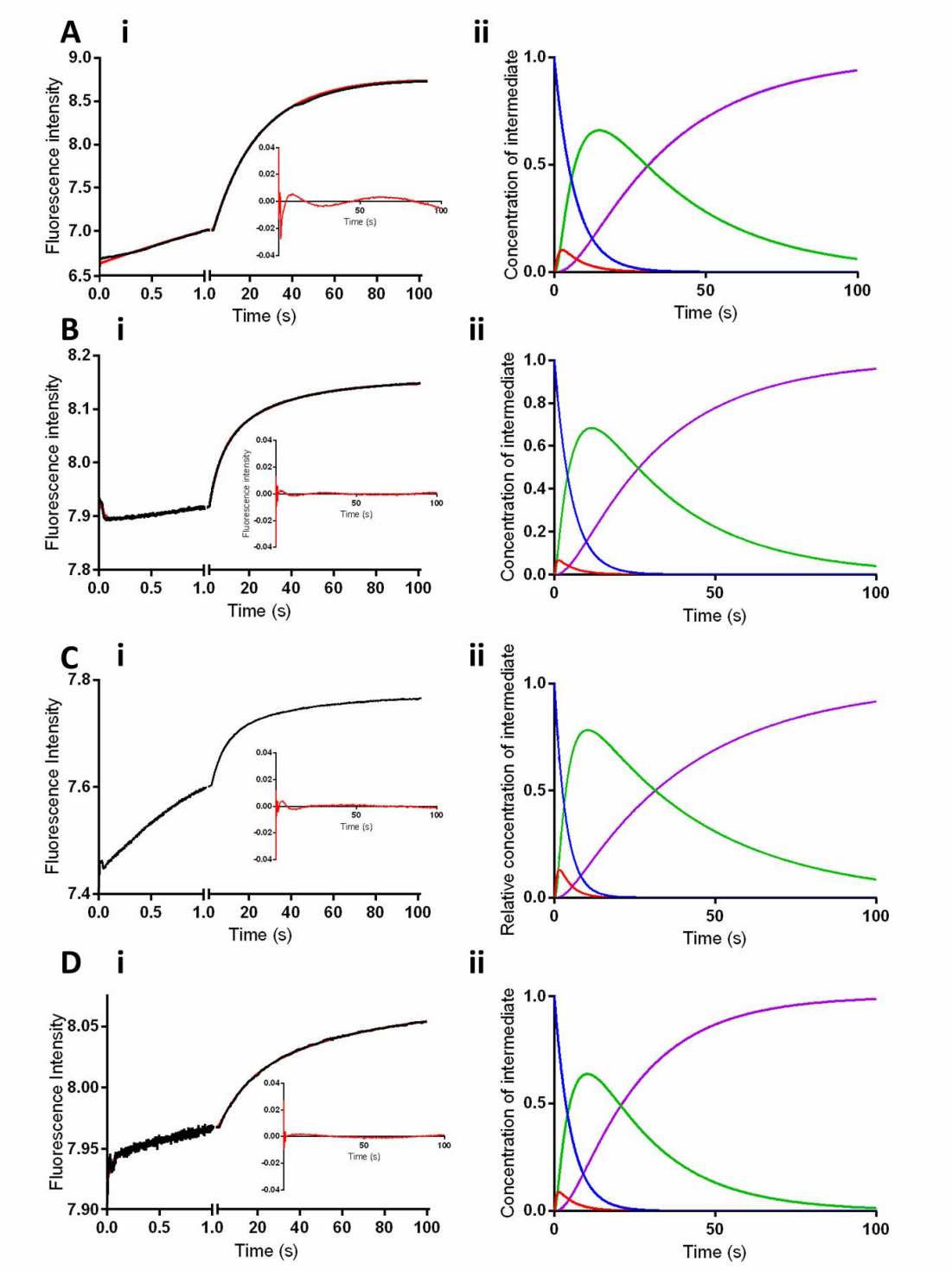


Figure 5.1.12. Kinetic modelling of 40 µg/ml PolyKcc interacting with FPE labelled PC_{100} vesicles. (A) Tris, (B) PBS, (C) NaSCN and (D) Gly-Gly-Gly. (i) An averaged trace of PolyKcc interaction to PC_{100} (black). This interaction is modelled (red) with the residuals of the kinetic model shown in the insert. (ii) The relative concentration of intermediate species suggested by the binding model, each colour represents a different intermediate in the reaction A→B→C→D. At any time point A+B+C+D= 1. All experiments were conducted at pH 7.4 at 25°C.

	PC_{100}					
	K_1 ($\mu gml^{-1}s^{-1}$)	**sd ±**	**K_2 ($\mu gml^{-1}s^{-1}$)**	**sd ±**	**K_3 ($\mu gml^{-1}s^{-1}$)**	**sd ±**
Tris	0.148	0.0018	2.54	0.016	0.031	0.0002
PBS	0.189	0.0028	21.58	0.37	0.034	0.0003
Gly-Gly-Gly	0.278	0.0065	6.45	0.019	0.026	0.0006
NaSCN	0.326	0.0026	3.026	0.003	0.010	0.0007

Table 5.1.11. Kinetic rates of 40 µg/ml $PolyK_{cc}$ interacting with FPE labelled PC_{100} vesicles in various media pH 7.4; experiments were conducted at 25°C. K_1 represents the rate between A→B; K_2 represents the rate between B→C and K_3 represent the rate between C→D in binding concentration intermediates such as in Figure 5.1.8B.

The increased mechanistic step, suggested by the kinetic modelling with PC_{100} membranes, is associated with the cooperative binding of the long-chain PolyK that interacts with the membrane (Figure 5.1.11).

5.1.3.2 *$PC_{70}Chol_{30}$ membranes*

$PolyK_{cc}$ interaction with FPE labelled $PC_{70}Chol_{30}$ resulted in an increase in fluorescence intensity. SFRM traces were examined for their binding capacity and affinities as shown previously (Figure 5.1.11). All media employed during the $PolyK_{cc}$ interactions with $PC_{70}Chol_{30}$ membranes, following an F-test, were best fitted to cooperative binding curves (Table 5.1.12).

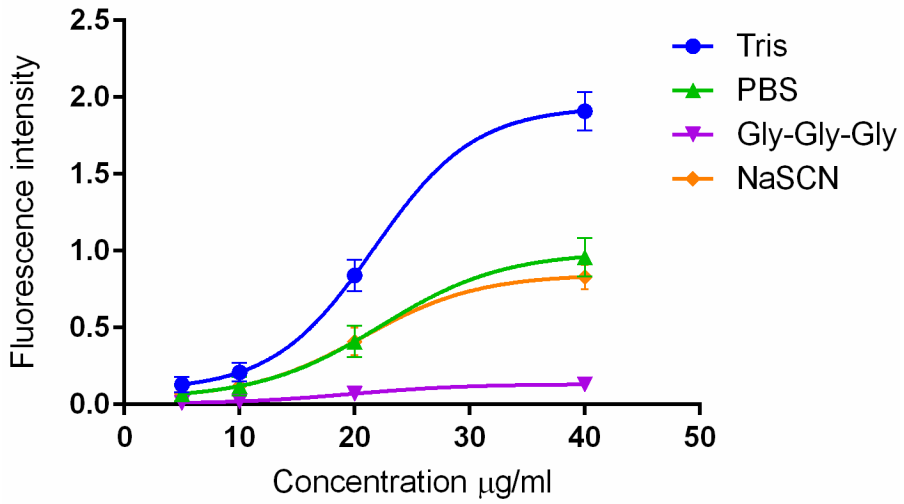


Figure 5.1.13. Plateau Δ*FI* values from SFRM of $PolyK_{cc}$ binding to $PC_{70}Chol_{30}$ membranes. Different media, Tris (blue), PBS (green), Gly-Gly-Gly (purple) and NaSCN (orange), were at pH7.4 (Table 2.2.1), with experiments conducted at 25°C.

	$PC_{70}Chol_{30}$					
	B_{max} (a.u.)	**sd ±**	**K_d (µg/ml)**	**sd ±**	**h**	**sd ±**
Tris	1.91	0.51	10.70	4.40	2.13	1.49
PBS	0.96	0.07	13.29	1.29	2.43	0.42
Gly-Gly-Gly	0.13	0.11	14.66	6.82	4.75	0.98
NaSCN	0.83	0.078	12.88	1.75	5.29	2.30

Table 5.1.12. B_{max} and K_d values for $PolyK_{cc}$ binding to $PC_{70}Chol_{30}$ membranes. SFRM Δ*FI* values were fitted to a hyperbolic binding curve and hyperbolic binding curve will Hill coefficient, the best fit was determined by an F-test. All media used were at pH7.4 (Table 2.2.1), with experiments conducted at 25°C.

There is a decrease in binding capacity in the presence of salt, as demonstrated previously with $PolyK_{cc}$ interaction with PC_{100} (Table 5.1.10). Between PC_{100} and $PC_{70}Chol_{30}$ membranes, the affinity did not differ significantly in either Tris or PBS media (PBS PC_{100} K_d; 13.29 ± 3.14, $PC_{70}Chol_{30}$ K_d; 13.29 ± 1.292, ($P>0.05$ one-way t-test)). This result would suggest that there is no preferential interaction with cholesterol, as seen with $PolyK_{10}$ interactions, however, a significant increase in binding capacity demonstrates an increase in binding to cholesterol-containing membranes (Table 5.1.12, $P>0.05$ one-way t-test).

$PolyK_{cc}$ binding in Tris and PBS media has a Hill coefficient of ~2 suggesting cooperative binding to the membrane like that of the $PolyK_{cc}$ interaction with PC_{100} membranes. Gly-Gly-Gly and NaSCN have a reduced affinity and binding capacity to the $PC_{70}Chol_{30}$ membranes however, they have Hill coefficients of ~5, suggesting a high level of cooperativity. This may be the binding of the polypeptide as multimers or the initial polypeptide interaction with the membrane priming the membrane for the further association.

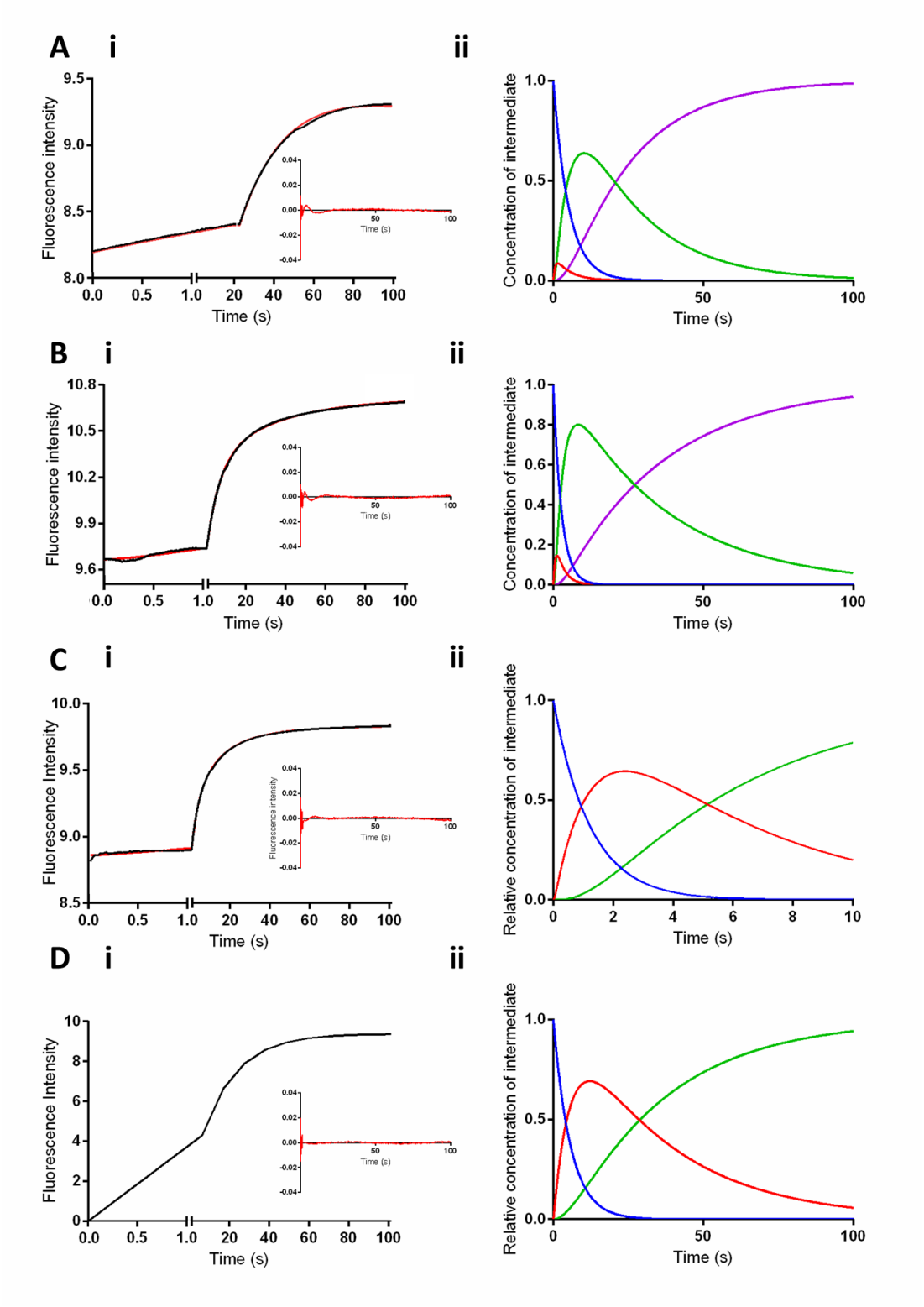


Figure 5.1.14. Kinetic modelling of 40 µg/ml PolyK$_{cc}$ interacting with FPE labelled PC$_{70}$Chol$_{30}$ vesicles. (A) Tris, (B) PBS, (C) NaSCN and (D) Gly-Gly-Gly. (i) An averaged trace of PolyK$_{cc}$ interaction to PC$_{70}$Chol$_{30}$ (black). This interaction is modelled (red) with the residuals of the kinetic model shown in the insert. (ii) The relative concentration of intermediate species suggested by the binding model, each colour represents a different intermediate in the reaction A→B→C→D. At any time point A+B+C+D= 1. All experiments were conducted at pH 7.4 at 25°C.

	$PC_{70}Chol_{30}$					
	K_1 ($\mu gml^{-1}s^{-1}$)	**sd ±**	**K_2 ($\mu gml^{-1}s^{-1}$)**	**sd ±**	**K_3 ($\mu gml^{-1}s^{-1}$)**	**sd ±**
Tris	0.196	0.002	1.71	0.0034	0.046	0.0002
PBS	0.367	0.005	1.64	0.012	0.029	0.0003
Gly-Gly-Gly	0.1813	0.01	1.88	0.0032	-	-
NaSCN	0.175	0.005	1.37	0.027	-	-

Table 5.1.13. Kinetic rates of 40 µg/ml $PolyK_{cc}$ interacting with FPE labelled $PC_{70}Chol_{30}$ vesicles in various media at pH 7.4, experiments were conducted at 25°C. K_1 represents the rate between A→B, K_2 represents the rate between B→C and K_3 represent the rate between C→D in binding concentration intermediates such as Figure 5.1.14.

Figure 5.1.14A illustrates that $PolyK_{cc}$ interactions with $PC_{70}Chol_{30}$ are best fitted to a three-step kinetic model, with all media tested (Table 5.1.13).

The initial association rate, K_1, is faster in $PC_{70}Chol_{30}$ membranes than PC_{100} membranes. This result, in combination with the increased binding capacity, suggests that the cooperative binding of $PolyK_{cc}$ is faster than the non-cooperative binding shown with PC_{100} membranes. $PC_{70}Chol_{30}$ membranes have a higher percentage of intermediate B formation (~20%) than in PC_{100} (~10%). Intermediate B was previously attributed to two potential mechanisms. Firstly an intermediate formed due to the cooperative binding (in the case of $PolyK_{cc}$ interaction with PC_{100} membranes), or cholesterol-mediated binding (in the case of $PolyK_{10}$ interaction with $PC_{70}Chol_{30}$ membranes). The two-fold increase of the intermediate suggests that the both mechanisms could be represented by the one kinetic step.

5.1.3.3 *$PC_{70}PS_{30}$ membranes*

The addition of $PolyK_{cc}$ to FPE labelled $PC_{70}PS_{30}$ vesicles causes an increase in fluorescence intensity as the membrane surface potential becomes more electropositive. The binding profiles of $PolyK_{cc}$ interaction to $PC_{70}PS_{30}$ membranes in the different media employed were all preferentially fitted to a cooperative binding model (Figure 5.1.15).

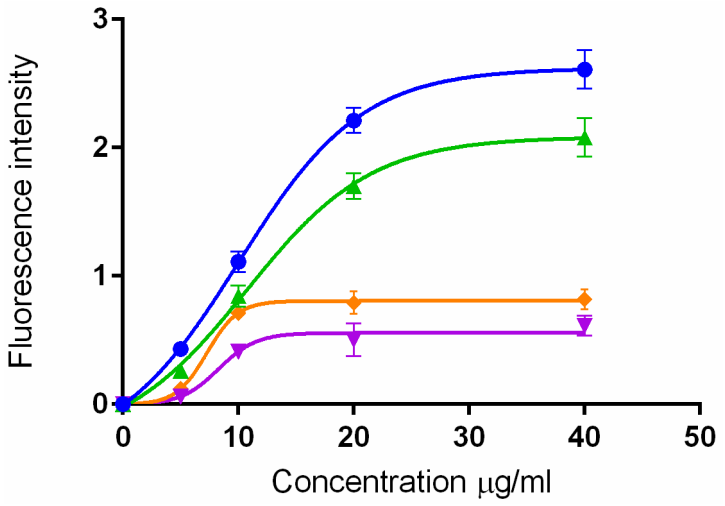


Figure 5.1.15. Plateau Δ*FI* values from SFRM of PolyK$_{cc}$ binding to PC$_{70}$PS$_{30}$ membranes. Different media, Tris (blue), PBS (green), Gly-Gly-Gly (purple) and NaSCN (orange), were at pH7.4 (Table 2.2.1), with experiments conducted at 25°C.

	PC$_{70}$PS$_{30}$					
	B$_{max}$ (a.u.)	**sd ±**	**K$_d$ (µg/ml)**	**sd ±**	**h**	**sd ±**
Tris	2.61	0.10	1.26	0.01	2.61	0.10
PBS	2.13	0.21	2.66	0.02	1.46	0.01
Gly-Gly-Gly	0.61	0.17	20.65	0.05	1.06	0.11
NaSCN	0.82	0.07	27.46	0.07	0.82	0.01

Table 5.1.14. B$_{max}$ and K$_d$ values PolyK$_{cc}$ binding to PC$_{70}$PS$_{30}$ membranes. SFRM Δ*FI* values was fitted to a hyperbolic binding curve and hyperbolic binding curve with a Hill coefficient. The best fit was determined by an F-test. All media used were at pH7.4 (Table 2.2.1), with experiments conducted at 25°C.

The binding affinity of PolyK$_{cc}$ to PC$_{70}$PS$_{30}$ membranes, was greater than the interaction to both PC$_{100}$ and PC$_{70}$Chol$_{30}$ membranes (Tris K$_d$ PC$_{100}$ 12.15 ± 0.35, PC$_{70}$Chol$_{30}$ 10.70 ± 4.40, PC$_{70}$PS$_{30}$ 1.26 ± 0.01, ($P<0.01$ ANOVA)). The PolyK$_{cc}$ binds to PC$_{70}$Chol$_{30}$ membranes with the same affinity as PolyK$_{10}$ (Tris K$_d$ PolyK$_{10}$ 1.06 ± 0.01, PolyK$_{cc}$ 1.26 ± 0.01) however, with a lower binding capacity (Tris B$_{max}$; PolyK$_{10}$ 6.04 ± 0.24, PolyK$_{cc}$ 2.61 ± 0.10). Therefore, the longer-chain PolyK species binds to the membrane with the same affinity, but to fewer binding sites, potentially due to the increased size of the chains that are associating. The cooperativity demonstrated by PolyK$_{cc}$ may account for the decreased capacity when compared to PolyK$_{10}$. Although the number of residues in the reaction is constant between the

polypeptides, the long chains of $PolyK_{cc}$ are more likely to overlap when binding than the short $PolyK_{10}$.

A drop in fluorescence intensity was observed after the initial ~2.5s of polypeptide association, as seen previously with $PolyK_{10}$ interaction with $PC_{70}PS_{30}$ membranes (Figure 5.1.8). The kinetic data fits to the most complex model of any polypeptide-membrane interaction with four steps (Figure 5.1.16).

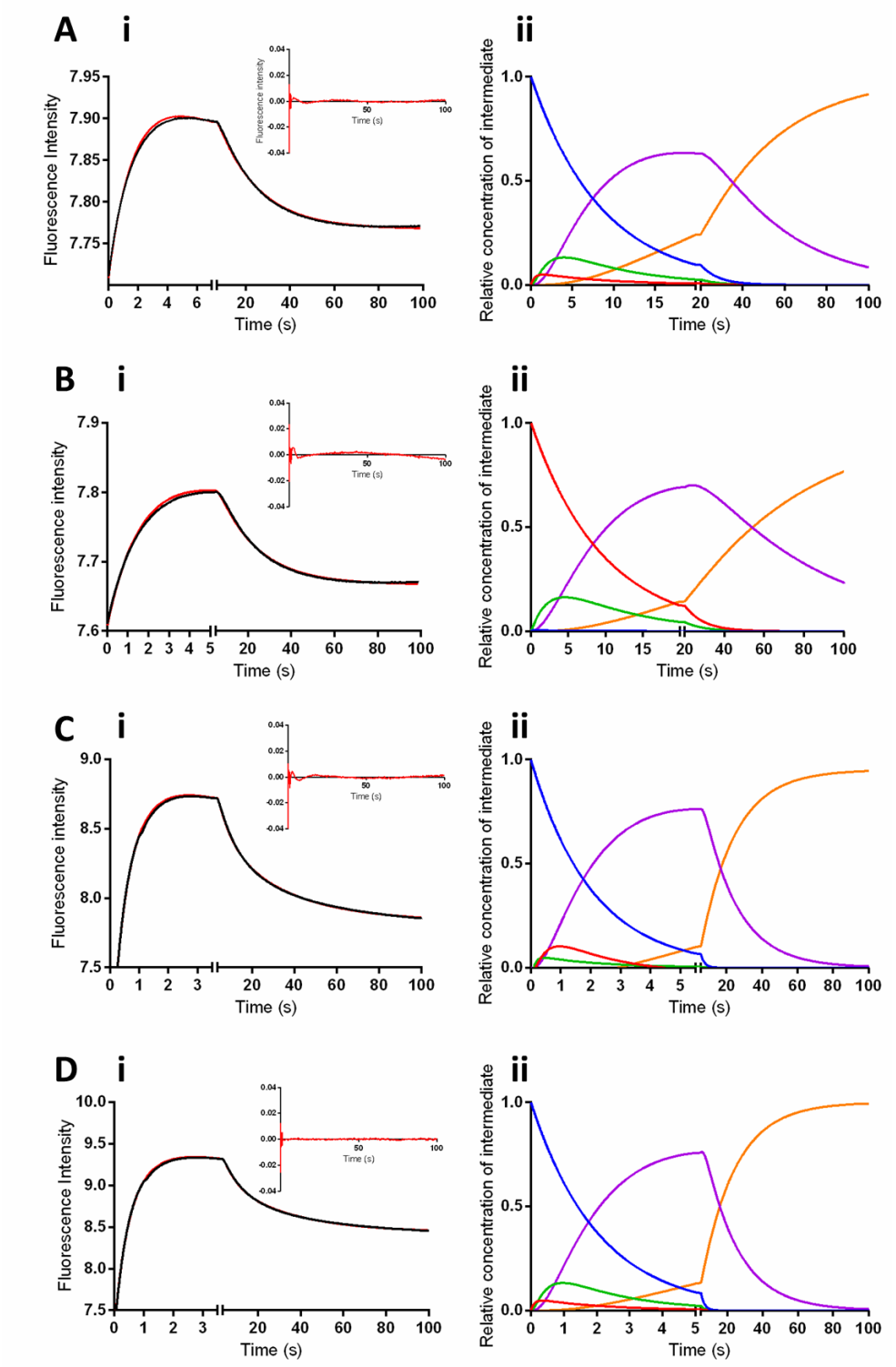


Figure 5.1.16. Kinetic modelling of 40 µg/ml PolyK$_{cc}$ interacting with FPE labelled PC$_{70}$PS$_{30}$ vesicles. (A) Tris, (B) PBS, (C) NaSCN and (D) Gly-Gly-Gly. (i) An averaged trace of PolyK$_{cc}$ interaction to PC$_{70}$PS$_{30}$ (black). This interaction is modelled (red) with the residuals of th1e kinetic model shown in the insert. (ii) The relative concentration of intermediate species suggested by the binding model, each colour represents a different intermediate in the reaction A→B→C→D→E. At any time point A+B+C+D+E= 1. All experiments were conducted at pH 7.4 at 25°C.

	$PC_{70}PS_{30}$							
	K_1 ($\mu gml^{-1}s^{-1}$)	**sd ±**	**K_2 ($\mu gml^{-1}s^{-1}$)**	**sd ±**	**K_3 ($\mu gml^{-1}s^{-1}$)**	**sd ±**	**K_4 ($\mu gml^{-1}s^{-1}$)**	**sd ±**
Tris	3.2407	24.022	14.084	27.26	0.94	0.91	0.0009	0.018
PBS	0.133	0.0042	10.393	0.11	2.74	0.029	0.6175	0.017
NaSCN	0.489	0.006	8.7001	0.08	2.45	0.024	0.0528	0.0007
Gly-Gly-Gly	0.1051	0.0096	24.922	0.71	0.40	0.018	0.0167	0.002

Table 5.1.15. Kinetic rates of 40 µg/ml $PolyK_{cc}$ interacting with FPE labelled $PC_{70}PS_{30}$ vesicles in media (at pH 7.4, experiments were conducted at 25°C. K_1 represents the rate between A→B, K_2 represents the rate between B→C, K_3 represents the rate between C→D and K_4 represents the rate between D→E in binding concentration intermediates such as Figure 5.1.16.

The kinetic modelling of the reaction matched that a four-step interaction. The initial three steps are similar to those shown with a $PolyK_{cc}$ interaction with $PC_{70}Chol_{30}$ membranes (Figure 5.1.14), and a $PolyK_{10}$ interaction with $PC_{70}PS_{30}$ membranes (Figure 5.1.8). The interaction steps discussed with $PolyK_{cc}$ to $PC_{70}Chol_{30}$ and $PolyK_{10}$ to $PC_{70}PS_{30}$ are ongoing after the 100 s of observation. However, the $PolyK_{cc}$ $PC_{70}PS_{30}$ interactions are completed after 15s with one further reaction step occurring for the remainder of the 100s observation period. The concentration peak of intermediate D (~15 s) (Figure 5.1.16) is much later than the ΔFI of ~2.5 s which suggests that the initial polypeptide association reaches equilibrium with the decreasing fluorescence. This is caused by step E after 2.5s and continues for a total of 15s. The mechanism behind the fluorescence decrease is investigated further in Section 5.3.2.

5.1.3.4 *Summary of PolyK$_{cc}$ Interaction to Various Membranes*

	PC$_{100}$				**PC$_{70}$Chol$_{30}$**				**PC$_{70}$PS$_{30}$**			
	Tris	PBS	NaSCN	Gly-Gly-Gly	Tris	PBS	NaSCN	Gly-Gly-Gly	Tris	PBS	NaSCN	Gly-Gly-Gly
Number of kinetic steps	2	2	2	2	3	3	2	2	4	4	4	4
Apparent K_D (μM)	12.15	13.3	21.25	>40	10.7	13.3	14.7	12.9	1.3	2.7	20.7	27.5
Binding mode	C	C	-	-	C	C	C	C	C	H	H	H

Table 5.1.16. Summary of interactions between PolyK$_{cc}$ and membranes. Kinetic steps and binding affinities are summarised from tables above. Binding mode denoted as either hyperbolic (H) or cooperative (C).

Interactions of PolyK$_{cc}$ with various membranes elicited the same trends of binding interactions as seen with PolyK$_{10}$ interactions. These include cholesterol preferential binding and the increased electrostatic interaction to PS in the membrane. Increasing the chain length altered the binding profiles of the polypeptide from hyperbolic to sigmoidal thus increasing the steps needed for the kinetic modelling (Figure 5.1.12, Figure 5.1.14 and Figure 5.1.16).

5.1.3.5 *Thioflavin T Interaction with PolyKcc in the Presence of Membrane Vesicles*

The interaction of PolyK$_{cc}$ to the various membrane compositions was shown to be a multi-step reaction in all the different media compositions. By interrogating the kinetic modelling of the interaction, one of the intermediate steps has been suggested to be a conformational change on the membrane surface.

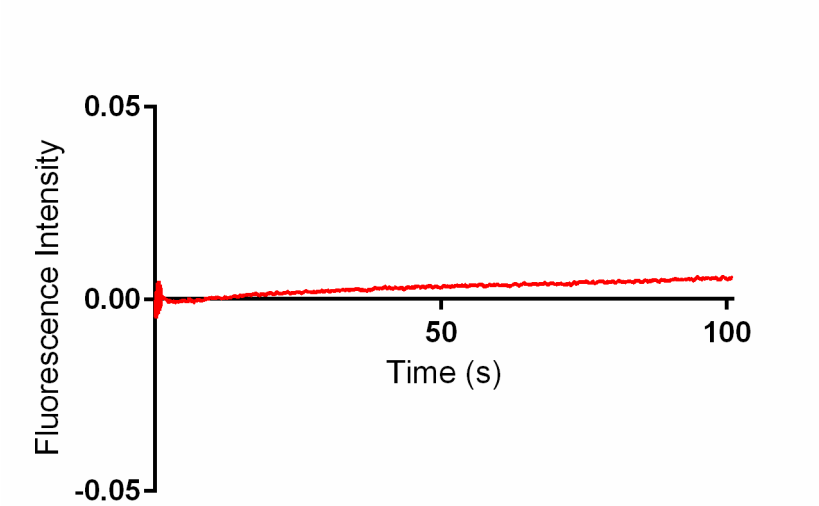


Figure 5.1.17. SFRM trace of Δ*FI* of ThT in solution following excitation at 482 nm in PBS interacting with PolyK$_{cc}$ (40µg/ml), at pH7.4, experiments were conducted 25°C

The interaction between the PolyK$_{cc}$ and ThT in the absence of membrane demonstrated that the PolyK$_{cc}$ stock used is not aggregated, and does not spontaneously aggregate in solution.

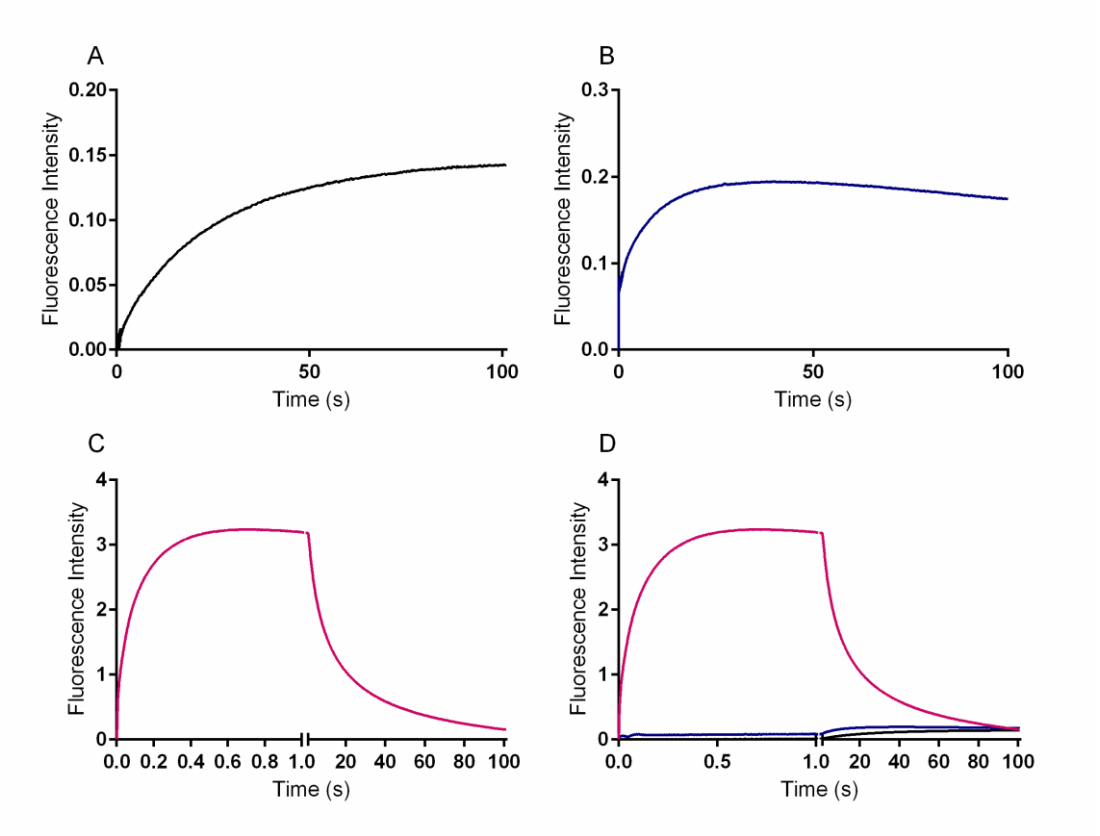


Figure 5.1.18. SFRM trace of Δ*FI* of membranes labelled ThT interacting with PolyK$_{cc}$ 40µg/ml and (red) 400 µM unlabelled PC$_{100}$ membranes. (A) PC$_{100}$ membranes (B) PC$_{70}$Chol$_{30}$ and (C) PC$_{70}$PS$_{30}$. Relative effects of fluorescence changes in different membranes in (D). Experiments were carried out in PBS pH7.4 at 25°C, with fluorescence intensity measured following excitation at 482 nm.

The PolyK$_{cc}$ interaction with ThT in the presence of membranes resulted in an increase in fluorescence intensity which suggests β-sheet formation. Figure 5.1.18 denotes a modest increase of the fluorescence in PC$_{100}$ and PC$_{70}$Chol$_{30}$ membranes. The fluorescence profile of ThT is complimentary to the fluorescence observed with the membrane surface potential of FPE (Figure 5.1.11, Figure 5.1.13 and Figure 5.1.15). This suggests that binding and β-sheet formation occur sequentially i.e. as more PolyK$_{cc}$ binds, more β-sheets are formed. β-sheet formation in the presence of PC$_{70}$PS$_{30}$ membranes correlates with the binding shown in Figure 5.1.16, with an increase in fluorescence, followed by a decreases in the ThT fluorescence, suggesting that there is a further reaction step that results in the dissociation of the secondary structure (see Section 5.2).

5.1.4 PolyQ$_{28}$ Interaction to Membranes

Polypeptide binding to the membrane has been examined with both short (PolyK$_{10}$) and long poly-lysine chains (PolyK$_{cc}$). The function of the Huntingtin protein is still unknown however, the first exon, containing the polyglutamine expansion, has been shown to be important in directing the association of the peptide (Section 1.2.4). Here, the binding interaction of the first exon of Htt, termed PolyQ$_{28}$, is examined to determine the extent that the polypeptide interactions characterised above are responsible for Huntingtin interactions.

5.1.4.1 *PC$_{100}$ membranes*

Initially, interactions were examined by titration assays in a fluoromax spectrometer however; the polypeptide did not elicit a detectable fluorescence change. As a result, the previously validated SFRM was employed in similar processes to the PolyK$_{10}$ and PolyK$_{cc}$ interaction with membranes.

PolyQ$_{28}$ interaction with FPE labelled PC$_{100}$ membranes, detected with SFRM, still did not affect the electrostatic membrane potential enough to elicit a fluorescence in any of the media employed (Table 5.1.2, Figure 5.1.19).

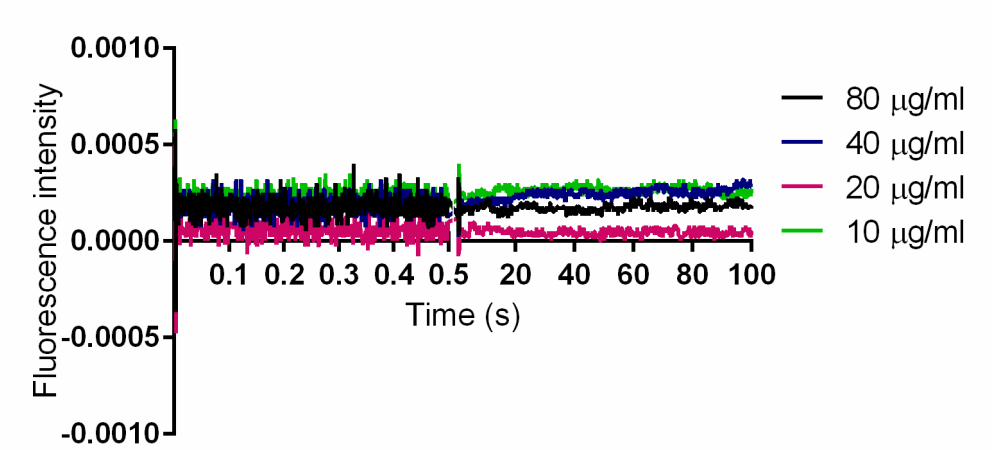


Figure 5.1.19. SFRM trace of PolyQ$_{28}$ interaction with PC$_{100}$ membranes in PBS media, at pH7.4, experiments were conducted at 25°C. Each trace is an average of five binding reactions.

5.1.4.2 *$PC_{70}Chol_{30}$ membranes*

The interaction between $PolyQ_{28}$ and $PC_{70}Chol_{30}$ membranes demonstrates that $PolyQ_{28}$ specifically binds to cholesterol-containing membranes.

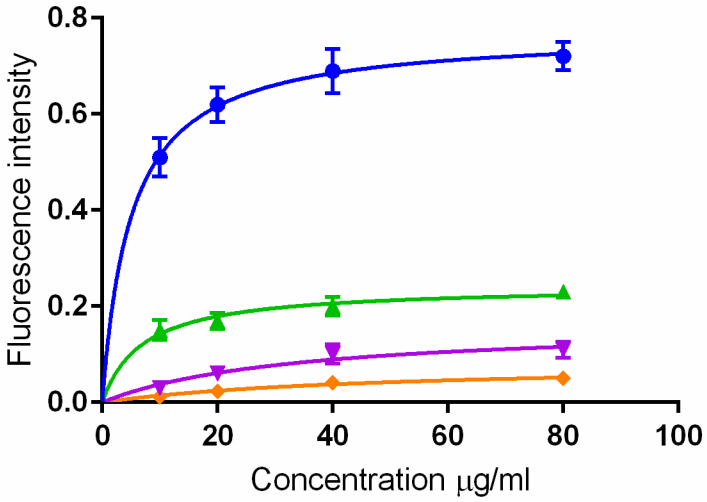


Figure 5.1.20. Plateau Δ*FI* values from SFRM of $PolyQ_{28}$ binding to $PC_{70}Chol_{30}$. Different media, Tris (blue), PBS (green), Gly-Gly-Gly (purple) and NaSCN (orange), were at pH7.4 (Table 2.2.1), with experiments conducted at 25°C.

	$PC_{70}Chol_{30}$			
	B_{max} (a.u.)	**sd ±**	**K_d (μg/ml)**	**sd ±**
Tris	0.72	0.005	3.59	0.21
PBS	0.23	0.003	4.01	0.20
Gly-Gly-Gly	0.11	0.013	12.32	0.47
NaSCN	0.05	0.001	21.13	0.40

Table 5.1.17. B_{max} and K_d values $PolyQ_{28}$ binding to $PC_{70}Chol_{30}$ membranes. SRFM Δ*FI* values were fitted to a hyperbolic binding curve and hyperbolic binding curve with a Hill coefficient. The best fit was determined by an F-test. All media were used at pH7.4 (Table 2.2.1), with experiments conducted at 25°C.

$PolyQ_{28}$ interaction with $PC_{70}Chol_{30}$ membranes in the various media were best fitted to a hyperbolic binding model and did not exhibit cooperativity, determined by an F-test. The binding capacity was decreased three-fold in the presence of salt (PBS and Tris Table 5.1.17, ($P<0.01$, one-way t-test)); however the binding affinity was not significantly decreased ($P>0.05$). This suggests that either that the binding sites on the membrane are ionically screened resulting in decreased PolyQ binding, or the sensitivity of the probe is decreased due to screening the effective range of the probe

by the increased salt, however there is no evidence for this (Figure 5.1.1). Gly-Gly-Gly decreased the binding capacity of PolyQ to membranes a further two-fold, and the affinity a further four-fold. More severely, NaSCN decreased the binding capacity of the PolyQ four-fold and the binding affinity five-fold. From previous observations, this suggests that the PolyQ binding is primarily driven by charge-charge interactions, which is unsurprising considering the nature of the polypeptide (see discussion). The preferential interaction with the cholesterol-containing membranes suggests that hydrogen bonding occurs between the $PolyQ_{28}$ and the cholesterol in the membrane.

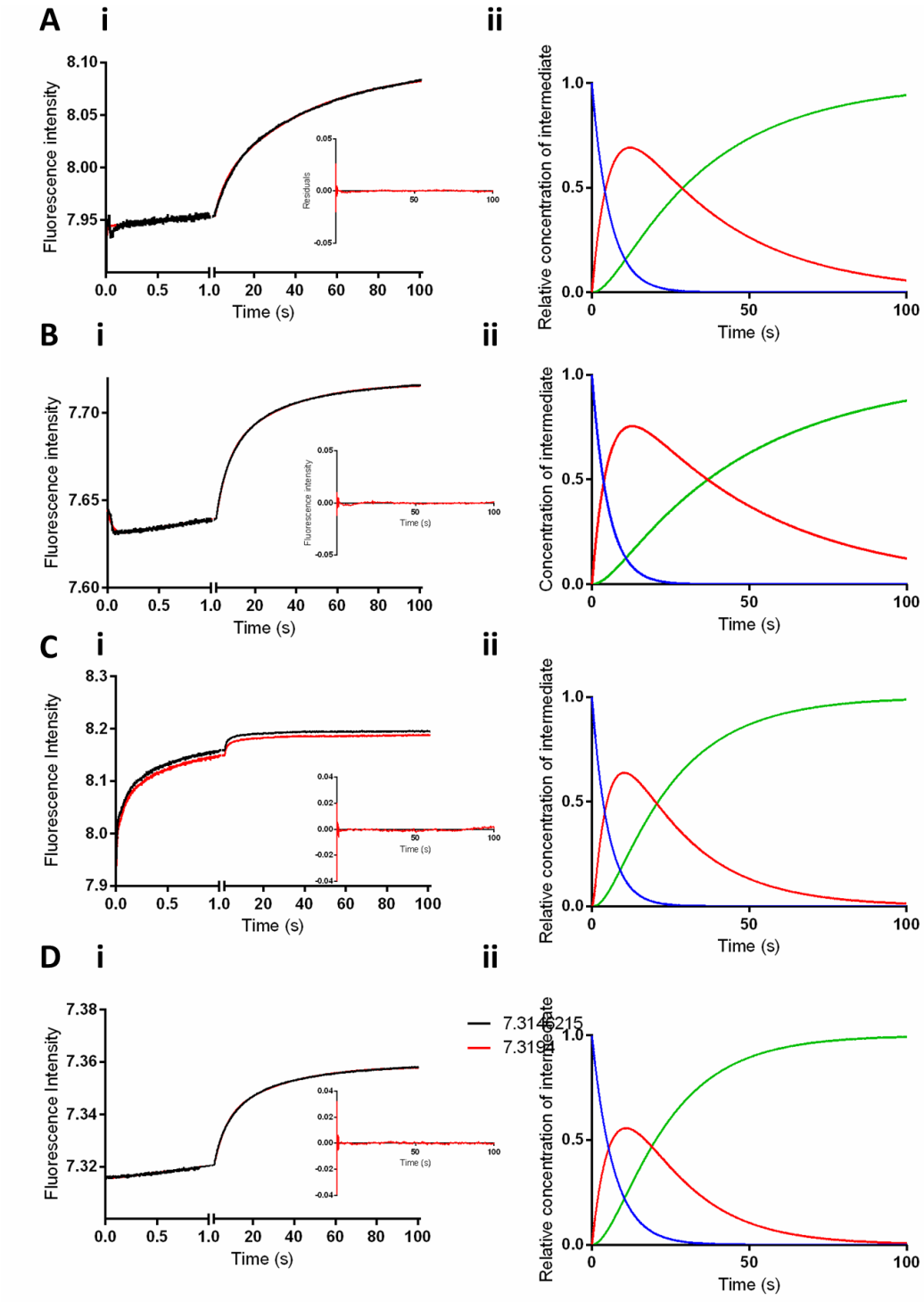


Figure 5.1.21. Kinetic modelling of 40 µg/ml PolyQ$_{28}$ interacting with FPE labelled PC$_{70}$Chol$_{30}$ vesicles. (A) Tris, (B) PBS, (C) NaSCN and (D) Gly-Gly-Gly. (i) An averaged trace of PolyQ$_{28}$ interaction to PC$_{70}$Chol$_{30}$ (black). This interaction is modelled (red) with the residuals of th1e kinetic model shown in the insert. (ii) The relative concentration of intermediate species suggested by the binding model, each colour represents a different intermediate in the reaction A→B→C. At any time point A+B+C= 1. All experiments were conducted at pH 7.4 at 25°C.

	$PC_{70}Chol_{30}$			
	K_1 ($\mu gml^{-1}s^{-1}$)	**sd ±**	**K_2 ($\mu gml^{-1}s^{-1}$)**	**sd ±**
Tris	1.87	0.358	7.23	0.32
.0PBS	0.91	0.12	9.54	0.19
Gly-Gly-Gly	0.15	0.05	23.91	0.41
Na0SCN	0.020	0.04	32.29	0.36

Table 5.1.18. Kinetic rates of 40 µg/ml $PolyQ_{28}$ interacting with FPE labelled $PC_{70}Chol_{30}$ vesicles in media (Table 2.2.1) at pH 7.4, experiments were conducted at 25°C. K_1 represents the rate between A→B and K_2 represents the rate between B→C such as Figure 5.1.21.

Kinetic modelling was undertaken to understand the binding reaction further. The interaction of $PolyQ_{28}$ with $PC_{70}Chol_{30}$ membranes offers a two-step reaction of A→B→C with one intermediate between the unbound and the bound peptide. Both PolyK species interaction with cholesterol-containing membranes were fitted to a three-step mechanism, with one of the steps attributed to the cholesterol preferential binding (Figure 5.1.6). However, the lack of interaction to PC_{100} membranes and the simpler two-step interaction suggests that $PolyQ_{28}$ exclusively binds cholesterol in $PC_{70}Chol_{30}$ membranes.

5.1.4.3 *$PC_{70}PS_{30}$ membranes*

The binding of $PolyQ_{28}$ to $PC_{70}PS_{30}$ membranes in PBS media is best described by a sigmoidal (cooperative) binding model, than a hyperbolic binding model (Figure 5.1.22). Cooperative binding was not observed in PC_{100} membranes (no binding), $PC_{70}Chol_{30}$ membranes (hyperbolic binding) or any other media (Tris, Gly-Gly-Gly or NaSCN) when binding to $PC_{70}PS_{30}$ membranes. The cooperativity in PBS suggests that the presence of salt promotes dimer formation (demonstrated by a Hill coefficient of ~2). Alternatively, the binding of one electrolyte increases the affinity for further electrolytes in the presence of salt (Table 5.1.19).

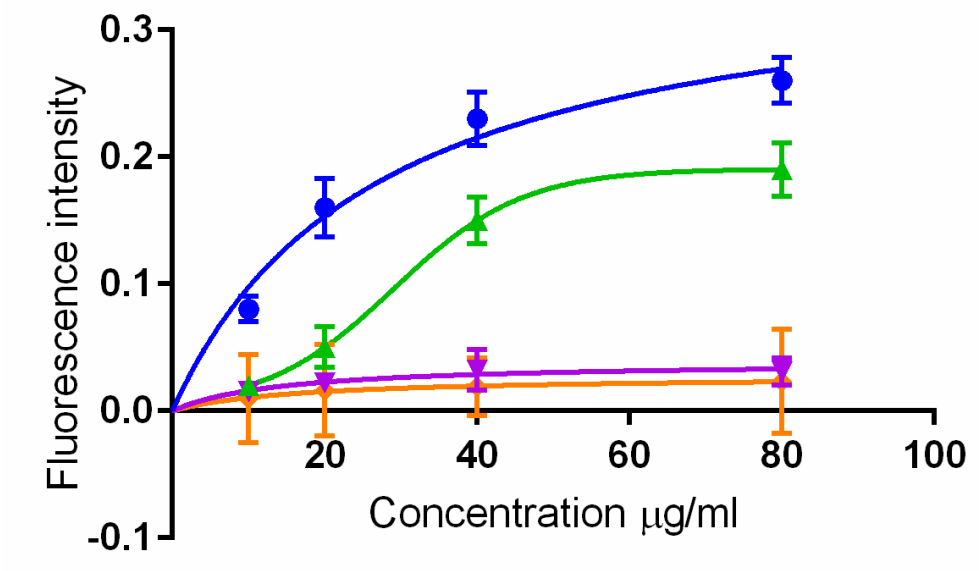


Figure 5.1.22. Plateau Δ*FI* values from SFRM of PolyQ$_{28}$ binding to PC$_{70}$PS$_{30}$. Different media, Tris (blue), PBS (green), Gly-Gly-Gly (purple) and NaSCN (orange), were at pH7.4 (Table 2.2.1), with experiments conducted at 25°C.

	PC$_{70}$PS$_{30}$					
	B_{max} (a.u.)	**sd ±**	**K_d (μg/ml)**	**sd ±**	**h**	**sd ±**
Tris	0.28	0.056	15.26	2.34	-	-
PBS	0.19	0.026	29.06	5.22	2.35	0.68
Gly-Gly-Gly	0.031	0.057	136.26	15.23	-	-
NaSCN	0.017	0.035	83.74	20.49	-	-

Table 5.1.19. B_{max} and K_d values for PolyQ$_{28}$ binding to PC$_{70}$PS$_{30}$ membranes. SFRM Δ*FI* values was fitted to a hyperbolic binding curve and hyperbolic binding curve will Hill coefficient. The best fit was determined by an F-test. All media were used at pH7.4 (Table 2.2.1), with experiments conducted at 25°C.

PolyQ$_{28}$ interactions with PC$_{70}$PS$_{30}$ membranes in PBS and Tris have similar binding capacities and affinities (Table 5.1.19). The presence of Gly-Gly-Gly and NaSCN media decreases the affinity of the PolyQ$_{28}$ dramatically (Tris K_d 15.26 ± 2.34, Gly-Gly-Gly K_d 136.26 ± 15.23, NaSCN K_d 83.74 ± 20.49). The elimination of the interactions in both Gly-Gly-Gly and NaSCN media suggest that the interactions are not as strong the electrostatic interaction between PolyK$_{cc}$ and PS. The binding capacity of PolyQ$_{28}$ to PC$_{70}$PS$_{30}$ membranes was decreased compared to that of PC$_{70}$Chol$_{30}$ membranes (Tris B_{max} PC$_{70}$Chol$_{30}$; 0.72 ± 0.005, PC$_{70}$PS$_{30}$; 0.28 ±

0.056). These results suggest that $PolyQ_{28}$ has a greater affinity to cholesterol than PS.

The kinetic modelling of $PolyQ_{28}$ interaction to $PC_{70}PS_{30}$ membranes denotes a two-step reaction akin to $PC_{70}Chol_{30}$ interaction with only one intermediate.

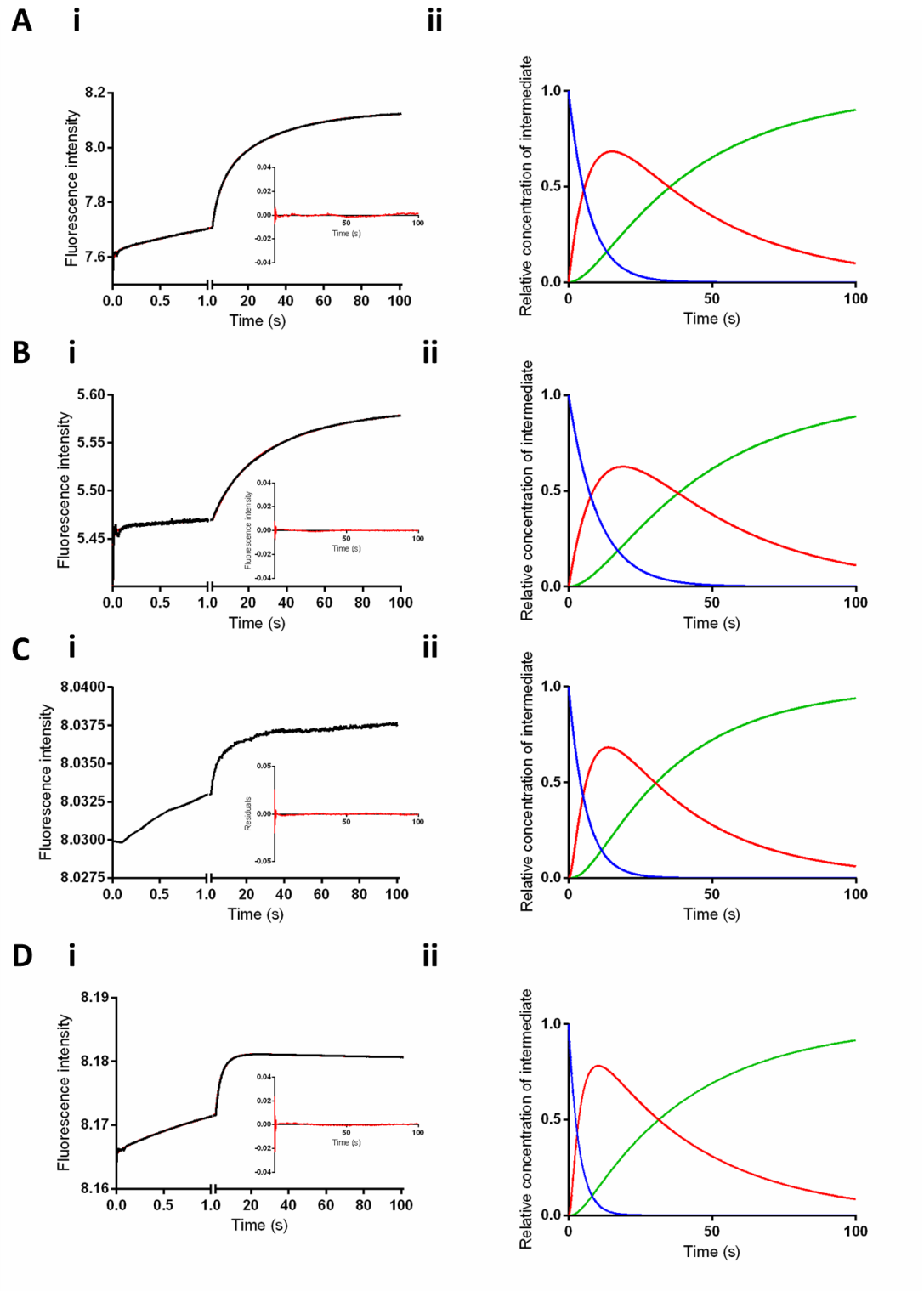


Figure 5.1.23. Kinetic modelling of 40 µg/ml PolyQ$_{28}$ interacting with FPE labelled PC$_{70}$PS$_{30}$ vesicles. (A) Tris, (B) PBS, (C) NaSCN and (D) Gly-Gly-Gly. (i) An averaged trace of PolyQ$_{28}$ interaction to PC$_{70}$PS$_{30}$ (black). This interaction is modelled (red) with the residuals of the kinetic model shown in the insert. (ii) The relative concentration of intermediate species suggested by the binding model, each colour represents a different intermediate in the reaction A→B→C. At any time point A+B+C= 1. All experiments were conducted at pH 7.4 at 25°C.

	$PC_{70}PS_{30}$			
	K_1 ($\mu gml^{-1}s^{-1}$)	**sd ±**	**K_2 ($\mu gml^{-1}s^{-1}$)**	**sd ±**
Tris	3.6	0.26	2.26	0.21
.0PBS	2.59	0.17	3.56	0.27
Gly-Gly-Gly	1.03	0.11	15.26	0.16
Na0SCN	1.26	0.21	11.65	0.19

Table 5.1.20. Kinetic rates of 40 µg/ml $PolyQ_{28}$ interacting with FPE labelled $PC_{70}PS_{30}$ vesicles in media (Table 2.2.1) at pH 7.4, experiments were conducted at 25°C. K_1 represents the rate between A→B and K_2 represents the rate between B→C such as Figure 5.1.23.

5.1.4.4 *Summary of $PolyQ_{28}$ Interaction to Various Membranes*

	PC_{100}				$PC_{70}Chol_{30}$				$PC_{70}PS_{30}$			
	Tris	PBS	NaSCN	Gly-Gly-Gly	Tris	PBS	NaSCN	Gly-Gly-Gly	Tris	PBS	NaSCN	Gly-Gly-Gly
Number of kinetic steps	-	-	-	-	2	2	2	2	2	2	2	2
Apparent K_D (µM)	-	-	-	-	3.6	4	12.3	21.13	15.26	29.1	>40	>40
Binding mode	-	-	-	-	H	H	H	H	H	C	H	H

Table 5.1.21. Summary of interactions between $PolyQ_{28}$ and membranes. Kinetic steps and binding affinities are summarised from tables above. Binding mode denoted as either hyperbolic (H) or cooperative (C).

$PolyQ_{28}$ exhibited unique binding qualities in comparison to $PolyK_{10}$ and $PolyK_{cc}$. FPE did not respond to the $PolyQ_{28}$ interaction with PC_{100} membranes, whereas both PolyK species elicited weak, yet present binding profiles. This suggests that the polypeptide does not interact with PC_{100} membranes or, that the interaction with the membrane does not alter the membrane surface potential and hence, does not modify the fluorescence intensity of the FPE. While observing $PolyQ_{28}$ interactions with the various membrane types, no dissociation kinetics were observed suggesting that the polypeptide exhibits simple binding kinetics instead of more complex association to that of the PolyK species. The intermolecular interactions associated with PolyQ interaction will be discussed further in the discussion.

5.1.4.5 *Thioflavin T Interaction with PolyQ$_{28}$*

PolyQ$_{28}$ interacts with PC$_{70}$Chol$_{30}$ and PC$_{30}$PS$_{70}$ membranes via a two-step mechanism. The intermediate at one stage (approx. 25 s) dominates the total peptide conformation with approximately 20% of A, the unbound peptide, 60% of B the intermediate and 20% C the bound peptide. Thioflavin T was employed to examine hydrogen bond formation, representative of polypeptide clustering on the membrane surface forming β-sheets.

Initially, the ThT interaction with PolyQ$_{28}$ was observed in the absence of membranes. Figure 5.1.24 shows that ThT did not respond the PolyQ$_{28}$ in solution, meaning that the peptide stock is not aggregated.

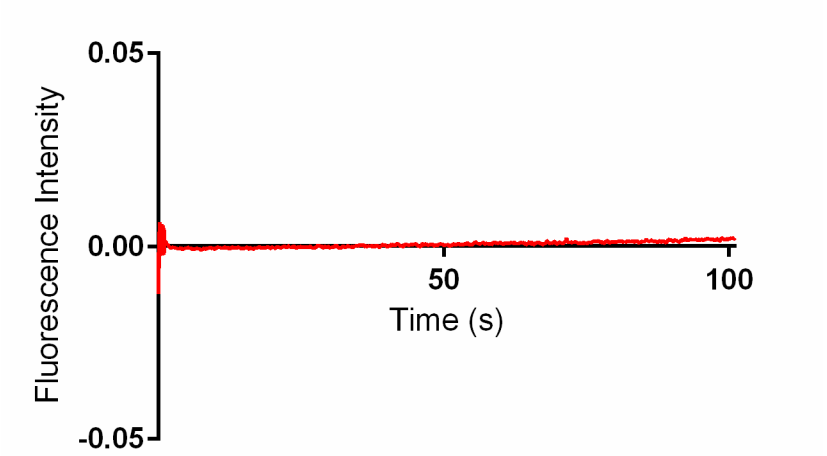


Figure 5.1.24. SFRM trace of Δ*FI* of ThT in solution interacting with PolyQ$_{28}$ (40 µg/ml) following excitation at 482 nm in PBS at pH7.4, experiments were conducted at 25°C.

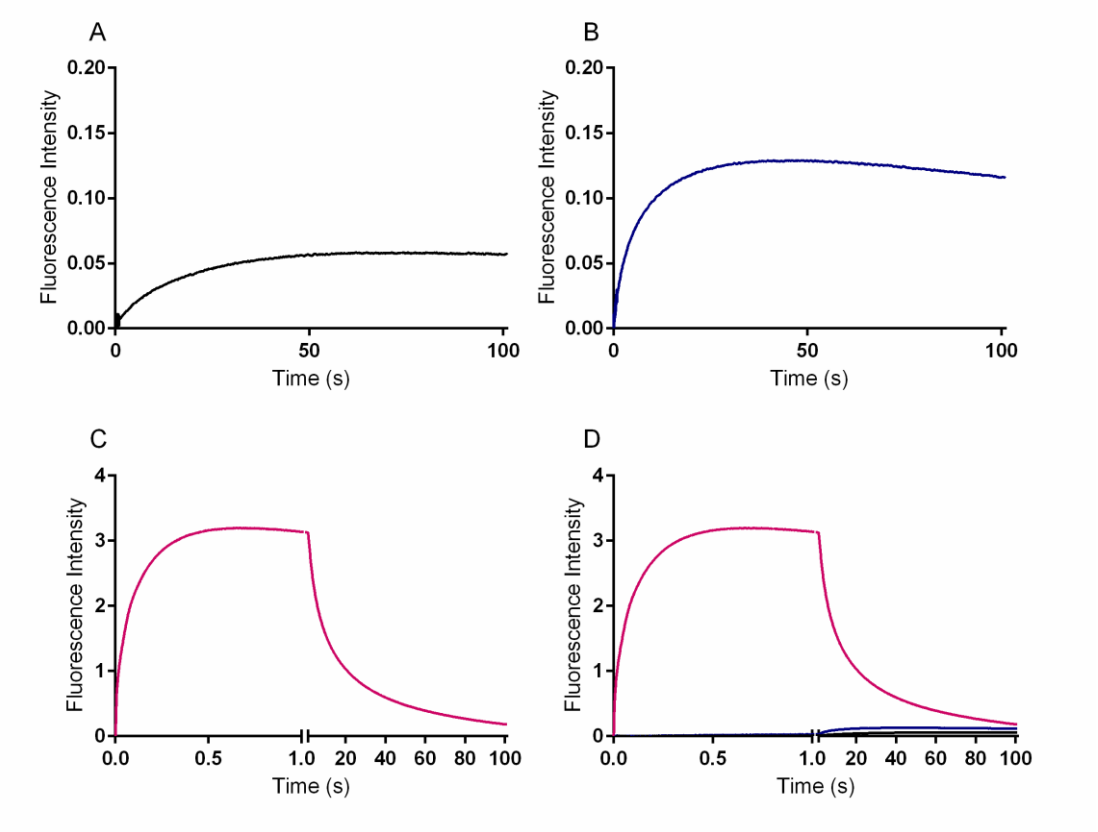


Figure 5.1.25. SFRM trace of Δ*FI* of membranes labelled ThT interacting with PolyQ$_{28}$ 40µg/ml in PBS at pH7.4, experiments were conducted at 25°C. (A) PC_{100} membranes (B) $PC_{70}Chol_{30}$ and (C) $PC_{70}PS_{30}$. Relative effects of fluorescence changes in different membranes in (D).

The addition of PolyQ$_{28}$ to PC_{100} membranes in the presence of ThT resulted in an increase in fluorescence (Figure 5.1.25A) The increment in fluorescence is a result of the formation of hydrogen bonds, indicative of secondary structure formation following peptide interaction. This suggests that the binding of PolyQ$_{28}$ does not elicit a change in the surface potential needed for detection by FPE when binding to PC_{100} membranes. This may be due to the charge of the glutamine at pH 7.4 not being strong enough to elicit a response with FPE detection. PolyQ$_{28}$ interacts with $PC_{70}Chol_{30}$ detected with both FPE and ThT. Given the polar R group of glutamine, it may form hydrogen bonds with the hydroxyl group of the cholesterol, increasing the affinity of the interactions and subsequently resulting in detection by the FPE in the membrane. The interaction between PolyQ$_{28}$ and $PC_{70}PS_{30}$, resulted in ThT fluorescence changes ~40 larger than those seen with PC_{100} and $PC_{70}Chol_{30}$. This

suggests that highly ordered hydrogen-bond networks are formed (in the form of β-sheets) between 0-1 s which then dissociate over time (1-100s) in a comparable process to both PolyK species interaction with $PC_{70}PS_{30}$ membranes. The kinetic profiling of the interaction with FPE-labelled $PC_{70}PS_{30}$ membranes had a very modest fluorescence increase in the first 1 s, followed by an incremental increase of fluorescence from 1-00 s. This suggests that the second process is what is detected by both the ThT and FPE probes.

5.2 Effect of Polypeptides on Membrane Microdomain Formation

The different membranes employed in these studies have shown a range of different binding affinities and mechanisms for PolyK and PolyQ. These forces have been modulated in the presence of NaSCN and Gly-Gly-Gly media to reduce the intermolecular interactions. However, questions remain as to the identity of the final step in the kinetic modelling related to: the FPE *FI* decrease with $PolyK_{10}$ and PolyKcc $PC_{70}PS_{30}$ membrane interactions (Figure 5.1.6), and the ThT *FI* decrease with $PolyQ_{28}$ and $PC_{70}PS_{30}$ membranes.

These results coupled with the literature suggest that a poly-lysine interaction with certain membranes can form aggregates, which localise to membrane microdomains [31]. The kinetic characterisation of the interactions between the amino acids coded for by the first exon of huntingtin proteins (with PolyQ expansions) and various membranes suggest that the PolyQ extension is responsible for the peptide localisation to membrane microdomains [237]. These results suggest that different membrane organisations may mediate the final reaction step. Therefore the effect on membrane microdomains was examined over time following polypeptide interactions.

5.2.1 Effect of $PolyK_{10}$ on Various Supported Lipid Bilayers in Different Media

Initially, SLBs were quantified in control conditions to examine the effect of imaging over time. Previous results have shown the membrane to be fluid (Table 4.1.1) with a diffusion coefficient of ~2.5 $\mu m^2/s$. With an imaging window of 238 x 238 μm, the whole bilayer imaged could theoretically be replaced by new lipids within ~2 minutes (Equation 2.10.1, Section 2.10.2). Image capture was taken every 15 minutes to account for any differences between different lipid compositions and media as

well as the time to capture the image. Previous results have demonstrated that during image capture (approx. 3-4 minutes) the microdomains are stable, as observed by an absence of movement through the z-axis image stacks. These observations are in line with the literature results that suggest the microdomain structures are long-lived, where lipids diffuse in and out of the structures [125].

Figure 5.2.1 stands as the negative control experiment and demonstrates the effect of imaging a $PC_{70}Chol_{30}$ membrane four times over an hour. Domain numbers decrease after the initial image capture, followed by a plateau for the remaining time-course. This suggests that the membrane exhibits limited photobleaching, where some of the domains have a drop in fluorescence which causes them to drop below the threshold detection limit. Further image capture does not further decrease the number of domains detected, suggesting that photobleaching is in equilibrium with membrane fluidity and fluorescence recovery.

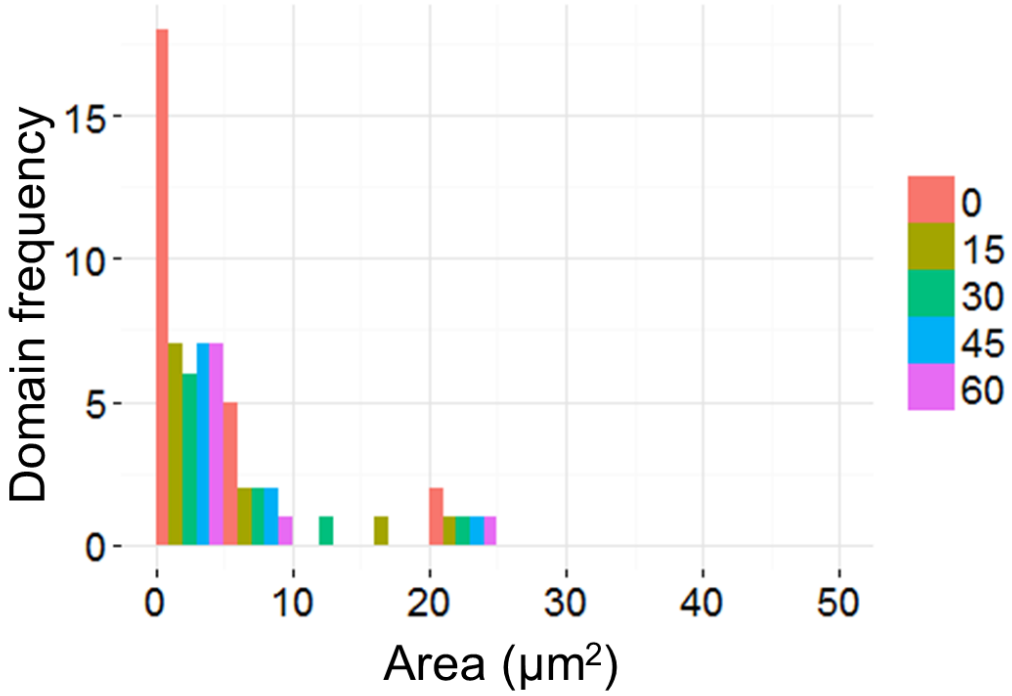


Figure 5.2.1. Negative control histogram of domains processed through particle quantification analysis of z-average $PC_{70}Chol_{30}$ supported lipid bilayers. Membranes were imaged every 15

minutes following the addition of 0.05% (v/v) of PBS in PBS at pH7.4; experiments were conducted at 25°C. The microdomain bin size was 5μm, with each time represented by a different colour.

$PolyK_{10}$ interaction with SLBs was observed with the same three membrane compositions used for polypeptide binding; PC_{100}, $PC_{70}Chol_{30}$, $PC_{70}PS_{30}$. PC_{100} membranes are relatively homogeneous with a small population of domains. Any domains present decrease over time, (Figure 5.2.2A), which correlates with the previous photobleaching effects shown in Figure 5.2.1. $PC_{70}Chol_{30}$ membranes are heterogeneous, with a population of cholesterol-rich lipid ordered domains (as characterised in Chapter 4 (Figure 4.1.8)). Following the interaction of $PolyK_{10}$ with the membrane, the number of domains decreased over time suggesting that the $PolyK_{10}$ does not promote domain formation. In $PC_{70}PS_{30}$ membranes, the binding of $PolyK_{10}$ to the membrane is much stronger, and elicits a far greater increase in fluorescence than PC_{100} and $PC_{70}Chol_{30}$ membranes (Figure 5.1.8). During the $PolyK_{10}$ interaction with $PC_{70}PS_{30}$ membranes, the FPE fluorescence increases between 0-2.5 s, followed by a slower fluorescence decay up to the observed 100 s. The $PolyK_{10}$ interactions with $PC_{70}PS_{30}$ SLBs rely on the polypeptide diffusion in solution, instead of the rapid mixing, and hence will have slower association with the membrane. $PC_{70}PS_{30}$ membranes are heterogeneous (see Figure 5.2.2 and Section 4.1.2.2) with the FPE co-localising with PS in the membrane to form microdomains [238]. The interaction of $PolyK_{10}$ with the $PC_{70}PS_{30}$ membranes, promotes the formation of not only more domains, but domains that are greater in size (Figure 5.2.2C). Figure 5.2.3 demonstrates this effect visually with the fluorescence microscopy of the bilayer following a single addition of the polypeptide at time 0 and the subsequent increase in domain population.

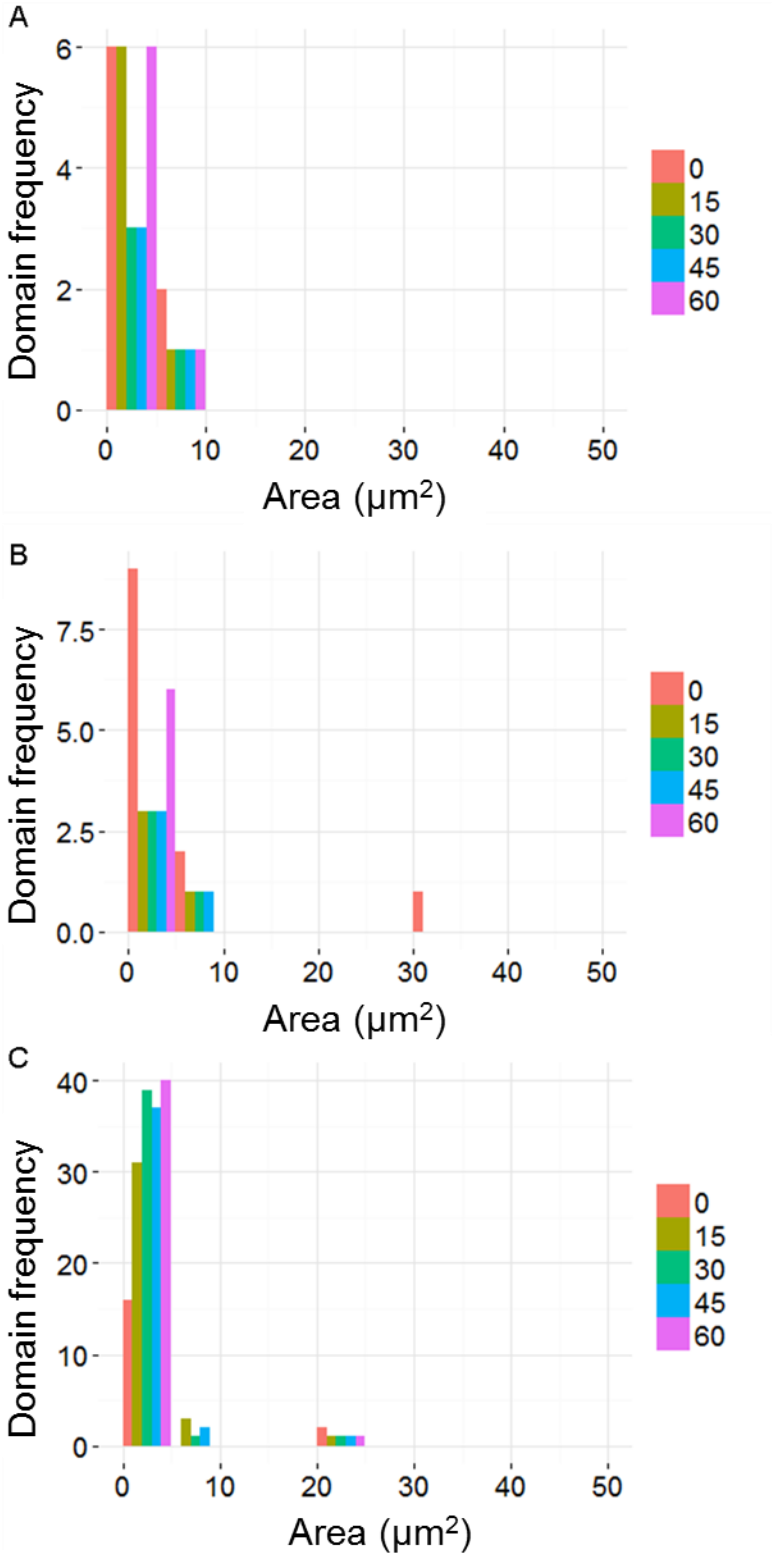


Figure 5.2.2 Interaction of PolyK$_{10}$ with membranes in PBS. (A) PC$_{100}$ bilayer, (B) PC$_{70}$Chol$_{30}$ bilayer, (C) PC$_{70}$PS$_{30}$ bilayer in PBS at pH7.4, experiments were conducted at 25°C. SLBs were imaged every 15 minutes and plotted as histograms.

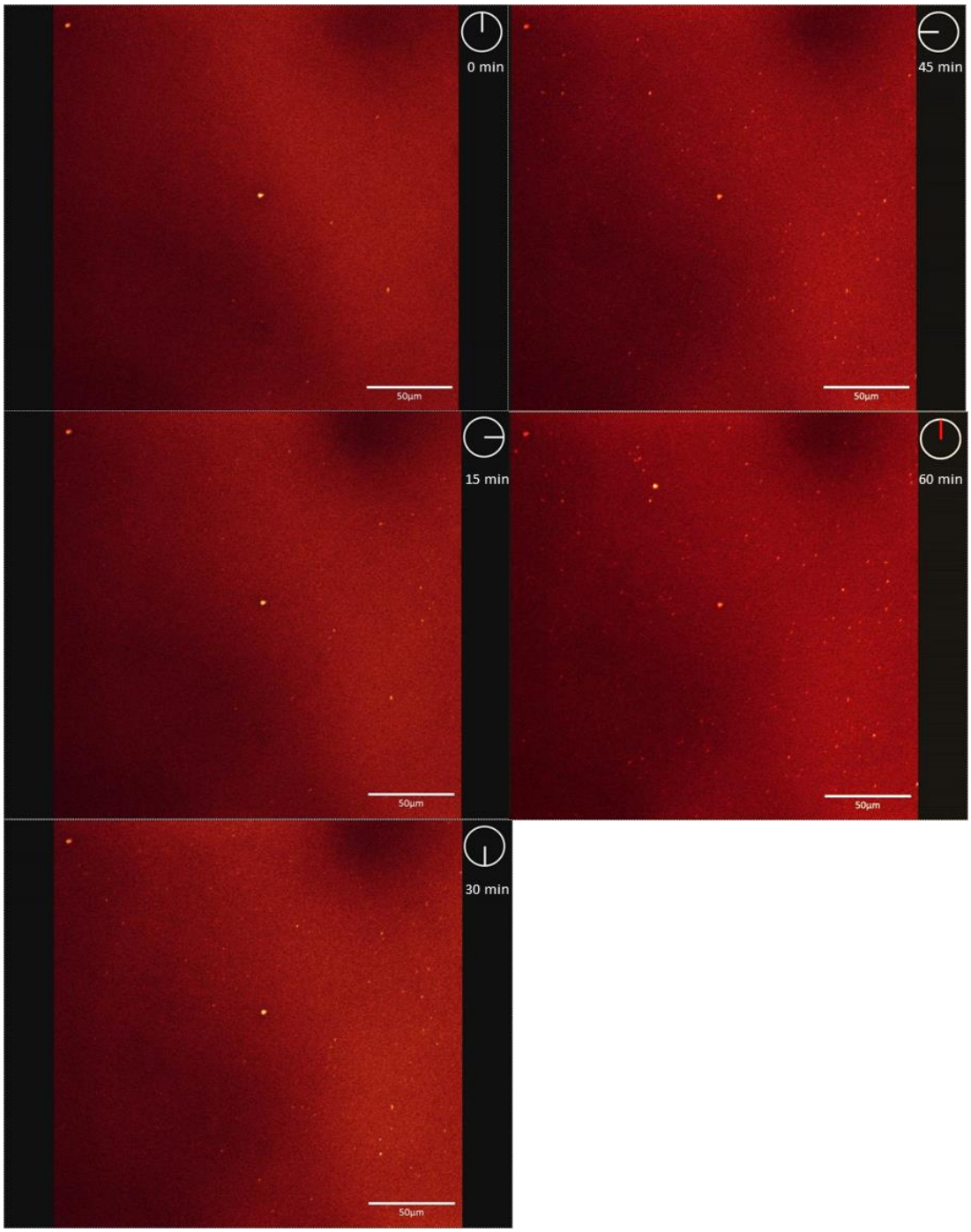


Figure 5.2.3. $PC_{70}PS_{30}$membrane interaction with (40 µg/ml) $PolyK_{10}$ over time. The bilayer is imaged every 15 minutes in PBS at pH7.4; experiments were conducted at 25°C.

Soluble reagents in the media have shown to be effective in reducing the intermolecular forces that govern different protein interactions (Section 3.1), in addition to modulating the headgroup interactions in lipid microdomain formation. In this study, the relative binding capacity and affinity of $PolyK_{10}$ to all membranes

decreased in the presence of Gly-Gly-Gly and NaSCN (Table 5.1.3, Table 5.1.5 and Table 5.1.7).

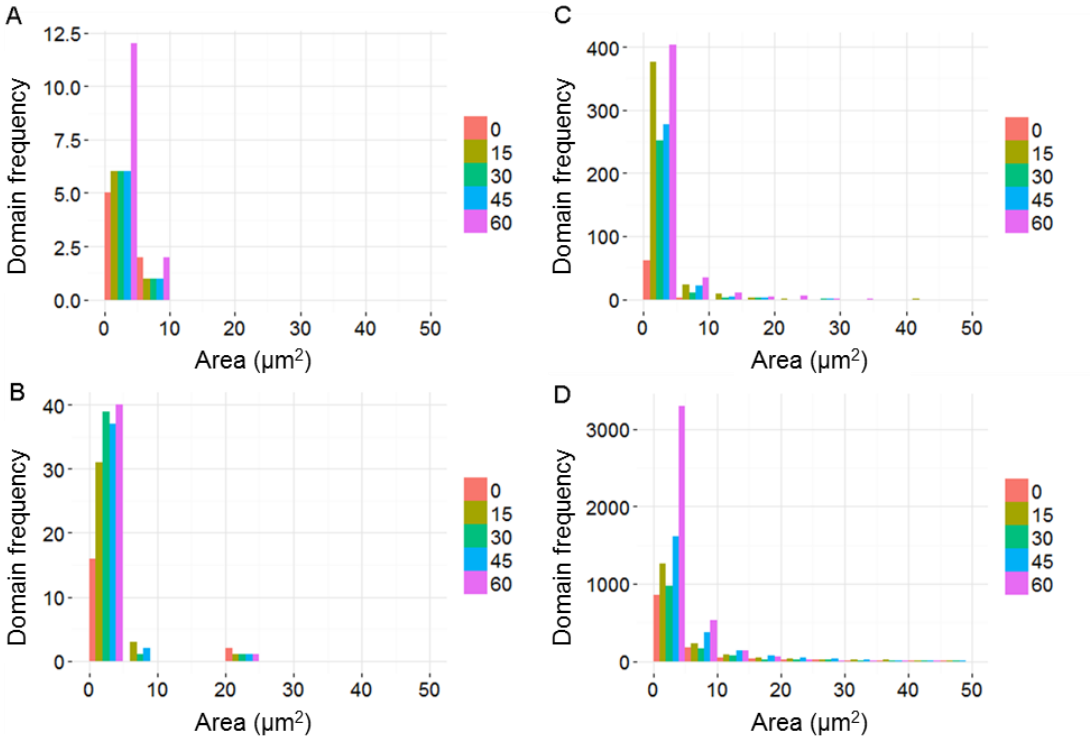


Figure 5.2.4. Histogram of membrane microdomains following PolyK$_{10}$ 40 μg/ml interaction with PC$_{70}$PS$_{30}$ membranes in different media conditions. (A) Tris, (B) PBS, (C) NaSCN and (D) Gly-Gly-Gly (Table 2.2.1) at pH7.4, experiments were conducted at 25°C.

The presence of NaSCN and Gly-Gly-Gly in the media has been shown to increase the numbers of domains in the membrane bilayers before the polypeptide interaction (Section 3.1). Figure 5.2.4 demonstrates that the membrane microdomains in PC$_{70}$PS$_{30}$ membranes are increased in both frequency and size in the presence of PolyK$_{10}$ over time, in all media tested. In Tris and PBS media, PolyK$_{10}$ increased domain formation approximately two-fold. NaSCN media (Figure 5.2.4C) resulted in a four-fold increase in domains ≤ 5 μm^2. In combination with the binding results, NaSCN decreases the affinity of the PolyK$_{10}$ to the membrane, but increases the domain population dramatically. Gly-Gly-Gly produces results similar to those with

NaSCN media with a three-fold increase in domains $\leq 5\ \mu m^2$, and a four-fold increase in domains $\geq 5\ \mu m^2$.

The increase in domain frequency and size correlates with the ΔFI decrease shown in the SFRM experiments. This suggests that membrane reorganisation is at least partially responsible for the fluorescence decrease.

5.2.1.1 *Effect of PolyQ$_{28}$ on Various Supported Lipid Bilayers in Different Media*

The effect of PolyQ$_{28}$ on the membrane reorganisation was examined as a causative factor between the contradictory results of the fluorescent intensity changes between FPE and ThT. FPE reported a steady increase in fluorescence that relates to an increase in the membrane surface potential. ThT reported an increase in fluorescence between 0-1 s, followed by a decrease between 1-100 s. This correlates with an increase in hydrogen bond formation, followed by a decrease.

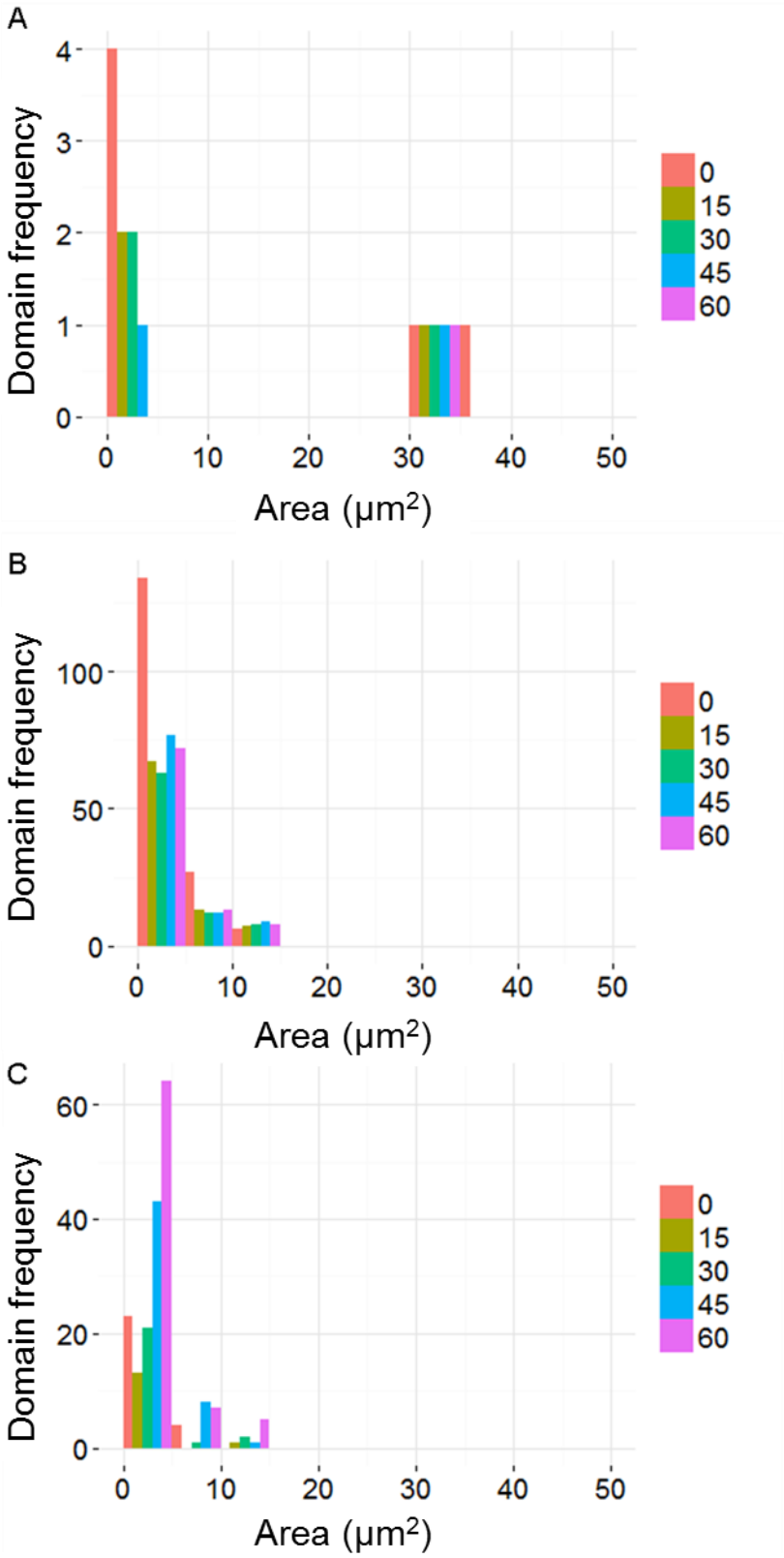


Figure 5.2.5. Interaction of PolyQ$_{28}$ to membranes in PBS. (A) PC_{100} bilayer, (B) $PC_{70}Chol_{30}$ bilayer, (C) $PC_{70}PS_{30}$ bilayer in PBS at pH7.4, experiments were conducted at 25°C. SLBs are imaged every 15 minutes and plotted as microdomain size distribution histograms.

The membrane dependence of the $PolyQ_{28}$ reorganisation is highlighted in Figure 5.2.5. Interrogation of PC_{100} membranes is inherently difficult due the homogenous nature of the bilayers hence, the domain counts are negligible (Figure 5.2.5A). $PC_{70}Chol_{30}$ SLBs are heterogeneous, which allows the observation of the membrane microdomains over time. The interaction of $PolyQ_{28}$ with $PC_{70}Chol_{30}$ membranes resulted in an initial decrease of the domains, followed by a plateau over time (Figure 5.2.5B) (similar to the photobleaching control and $PolyK_{10}$ experiments (Figure 5.2.1)). The $PolyQ_{28}$ interaction with $PC_{70}PS_{30}$ membranes resulted in an initial decrease of domains detected (attributed to photobleaching) followed by an increase in domains, shown in Figure 5.2.5C.

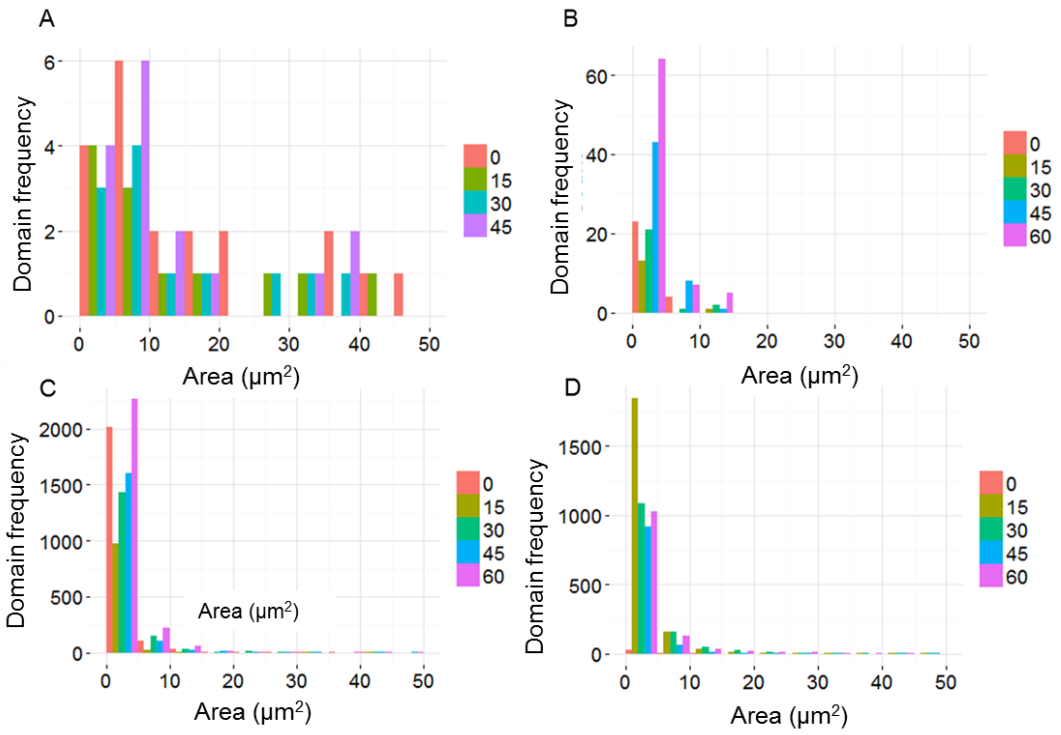


Figure 5.2.6. Histogram of confocal microscopy images with $PolyQ_{28}$ 40 µg/ml interaction with $PC_{70}PS_{30}$ membranes in different media conditions. (A) Tris, (B) PBS, (C) NaSCN and (D) Gly-Gly-Gly (Table 2.2.1) at pH7.4, experiments were conducted at 25°C.

Figure 5.2.6, shows that $PolyQ_{28}$ mediates membrane microdomain formation in the same way as $PolyK_{10}$. This suggests that the phenomenon is driven by the interaction

and clustering of like charges to the membrane to stabilise PS-containing domains. The interaction of $PolyQ_{28}$ with $PC_{70}PS_{30}$ membranes in Tris media resulted in a plateau in the domain number however, microdomains in PBS observed the same effect between polypeptide species employed. NaSCN increased the domains as a function of time, however initially the samples showed a decrease in domain frequency followed by slow recovery and subsequent increase. In control experiments, domain counts never increased above the initial non-photobleached values (Figure 5.2.1, Figure 5.2.2A & B, Figure 5.2.5A & B). This suggests that the decrease and increase of domains in the presence of NaSCN, is potentially due to a slower reaction due to the decreased affinity to the membrane in comparison to PBS (Table 5.1.19). Gly-Gly-Gly resulted in a marked increase in domain frequency and size. This is expected due to favourable conditions for microdomains formation by the media, as previously shown in Section 4.3. The interaction of $PolyQ_{28}$ with the membrane under these conditions may promote the microdomain nucleation observed.

The interaction of polypeptides to membranes, both as vesicles and SLBs, helps to characterise an important mechanism in allowing the rational control of membrane microdomain association and dissociation.

5.3 Discussion

The interactions of polypeptides to membrane surfaces have not been fully understood. Several studies have focussed on the binding kinetics of various proteins/ peptides [36, 239], however these studies have failed to extend the study to cover the downstream processes that follow the initial interaction, i.e. characterising protein binding an insertion, without investigating how that may affect membrane function or formation. In the present study, different polypeptides were incubated with both lipid vesicles and supported lipid bilayers in order to characterise the binding kinetics to provide insight into the binding mechanism.

Initially, SFRM was used employing FPE and ThT probes to examine polypeptide binding of different chain lengths and residue types. The interactions were investigated in media known to target different intermolecular interactions. The effects of the polypeptides were then examined for effects on membrane microdomain assembly. The PolyK polypeptide interactions in the SLB model system, highlight the key roles of polypeptide chains in microdomain assembly. The $PolyQ_{28}$ polypeptide is used to relate the observed effects to the role of native huntingtin proteins and provides a potential insight into the pathology of Huntington's disease.

5.3.1 Effect of Ionic Strength on Polypeptide Binding

Electrostatic attraction is one of the strongest intermolecular forces that govern molecular interactions between proteins and membranes. This study shows that two polypeptide species, namely lysine and glutamine oligomers, exhibit temporal and spatial differences in their interaction profiles to a range of membranes. These interactions may be modified with soluble reagents that change the polypeptide membrane interaction and membrane microdomain assembly/disassembly.

Polypeptide association was first examined, in the presence of low or high salt conditions (Figure 5.3.1). Neutral membranes of PC contain a mixture of different lipids (Table 2.1.1). The lipid head groups exhibit zwitterion capabilities resulting from the anionic phosphate and cationic quaternary ammonium centres. Considering this, the interaction of a charged polypeptide is still likely to be electrostatic in nature, and to be representative of charge-induced dipole interactions. The ions and phosphates in PBS medium have been shown to localise to the Stern layer of the membrane surface as well as the positive charges of the peptide [66]. This is expected to create a steric hindrance of peptide-lipid interaction and reduce the association of the peptide with the lipid bilayers. This phenomenon has been observed within the polypeptide additions to all membranes types when observing the difference between PBS and Tris media (as illustrated in Figure 5.3.1 and summarised in Table 5.1.9).

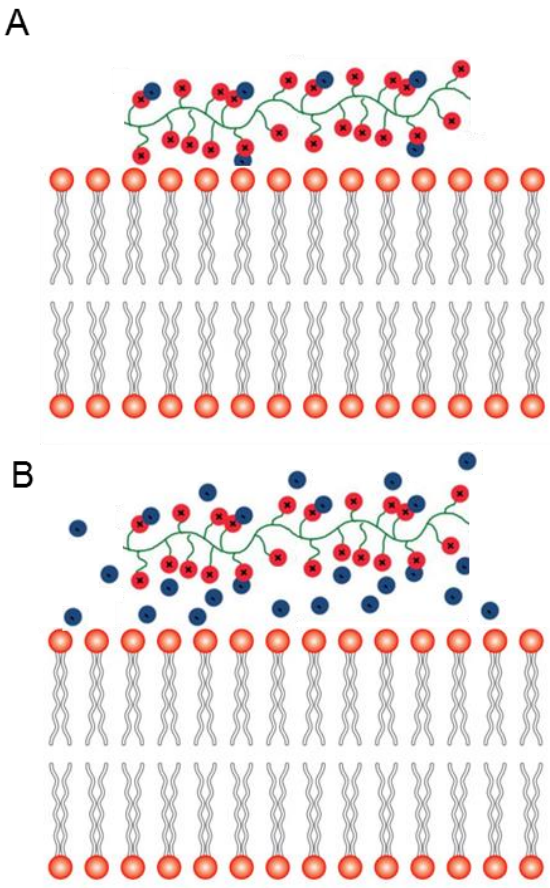


Figure 5.3.1. Schematic interaction of a polypeptide to an uncharged surface in the presence of (A) low salt (Tris) and (B) high salt (PBS) media.

5.3.2 Dissection of the Membrane Binding Profile of Polypeptides in Various Media

The decreased affinity of polypeptide binding in the presence of salt was shown across the whole range of polypeptides employed; $PolyK_{10}$, $PolyK_{cc}$ and $PolyQ_{28}$. This suggests that charge-charge and induced dipole interactions that contribute to the binding interactions are affected in the same way.

In the presence of the different reagent media, Gly-Gly-Gly or NaSCN, the binding capacity and affinity of $PolyK_{10,}$ $PolyK_{cc}$ and PolyQ were decreased . The binding of polypeptide is expected to be similar to those observed with fibrinogen interactions, outlined in Section 3.4.2, with the presence of clustered point charges. NaSCN is proposed to localise to the membrane as well as having a presence in the bulk water.

It is a known chaotrope, which has been shown to break hydrogen bonds between water [59, 225] and can form a solvation layer around the ion surface [57, 66], increasing the local dielectric constant and subsequently decreasing electrostatic interactions. Gly-Gly-Gly is a DCMR, which has been shown to reduce all intermolecular attractive forces (except dispersion force) by increasing the dielectric constant of the bulk solution. The effect of the different reagents employed here is also evident in the cooperativity of the polypeptide interaction with the membrane. $PolyK_{cc}$ exhibits a cooperativity of ~2 in PBS and Tris in all three membrane compositions however, in the presence of NaSCN and Gly-Gly-Gly, the cooperativity is altered. In PC_{100} and $PC_{70}PS_{30}$ membranes, cooperativity is diminished. In $PC_{70}Chol_{30}$ membranes, the cooperativity is greatly increased with a Hill coefficient of ~4, however, the binding affinity and capacity are significantly reduced suggesting that the few polypeptides that do bind, use cooperation to binding in larger numbers, following initial interaction.

5.3.3 $PolyQ_{28}$ interaction with Membranes

The $PolyQ_{28}$ interaction to membranes has to be considered from two standpoints. The $PolyQ_{28}$ employed here is the first exon of the huntingtin protein, which contains a 'leader peptide' before the polypeptide expansion. Recent literature suggests that these two regions of the peptide may have differing effects. The leader sequence has been shown to have 17 key residues in the N-terminus that are essential in the interaction with cell membranes [240-242]. The leader sequence has also been shown to form an alpha helix when inserting into the membrane [240]. This formation allows us to distinguish between the leader sequence (forming a α-helix) and the glutamine expansion (forming β-sheets). Given the increase in ThT fluorescence, denoting β-sheet formation, the electrostatic interaction shown by FPE can be

attributed to the glutamine expansion. The length of the PolyQ has been directly related to the aggregation state of the membrane [36, 198]. In this study, the FPE kinetic modelling of the interaction resulted in simple association kinetics with a maximum of three steps: A→B, initial of free polypeptide to the membrane, B→C conformational change on the surface (formation of β-sheets) and C→D, redistribution of lipids into different microdomain structures. Analysis of the kinetic data alone would suggest that there is no evidence of leader association in this study (summarised in Table 5.1.21). However, the $PolyQ_{28}$ interaction to FPE-labelled membranes did not faithfully represent all the mechanistic steps due to fluorescence increase shown with the ThT probe, suggesting formation of hydrogen bonded structure on the membrane surface.

The interaction of the leader sequence, whether represented here or not, has little evidence in affecting the assembly or disassembly of microdomain populations. Nagarjan et al., 2014 suggested that the binding of the polyglutamine expansion of huntingtin protein results in a disordered lipid structure, which subsequently disrupts normal cellular function. Others have highlighted the formation of β-sheets on the membrane surface as a key mechanism for disease pathology with the accumulation of Huntingtin protein [239]. The evidence here lends credence to the β-sheet hypothesis due to the increased hydrogen-bonded structures created by the polypeptides following interaction (detected via the ThT probe). However, the evidence presented does not preclude both hypotheses to exist.

5.3.4 Membrane Specificity of Polypeptide Interactions

All polypeptide species exhibited differential binding to different membrane compositions. $PolyK_{10}$ and $PolyK_{cc}$ both had the least affinity to PC_{100} membranes, as detected by both FPE and ThT probes. $PolyQ_{28}$ was shown to weakly bind PC_{100}

when detected by ThT however, the interaction did not yield a fluorescence change with FPE (Figure 5.1.19).

PC_{100} membranes contain neutral lipids, which have zwitterionic properties, yet do not have any chemical properties that may lead to stronger affinity interactions, such as the negative charge of PS. The ThT *FI* increase, as shown in $PolyQ_{28}$ interaction to PC_{100} membranes, suggests that there is a membrane association that FPE is unable to detect. The ability of FPE to detect interactions in the other membrane types suggests that PC interactions are different to the cholesterol or PS interactions, in which the glutamine residues may hydrogen bond with the hydroxyl group of the cholesterol, demonstrated in Figure 5.3.2.

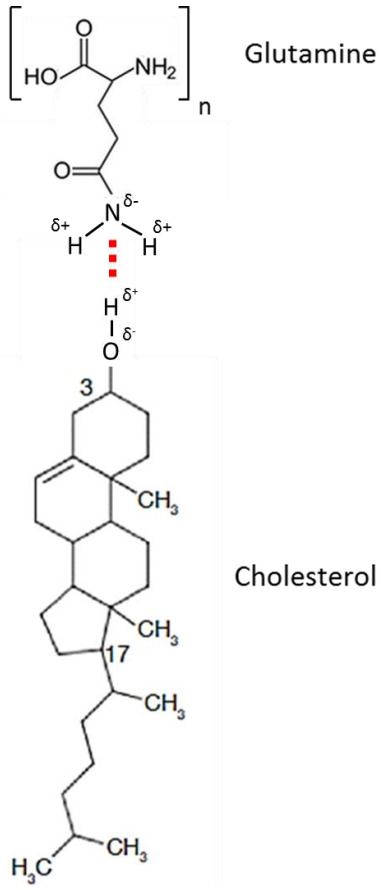


Figure 5.3.2. Diagram of hydrogen bonding between the hydroxyl group of cholesterol with the NH_2 in the R group of glutamine. Alternatively, the oxygen of cholesterol could hydrogen bond with the hydrogen of the glutamine.

Cholesterol containing membranes increased the binding affinity and capacity of the different electrolytes in various ways. FPE labelled $PC_{70}Chol_{30}$ membranes exhibited an *FI* increase following the interactions of all three polypeptides. No *FI* decrease occurred at any point during the interactions. Both PolyK species were kinetically modelled to a minimum of a two-step mechanism of A→B→C. The Δ*FI* of ThT demonstrated that the intermediate B in each model represents the formation of β-sheets, with A and C representing the unbound and bound configurations respectively. $PolyK_{10}$ PC_{100} interactions were modelled to a two-step mechanism. $PolyK_{10}$ has an increased binding capacity and affinity to $PC_{70}Chol_{30}$ membranes when compared to PC_{100} membranes. The increased binding affinity did not increase the complexity of the binding model however, there is an increased A→B transition representing the increased binding affinity.

Cholesterol dependence of $PolyQ_{28}$ interactions (Figure 5.1.20) suggests that the polypeptide has specificity for different membrane types. Recent studies have shown that $PolyQ_{28}$ selectively binds membrane microdomains in cells [237] with both wild-type $PolyQ_{28}$ and more so with mutant PolyQ (typically a polyglutamine expansion of 37 or above) [198]. SLB formations of $PC_{70}Chol_{30}$ membranes here, have shown to phase-separate into cholesterol-rich microdomains and a liquid disordered background (Figure 4.1.8). Increased binding to membrane vesicles of the same composition, suggests that the PolyQ preferentially binds to microdomains. $PolyK_{10}$ and $PolyK_{cc}$ bind $PC_{70}Chol_{30}$ membranes with higher affinity (as shown in Table 5.1.12) than PC_{100} membranes (Table 5.1.10).

Charged lipids in the membrane increased the binding of both PolyK species greatly, which was expected to be an electrostatic interaction between the positively charged lysine residues of the polypeptide and negatively phosphatidylserines lipids in the

membrane. This has been recently studied with 12-residue long poly-lysine chains [30], in which they observed dose-dependent change of zeta-potential, in line with the Gouy-Chapman-Stern model. This group demonstrated that the binding of lysine was independent of potassium adsorption, suggesting the interaction is not inhibited by salt screening. PolyQ binding elicited a slight increase in binding capacity and affinity to PS-containing membranes compared to the cholesterol-containing membrane. The interactions observed by ThT fluorescence in this study suggests that upon binding $PolyQ_{28}$ β-sheets are formed. Given that the kinetic modelling of $PolyQ_{28}$ only has one intermediate step (i.e. A→B→C) (Table 5.1.18) with the binding to cholesterol containing membranes is relatively simple. This suggests that there are no complexities associated with the leader sequence, such as clear secondary structure formation. $PolyQ_{28}$ binding to $PC_{70}PS_{30}$ membranes elicited a much greater change in fluorescent intensity with the ThT probe than the FPE probe. This suggests that the PolyQ interaction does not affect the surface potential and hence is less electrostatically driven than PolyK interactions due to the respective charges of the polypeptide.

5.3.5 Effect of Chain Length of PolyK Interactions

The different PolyK species have different binding capacities as well as distinct interaction profiles. Long chain PolyK exhibits hyperbolic binding curves with a Hill coefficient of approximately 2. The Hill coefficient is a representative value of the conformation of the binding species in an interaction. A Hill coefficient of 2 suggests that the long-chain PolyK may form dimers in order to interact, or that the initial interaction primes the membrane for further PolyK interaction in a mechanism illustrated in Figure 5.3.3 and Table 5.1.16. The cooperative binding model is also highlighted in the kinetic modelling differences between $PolyK_{10}$ and $PolyK_{cc}$. Table

5.1.14 demonstrates that all PolyK$_{cc}$ interactions have an additional mechanistic step upon membrane interaction.

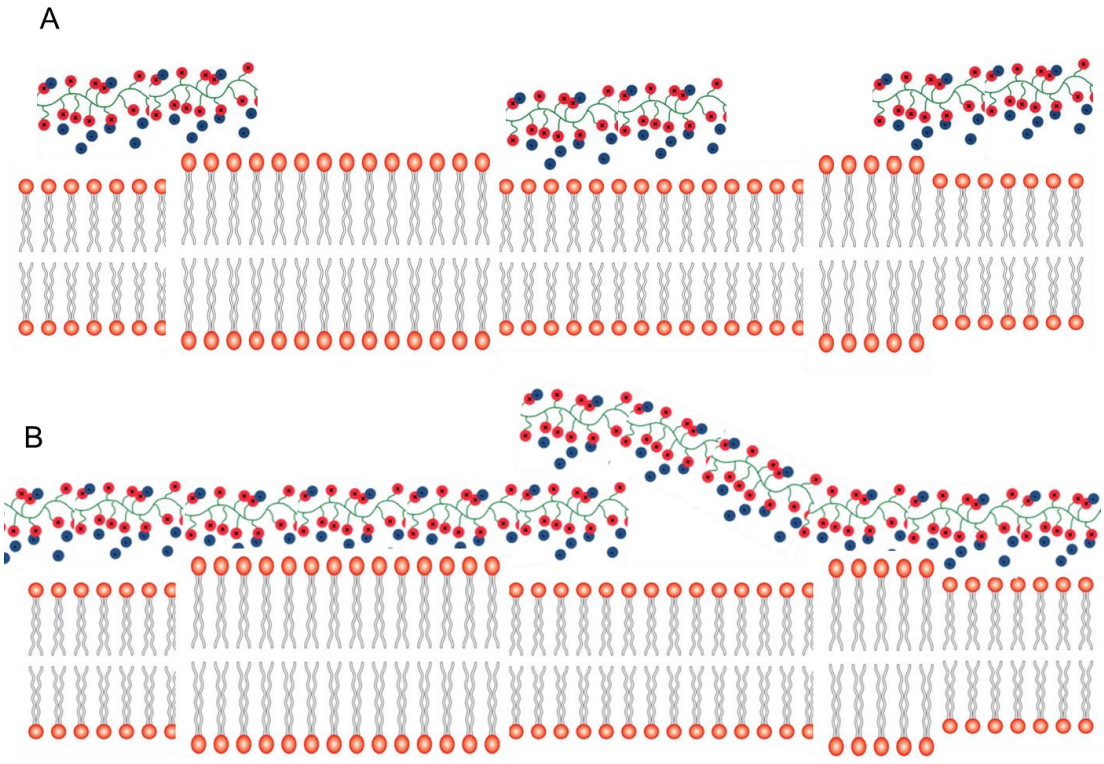


Figure 5.3.3. Diagrammatic representation of (A) short-chain PolyK$_{10}$ interaction as single chain and (B) long-chain PolyK$_{cc}$ binding cooperatively. Increased lipid heights represent membrane microdomains.

5.3.6 β-Sheet Formation on Membrane Surfaces

Both PolyQ and PolyK have been shown to have a random coil formation in neutral pH solutions as employed here [31, 243, 244]. In these systems, the polypeptides were shown to have no hydrogen-bonded secondary structure in solution. The kinetic modelling of PolyK and PolyQ interactions with various membranes indicated a binding intermediate during the interaction. During protein aggregation on the membrane surfaces, PolyQ has been shown to form β-sheets [36, 239] hence β-sheet formation was determined using ThT. In the presence of membranes and polypeptides β-sheets were formed with representative levels of binding in both PolyK species, suggesting that the β-sheet formation occurs directly after binding.

PolyQ interaction with membranes was dependent on lipid composition; however β-sheet formation was much greater than in the observed binding by electrostatic interaction as detected by FPE (Figure 5.1.25). The formation of β-sheets can occur through two processes: the binding of the polypeptide undergoing a conformational change (Figure 5.3.4A) or binding of new polypeptide onto the surface of another (Figure 5.3.4B).

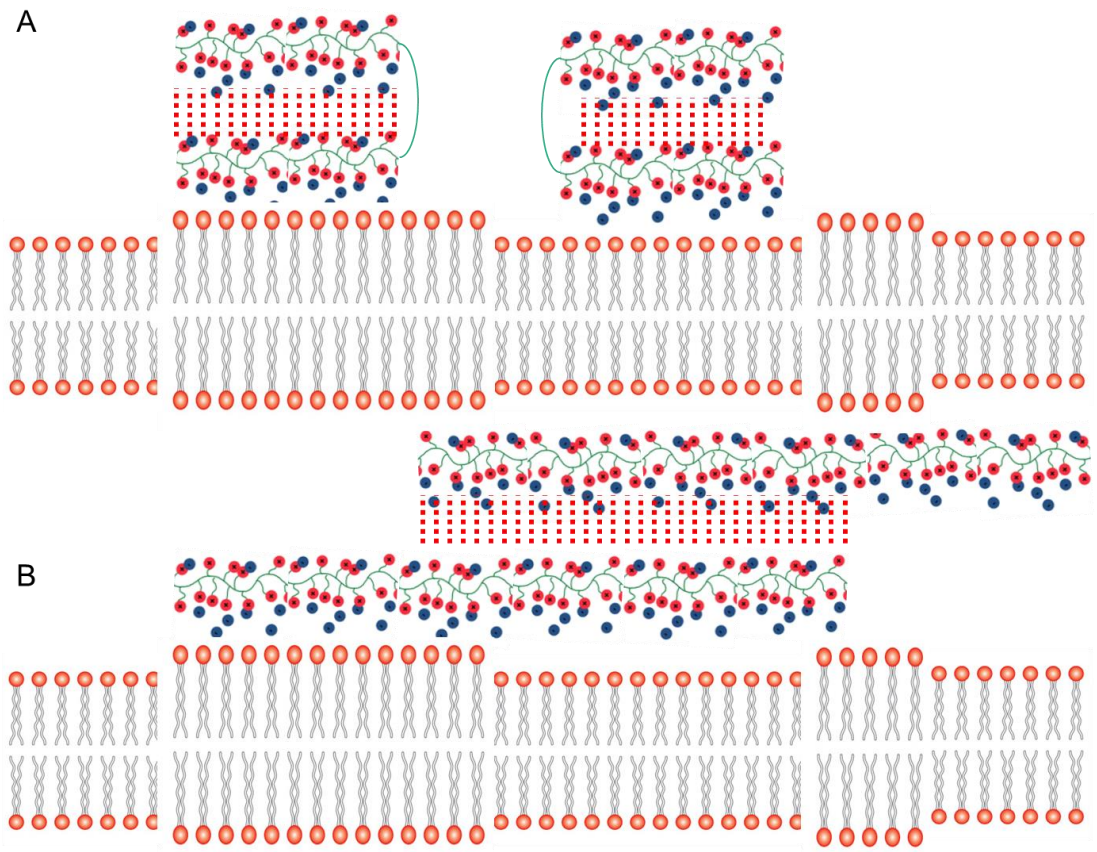


Figure 5.3.4. Diagrammatic representation of hydrogen bond formation in two mechanisms: (A) chain folding (B) more polypeptide binding and forming secondary structure.

The relative Δ*FI* between $PolyQ_{28}$ FPE and ThT suggests that the β-sheet formation occurs through the polypeptide folding on the surface through the proposed mechanism in Figure 5.3.4A of. The fluorescent intensity profiles, of both FPE and ThT, overlap during the interaction of $PolyK_{10}$ and $PolyK_{cc}$, to the various membranes employed. This suggests that as more binding occurs, so does β-sheet

formation. The interaction of PolyQ species with membranes is one of the most likely mechanisms of Huntington's disease [36]. Following the clustering of the peptide on the membrane surface, normal cell activity is hampered. Recent work has suggested that the conversion of the PolyQ peptide into β-sheets is one of the main mechanisms of disease toxicity [239]. This study shows for the first time, that the presence of charged lipids greatly induced β-sheet formation in PolyK and PolyQ species. This result, in combination with the membrane dependence and modulation of lipid rafts, expands the knowledge base of polypeptide interactions and offers potential insights into the mechanisms of Huntington's or protein misfolding diseases.

5.3.7 Supported Bilayer Interaction of Polypeptides

The propensity for PolyQ and PolyK to bind to cholesterol and PS in the membrane, raises the question of whether the polypeptides are attracted to the unique properties of the lipids within the bilayer (such as nonpolar cholesterol or negative PS), or preferentially binding to more ordered regions of lipids such as L_o compared to the unordered L_d phase.

In the systems employed here, it is evident to see that the presence of PS promotes the formation of new membrane microdomains (Figure 5.2.2). $PC_{70}PS_{30}$ membranes therefore consist of electrically neutral zwitterionic PC lipids, and a negatively charged PS lipid. In the membranes shown in PBS and Tris media, the membranes are spatially organised into a heterogeneous membrane. The local patches of fluorescent intensity arise from clustering of the FPE probe in the membrane in microdomains. Upon interaction with the polypeptide species of both $PolyK_{10}$ and $PolyQ_{28,}$ the membrane microdomain species were shown to increase (Figure 5.2.2

and Figure 5.2.5). This suggests that the new domains are electrostatically driven through the positive polypeptide on the surface and the negatively charged lipids.

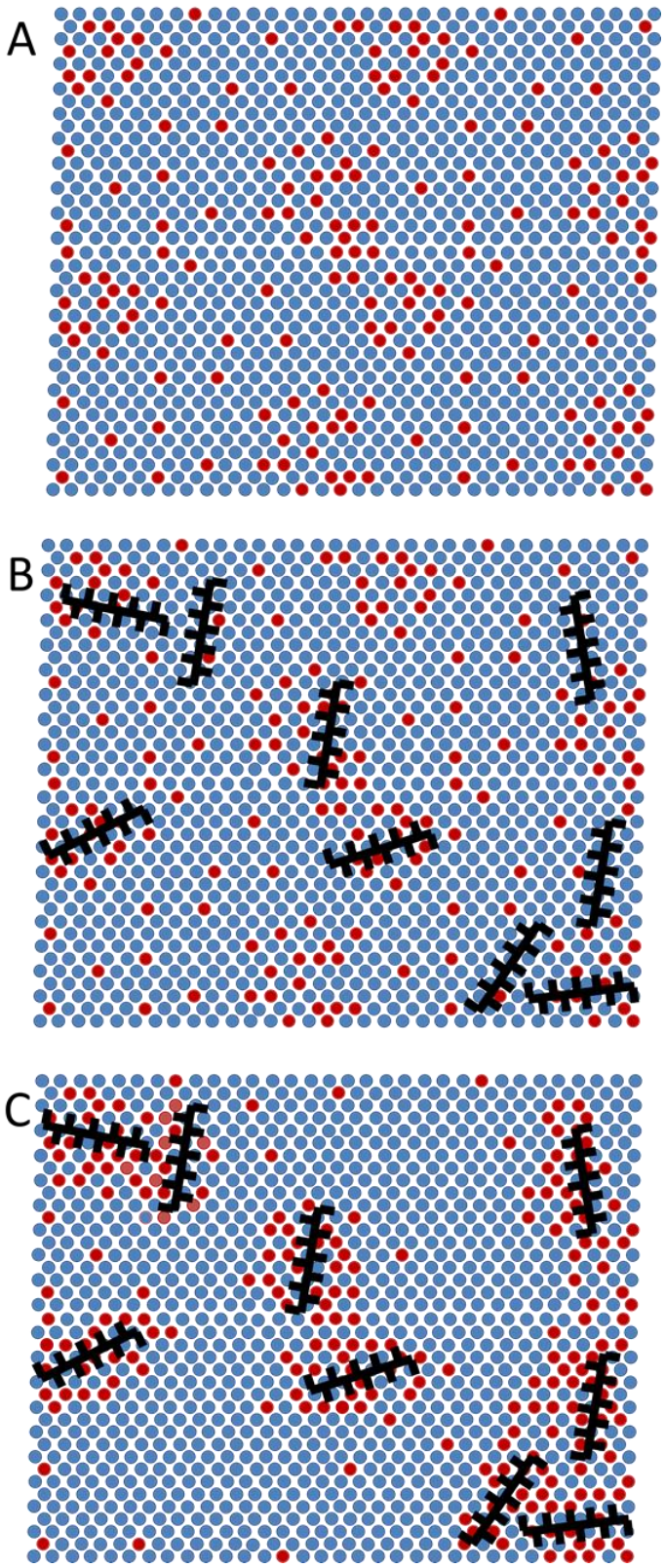


Figure 5.3.5. Proposed mechanism of microdomain assembly. Blue circles represent zwitterionic PC lipids and red circles represent negatively charged PS lipids. (A) PS lipids form liquid ordered microdomains with the PC lipids. (B) When a polypeptide species is added to the membrane it binds preferentially to negatively charged PS lipids. (C) This stabilises the microdomains by decreasing the Gibbs free energy and promotes domain formation.

When the polypeptide binds the membrane, it reduces the net charge density and the electrostatic free energy stored in the diffuse double layer. Reducing the charge density and surface potential al of the membrane reduces the Gibbs free energy of the system. The binding of the polypeptides to the membrane microdomains and membrane surface, must reduce the electrostatic free energy enough to overcome the increase in free energy that arises from the entropic mixing of the PS lipids diffusing out of the ordered domains, and the electrostatic cost of association of the like charges of PS in the domains (illustrated in Figure 5.3.5). Due to the electrostatic attraction between the polypeptide and the PS in the membrane, the polypeptide will bind much more strongly to regions of the membrane that contain higher fractions of negatively charged lipids. Given that the membrane is already heterogeneous with charged lipids, the binding of the polypeptide is expected to initially bind to these microdomains. Given that PolyQ also binding PC and cholesterol lipids, upon later interaction, the polypeptide will bind regions of the membrane with decreasing fractions of negatively charged lipids. This then may induce asymmetry of the bilayer to promote flipping of PS lipids to the exposed surface, in order to create new microdomains, illustrated in Figure 5.3.6B. The results demonstrated in this study suggest a model in which the polypeptide electrostatic interaction could drive microdomain assembly.

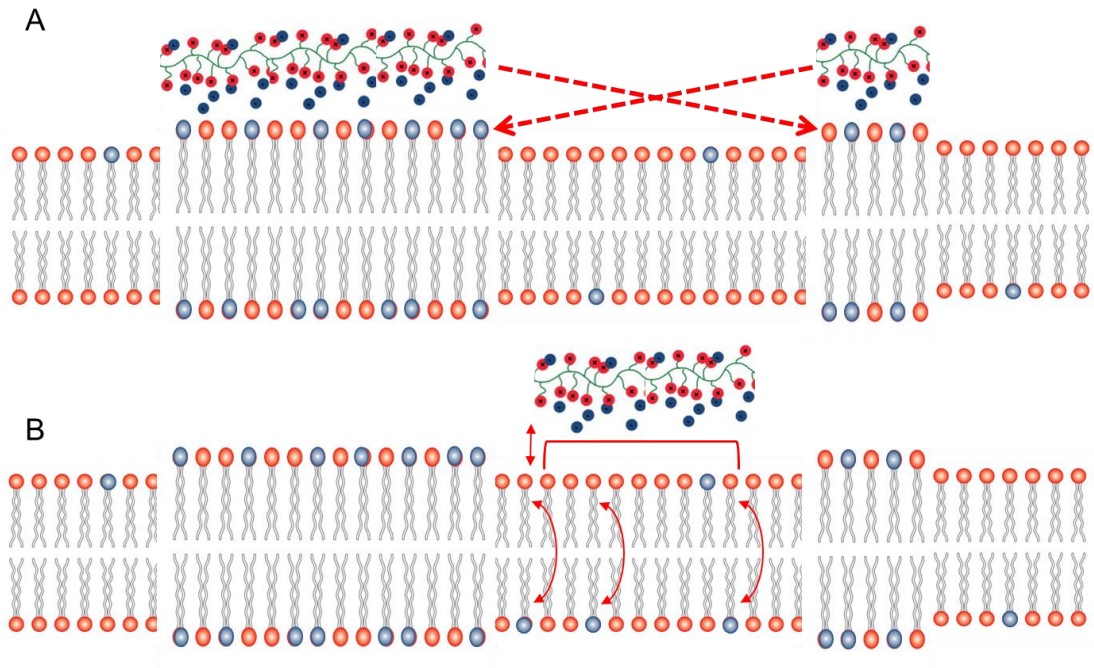


Figure 5.3.6. A possible mechanism for domain formation in the presence of PolyK and PolyQ. (A) Domain clustering from electrostatic attraction between positive polypeptides and negative domains to form larger domains. (B) The polypeptide induces asymmetric of PS in the membrane to create favourable conditions for domain formation.

The use of the media regents offers a further complication of the microdomain formation process. The interaction between PolyK and the membrane surface is shown to disrupt the water on the surface, and to form hydrogen bonds with the polypeptide [30]. These observations correlate with the water modulating effects of NaSCN shown here, which promoted domain formation (Figure 4.1.13). When PolyQ and PolyK are binding in the presence of NaSCN, the electrostatic interaction to the membrane is reduced (Table 5.1.17). This reduces the propensity for the mechanism in Figure 5.3.6A to be dominant. Microdomains in these systems increase dramatically, lending more evidence towards the domains being formed through the effect of NaSCN (Figure 4.3.3). This in turn would affect the capacitance of the membrane bilayer and further decrease the Gibbs free energy, propagating the association of the microdomains as shown in Figure 5.3.5.

The results of this study are unable to differentiate fully between effects of the leader sequence and the polypeptide expansion in the PolyQ species. However, with the demonstration of preferential binding of PolyQ to cholesterol and PS in the membrane (Table 5.1.19) coupled with the increase of microdomains following these interactions, it is reasonable to suggest that the electrolyte expansion is responsible for nucleation of new microdomains.

5.3.8 Future Work into Membrane Microdomain Modulation by Polypeptides

The investigation into the different polypeptides with various membrane surfaces, has proven successful in offering new insight into the modulation of membrane microdomains during these interactions. The ability for polypeptides to increase domain populations is of widespread interest in the field of disease pathologies such as Huntington's disease. It is also of great concern to the wider scientific community where the frequent use of polypeptide species such as $PolyK_{cc}$ in cell culture, may affect membrane microdomain formation. This has been highlighted by other research groups who have shown that the clustering of PolyK on glass slides induces microdomain formation [245]. This study has demonstrated that the addition of PolyK to the media also promotes the formation of microdomains in the presence of certain lipid types. Therefore, during the study of membrane microdomains the use of PolyK should be carefully monitored. The binding properties of PolyK have recently been applied to create 3D biomembranes, using PolyK to sandwich layers of charged membranes (in this case POPC and POPG) [246]

To investigate the binding parameters of huntingtin further, the different lengths of polyglutamine must be examined, ranging from the 28-residue wild type employed here, to the expansion of ~150 glutamines that are currently used to convey disease pathology in model mice systems [197]. This may be done with either the presence

or absence of the leader sequence. Once characterised, these interactions would further develop the β-sheet mechanism suggested here, and would offer further insights into the disease mechanism.

6 General Conclusions

Nonspecific binding is a problematic in a range of systems. This study examines this issue in both SPR and a bead-based detection instrument. This non-specific binding was then attenuated in the presence of various reagents added to the media (Section 3.1.1). A combination of NaSCN and Gly-Gly-Gly was shown to eliminate the binding of both albumin and fibrinogen (Section 3.1.5) in SPR and a range of cytokines with Luminex.

Within the field of SPR, nonspecific binding is a key limiting factor in the detection limits of the instrument [247]. Therefore, the utilisation of reagents, such as those demonstrated in this study, would potentially enhance the ability of SPR to detect analytes from crude samples such as blood plasma [248, 249] and cell lysates [250]. Another detection instrument characterised for nonspecific binding was the multi-analyte Luminex assay. Chapter 3 demonstrated that for this instrument the judicious choice of media reagents could decrease nonspecific binding of a whole panel of human cytokines, without decreasing the specific interactions (Section 1.4.6).

This level of control over intermolecular interactions has not been demonstrated with the use of soluble reagents before and thus, the mechanism in which it works is important. NaSCN are small chaotropic anions which have been shown to break hydrogen bonds, and re-order the water around the ions [225]. This reordering disrupts hydrogen bonding between interacting species. The NaSCN ions will also localise on the membrane surface due to an electrostatic interaction [66], and an increase in the zeta potential of the membrane, which ultimately decreases the electrostatic interactions. Gly-Gly-Gly is a small neutrally charged tri-peptide. Gly-Gly-Gly (among others (Table 1.6.1) (Section 3.1)) has been shown to increase the

dielectric constant of a solution due to the electronic capacitance of the dipole across the peptide. Increasing the ambient dielectric constant decreases the attractive intermolecular forces. This functional use a dielectric constant modifying reagent, DCMR, is the first known example where intermolecular interactions are targeted in this way. This work has focussed on the characterisation of a few selected chaotropes and DCMRs through a selection of techniques. However, it would be of great interest extend these studies further with systematic investigation of other reagents to determine if there is predictable beneficial effect of a particular DCMR or chaotrope.

The approach taken by this study has been replicated by the wider scientific field demonstrated by those that have referenced the published paper from Chapter 3 [251-254] and extensively in our collaborative laboratories [43, 255].

This work was undertaken in collaboration with the manufacturer, BioRad, and aided in the development of their new instrument media. It is our understanding that this is the first time a set of media conditions have been rationally formulated to decrease nonspecific binding. The media system is more effective than previous efforts to optimise the sensor slide therefore; it presents an exciting universal technique to optimise various binding assays.

In the second results chapter the work was extended to look at membrane bilayers. This research was driven by the recognition that reagents capable of modulating water structure would potentially affect the interfacial water molecules at the membrane bilayer surface. Due to the recent highlighted importance of interfacial water molecules in the formation fluorescence spectroscopy and atomic force microscopy (AFM) of supported lipid bilayers (SLBs) was undertaken to observe changes in microdomain assembly/disassembly.

Chapter 4 presents evidence to suggest that the lipid organisation of the membranes microdomain formation is affected by the presence of DCMRs and mild chaotropes. Initially, the microdomain populations were characterised with different membrane compositions. Both synthetic and naturally derived lipids mixtures were used. Naturally derived lipids were chosen to be more physiologically relevant whereas synthetic lipids were chosen, due to their widespread usage in phase characterisation experiments, such as Connell et al. [132]. The presence of NaSCN or Gly-Gly-Gly in the media was observed to significantly increase the frequency of microdomains in all different lipid compositions. Given that the lipid composition did not change during the experiment, this suggests that the reagents modulate interactions with the head groups. It is well established that water structure is different dependant on the lipid phase, i.e. the difference between liquid disordered, liquid ordered and gel phase, [47, 146, 204]. The density of water increases with an increased packing of lipid molecules; hence, the interaction of the reagents and the membrane is hypothesised to affect the water network on the surface of the membrane. The work in this study offers experimental evidence that the modulation of this network has dramatic effects on the organisation of the membrane microdomains (Section 4.1.2).

This work has led to the development of more sophisticated simulations to try to provide a molecular/chemical explanation for the effects of SCN^- ions on microdomain formation [256]. These simulations suggest that the SCN^- ions disrupt the natural water network and to order the water molecules around the ions [226]; therefore, the ions on the non-microdomain membrane are expected to increase the hydration of the lipids in the bilayer. The hydrated lipids extend, as depicted in Figure 4.3.2, which may result in tighter packing of unsaturated lipids.

To our knowledge, these results give the first evidence that membrane microdomain assembly can be controlled at a given temperature post membrane formation. The interaction between lipid head groups in the membrane could elucidate further complexities of the membrane bilayer, where the interaction between the lipid head group and the media can no longer be ignored as a causative factor in microdomain assembly. The ability to control these interactions warrants further investigation of other head-group mediating molecules that may result in aberrant microdomain detection. This study presents data that microdomain lipid membrane biologists should be aware of – how something as simple as buffer components might have a significant impact on the membrane being studied.

The approach taken during this study was replicated to characterise the effects of commonly used oils in the formation of droplet interface bilayers (DIBs) [257]. DIBs are formed with aqueous droplets introduced in a lipid and oil environment, this then promotes the self-assembly of a lipid monolayer. The interaction between two monolayers, forms a bilayer which is used to characterise any microdomain that may form. The fluorescence microscopy developed in this study was utilised to show that oils below the critical micelle concentration, and hence likely to be disperse within the aqueous droplet of a DIB, can cause aberrant microdomain formation [257]. These results demonstrate that the approaches used in this study are transferable to a host of different fields. More importantly, it also highlights that there are a host of different factors that have to be considered when characterising membrane bilayers, not simply the ratio of saturated and unsaturated lipids.

These results may have larger implications in the field of membrane biology, specifically with the interaction and characterisation of membrane proteins. Much is

unknown about the folding and structure of many integral membrane proteins [258]. The microdomain localisation of these proteins has been demonstrated to affect the function [72, 112] and the lipids that co-localise with membrane proteins are expected to be highly physiologically relevant [80]. This has led to the development of different solubilisation techniques that retain the native lipids, such as the formation of nanodiscs [5] or styrene-maleic acid lipid particles [259]. These contrast the historical detergent solubilisation that removes the native lipids [260]. In a cellular environment, the promotion of new microdomains may alter the location of the membrane proteins, or the lipid type that co-localises with the membrane. A combination of these new techniques with the altered microdomain formation, as demonstrated in this study, would allow for the investigation of protein association with microdomains in addition to the co-localising lipids. This work however, would require the optimisation of *in vitro* microdomain detection, and the validation of any cytotoxic effects of either NaSCN or Gly-Gly-Gly.

Increasing the complexity of the systems in which these interactions takes place is a key step for the development of next-generation biomimetic systems. The reagents were used to elucidate the interactions between polypeptides and membrane vesicles, and SLBs to characterise the binding mechanism and kinetics.

Initially, the binding of the different PolyK lengths was examined in the presence of various media. The binding of in solution PolyK to cells highlighted binding to both phosphatidylserine and cholesterol. These observations led to larger studies on how PolyK may affect in vitro assays. Increasing chain lengths of PolyK increase the cooperativity of the binding interactions. The cooperative nature of $PolyK_{cc}$ may therefore, result in clustering and aggregation on the membrane. The addition of $PolyK_{10}$ to the membrane surface in solution was examined over time. The addition

of PolyK to $PC_{70}PS_{30}$ membranes however, resulted in an increase in membrane microdomains over time. This suggests that the electrostatic interaction between the positively charged polypeptide, and negatively charged phospholipid, results in the stabilisation of PS molecules by reducing the free energy of the system. This promotes the redistribution of the lipids into tightly packed membrane microdomains.

The formation of membrane microdomains in the presence of PolyK tracts has already been studied with cytoplasmic proteins such as protein kinase C [261, 262]. PolyK on cell culture surfaces has been shown to result in the formation of ripples and microdomain-like structures following cellular adhesion [245]. This work reaffirms that PolyK, such as that frequently used to coat cell culture plates, may drastically alter the membrane bilayer of cells grown in these conditions. The NaSCN and DCMRs employed have been shown to further enhance the membrane association of these studies and offers a further level of control on microdomains.

The study of polypeptides association to the membrane included the association of $PolyQ_{28}$ to the membrane. The correlation of the PolyK and PolyQ offers physiological credence to the fundamental association shown with the PolyK association

The function of the huntingtin protein responsible for Huntington's disease is unknown [34] however, there is a clear correlation between the expansion of the glutamine tract with disease severity [32]. This study offers evidence that PolyQ preferentially binds PS in the membrane, as well as promoting microdomain formation in PS-containing membranes over time. In cell membranes, PS is held in the inner leaflet of the plasma membrane however, upon apoptosis, the PS is released

to the external leaflet [263]. The binding and clustering of PS-containing microdomains suggest that the huntingtin protein may be important in an apoptosis pathway. The binding of PolyQ is driven through hydrogen bonding and β-sheet formation (observed with ThT fluorescence). The expansion of the PolyQ tract to pathological levels is expected to increase the membrane association and β-sheet formation. This theory is strengthened by recent literature that highlights β-sheet formation as a causative mechanism for cell death in Huntington's disease [35, 239, 264].

The ability to extend the previous studies of the field, increasing their complexity, offers a step in *in vitro* models which allows for more faithful representation of the *in vivo* environment.

7 REFERENCES

[1] A. D. BANGHAM AND R. W. HORNE, "NEGATIVE STAINING OF PHOSPHOLIPIDS + THEIR STRUCTURAL MODIFICATION BY-SURFACE ACTIVE AGENTS AS OBSERVED IN ELECTRON MICROSCOPE," *JOURNAL OF MOLECULAR BIOLOGY,* VOL. 8, NO. 5, PP. 660-&, 1964 1964.

[2] H. P. WACKLIN, "COMPOSITION AND ASYMMETRY IN SUPPORTED MEMBRANES FORMED BY VESICLE FUSION," (IN ENGLISH), *LANGMUIR,* ARTICLE VOL. 27, NO. 12, PP. 7698-7707, JUN 2011.

[3] P. MUELLER, D. O. RUDIN, H. T. TIEN, AND W. C. WESCOTT, "RECONSTITUTION OF CELL MEMBRANE STRUCTURE IN VITRO AND ITS TRANSFORMATION INTO AN EXCITABLE SYSTEM," *NATURE,* VOL. 194, NO. 4832, PP. 979-&, 1962 1962.

[4] S. L. VEATCH AND S. L. KELLER, "SEPARATION OF LIQUID PHASES IN GIANT VESICLES OF TERNARY MIXTURES OF PHOSPHOLIPIDS AND CHOLESTEROL," *BIOPHYSICAL JOURNAL,* VOL. 85, NO. 5, PP. 3074-3083, NOV 1 2003.

[5] T. K. RITCHIE *ET AL.*, "RECONSTITUTION OF MEMBRANE PROTEINS IN PHOSPHOLIPID BILAYER NANODISCS," *METHODS IN ENZYMOLOGY; LIPOSOMES, PT F,* VOL. 464, PP. 211-231, 2009 2009.

[6] S. CAVAGNERO, H. J. DYSON, AND P. E. WRIGHT, "IMPROVED LOW PH BICELLE SYSTEM FOR ORIENTING MACROMOLECULES OVER A WIDE TEMPERATURE RANGE," *JOURNAL OF BIOMOLECULAR NMR,* VOL. 13, NO. 4, PP. 387-391, APR 1999.

[7] S. O. DODONOVA *ET AL.*, "A STRUCTURE OF THE COPI COAT AND THE ROLE OF COAT PROTEINS IN MEMBRANE VESICLE ASSEMBLY," *SCIENCE,* VOL. 349, NO. 6244, PP. 195-198, JUL 10 2015.

[8] N. G. D'LIMA AND C. M. TESCHKE, "A METHOD TO INVESTIGATE PROTEIN ASSOCIATION WITH INTACT SEALED MYCOBACTERIAL MEMBRANE VESICLES," *ANALYTICAL BIOCHEMISTRY,* VOL. 485, PP. 109-11, 2015-SEP-15 2015.

[9] S. J. SINGER AND G. L. NICOLSON, "FLUID MOSAIC MODEL OF STRUCTURE OF CELL-MEMBRANES," *SCIENCE,* VOL. 175, NO. 4023, PP. 720-&, 1972 1972.

[10] R. D. KLAUSNER, J. G. DONALDSON, AND J. LIPPINCOTTSCHWARTZ, "BREFELDIN-A - INSIGHTS INTO THE CONTROL OF MEMBRANE TRAFFIC AND ORGANELLE STRUCTURE," *JOURNAL OF CELL BIOLOGY,* VOL. 116, NO. 5, PP. 1071-1080, MAR 1992.

[11] A. MASELLI, M. PIERDOMINICI, C. VITALE, AND E. ORTONA, "MEMBRANE LIPID RAFTS AND ESTROGENIC SIGNALLING: A FUNCTIONAL ROLE IN THE MODULATION OF CELL HOMEOSTASIS," *APOPTOSIS,* VOL. 20, NO. 5, PP. 671-678, MAY 2015.

[12] D. S. FRIEND AND D. W. FAWCETT, "MEMBRANE DIFFERENTIATIONS IN FREEZE-FRACTURED MAMMALIAN SPERM," *JOURNAL OF CELL BIOLOGY,* VOL. 63, NO. 2, PP. 641-664, 1974 1974.

[13] U. MAURER, C. CHARVET, A. S. WAGMAN, E. DEJARDIN, AND D. R. GREEN, "GLYCOGEN SYNTHASE KINASE-3 REGULATES MITOCHONDRIAL OUTER MEMBRANE PERMEABILIZATION AND APOPTOSIS BY DESTABILIZATION OF MCL-1," *MOLECULAR CELL,* VOL. 21, NO. 6, PP. 749-760, MAR 17 2006.

[14] K. SIMONS AND R. EHEHALT, "CHOLESTEROL, LIPID RAFTS, AND DISEASE," (IN ENGLISH), *JOURNAL OF CLINICAL INVESTIGATION,* ARTICLE VOL. 110, NO. 5, PP. 597-603, SEP 2002.

[15] W. C. LIN, C. D. BLANCHETTE, T. V. RATTO, AND M. L. LONGO, "LIPID ASYMMETRY IN DLPC/DSPC-SUPPORTED LIPID BILAYERS: A COMBINED AFM AND FLUORESCENCE MICROSCOPY STUDY," (IN ENGLISH), *BIOPHYSICAL JOURNAL*, ARTICLE VOL. 90, NO. 1, PP. 228-237, JAN 2006.

[16] T. PETERS, JR., "ALL ABOUT ALBUMIN; BIOCHEMISTRY, GENETICS AND MEDICAL APPLICATIONS," ED. SAN DIEGO, CA,: ACADEMIC PRESS, 1995, PP. 9-75.

[17] F. YANG, Y. ZHANG, AND H. LIANG, "INTERACTIVE ASSOCIATION OF DRUGS BINDING TO HUMAN SERUM ALBUMIN," *INTERNATIONAL JOURNAL OF MOLECULAR SCIENCES*, VOL. 15, NO. 3, PP. 3580-3595, MAR 2014.

[18] A. A. SPECTOR, "FATTY-ACID BINDING TO PLASMA ALBUMIN," *JOURNAL OF LIPID RESEARCH*, VOL. 16, NO. 3, PP. 165-179, 1975 1975.

[19] N. CHADBORN, J. BRYANT, A. J. BAIN, AND P. O'SHEA, "LIGAND-DEPENDENT CONFORMATIONAL EQUILIBRIA OF SERUM ALBUMIN REVEALED BY TRYPTOPHAN FLUORESCENCE QUENCHING," (IN ENGLISH), *BIOPHYSICAL JOURNAL*, ARTICLE VOL. 76, NO. 4, PP. 2198-2207, APR 1999.

[20] G. STEHLE, A. WUNDER, H. H. SCHRENK, G. HARTUNG, D. L. HEENE, AND H. SINN, "ALBUMIN-BASED DRUG CARRIERS: COMPARISON BETWEEN SERUM ALBUMINS OF DIFFERENT SPECIES ON PHARMACOKINETICS AND TUMOR UPTAKE OF THE CONJUGATE," (IN ENGLISH), *ANTI-CANCER DRUGS*, ARTICLE VOL. 10, NO. 8, PP. 785-790, SEP 1999.

[21] M. ROZGA, M. KLONIECKI, A. JABLONOWSKA, M. DANDLEZ, AND W. BAL, "THE BINDING CONSTANT FOR AMYLOID A BETA 40 PEPTIDE INTERACTION WITH HUMAN SERUM ALBUMIN," (IN ENGLISH), *BIOCHEMICAL AND BIOPHYSICAL RESEARCH COMMUNICATIONS*, ARTICLE VOL. 364, NO. 3, PP. 714-718, DEC 2007.

[22] B. J. VAN VUUREN, T. READ, R. V. OLKHOV, AND A. M. SHAW, "HUMAN SERUM ALBUMIN INTERFERENCE ON PLASMON-BASED IMMUNOKINETIC ASSAY FOR ANTIBODY SCREENING IN MODEL BLOOD SERA," (IN ENGLISH), *ANALYTICAL BIOCHEMISTRY*, ARTICLE VOL. 405, NO. 1, PP. 114-120, OCT 2010.

[23] R. MILLIONI *ET AL.*, "HIGH ABUNDANCE PROTEINS DEPLETION VS LOW ABUNDANCE PROTEINS ENRICHMENT: COMPARISON OF METHODS TO REDUCE THE PLASMA PROTEOME COMPLEXITY," (IN ENGLISH), *PLOS ONE*, ARTICLE VOL. 6, NO. 5, P. 7, MAY 2011, ART. NO. E19603.

[24] J. GRANGER, J. SIDDIQUI, S. COPELAND, AND D. REMICK, "ALBUMIN DEPLETION OF HUMAN PLASMA ALSO REMOVES LOW ABUNDANCE PROTEINS INCLUDING THE CYTOKINES," *PROTEOMICS*, VOL. 5, NO. 18, PP. 4713-4718, DEC 2005.

[25] S. KALASIN AND M. M. SANTORE, "NON-SPECIFIC ADHESION ON BIOMATERIAL SURFACES DRIVEN BY SMALL AMOUNTS OF PROTEIN ADSORPTION," (IN ENGLISH), *COLLOIDS AND SURFACES B-BIOINTERFACES*, ARTICLE VOL. 73, NO. 2, PP. 229-236, OCT 2009.

[26] J. M. KOLLMAN, L. PANDI, M. R. SAWAYA, M. RILEY, AND R. F. DOOLITTLE, "CRYSTAL STRUCTURE OF HUMAN FIBRINOGEN," *BIOCHEMISTRY*, VOL. 48, NO. 18, PP. 3877-3886, MAY 12 2009.

[27] A. R. FOLSOM, "EPIDEMIOLOGY OF FIBRINOGEN," (IN ENGLISH), *EUROPEAN HEART JOURNAL*, ARTICLE; PROCEEDINGS PAPER VOL. 16, PP. 21-24, MAR 1995.

[28] H. Y. NI *ET AL.*, "PERSISTENCE OF PLATELET THROMBUS FORMATION IN ARTERIOLES OF MICE LACKING BOTH VON WILLEBRAND FACTOR AND

FIBRINOGEN," *JOURNAL OF CLINICAL INVESTIGATION,* VOL. 106, NO. 3, PP. 385-392, AUG 2000.

[29] J. S. REES AND K. S. LILLEY, "METHOD FOR SUPPRESSING NON-SPECIFIC PROTEIN INTERACTIONS OBSERVED WITH AFFINITY RESINS," (IN ENGLISH), *METHODS,* ARTICLE VOL. 54, NO. 4, PP. 407-412, AUG 2011.

[30] N. I. MARUKOVICH, A. M. NESTERENKO, AND Y. A. ERMAKOV, "STRUCTURAL FACTORS IN LYSINE AND POLYLYSINE INTERACTIONS WITH LIPID MEMBRANES," (IN RUSSIAN), *BIOLOGICHESKIE MEMBRANY,* ARTICLE VOL. 31, NO. 6, PP. 401-409, NOV-DEC 2014.

[31] W. DZWOLAK, T. MURAKI, M. KATO, AND Y. TANIGUCHI, "CHAIN-LENGTH DEPENDENCE OF ALPHA-HELIX TO BETA-SHEET TRANSITION IN POLYLYSINE: MODEL OF PROTEIN AGGREGATION STUDIED BY TEMPERATURE-TUNED FTIR SPECTROSCOPY," (IN ENGLISH), *BIOPOLYMERS,* ARTICLE VOL. 73, NO. 4, PP. 463-469, MAR 2004.

[32] L. PIERI, K. MADIONA, L. BOUSSET, AND R. MELKI, "FIBRILLAR ALPHA-SYNUCLEIN AND HUNTINGTIN EXON 1 ASSEMBLIES ARE TOXIC TO THE CELLS," (IN ENGLISH), *BIOPHYSICAL JOURNAL,* ARTICLE VOL. 102, NO. 12, PP. 2894-2905, JUN 2012.

[33] P. HARJES AND E. E. WANKER, "THE HUNT FOR HUNTINGTIN FUNCTION: INTERACTION PARTNERS TELL MANY DIFFERENT STORIES," *TRENDS IN BIOCHEMICAL SCIENCES,* VOL. 28, NO. 8, PP. 425-433, AUG 2003.

[34] E. CATTANEO, C. ZUCCATO, AND M. TARTARI, "NORMAL HUNTINGTIN FUNCTION: AN ALTERNATIVE APPROACH TO HUNTINGTON'S DISEASE," *NATURE REVIEWS NEUROSCIENCE,* VOL. 6, NO. 12, PP. 919-930, DEC 2005.

[35] C.-S. SUN *ET AL.*, "CONFORMATIONAL SWITCH OF POLYGLUTAMINE-EXPANDED HUNTINGTIN INTO BENIGN AGGREGATES LEADS TO NEUROPROTECTIVE EFFECT," *SCIENTIFIC REPORTS,* VOL. 5, OCT 9 2015, ART. NO. 14992.

[36] K. A. BURKE, K. M. HENSAL, C. S. UMBAUGH, M. CHAIBVA, AND J. LEGLEITER, "HUNTINGTIN DISRUPTS LIPID BILAYERS IN A POLYQ-LENGTH DEPENDENT MANNER," *BIOCHIMICA ET BIOPHYSICA ACTA-BIOMEMBRANES,* VOL. 1828, NO. 8, PP. 1953-1961, AUG 2013.

[37] M. F. PERUTZ, T. JOHNSON, M. SUZUKI, AND J. T. FINCH, "GLUTAMINE REPEATS AS POLAR ZIPPERS - THEIR POSSIBLE ROLE IN INHERITED NEURODEGENERATIVE DISEASES," *PROCEEDINGS OF THE NATIONAL ACADEMY OF SCIENCES OF THE UNITED STATES OF AMERICA,* VOL. 91, NO. 12, PP. 5355-5358, JUN 7 1994.

[38] J. M. GIL AND A. C. REGO, "MECHANISMS OF NEURODEGENERATION IN HUNTINGTON'S DISEASE," *EUROPEAN JOURNAL OF NEUROSCIENCE,* VOL. 27, NO. 11, PP. 2803-2820, JUN 2008.

[39] S. TAM *ET AL.*, "THE CHAPERONIN TRIC BLOCKS A HUNTINGTIN SEQUENCE ELEMENT THAT PROMOTES THE CONFORMATIONAL SWITCH TO AGGREGATION," *NATURE STRUCTURAL & MOLECULAR BIOLOGY,* VOL. 16, NO. 12, PP. 1279-U98, DEC 2009.

[40] P. R. DAHLGREN *ET AL.*, "ATOMIC FORCE MICROSCOPY ANALYSIS OF THE HUNTINGTON PROTEIN NANOFIBRIL FORMATION," *NANOMEDICINE : NANOTECHNOLOGY, BIOLOGY, AND MEDICINE,* VOL. 1, NO. 1, PP. 52-7, 2005-MAR 2005.

[41] J. N. ISRAELACHVILI, "INTERMOLECULAR AND SURFACE FORCES, 3RD EDITION," (IN ENGLISH), *INTERMOLECULAR AND SURFACE FORCES, 3RD EDITION,* BOOK PP. 1-674, 2011.

[42] T. LAUE, "PROXIMITY ENERGIES: A FRAMEWORK FOR UNDERSTANDING CONCENTRATED SOLUTIONS," (IN ENGLISH),

JOURNAL OF MOLECULAR RECOGNITION, ARTICLE VOL. 25, NO. 3, PP. 165-173, MAR 2012.

[43] J. L. RICHENS, J. S. LANE, J. P. BRAMBLE, AND P. O'SHEA, "THE ELECTRICAL INTERPLAY BETWEEN PROTEINS AND LIPIDS IN MEMBRANES," *BIOCHIMICA ET BIOPHYSICA ACTA-BIOMEMBRANES*, VOL. 1848, NO. 9, PP. 1828-1836, SEP 2015.

[44] "NANOSCOPY AND MULTIDIMENSIONAL OPTICAL FLUORESCENCE MICROSCOPY," *NANOSCOPY AND MULTIDIMENSIONAL OPTICAL FLUORESCENCE MICROSCOPY*, PP. 1-360, 2010 2010.

[45] J. L. RICHENS, P. WEIGHTMAN, B. L. BARNES, AND P. O'SHEA, "IN VIVO SPECTROSCOPIC IMAGING OF BIOLOGICAL MEMBRANES AND SURFACE IMAGING FOR HIGH-THROUGHPUT SCREENING," *NANOSCOPY AND MULTIDIMENSIONAL OPTICAL FLUORESCENCE MICROSCOPY*, 2010 2010.

[46] D. CHANDLER, "INTERFACES AND THE DRIVING FORCE OF HYDROPHOBIC ASSEMBLY," *NATURE*, VOL. 437, NO. 7059, PP. 640-647, SEP 29 2005.

[47] D. ROBINSON, N. A. BESLEY, P. O'SHEA, AND J. D. HIRST, "WATER ORDER PROFILES ON PHOSPHOLIPID/CHOLESTEROL MEMBRANE BILAYER SURFACES," *JOURNAL OF COMPUTATIONAL CHEMISTRY*, VOL. 32, NO. 12, PP. 2613-2618, SEP 2011.

[48] D. LECKBAND AND J. ISRAELACHVILI, "INTERMOLECULAR FORCES IN BIOLOGY," *QUARTERLY REVIEWS OF BIOPHYSICS*, VOL. 34, NO. 2, PP. 105-267, MAY 2001.

[49] A. H. ELCOCK AND J. A. MCCAMMON, "ELECTROSTATIC CONTRIBUTIONS TO THE STABILITY OF HALOPHILIC PROTEINS," (IN ENGLISH), *JOURNAL OF MOLECULAR BIOLOGY*, ARTICLE VOL. 280, NO. 4, PP. 731-748, JUL 1998.

[50] S. IZRAILEV, S. STEPANIANTS, M. BALSERA, Y. OONO, AND K. SCHULTEN, "MOLECULAR DYNAMICS STUDY OF UNBINDING OF THE AVIDIN-BIOTIN COMPLEX," *BIOPHYSICAL JOURNAL*, VOL. 72, NO. 4, PP. 1568-1581, APR 1997.

[51] J. WALL, F. AYOUB, AND P. OSHEA, "INTERACTIONS OF MACROMOLECULES WITH THE MAMMALIAN-CELL SURFACE," (IN ENGLISH), *JOURNAL OF CELL SCIENCE*, ARTICLE VOL. 108, PP. 2673-2682, JUL 1995.

[52] R. W. MAURER, S. I. SANDLER, AND A. M. LENHOFF, "SALTING-IN CHARACTERISTICS OF GLOBULAR PROTEINS," *BIOPHYSICAL CHEMISTRY*, VOL. 156, NO. 1, PP. 72-78, JUN 2011.

[53] L. JONES AND P. OSHEA, "THE ELECTROSTATIC NATURE OF THE CELL-SURFACE OF CANDIDA-ALBICANS - A ROLE IN ADHESION," *EXPERIMENTAL MYCOLOGY*, VOL. 18, NO. 2, PP. 111-120, JUN 1994.

[54] J. L. RICHENS, E. A. M. LUNT, D. SANGER, G. MCKENZIE, AND P. O'SHEA, "AVOIDING NONSPECIFIC INTERACTIONS IN STUDIES OF THE PLASMA PROTEOME: PRACTICAL SOLUTIONS TO PREVENTION OF NONSPECIFIC INTERACTIONS FOR LABEL-FREE DETECTION OF LOW-ABUNDANCE PLASMA PROTEINS," *JOURNAL OF PROTEOME RESEARCH*, VOL. 8, NO. 11, PP. 5103-5110, NOV 2009.

[55] W. KUNZ, J. HENLE, AND B. W. NINHAM, "'ZUR LEHRE VON DER WIRKUNG DER SALZE' (ABOUT THE SCIENCE OF THE EFFECT OF SALTS): FRANZ HOFMEISTER'S HISTORICAL PAPERS," (IN ENGLISH), *CURRENT OPINION IN COLLOID & INTERFACE SCIENCE*, REVIEW VOL. 9, NO. 1-2, PP. 19-37, AUG 2004.

[56] P. SCHONFELD, L. MONTERO, AND J. FABIAN, "A COMBINED EXPERIMENTAL AND QUANTUM CHEMICAL STUDY ON THE PUTATIVE

PROTONOPHORIC ACTIVITY OF THIOCYANATE," *BIOPHYSICAL JOURNAL,* VOL. 89, NO. 3, PP. 1504-1515, SEP 2005.

[57] D. F. PARSONS, M. BOSTROM, P. LO NOSTRO, AND B. W. NINHAM, "HOFMEISTER EFFECTS: INTERPLAY OF HYDRATION, NONELECTROSTATIC POTENTIALS, AND ION SIZE," (IN ENGLISH), *PHYSICAL CHEMISTRY CHEMICAL PHYSICS,* ARTICLE VOL. 13, NO. 27, PP. 12352-12367, 2011.

[58] Y. KOGA, P. WESTH, J. V. DAVIES, K. MIKI, K. NISHIKAWA, AND H. KATAYANAGI, "TOWARD UNDERSTANDING THE HOFMEISTER SERIES. 1. EFFECTS OF SODIUM SALTS OF SOME ANIONS ON THE MOLECULAR ORGANIZATION OF H2O," (IN ENGLISH), *JOURNAL OF PHYSICAL CHEMISTRY A,* ARTICLE VOL. 108, NO. 40, PP. 8533-8541, OCT 2004.

[59] H. KIM, S. PARK, AND M. CHO, "ROTATIONAL DYNAMICS OF THIOCYANATE IONS IN HIGHLY CONCENTRATED AQUEOUS SOLUTIONS," (IN ENGLISH), *PHYSICAL CHEMISTRY CHEMICAL PHYSICS,* ARTICLE VOL. 14, NO. 18, PP. 6233-6240, 2012.

[60] K. D. COLLINS AND M. W. WASHABAUGH, "THE HOFMEISTER EFFECT AND THE BEHAVIOR OF WATER AT INTERFACES," *QUARTERLY REVIEWS OF BIOPHYSICS,* VOL. 18, NO. 4, PP. 323-422, NOV 1985.

[61] M. G. CACACE, E. M. LANDAU, AND J. J. RAMSDEN, "THE HOFMEISTER SERIES: SALT AND SOLVENT EFFECTS ON INTERFACIAL PHENOMENA," *QUARTERLY REVIEWS OF BIOPHYSICS,* VOL. 30, NO. 3, PP. 241-277, AUG 1997.

[62] A. W. OMTA, M. F. KROPMAN, S. WOUTERSEN, AND H. J. BAKKER, "NEGLIGIBLE EFFECT OF IONS ON THE HYDROGEN-BOND STRUCTURE IN LIQUID WATER," *SCIENCE,* VOL. 301, NO. 5631, PP. 347-349, JUL 18 2003.

[63] J. D. BATCHELOR, A. OLTEANU, A. TRIPATHY, AND G. J. PIELAK, "IMPACT OF PROTEIN DENATURANTS AND STABILIZERS ON WATER STRUCTURE," *JOURNAL OF THE AMERICAN CHEMICAL SOCIETY,* VOL. 126, NO. 7, PP. 1958-1961, FEB 25 2004.

[64] M. BOSTROM, W. KUNZ, AND B. W. NINHAM, "HOFMEISTER EFFECTS IN SURFACE TENSION OF AQUEOUS ELECTROLYTE SOLUTION," *LANGMUIR,* VOL. 21, NO. 6, PP. 2619-2623, MAR 15 2005.

[65] M. BOSTROM, D. R. M. WILLIAMS, AND B. W. NINHAM, "SPECIFIC ION EFFECTS: WHY DLVO THEORY FAILS FOR BIOLOGY AND COLLOID SYSTEMS," *PHYSICAL REVIEW LETTERS,* VOL. 87, NO. 16, OCT 15 2001, ART. NO. 168103.

[66] P. JUNGWIRTH AND B. WINTER, "IONS AT AQUEOUS INTERFACES: FROM WATER SURFACE TO HYDRATED PROTEINS," IN *ANNUAL REVIEW OF PHYSICAL CHEMISTRY,* VOL. 59(ANNUAL REVIEW OF PHYSICAL CHEMISTRY, PALO ALTO: ANNUAL REVIEWS, 2008, PP. 343-366.

[67] J. E. RICCI AND T. W. DAVIS, "AN EMPIRICAL RELATION BETWEEN SOLUBILITY OF SLIGHTLY SOLUBLE ELECTROLYTES AND DIELECTRIC CONSTANT OF THE SOLVENT," *JOURNAL OF THE AMERICAN CHEMICAL SOCIETY,* VOL. 62, PP. 407-413, JAN-JUN 1940.

[68] T. RABILLOUD, C. ADESSI, A. GIRAUDEL, AND J. LUNARDI, "IMPROVEMENT OF THE SOLUBILIZATION OF PROTEINS IN TWO-DIMENSIONAL ELECTROPHORESIS WITH IMMOBILIZED PH GRADIENTS," *ELECTROPHORESIS,* VOL. 18, NO. 3-4, PP. 307-316, MAR-APR 1997.

[69] F. ROSENBERGER, S. B. HOWARD, J. W. SOWERS, AND T. A. NYCE, "TEMPERATURE-DEPENDENCE OF PROTEIN SOLUBILITY - DETERMINATION AND APPLICATION TO CRYSTALLIZATION IN X-RAY CAPILLARIES," *JOURNAL OF CRYSTAL GROWTH,* VOL. 129, NO. 1-2, PP. 1-12, MAR 1993.

[70] B. Q. WANG, S. TCHESSALOV, M. T. CICERONE, N. W. WARNE, AND M. J. PIKAL, "IMPACT OF SUCROSE LEVEL ON STORAGE STABILITY OF PROTEINS IN FREEZE-DRIED SOLIDS: II. CORRELATION OF AGGREGATION RATE WITH PROTEIN STRUCTURE AND MOLECULAR MOBILITY," (IN ENGLISH), *JOURNAL OF PHARMACEUTICAL SCIENCES,* ARTICLE VOL. 98, NO. 9, PP. 3145-3166, SEP 2009.

[71] B. M. BAYNES, D. I. C. WANG, AND B. L. TROUT, "ROLE OF ARGININE IN THE STABILIZATION OF PROTEINS AGAINST AGGREGATION," (IN ENGLISH), *BIOCHEMISTRY,* ARTICLE VOL. 44, NO. 12, PP. 4919-4925, MAR 2005.

[72] S. JANOSCH *ET AL.*, "PARTITIONING OF DUAL-LIPIDATED PEPTIDES INTO MEMBRANE MICRODOMAINS: LIPID SORTING VS PEPTIDE AGGREGATION," (IN ENGLISH), *JOURNAL OF THE AMERICAN CHEMICAL SOCIETY,* ARTICLE VOL. 126, NO. 24, PP. 7496-7503, JUN 2004.

[73] E. J. COHN AND J. T. EDSALL, H. E. HOWE, ED. *PROTEINS, AMINO ACIDS AND PEPTIDES AS IONS AND DIPOLAR IONS* (AMERICAN CHEMICAL SOCIETY). 330 WEST FORTY-SECOND ST., NEW YORK, U.S.A: REINHOLD PUBLISHING CORPORATION, 1943, P. 686.

[74] T. ARAKAWA *ET AL.*, "SUPPRESSION OF PROTEIN INTERACTIONS BY ARGININE: A PROPOSED MECHANISM OF THE ARGININE EFFECTS," (IN ENGLISH), *BIOPHYSICAL CHEMISTRY,* REVIEW VOL. 127, NO. 1-2, PP. 1-8, APR 2007.

[75] M. FURUYA, M. HARAMURA, AND A. TANAKA, "REDUCTION OF NONSPECIFIC BINDING PROTEINS TO SELF-ASSEMBLED MONOLAYER ON GOLD SURFACE," *BIOORGANIC & MEDICINAL CHEMISTRY,* VOL. 14, NO. 2, PP. 537-543, JAN 15 2006.

[76] A. C. KLAVER, L. M. PATRIAS, M. P. COFFEY, J. M. FINKE, AND D. A. LOEFFLER, "MEASUREMENT OF ANTI-A BETA 1-42 ANTIBODIES IN INTRAVENOUS IMMUNOGLOBULIN WITH INDIRECT ELISA: THE PROBLEM OF NONSPECIFIC BINDING," *JOURNAL OF NEUROSCIENCE METHODS,* VOL. 187, NO. 2, PP. 263-269, MAR 30 2010.

[77] S. ROMERO, A. REILLO, B. ESCALERA, AND P. BUSTAMANTE, "THE BEHAVIOR OF PARACETAMOL IN MIXTURES OF AMPHIPROTIC AND AMPHIPROTIC-APROTIC SOLVENTS. RELATIONSHIP OF SOLUBILITY CURVES TO SPECIFIC AND NONSPECIFIC INTERACTIONS," (IN ENGLISH), *CHEMICAL & PHARMACEUTICAL BULLETIN,* ARTICLE VOL. 44, NO. 5, PP. 1061-1064, MAY 1996.

[78] G. G. PRIVE, "DETERGENTS FOR THE STABILIZATION AND CRYSTALLIZATION OF MEMBRANE PROTEINS," *METHODS,* VOL. 41, NO. 4, PP. 388-397, APR 2007.

[79] J. YU, D. A. FISCHMAN, AND T. L. STECK, "SELECTIVE SOLUBILIZATION OF PROTEINS AND PHOSPHO LIPIDS FROM RED BLOOD CELL MEMBRANES BY NONIONIC DETERGENTS," *JOURNAL OF SUPRAMOLECULAR STRUCTURE,* VOL. 1, NO. 3, PP. 233-248, 1973 1973.

[80] A. M. SEDDON, P. CURNOW, AND P. J. BOOTH, "MEMBRANE PROTEINS, LIPIDS AND DETERGENTS: NOT JUST A SOAP OPERA," *BIOCHIMICA ET BIOPHYSICA ACTA-BIOMEMBRANES,* VOL. 1666, NO. 1-2, PP. 105-117, NOV 3 2004.

[81] B. BATTEIGER, W. J. NEWHALL, AND R. B. JONES, "THE USE OF TWEEN-20 AS A BLOCKING-AGENT IN THE IMMUNOLOGICAL DETECTION OF PROTEINS TRANSFERRED TO NITROCELLULOSE MEMBRANES," (IN ENGLISH), *JOURNAL OF IMMUNOLOGICAL METHODS,* ARTICLE VOL. 55, NO. 3, PP. 297-307, 1982.

[82] P. O'SHEA, "MEMBRANE POTENTIALS: MEASUREMENT, OCCURRENCE AND ROLES IN CELLULAR FUNCTIONS," (IN ENGLISH),

BIOELECTROCHEMISTRY OF MEMBRANES, ARTICLE VOL. 6, PP. 23-59, 2004.

[83] E. FAHY *ET AL.*, "A COMPREHENSIVE CLASSIFICATION SYSTEM FOR LIPIDS," *JOURNAL OF LIPID RESEARCH*, VOL. 46, NO. 5, PP. 839-861, MAY 2005.

[84] J. F. NAGLE AND S. TRISTRAM-NAGLE, "STRUCTURE OF LIPID BILAYERS," (IN ENGLISH), *BIOCHIMICA ET BIOPHYSICA ACTA-REVIEWS ON BIOMEMBRANES*, REVIEW VOL. 1469, NO. 3, PP. 159-195, NOV 2000.

[85] Y. A. HANNUN, "THE SPHINGOMYELIN CYCLE AND THE 2ND MESSENGER FUNCTION OF CERAMIDE," (IN ENGLISH), *JOURNAL OF BIOLOGICAL CHEMISTRY*, REVIEW VOL. 269, NO. 5, PP. 3125-3128, FEB 1994.

[86] O. CUVILLIER *ET AL.*, "SUPPRESSION OF CERAMIDE-MEDIATED PROGRAMMED CELL DEATH BY SPHINGOSINE-1-PHOSPHATE," *NATURE*, VOL. 381, NO. 6585, PP. 800-803, JUN 27 1996.

[87] M. EEMAN AND M. DELEU, "FROM BIOLOGICAL MEMBRANES TO BIOMIMETIC MODEL MEMBRANES," *BIOTECHNOLOGIE AGRONOMIE SOCIETE ET ENVIRONNEMENT*, VOL. 14, NO. 4, PP. 719-736, 2010 2010.

[88] H. BROCKMAN, "DIPOLE POTENTIAL OF LIPID-MEMBRANES," *CHEMISTRY AND PHYSICS OF LIPIDS*, VOL. 73, NO. 1-2, PP. 57-79, SEP 6 1994.

[89] R. J. CLARKE, "EFFECT OF LIPID STRUCTURE ON THE DIPOLE POTENTIAL OF PHOSPHATIDYLCHOLINE BILAYERS," *BIOCHIMICA ET BIOPHYSICA ACTA-BIOMEMBRANES*, VOL. 1327, NO. 2, PP. 269-278, JUL 25 1997.

[90] J. N. ISRAELACHVILI, D. J. MITCHELL, AND B. W. NINHAM, "THEORY OF SELF-ASSEMBLY OF HYDROCARBON AMPHIPHILES INTO MICELLES AND BILAYERS," *JOURNAL OF THE CHEMICAL SOCIETY-FARADAY TRANSACTIONS II*, VOL. 72, PP. 1525-1568, 1976 1976.

[91] J. M. SEDDON, "STRUCTURE OF THE INVERTED HEXAGONAL (HII) PHASE, AND NON-LAMELLAR PHASE-TRANSITIONS OF LIPIDS," (IN ENGLISH), *BIOCHIMICA ET BIOPHYSICA ACTA*, REVIEW VOL. 1031, NO. 1, PP. 1-69, FEB 1990.

[92] H. SPRONG, P. VAN DER SLUIJS, AND G. VAN MEER, "HOW PROTEINS MOVE LIPIDS AND LIPIDS MOVE PROTEINS," *NATURE REVIEWS MOLECULAR CELL BIOLOGY*, VOL. 2, NO. 7, PP. 504-513, JUL 2001.

[93] A. V. FILIPPOV, M. A. RUDAKOVA, AND B. V. MUNAVIROV, "LATERAL DIFFUSION IN SPHINGOMYELIN BILAYERS," (IN ENGLISH), *MAGNETIC RESONANCE IN CHEMISTRY*, ARTICLE VOL. 48, NO. 12, PP. 945-950, DEC 2010.

[94] J. E. ROTHMAN AND J. LENARD, "MEMBRANE ASYMMETRY," *SCIENCE*, VOL. 195, NO. 4280, PP. 743-753, 1977 1977.

[95] T. P. TROUARD, A. A. NEVZOROV, T. M. ALAM, C. JOB, J. ZAJICEK, AND M. F. BROWN, "INFLUENCE OF CHOLESTEROL ON DYNAMICS OF DIMYRISTOYLPHOSPHATIDYLCHOLINE BILAYERS AS STUDIED BY DEUTERIUM NMR RELAXATION," (IN ENGLISH), *JOURNAL OF CHEMICAL PHYSICS*, REVIEW VOL. 110, NO. 17, PP. 8802-8818, MAY 1999.

[96] R. D. KORNBERG AND MCCONNEL.HM, "INSIDE-OUTSIDE TRANSITIONS OF PHOSPHOLIPIDS IN VESICLE MEMBRANES," (IN ENGLISH), *BIOCHEMISTRY*, ARTICLE VOL. 10, NO. 7, PP. 1111-&, 1971.

[97] J. LIU AND J. C. CONBOY, "1,2-DIACYL-PHOSPHATIDYLCHOLINE FLIP-FLOP MEASURED DIRECTLY BY SUM-FREQUENCY VIBRATIONAL SPECTROSCOPY," *BIOPHYSICAL JOURNAL*, VOL. 89, NO. 4, PP. 2522-2532, OCT 2005.

[98] N. SAPAY, W. F. D. BENNETT, AND D. P. TIELEMAN, "THERMODYNAMICS OF FLIP-FLOP AND DESORPTION FOR A SYSTEMATIC SERIES OF PHOSPHATIDYLCHOLINE LIPIDS," *SOFT MATTER*, VOL. 5, NO. 17, PP. 3295-3302, 2009.

[99] T. POMORSKI AND A. K. MENON, "LIPID FLIPPASES AND THEIR BIOLOGICAL FUNCTIONS," *CELLULAR AND MOLECULAR LIFE SCIENCES*, VOL. 63, NO. 24, PP. 2908-2921, DEC 2006.

[100] S. C. CHEN, J. M. STURTEVANT, AND B. J. GAFFNEY, "SCANNING CALORIMETRIC EVIDENCE FOR A 3RD PHASE-TRANSITION IN PHOSPHATIDYLCHOLINE BILAYERS," (IN ENGLISH), *PROCEEDINGS OF THE NATIONAL ACADEMY OF SCIENCES OF THE UNITED STATES OF AMERICA-BIOLOGICAL SCIENCES*, ARTICLE VOL. 77, NO. 9, PP. 5060-5063, 1980.

[101] G. CEVC, J. M. SEDDON, AND D. MARSH, "THE MECHANISM OF REGULATION OF MEMBRANE PHASE-BEHAVIOR, STRUCTURE AND INTERACTIONS BY LIPID HEADGROUPS AND ELECTROLYTE SOLUTION," *FARADAY DISCUSSIONS*, VOL. 81, PP. 179-189, 1986 1986.

[102] K. J. SEU, L. R. CAMBREA, R. M. EVERLY, AND J. S. HOVIS, "INFLUENCE OF LIPID CHEMISTRY ON MEMBRANE FLUIDITY: TAIL AND HEADGROUP INTERACTIONS," *BIOPHYSICAL JOURNAL*, VOL. 91, NO. 10, PP. 3727-3735, NOV 2006.

[103] J. H. IPSEN, G. KARLSTROM, O. G. MOURITSEN, H. WENNERSTROM, AND M. J. ZUCKERMANN, "PHASE-EQUILIBRIA IN THE PHOSPHATIDYLCHOLINE-CHOLESTEROL SYSTEM," *BIOCHIMICA ET BIOPHYSICA ACTA*, VOL. 905, NO. 1, PP. 162-172, NOV 27 1987.

[104] M. B. SANKARAM AND T. E. THOMPSON, "CHOLESTEROL-INDUCED FLUID-PHASE IMMISCIBILITY IN MEMBRANES," *PROCEEDINGS OF THE NATIONAL ACADEMY OF SCIENCES OF THE UNITED STATES OF AMERICA*, VOL. 88, NO. 19, PP. 8686-8690, OCT 1991.

[105] M. R. VIST AND J. H. DAVIS, "PHASE-EQUILIBRIA OF CHOLESTEROL DIPALMITOYLPHOSPHATIDYLCHOLINE MIXTURES - H-2 NUCLEAR MAGNETIC-RESONANCE AND DIFFERENTIAL SCANNING CALORIMETRY," *BIOCHEMISTRY*, VOL. 29, NO. 2, PP. 451-464, JAN 16 1990.

[106] R. F. M. DE ALMEIDA, A. FEDOROV, AND M. PRIETO, "SPHINGOMYELIN/PHOSPHATIDYLCHOLINE/CHOLESTEROL PHASE DIAGRAM: BOUNDARIES AND COMPOSITION OF LIPID RAFTS," *BIOPHYSICAL JOURNAL*, VOL. 85, NO. 4, PP. 2406-2416, OCT 2003.

[107] S. L. VEATCH AND S. L. KELLER, "SEEING SPOTS: COMPLEX PHASE BEHAVIOR IN SIMPLE MEMBRANES," *BIOCHIMICA ET BIOPHYSICA ACTA-MOLECULAR CELL RESEARCH*, VOL. 1746, NO. 3, PP. 172-185, DEC 30 2005.

[108] D. A. BROWN AND J. K. ROSE, "SORTING OF GPI-ANCHORED PROTEINS TO GLYCOLIPID-ENRICHED MEMBRANE SUBDOMAINS DURING TRANSPORT TO THE APICAL CELL-SURFACE," (IN ENGLISH), *CELL*, ARTICLE VOL. 68, NO. 3, PP. 533-544, FEB 1992.

[109] S. N. AHMED, D. A. BROWN, AND E. LONDON, "ON THE ORIGIN OF SPHINGOLIPID/CHOLESTEROL-RICH DETERGENT-INSOLUBLE CELL MEMBRANES: PHYSIOLOGICAL CONCENTRATIONS OF CHOLESTEROL AND SPHINGOLIPID INDUCE FORMATION OF A DETERGENT-INSOLUBLE, LIQUID-ORDERED LIPID PHASE IN MODEL MEMBRANES," *BIOCHEMISTRY*, VOL. 36, NO. 36, PP. 10944-10953, SEP 9 1997.

[110] T. Y. WANG, R. LEVENTIS, AND J. R. SILVIUS, "PARTITIONING OF LIPIDATED PEPTIDE SEQUENCES INTO LIQUID-ORDERED LIPID DOMAINS IN MODEL AND BIOLOGICAL MEMBRANES," *BIOCHEMISTRY*, VOL. 40, NO. 43, PP. 13031-13040, OCT 30 2001.

[111] D. A. BROWN AND E. LONDON, "FUNCTIONS OF LIPID RAFTS IN BIOLOGICAL MEMBRANES," *ANNUAL REVIEW OF CELL AND DEVELOPMENTAL BIOLOGY,* VOL. 14, PP. 111-136, 1998 1998.

[112] P. S. PYENTA, D. HOLOWKA, AND B. BAIRD, "CROSS-CORRELATION ANALYSIS OF INNER-LEAFLET-ANCHORED GREEN FLUORESCENT PROTEIN CO-REDISTRIBUTED WITH IGE RECEPTORS AND OUTER LEAFLET LIPID RAFT COMPONENTS," *BIOPHYSICAL JOURNAL,* VOL. 80, NO. 5, PP. 2120-2132, MAY 2001.

[113] T. J. MCINTOSH, A. VIDAL, AND S. A. SIMON, "SORTING OF LIPIDS AND TRANSMEMBRANE PEPTIDES BETWEEN DETERGENT-SOLUBLE BILAYERS AND DETERGENT-RESISTANT RAFTS," *BIOPHYSICAL JOURNAL,* VOL. 85, NO. 3, PP. 1656-1666, SEP 2003.

[114] R. FRAGOSO, D. J. REN, X. P. ZHANG, M. W. C. SU, S. J. BURAKOFF, AND Y. J. JIN, "LIPID RAFT DISTRIBUTION OF CD4 DEPENDS ON ITS PALMITOYLATION AND ASSOCIATION WITH LCK, AND EVIDENCE FOR CD4-INDUCED LIPID RAFT AGGREGATION AS AN ADDITIONAL MECHANISM TO ENHANCE CD3 SIGNALING," *JOURNAL OF IMMUNOLOGY,* VOL. 170, NO. 2, PP. 913-921, JAN 15 2003.

[115] A. ARCARO *ET AL.*, "ESSENTIAL ROLE OF CD8 PALMITOYLATION IN CD8 CORECEPTOR FUNCTION," *JOURNAL OF IMMUNOLOGY,* VOL. 165, NO. 4, PP. 2068-2076, AUG 15 2000.

[116] H. SHOGOMORI *ET AL.*, "PALMITOYLATION AND INTRACELLULAR DOMAIN INTERACTIONS BOTH CONTRIBUTE TO RAFT TARGETING OF LINKER FOR ACTIVATION OF T CELLS," *JOURNAL OF BIOLOGICAL CHEMISTRY,* VOL. 280, NO. 19, PP. 18931-18942, MAY 13 2005.

[117] R. BHATTACHARYYA, C. BARREN, AND D. M. KOVACS, "PALMITOYLATION OF AMYLOID PRECURSOR PROTEIN REGULATES AMYLOIDOGENIC PROCESSING IN LIPID RAFTS," *JOURNAL OF NEUROSCIENCE,* VOL. 33, NO. 27, PP. 11169-11183, JUL 3 2013.

[118] A. PRALLE, P. KELLER, E. L. FLORIN, K. SIMONS, AND J. K. H. HORBER, "SPHINGOLIPID-CHOLESTEROL RAFTS DIFFUSE AS SMALL ENTITIES IN THE PLASMA MEMBRANE OF MAMMALIAN CELLS," *JOURNAL OF CELL BIOLOGY,* VOL. 148, NO. 5, PP. 997-1007, MAR 6 2000.

[119] A. FILIPPOV, G. ORADD, AND G. LINDBLOM, "LIPID LATERAL DIFFUSION IN ORDERED AND DISORDERED PHASES IN RAFT MIXTURES," (IN ENGLISH), *BIOPHYSICAL JOURNAL,* ARTICLE VOL. 86, NO. 2, PP. 891-896, FEB 2004.

[120] K. SIMONS AND D. TOOMRE, "LIPID RAFTS AND SIGNAL TRANSDUCTION," (IN ENGLISH), *NATURE REVIEWS MOLECULAR CELL BIOLOGY,* REVIEW VOL. 1, NO. 1, PP. 31-39, OCT 2000.

[121] K. ROPER, D. CORBEIL, AND W. B. HUTTNER, "RETENTION OF PROMININ IN MICROVILLI REVEALS DISTINCT CHOLESTEROL-BASED LIPID MICRO-DOMAINS IN THE APICAL PLASMA MEMBRANE," (IN ENGLISH), *NATURE CELL BIOLOGY,* ARTICLE VOL. 2, NO. 9, PP. 582-592, SEP 2000.

[122] A. T. HAMMOND, F. A. HEBERLE, T. BAUMGART, D. HOLOWKA, B. BAIRD, AND G. W. FEIGENSON, "CROSSLINKING A LIPID RAFT COMPONENT TRIGGERS LIQUID ORDERED-LIQUID DISORDERED PHASE SEPARATION IN MODEL PLASMA MEMBRANES," *PROCEEDINGS OF THE NATIONAL ACADEMY OF SCIENCES OF THE UNITED STATES OF AMERICA,* VOL. 102, NO. 18, PP. 6320-6325, MAY 3 2005.

[123] F. A. HEBERLE AND G. W. FEIGENSON, "PHASE SEPARATION IN LIPID MEMBRANES," *COLD SPRING HARBOR PERSPECTIVES IN BIOLOGY,* VOL. 3, NO. 4, APR 2011, ART. NO. A004630.

[124] J. DUGGAN *ET AL.*, "FUNCTIONAL IMAGING OF MICRODOMAINS IN CELL MEMBRANES," (IN ENGLISH), *EUROPEAN BIOPHYSICS JOURNAL WITH BIOPHYSICS LETTERS*, REVIEW VOL. 37, NO. 8, PP. 1279-1289, OCT 2008.

[125] G. RICHARDSON, L. J. CUMMINGS, H. J. HARRIS, AND P. O'SHEA, "TOWARD A MATHEMATICAL MODEL OF THE ASSEMBLY AND DISASSEMBLY OF MEMBRANE MICRODOMAINS: COMPARISON WITH EXPERIMENTAL MODELS," *BIOPHYSICAL JOURNAL*, VOL. 92, NO. 12, PP. 4145-4156, JUN 2007.

[126] P. SHARMA *ET AL.*, "NANOSCALE ORGANIZATION OF MULTIPLE GPI-ANCHORED PROTEINS IN LIVING CELL MEMBRANES," (IN ENGLISH), *CELL*, ARTICLE VOL. 116, NO. 4, PP. 577-589, FEB 2004.

[127] S. MAYOR AND M. RAO, "RAFTS: SCALE-DEPENDENT, ACTIVE LIPID ORGANIZATION AT THE CELL SURFACE," *TRAFFIC*, VOL. 5, NO. 4, PP. 231-240, APR 2004.

[128] J. WALL, C. A. GOLDING, M. VANVEEN, AND P. OSHEA, "THE USE OF FLUORSCEINPHOSPHATIDYLETHANOLAMINE (FPE) AS A REAL-TIME PROBE FOR PEPTIDE MEMBRANE INTERACTIONS.," (IN ENGLISH), *MOLECULAR MEMBRANE BIOLOGY*, ARTICLE VOL. 12, NO. 2, PP. 183-192, APR-JUN 1995.

[129] M. FERNANDEZ-SUAREZ AND A. Y. TING, "FLUORESCENT PROBES FOR SUPER-RESOLUTION IMAGING IN LIVING CELLS," *NATURE REVIEWS MOLECULAR CELL BIOLOGY*, VOL. 9, NO. 12, PP. 929-943, DEC 2008.

[130] G. BINNIG, C. F. QUATE, AND C. GERBER, "ATOMIC FORCE MICROSCOPE," *PHYSICAL REVIEW LETTERS*, VOL. 56, NO. 9, PP. 930-933, MAR 3 1986.

[131] K. H. SHEIKH AND S. P. JARVIS, "CRYSTALLINE HYDRATION STRUCTURE AT THE MEMBRANE-FLUID INTERFACE OF MODEL LIPID RAFTS INDICATES A HIGHLY REACTIVE BOUNDARY REGION," *JOURNAL OF THE AMERICAN CHEMICAL SOCIETY*, VOL. 133, NO. 45, PP. 18296-18303, NOV 16 2011.

[132] S. D. CONNELL, G. HEATH, P. D. OLMSTED, AND A. KISIL, "CRITICAL POINT FLUCTUATIONS IN SUPPORTED LIPID MEMBRANES," *FARADAY DISCUSSIONS*, VOL. 161, PP. 91-111, 2013.

[133] L. J. PIKE, "LIPID RAFTS: BRINGING ORDER TO CHAOS," *JOURNAL OF LIPID RESEARCH*, VOL. 44, NO. 4, PP. 655-667, APR 2003.

[134] C. GOMEZ-MOUTON *ET AL.*, "DYNAMIC REDISTRIBUTION OF RAFT DOMAINS AS AN ORGANIZING PLATFORM FOR SIGNALING DURING CELL CHEMOTAXIS," *JOURNAL OF CELL BIOLOGY*, VOL. 164, NO. 5, PP. 759-768, MAR 2004.

[135] K. GAUS *ET AL.*, "VISUALIZING LIPID STRUCTURE AND RAFT DOMAINS IN LIVING CELLS WITH TWO-PHOTON MICROSCOPY," *PROCEEDINGS OF THE NATIONAL ACADEMY OF SCIENCES OF THE UNITED STATES OF AMERICA*, VOL. 100, NO. 26, PP. 15554-15559, DEC 2003.

[136] S. SAKAMOTO, H. NAKAHARA, T. UTO, Y. SHOYAMA, AND O. SHIBATA, "INVESTIGATION OF INTERFACIAL BEHAVIOR OF GLYCYRRHIZIN WITH A LIPID RAFT MODEL VIA A LANGMUIR MONOLAYER STUDY," (IN ENGLISH), *BIOCHIMICA ET BIOPHYSICA ACTA-BIOMEMBRANES*, ARTICLE VOL. 1828, NO. 4, PP. 1271-1283, APR 2013.

[137] G. CEVC, "MEMBRANE ELECTROSTATICS," *BIOCHIMICA ET BIOPHYSICA ACTA*, VOL. 1031, NO. 3, PP. 311-382, OCT 8 1990.

[138] P. O'SHEA, "INTERMOLECULAR INTERACTIONS WITH/WITHIN CELL MEMBRANES AND THE TTRINITY OF MEMBRANE POTENTIALS: KINETICS AND IMAGING," (IN ENGLISH), *BIOCHEMICAL SOCIETY TRANSACTIONS*, ARTICLE; PROCEEDINGS PAPER VOL. 31, PP. 990-996, OCT 2003.

[139] U. PETERSON, D. A. MANNOCK, R. LEWIS, P. POHL, R. N. MCELHANEY, AND E. E. POHL, "ORIGIN OF MEMBRANE DIPOLE POTENTIAL: CONTRIBUTION OF THE PHOSPHOLIPID FATTY ACID CHAINS," *CHEMISTRY AND PHYSICS OF LIPIDS*, VOL. 117, NO. 1-2, PP. 19-27, AUG 2002, ART. NO. PII S0009-3084(02)00013-0.

[140] S. MCLAUGHLIN, "THE ELECTROSTATIC PROPERTIES OF MEMBRANES," *ANNUAL REVIEW OF BIOPHYSICS AND BIOPHYSICAL CHEMISTRY*, VOL. 18, PP. 113-136, 1989 1989.

[141] P. O'SHEA, "PHYSICAL LANDSCAPES IN BIOLOGICAL MEMBRANES: PHYSICO-CHEMICAL TERRAINS FOR SPATIO-TEMPORAL CONTROL OF BIOMOLECULAR INTERACTIONS AND BEHAVIOUR," *PHILOSOPHICAL TRANSACTIONS OF THE ROYAL SOCIETY OF LONDON SERIES A-MATHEMATICAL PHYSICAL AND ENGINEERING SCIENCES*, VOL. 363, NO. 1827, PP. 575-588, FEB 15 2005.

[142] P. D. MCQUEEN, S. SAGOO, H. YAO, AND R. A. JOCKUSCH, "ON THE INTRINSIC PHOTOPHYSICS OF FLUORESCEIN," *ANGEWANDTE CHEMIE-INTERNATIONAL EDITION*, VOL. 49, NO. 48, PP. 9193-9196, 2010.

[143] J. CLADERA AND P. O'SHEA, "GENERIC TECHNIQUES FOR FLUORESCENCE MEASUREMENTS OF PROTEIN-LIGAND INTERACTIONS; REAL-TIME KINETICS AND SPATIAL IMAGING," *PROTEIN-LIGAND INTERACTIONS: STRUCTURE AND SPECTROSCOPY*, PP. 169-200, 2001 2001.

[144] C. WOLFE, J. CLADERA, AND P. O'SHEA, "AMINO ACID SEQUENCES WHICH PROMOTE AND PREVENT THE BINDING AND MEMBRANE INSERTION OF SURFACE-ACTIVE PEPTIDES: COMPARISON OF MELITTIN AND PROMELITTIN," *MOLECULAR MEMBRANE BIOLOGY*, VOL. 15, NO. 4, PP. 221-227, OCT-DEC 1998.

[145] T. ASAWAKARN, J. CLADERA, AND P. O'SHEA, "EFFECTS OF THE MEMBRANE DIPOLE POTENTIAL ON THE INTERACTION OF SAQUINAVIR WITH PHOSPHOLIPID MEMBRANES AND PLASMA MEMBRANE RECEPTORS OF CACO-2 CELLS," *JOURNAL OF BIOLOGICAL CHEMISTRY*, VOL. 276, NO. 42, PP. 38457-38463, OCT 19 2001.

[146] A. M. NESTERENKO AND Y. A. ERMAKOV, "MOLECULAR-DYNAMIC SIMULATION OF PHOSPHOLIPID BILAYERS: ION DISTRIBUTION AT THE SURFACE OF NEUTRAL AND CHARGED BILAYER IN THE LIQUID-CRYSTALLINE STATE," (IN RUSSIAN), *BIOLOGICHESKIE MEMBRANY*, ARTICLE VOL. 29, NO. 5, PP. 374-384, SEP-OCT 2012.

[147] L. M. LOEW, S. SCULLY, L. SIMPSON, AND A. S. WAGGONER, "EVIDENCE FOR A CHARGE-SHIFT ELECTROCHROMIC MECHANISM IN A PROBE OF MEMBRANE-POTENTIAL," *NATURE*, VOL. 281, NO. 5731, PP. 497-499, 1979 1979.

[148] B. J. FRISKEN, C. ASMAN, AND P. J. PATTY, "STUDIES OF VESICLE EXTRUSION," *LANGMUIR*, VOL. 16, NO. 3, PP. 928-933, FEB 8 2000.

[149] L. D. MAYER, M. J. HOPE, AND P. R. CULLIS, "VESICLES OF VARIABLE SIZES PRODUCED BY A RAPID EXTRUSION PROCEDURE," *BIOCHIM BIOPHYS ACTA*, VOL. 858, NO. 1, PP. 161-8, JUN 13 1986.

[150] P. D. LAMPE, G. J. WEI, AND G. L. NELSESTUEN, "STOPPED-FLOW STUDIES OF MYELIN BASIC-PROTEIN ASSOCIATION WITH PHOSPHOLIPID-VESICLES AND SUBSEQUENT VESICLE AGGREGATION," *BIOCHEMISTRY*, VOL. 22, NO. 7, PP. 1594-1599, 1983 1983.

[151] A. PHOTOPHYSICS, "SCHEMATIC OVERVIEW OF THE SEQUENTIAL-MIXING SETUP FOR THE APPLIED PHOTOPHYSICS SX20 STOPPED-FLOW SPECTROPHOTOMETER WITH OPTION SX/SQ," ED: APPLIED PHOTOPHYSICS, 2015.

[152] H. LEVINE, "QUANTIFICATION OF BETA-SHEET AMYLOID FIBRIL STRUCTURES WITH THIOFLAVIN T," *AMYLOID, PRIONS, AND OTHER PROTEIN AGGREGATES*, VOL. 309, PP. 274-284, 1999 1999.
[153] T. H. WATTS, A. A. BRIAN, J. W. KAPPLER, P. MARRACK, AND H. M. MCCONNELL, "ANTIGEN PRESENTATION BY SUPPORTED PLANAR MEMBRANES CONTAINING AFFINITY-PURIFIED I-AD," *PROCEEDINGS OF THE NATIONAL ACADEMY OF SCIENCES OF THE UNITED STATES OF AMERICA-BIOLOGICAL SCIENCES*, VOL. 81, NO. 23, PP. 7564-7568, 1984 1984.
[154] D. M. SOUMPASIS, "THEORETICAL-ANALYSIS OF FLUORESCENCE PHOTOBLEACHING RECOVERY EXPERIMENTS," *BIOPHYSICAL JOURNAL*, VOL. 41, NO. 1, PP. 95-97, 1983 1983.
[155] N. J. CHO, L. Y. HWANG, J. J. R. SOLANDT, AND C. W. FRANK, "COMPARISON OF EXTRUDED AND SONICATED VESICLES FOR PLANAR BILAYER SELF-ASSEMBLY," (IN ENGLISH), *MATERIALS*, ARTICLE VOL. 6, NO. 8, PP. 3294-3308, AUG 2013.
[156] A. SAVITZKY AND M. J. E. GOLAY, "SMOOTHING + DIFFERENTIATION OF DATA BY SIMPLIFIED LEAST SQUARES PROCEDURES," *ANALYTICAL CHEMISTRY*, VOL. 36, NO. 8, PP. 1627-&, 1964 1964.
[157] D. NECAS AND P. KLAPETEK, "GWYDDION: AN OPEN-SOURCE SOFTWARE FOR SPM DATA ANALYSIS," *CENTRAL EUROPEAN JOURNAL OF PHYSICS*, VOL. 10, NO. 1, PP. 181-188, FEB 2012.
[158] P. ENGLEBIENNE, A. VAN HOONACKER, AND M. VERHAS, "SURFACE PLASMON RESONANCE: PRINCIPLES, METHODS AND APPLICATIONS IN BIOMEDICAL SCIENCES," (IN ENGLISH), *SPECTROSCOPY-AN INTERNATIONAL JOURNAL*, ARTICLE; PROCEEDINGS PAPER VOL. 17, NO. 2-3, PP. 255-273, 2003.
[159] J. HOMOLA, "PRESENT AND FUTURE OF SURFACE PLASMON RESONANCE BIOSENSORS," (IN ENGLISH), *ANALYTICAL AND BIOANALYTICAL CHEMISTRY*, REVIEW VOL. 377, NO. 3, PP. 528-539, OCT 2003.
[160] O. SHOVMAN *ET AL.*, "EVALUATION OF THE BIOPLEX (TM) 2200 ANA SCREEN - ANALYSIS OF 510 HEALTHY SUBJECTS: INCIDENCE OF NATURAL/PREDICTIVE AUTOANTIBODIES," *AUTOIMMUNITY: CONCEPTS AND DIAGNOSIS AT THE CUTTING EDGE*, VOL. 1050, PP. 380-388, 2005 2005.
[161] P. GOTTSCHALK AND J. DUNN, "FITTING BRENDAN'S FIVE-PARAMETER LOGISTIC CURVE.," IN "BIO-RAD BULLETIN," BIO-RAD, BIO-RAD2005, VOL. 3022.
[162] S. KHALIFIAN, G. RAIMONDI, AND G. BRANDACHER, "THE USE OF LUMINEX ASSAYS TO MEASURE CYTOKINES," *THE JOURNAL OF INVESTIGATIVE DERMATOLOGY*, VOL. 135, NO. 4, PP. E31-E31, 2015-APR 2015.
[163] R. ZIMMERMAN, T. HAMILTON, L. MA, AND V. GUPTA, "COMPOSITE PROFILING OF ANGIOGENIC FACTORS USING BIO-PLEX PRO HUMAN CANCER BIOMARKER PANEL 1," VOL. 6156, ED. HERCULES, CA: BIO-RAD LABORATORIES, INC., 2000, PP. 1311-1318.
[164] J. F. D. SIAWAYA *ET AL.*, "AN EVALUATION OF COMMERCIAL FLUORESCENT BEAD-BASED LUMINEX CYTOKINE ASSAYS," *PLOS ONE*, VOL. 3, NO. 7, JUL 2 2008, ART. NO. E2535.
[165] B. CHESEBRO, A. RANGEL, J. STRIEBEL, AND B. RACE, "MULTIPLE EFFECTS OF PRION PROTEIN MEMBRANE ANCHORING ON PRION DISEASE PATHOGENESIS: INTERACTION OF PRPRES AMYLOID WITH THE BRAIN INTERSTITIAL FLUID (ISF) DRAINAGE PATHWAY," *PRION*, VOL. 7, PP. 6-6, APR-MAY 2013.

[166] C. SOTO, "ALZHEIMER'S AND PRION DISEASE AS DISORDERS OF PROTEIN CONFORMATION: IMPLICATIONS FOR THE DESIGN OF NOVEL THERAPEUTIC APPROACHES," *JOURNAL OF MOLECULAR MEDICINE-JMM*, VOL. 77, NO. 5, PP. 412-418, MAY 1999.

[167] J. RICHENS, K. VERE, AND P. O'SHEA, "OPTIMISATION OF PLASMONIC-BASED BIOSENSORS FOR LABEL-FREE IMAGING OF MOLECULAR ARRAYS; TOWARDS DIAGNOSIS OF NEURODEGENERATIVE DISEASES.," ED: IEEE, 2011.

[168] T. NOLAN, N. SINGH, AND C. R. MCCURDY, "LIGAND MACROMOLECULE INTERACTIONS: THEORETICAL PRINCIPLES OF MOLECULAR RECOGNITION," *LIGAND-MACROMOLECULAR INTERACTIONS IN DRUG DISCOVERY: METHODS AND PROTOCOLS*, VOL. 572, PP. 13-29, 2010 2010.

[169] J. L. RICHENS, E. A. LUNT, D. SANGER, G. MCKENZIE, AND P. O'SHEA, "AVOIDING NONSPECIFIC INTERACTIONS IN STUDIES OF THE PLASMA PROTEOME: PRACTICAL SOLUTIONS TO PREVENTION OF NONSPECIFIC INTERACTIONS FOR LABEL-FREE DETECTION OF LOW-ABUNDANCE PLASMA PROTEINS," (IN ENG), *J PROTEOME RES*, VOL. 8, NO. 11, PP. 5103-10, NOV 2009.

[170] W. M. MULLETT, E. P. LAI, AND J. M. YEUNG, "SURFACE PLASMON RESONANCE-BASED IMMUNOASSAYS," (IN ENG), *METHODS*, VOL. 22, NO. 1, PP. 77-91, SEP 2000.

[171] X. FAN, L. LIN, AND P. B. MESSERSMITH, "CELL FOULING RESISTANCE OF POLYMER BRUSHES GRAFTED FROM TI SUBSTRATES BY SURFACE-INITIATED POLYMERIZATION: EFFECT OF ETHYLENE GLYCOL SIDE CHAIN LENGTH," *BIOMACROMOLECULES*, VOL. 7, NO. 8, PP. 2443-2448, AUG 14 2006.

[172] G. L. KENAUSIS *ET AL.*, "POLY(L-LYSINE)-G-POLY(ETHYLENE GLYCOL) LAYERS ON METAL OXIDE SURFACES: ATTACHMENT MECHANISM AND EFFECTS OF POLYMER ARCHITECTURE ON RESISTANCE TO PROTEIN ADSORPTION," *JOURNAL OF PHYSICAL CHEMISTRY B*, VOL. 104, NO. 14, PP. 3298-3309, APR 13 2000.

[173] S. PASCHE, S. M. DE PAUL, J. VOROS, N. D. SPENCER, AND M. TEXTOR, "POLY(L-LYSINE)-GRAFT-POLY(ETHYLENE GLYCOL) ASSEMBLED MONOLAYERS ON NIOBIUM OXIDE SURFACES: A QUANTITATIVE STUDY OF THE INFLUENCE OF POLYMER INTERFACIAL ARCHITECTURE ON RESISTANCE TO PROTEIN ADSORPTION BY TOF-SIMS AND *IN SITU* OWLS," *LANGMUIR*, VOL. 19, NO. 22, PP. 9216-9225, OCT 28 2003.

[174] S. PASCHE, J. VOROS, H. J. GRIESSER, N. D. SPENCER, AND M. TEXTOR, "EFFECTS OF IONIC STRENGTH AND SURFACE CHARGE ON PROTEIN ADSORPTION AT PEGYLATED SURFACES," *JOURNAL OF PHYSICAL CHEMISTRY B*, VOL. 109, NO. 37, PP. 17545-17552, SEP 22 2005.

[175] A. ASADA AND M. SONOYAMA, "SOLUBILIZATION AND STRUCTURAL STABILITY OF BACTERIORHODOPSIN WITH A MILD NONIONIC DETERGENT, N-OCTYL-BETA-THIOGLUCOSIDE," *BIOSCIENCE BIOTECHNOLOGY AND BIOCHEMISTRY*, VOL. 75, NO. 2, PP. 376-378, FEB 2011.

[176] N. JADIDI, B. ADIB, AND F. B. MALIHI, "SYNERGISM AND PERFORMANCE OPTIMIZATION IN LIQUID DETERGENTS CONTAINING BINARY MIXTURES OF ANIONIC-NONIONIC, AND ANIONIC-CATIONIC SURFACTANTS," *JOURNAL OF SURFACTANTS AND DETERGENTS*, VOL. 16, NO. 1, PP. 115-121, JAN 2013.

[177] L. MAKOWSKI, D. J. RODI, S. MANDAVA, D. D. L. MINH, D. B. GORE, AND R. F. FISCHETTI, "MOLECULAR CROWDING INHIBITS INTRAMOLECULAR BREATHING MOTIONS IN PROTEINS," *JOURNAL OF MOLECULAR BIOLOGY*, VOL. 375, NO. 2, PP. 529-546, JAN 11 2008.

[178] H.-X. ZHOU, G. RIVAS, AND A. P. MINTON, "MACROMOLECULAR CROWDING AND CONFINEMENT: BIOCHEMICAL, BIOPHYSICAL, AND POTENTIAL PHYSIOLOGICAL CONSEQUENCES," *ANNUAL REVIEW OF BIOPHYSICS*, VOL. 37, PP. 375-397, 2008 2008.
[179] R. THORPE AND S. J. SWANSON, "CURRENT METHODS FOR DETECTING ANTIBODIES AGAINST ERYTHROPOIETIN AND OTHER RECOMBINANT PROTEINS," *CLINICAL AND DIAGNOSTIC LABORATORY IMMUNOLOGY*, VOL. 12, NO. 1, PP. 28-39, JAN 2005.
[180] P. JUNGWIRTH AND D. J. TOBIAS, "IONS AT THE AIR/WATER INTERFACE," *JOURNAL OF PHYSICAL CHEMISTRY B*, VOL. 106, NO. 25, PP. 6361-6373, JUN 27 2002.
[181] Y. ZHANG AND P. S. CREMER, "INTERACTIONS BETWEEN MACROMOLECULES AND IONS: THE HOFMEISTER SERIES," *CURRENT OPINION IN CHEMICAL BIOLOGY*, VOL. 10, NO. 6, PP. 658-663, DEC 2006.
[182] P. E. MASON, G. W. NEILSON, C. E. DEMPSEY, A. C. BARNES, AND J. M. CRUICKSHANK, "THE HYDRATION STRUCTURE OF GUANIDINIUM AND THIOCYANATE IONS: IMPLICATIONS FOR PROTEIN STABILITY IN AQUEOUS SOLUTION," *PROCEEDINGS OF THE NATIONAL ACADEMY OF SCIENCES OF THE UNITED STATES OF AMERICA*, VOL. 100, NO. 8, PP. 4557-4561, APR 15 2003.
[183] Z. ADAMCZYK, B. CICHOCKI, M. L. EKIEL-JEZEWSKA, A. SLOWICKA, E. WAJNRYB, AND M. WASILEWSKA, "FIBRINOGEN CONFORMATIONS AND CHARGE IN ELECTROLYTE SOLUTIONS DERIVED FROM DLS AND DYNAMIC VISCOSITY MEASUREMENTS," (IN ENGLISH), *JOURNAL OF COLLOID AND INTERFACE SCIENCE*, ARTICLE VOL. 385, PP. 244-257, NOV 2012.
[184] M. GEKLE, S. MILDENBERGER, R. FREUDINGER, AND S. SILBERNAGL, "FUNCTIONAL CHARACTERIZATION OF ALBUMIN BINDING TO THE APICAL MEMBRANE OF OK CELLS," *AMERICAN JOURNAL OF PHYSIOLOGY-RENAL FLUID AND ELECTROLYTE PHYSIOLOGY*, VOL. 271, NO. 2, PP. F286-F291, AUG 1996.
[185] B. Q. WANG, S. TCHESSALOV, N. W. WARNE, AND M. J. PIKAL, "IMPACT OF SUCROSE LEVEL ON STORAGE STABILITY OF PROTEINS IN FREEZE-DRIED SOLIDS: I. CORRELATION OF PROTEIN-SUGAR INTERACTION WITH NATIVE STRUCTURE PRESERVATION," (IN ENGLISH), *JOURNAL OF PHARMACEUTICAL SCIENCES*, ARTICLE VOL. 98, NO. 9, PP. 3131-3144, SEP 2009.
[186] N. JOVANOVIC, A. BOUCHARD, G. W. HOFLAND, G. J. WITKAMP, D. J. A. CROMMELIN, AND W. JISKOOT, "DISTINCT EFFECTS OF SUCROSE AND TREHALOSE ON PROTEIN STABILITY DURING SUPERCRITICAL FLUID DRYING AND FREEZE-DRYING," *EUROPEAN JOURNAL OF PHARMACEUTICAL SCIENCES*, VOL. 27, NO. 4, PP. 336-345, MAR 2006.
[187] J. A. TE, M. L. TAN, AND T. ICHIYE, "SOLVATION OF GLUCOSE, TREHALOSE, AND SUCROSE BY THE SOFT-STICKY DIPOLE-QUADRUPOLE-OCTUPOLE WATER MODEL," (IN ENGLISH), *CHEMICAL PHYSICS LETTERS*, ARTICLE VOL. 491, NO. 4-6, PP. 218-223, MAY 2010.
[188] J.-F. MASSON, T. M. BATTAGLIA, J. CRAMER, S. BEAUDOIN, M. SIERKS, AND K. S. BOOKSH, "REDUCTION OF NONSPECIFIC PROTEIN BINDING ON SURFACE PLASMON RESONANCE BIOSENSORS," *ANALYTICAL AND BIOANALYTICAL CHEMISTRY*, VOL. 386, NO. 7-8, PP. 1951-1959, DEC 2006.
[189] S. HAN, C. KIM, AND D. KWON, "THERMAL-DEGRADATION OF POLY(ETHYLENEGLYCOL)," *POLYMER DEGRADATION AND STABILITY*, VOL. 47, NO. 2, PP. 203-208, 1995 1995.

[190] S. HAN, C. KIM, AND D. KWON, "THERMAL/OXIDATIVE DEGRADATION AND STABILIZATION OF POLYETHYLENE GLYCOL," *POLYMER,* VOL. 38, NO. 2, PP. 317-323, JAN 1997.
[191] O. A. MKHATRESH AND F. HEATLEY, "A STUDY OF THE PRODUCTS AND MECHANISM OF THE THERMAL OXIDATIVE DEGRADATION OF POLY(ETHYLENE OXIDE) USING H-1 AND C-13 1-D AND 2-D NMR," *POLYMER INTERNATIONAL,* VOL. 53, NO. 9, PP. 1336-1342, SEP 2004.
[192] J. WALL, F. AYOUB, AND P. O'SHEA, "A STUDY OF THE INTERACTIONS OF AN IMMUNOGLOBULIN LIGHT CHAIN WITH ARTIFICIAL AND B-LYMPHOCYTE MEMBRANES.," VOL. AUG 1, ED. HUMAN IMMUNOLOGY & CANCER PROGRAM, UNIVERSITY OF TENNESSEE MEDICAL CENTER AT KNOXVILLE, 1924 ALCOA HIGHWAY, KNOXVILLE, TN 37920-6999. USA: FRONT BIOSCI. , 1996, PP. 46-58
[193] N. SINHA AND S. J. SMITH-GILL, "MOLECULAR DYNAMICS SIMULATION OF A HIGH-AFFINITY ANTIBODY-PROTEIN COMPLEX - THE BINDING SITE IS A MOSAIC OF LOCALLY FLEXIBLE AND PREORGANIZED RIGID REGIONS," (IN ENGLISH), *CELL BIOCHEMISTRY AND BIOPHYSICS,* ARTICLE VOL. 43, NO. 2, PP. 253-273, 2005.
[194] D. E. KOSHLAND, "THE KEY-LOCK THEORY AND THE INDUCED FIT THEORY," *ANGEWANDTE CHEMIE-INTERNATIONAL EDITION,* VOL. 33, NO. 23-24, PP. 2375-2378, JAN 3 1994.
[195] Y. NING *ET AL.*, "DEVELOPMENT AND ASSESSMENT OF A HIGH ABUNDANT HUMAN PLASMA PROTEIN DEPLETION KIT USING MONOCLONAL ANTIBODIES AGAINST NATIVE SERUM PROTEINS," (IN ENGLISH), *MOLECULAR & CELLULAR PROTEOMICS,* MEETING ABSTRACT VOL. 4, NO. 8, PP. S215-S215, AUG 2005.
[196] G. SADIK *ET AL.*, "*IN VITRO* PROCESSING OF AMYLOID PRECURSOR PROTEIN BY CATHEPSIN D," (IN ENGLISH), *INTERNATIONAL JOURNAL OF BIOCHEMISTRY & CELL BIOLOGY,* ARTICLE VOL. 31, NO. 11, PP. 1327-1337, NOV 1999.
[197] R. J. CARTER *ET AL.*, "CHARACTERIZATION OF PROGRESSIVE MOTOR DEFICITS IN MICE TRANSGENIC FOR THE HUMAN HUNTINGTON'S DISEASE MUTATION," (IN ENGLISH), *JOURNAL OF NEUROSCIENCE,* ARTICLE VOL. 19, NO. 8, PP. 3248-3257, APR 1999.
[198] K. B. KEGEL *ET AL.*, "POLYGLUTAMINE EXPANSION IN HUNTINGTIN INCREASES ITS INSERTION INTO LIPID BILAYERS," *BIOCHEMICAL AND BIOPHYSICAL RESEARCH COMMUNICATIONS,* VOL. 387, NO. 3, PP. 472-475, SEP 25 2009.
[199] S. LECOMTE, T. HA PHUONG, J. GEAN, K. BERTHELOT, AND C. CULLIN, "INTERACTION HET-S PRION / MEMBRANE TO GET A BETTER INSIGHT OF AMYLOID TOXICITY," *BIOPHYSICAL JOURNAL,* VOL. 98, NO. 3, PP. 459A-459A, JAN 2010.
[200] N. K. CHU *ET AL.*, "A C-TERMINAL MEMBRANE ANCHOR AFFECTS THE INTERACTIONS OF PRION PROTEINS WITH LIPID MEMBRANES," *JOURNAL OF BIOLOGICAL CHEMISTRY,* VOL. 289, NO. 43, PP. 30144-30160, OCT 24 2014.
[201] M. BOADA *ET AL.*, "AMYLOID-TARGETED THERAPEUTICS IN ALZHEIMER'S DISEASE: USE OF HUMAN ALBUMIN IN PLASMA EXHANGE AS A NOVEL APPORACH FOR A BETA MOBILIZATION," (IN ENGLISH), *DRUG NEWS & PERSPECTIVES,* ARTICLE VOL. 22, NO. 6, PP. 325-339, JUL-AUG 2009.
[202] *CURRENT STATE OF ALZHEIMER'S DISEASE RESEARCH AND THERAPEUTICS* (CURRENT STATE OF ALZHEIMER'S DISEASE RESEARCH AND THERAPEUTICS). 2012.

[203] E. MICHAELIS AND M. MICHAELIS, *CURRENT STATE OF ALZHEIMER'S DISEASE RESEARCH AND THERAPEUTICS* (CURRENT STATE OF ALZHEIMER'S DISEASE RESEARCH AND THERAPEUTICS). 2012.

[204] E. A. DISALVO, M. F. MARTINI, A. M. BOUCHET, A. HOLLMANN, AND M. A. FRIAS, "STRUCTURAL AND THERMODYNAMIC PROPERTIES OF WATER-MEMBRANE INTERPHASES: SIGNIFICANCE FOR PEPTIDE/MEMBRANE INTERACTIONS," *ADVANCES IN COLLOID AND INTERFACE SCIENCE,* VOL. 211, PP. 17-33, SEP 2014.

[205] D. ROBINSON, N. A. BESLEY, P. O'SHEA, AND J. D. HIRST, "DI-8-ANEPPS EMISSION SPECTRA IN PHOSPHOLIPID/CHOLESTEROL MEMBRANES: A THEORETICAL STUDY," *JOURNAL OF PHYSICAL CHEMISTRY B,* VOL. 115, NO. 14, PP. 4160-4167, APR 14 2011.

[206] R. VARMA AND S. MAYOR, "GPI-ANCHORED PROTEINS ARE ORGANIZED IN SUBMICRON DOMAINS AT THE CELL SURFACE," *NATURE,* VOL. 394, NO. 6695, PP. 798-801, AUG 20 1998.

[207] K. AMAN, E. LINDAHL, O. EDHOLM, P. HAKANSSON, AND P. O. WESTLUND, "STRUCTURE AND DYNAMICS OF INTERFACIAL WATER IN AN L-ALPHA PHASE LIPID BILAYER FROM MOLECULAR DYNAMICS SIMULATIONS," *BIOPHYSICAL JOURNAL,* VOL. 84, NO. 1, PP. 102-115, JAN 2003.

[208] J. R. SILVIUS, D. DELGIUDICE, AND M. LAFLEUR, "CHOLESTEROL AT DIFFERENT BILAYER CONCENTRATIONS CAN PROMOTE OR ANTAGONIZE LATERAL SEGREGATION OF PHOSPHOLIPIDS OF DIFFERING ACYL CHAIN LENGTH," (IN ENGLISH), *BIOCHEMISTRY,* ARTICLE VOL. 35, NO. 48, PP. 15198-15208, DEC 1996.

[209] K. SIMONS AND E. IKONEN, "FUNCTIONAL RAFTS IN CELL MEMBRANES," (IN ENGLISH), *NATURE,* ARTICLE VOL. 387, NO. 6633, PP. 569-572, JUN 1997.

[210] F. T. PRESTI, R. J. PACE, AND S. I. CHAN, "CHOLESTEROL PHOSPHOLIPID INTERACTION IN MEMBRANES .2. STOICHIOMETRY AND MOLECULAR PACKING OF CHOLESTEROL-RICH DOMAINS," *BIOCHEMISTRY,* VOL. 21, NO. 16, PP. 3831-3835, 1982 1982.

[211] B. WESTERLUND AND J. P. SLOTTE, "HOW THE MOLECULAR FEATURES OF GLYCOSPHINGOLIPIDS AFFECT DOMAIN FORMATION IN FLUID MEMBRANES," (IN ENGLISH), *BIOCHIMICA ET BIOPHYSICA ACTA-BIOMEMBRANES,* REVIEW VOL. 1788, NO. 1, PP. 194-201, JAN 2009.

[212] A. BJORKBOM *ET AL.*, "EFFECT OF SPHINGOMYELIN HEADGROUP SIZE ON MOLECULAR PROPERTIES AND INTERACTIONS WITH CHOLESTEROL," *BIOPHYSICAL JOURNAL,* VOL. 99, NO. 10, PP. 3300-3308, NOV 17 2010.

[213] J. P. SLOTTE, "THE IMPORTANCE OF HYDROGEN BONDING IN SPHINGOMYELIN'S MEMBRANE INTERACTIONS WITH CO-LIPIDS," *BIOCHIMICA ET BIOPHYSICA ACTA-BIOMEMBRANES,* VOL. 1858, NO. 2, PP. 304-310, FEB 2016.

[214] S. A. PANDIT, S. VASUDEVAN, S. W. CHIU, R. J. MASHL, E. JAKOBSSON, AND H. L. SCOTT, "SPHINGOMYELIN-CHOLESTEROL DOMAINS IN PHOSPHOLIPID MEMBRANES: ATOMISTIC SIMULATION," *BIOPHYSICAL JOURNAL,* VOL. 87, NO. 2, PP. 1092-1100, AUG 2004.

[215] T. STARKE-PETERKOVIC, N. TURNER, M. F. VITHA, M. P. WALLER, D. E. HIBBS, AND R. J. CLARKE, "CHOLESTEROL EFFECT ON THE DIPOLE POTENTIAL OF LIPID MEMBRANES," *BIOPHYSICAL JOURNAL,* VOL. 90, NO. 11, PP. 4060-4070, JUN 2006.

[216] R. PETHIG, "DIELECTRIC AND ELECTRONIC PROPERTIES OF BIOLOGICAL MATERIALS," *DI ELECTRIC AND ELECTRONIC PROPERTIES OF BIOLOGICAL MATERIALS,* PP. 376-376, 1979 1979.

[217] J. CLADERA AND P. O'SHEA, "INTRAMEMBRANE MOLECULAR DIPOLES AFFECT THE MEMBRANE INSERTION AND FOLDING OF A MODEL AMPHIPHILIC PEPTIDE," *BIOPHYSICAL JOURNAL,* VOL. 74, NO. 5, PP. 2434-2442, MAY 1998.
[218] E. GROSS, R. S. BEDLACK, AND L. M. LOEW, "DUAL-WAVELENGTH RATIOMETRIC FLUORESCENCE MEASUREMENT OF THE MEMBRANE DIPOLE POTENTIAL," *BIOPHYSICAL JOURNAL,* VOL. 67, NO. 1, PP. 208-216, JUL 1994.
[219] S. BANDARI, H. CHAKRABORTY, D. F. COVEY, AND A. CHATTOPADHYAY, "MEMBRANE DIPOLE POTENTIAL IS SENSITIVE TO CHOLESTEROL STEREOSPECIFICITY: IMPLICATIONS FOR RECEPTOR FUNCTION," *CHEMISTRY AND PHYSICS OF LIPIDS,* VOL. 184, PP. 25-29, DEC 2014.
[220] G. R. HEATH, B. R. G. JOHNSON, P. D. OLMSTED, S. D. CONNELL, AND S. D. EVANS, "ACTIN ASSEMBLY AT MODEL-SUPPORTED LIPID BILAYERS," *BIOPHYSICAL JOURNAL,* VOL. 105, NO. 10, PP. 2355-2365, NOV 19 2013.
[221] E. A. DISALVO *ET AL.*, "STRUCTURAL AND FUNCTIONAL PROPERTIES OF HYDRATION AND CONFINED WATER IN MEMBRANE INTERFACES," *BIOCHIMICA ET BIOPHYSICA ACTA-BIOMEMBRANES,* VOL. 1778, NO. 12, PP. 2655-2670, DEC 2008.
[222] H. HIMENO, N. SHIMOKAWA, S. KOMURA, D. ANDELMAN, T. HAMADA, AND M. TAKAGI, "CHARGE-INDUCED PHASE SEPARATION IN LIPID MEMBRANES," *SOFT MATTER,* VOL. 10, NO. 40, PP. 7959-7967, 2014 2014.
[223] Y. S. TARAHOVSKY, E. N. MUZAFAROV, AND Y. A. KIM, "RAFTS MAKING AND RAFTS BRAKING: HOW PLANT FLAVONOIDS MAY CONTROL MEMBRANE HETEROGENEITY," (IN ENGLISH), *MOLECULAR AND CELLULAR BIOCHEMISTRY,* ARTICLE VOL. 314, NO. 1-2, PP. 65-71, JUL 2008.
[224] H. BINDER, "WATER NEAR LIPID MEMBRANES AS SEEN BY INFRARED SPECTROSCOPY," *EUROPEAN BIOPHYSICS JOURNAL WITH BIOPHYSICS LETTERS,* VOL. 36, NO. 4-5, PP. 265-279, APR 2007.
[225] R. KOYNOVA, J. BRANKOV, AND B. TENCHOV, "MODULATION OF LIPID PHASE BEHAVIOR BY KOSMOTROPIC AND CHAOTROPIC SOLUTES - EXPERIMENT AND THERMODYNAMIC THEORY," *EUROPEAN BIOPHYSICS JOURNAL WITH BIOPHYSICS LETTERS,* VOL. 25, NO. 4, PP. 261-274, 1997 1997.
[226] Y. KAMEDA, R. TAKAHASHI, T. USUKI, AND O. UEMURA, "HYDRATION STRUCTURE OF SCN- IN CONCENTRATED AQUEOUS SODIUM THIOCYANATE SOLUTIONS," *BULLETIN OF THE CHEMICAL SOCIETY OF JAPAN,* VOL. 67, NO. 4, PP. 956-963, APR 1994.
[227] W. RAWICZ, B. A. SMITH, T. J. MCINTOSH, S. A. SIMON, AND E. EVANS, "ELASTICITY, STRENGTH, AND WATER PERMEABILITY OF BILAYERS THAT CONTAIN RAFT MICRODOMAIN-FORMING LIPIDS," *BIOPHYSICAL JOURNAL,* VOL. 94, NO. 12, PP. 4725-4736, JUN 15 2008.
[228] R. M. EPAND, S. D. RYCHNOVSKY, J. D. BELANI, AND R. F. EPAND, "ROLE OF CHIRALITY IN PEPTIDE-INDUCED FORMATION OF CHOLESTEROL-RICH DOMAINS," (IN ENGLISH), *BIOCHEMICAL JOURNAL,* ARTICLE VOL. 390, PP. 541-548, SEP 2005.
[229] D. R. MARTIN, D. FIORETTO, AND D. V. MATYUSHOV, "DEPOLARIZED LIGHT SCATTERING AND DIELECTRIC RESPONSE OF A PEPTIDE DISSOLVED IN WATER," *JOURNAL OF CHEMICAL PHYSICS,* VOL. 140, NO. 3, JAN 21 2014, ART. NO. 035101.
[230] D. R. MARTIN AND D. V. MATYUSHOV, "HYDRATION SHELLS OF PROTEINS PROBED BY DEPOLARIZED LIGHT SCATTERING AND

DIELECTRIC SPECTROSCOPY: ORIENTATIONAL STRUCTURE IS SIGNIFICANT, POSITIONAL STRUCTURE IS NOT," *JOURNAL OF CHEMICAL PHYSICS*, VOL. 141, NO. 22, DEC 14 2014, ART. NO. 22D501.

[231] A. GRAKOUI *ET AL.*, "THE IMMUNOLOGICAL SYNAPSE: A MOLECULAR MACHINE CONTROLLING T CELL ACTIVATION," *SCIENCE*, VOL. 285, NO. 5425, PP. 221-227, JUL 9 1999.

[232] E. YAMAMOTO, T. AKIMOTO, M. YASUI, AND K. YASUOKA, "ORIGIN OF SUBDIFFUSION OF WATER MOLECULES ON CELL MEMBRANE SURFACES," (IN ENGLISH), *SCIENTIFIC REPORTS*, ARTICLE VOL. 4, P. 7, APR 2014, ART. NO. 4720.

[233] A. E. NEL *ET AL.*, "UNDERSTANDING BIOPHYSICOCHEMICAL INTERACTIONS AT THE NANO-BIO INTERFACE," (IN ENGLISH), *NATURE MATERIALS*, REVIEW VOL. 8, NO. 7, PP. 543-557, JUL 2009.

[234] S. Y. OH *ET AL.*, "AMYLOID PRECURSOR PROTEIN INTERACTS WITH NOTCH RECEPTORS," (IN ENGLISH), *JOURNAL OF NEUROSCIENCE RESEARCH*, ARTICLE VOL. 82, NO. 1, PP. 32-42, OCT 2005.

[235] S. LEAR AND S. L. COBB, "PEP-CALC.COM: A SET OF WEB UTILITIES FOR THE CALCULATION OF PEPTIDE AND PEPTOID PROPERTIES AND AUTOMATIC MASS SPECTRAL PEAK ASSIGNMENT," *JOURNAL OF COMPUTER-AIDED MOLECULAR DESIGN*, VOL. 30, NO. 3, PP. 271-277, MAR 2016.

[236] P. F. F. ALMEIDA, A. POKORNY, AND A. HINDERLITER, "THERMODYNAMICS OF MEMBRANE DOMAINS," (IN ENGLISH), *BIOCHIMICA ET BIOPHYSICA ACTA-BIOMEMBRANES*, REVIEW VOL. 1720, NO. 1-2, PP. 1-13, DEC 2005.

[237] A. BERTONI *ET AL.*, "EARLY AND LATE EVENTS INDUCED BY POLYQ-EXPANDED PROTEINS IDENTIFICATION OF A COMMON PATHOGENIC PROPERTY OF POLYQ-EXPANDED PROTEINS," *JOURNAL OF BIOLOGICAL CHEMISTRY*, VOL. 286, NO. 6, PP. 4727-4741, FEB 2011.

[238] C. SONG, H. HOLMSEN, AND W. NERDAL, "EXISTENCE OF LIPID MICRODOMAINS IN BILAYER OF DIPALMITOYL PHOSPHATIDYLCHOLINE (DPPQ AND 1-STEAROYL-2-DOCOSAHEXENOYL PHOSPHATIDYLSERINE (SDPS) AND THEIR PERTURBATION BY CHLORPROMAZINE: A C-13 AND P-31 SOLID-STATE NMR STUDY," *BIOPHYSICAL CHEMISTRY*, VOL. 120, NO. 3, PP. 178-187, APR 2006.

[239] Q. C. ZHANG *ET AL.*, "A COMPACT BETA MODEL OF HUNTINGTIN TOXICITY," *JOURNAL OF BIOLOGICAL CHEMISTRY*, VOL. 286, NO. 10, PP. 8188-8196, MAR 11 2011.

[240] S. COTE, V. BINETTE, E. S. SALNIKOV, B. BECHINGER, AND N. MOUSSEAU, "PROBING THE HUNTINGTIN 1-17 MEMBRANE ANCHOR ON A PHOSPHOLIPID BILAYER BY USING ALL-ATOM SIMULATIONS," *BIOPHYSICAL JOURNAL*, VOL. 108, NO. 5, PP. 1187-1198, MAR 10 2015.

[241] A. NAGARAJAN, S. JAWAHERY, AND S. MATYSIAK, "THE EFFECTS OF FLANKING SEQUENCES IN THE INTERACTION OF POLYGLUTAMINE PEPTIDES WITH A MEMBRANE BILAYER," *JOURNAL OF PHYSICAL CHEMISTRY B*, VOL. 118, NO. 24, PP. 6368-6379, JUN 19 2014.

[242] K. A. BURKE, K. J. KAUFFMAN, C. S. UMBAUGH, S. L. FREY, AND J. LEGLEITER, "THE INTERACTION OF POLYGLUTAMINE PEPTIDES WITH LIPID MEMBRANES IS REGULATED BY FLANKING SEQUENCES ASSOCIATED WITH HUNTINGTIN," *JOURNAL OF BIOLOGICAL CHEMISTRY*, VOL. 288, NO. 21, PP. 14993-15005, MAY 24 2013.

[243] E. L. ALTSCHULER, N. V. HUD, J. A. MAZRIMAS, AND B. RUPP, "RANDOM COIL CONFORMATION FOR EXTENDED POLYGLUTAMINE STRETCHES

IN AQUEOUS SOLUBLE MONOMERIC PEPTIDES," *JOURNAL OF PEPTIDE RESEARCH*, VOL. 50, NO. 1, PP. 73-75, JUL 1997.
[244] P. C. PAINTER AND J. L. KOENIG, "SOLUTION CONFORMATION OF POLY(L-LYSINE) - RAMAN AND INFRARED SPECTROSCOPIC STUDY," *BIOPOLYMERS*, VOL. 15, NO. 2, PP. 229-240, 1976 1976.
[245] A. HATEGAN, K. SENGUPTA, S. KAHN, E. SACKMANN, AND D. E. DISCHER, "TOPOGRAPHICAL PATTERN DYNAMICS IN PASSIVE ADHESION OF CELL MEMBRANES," *BIOPHYSICAL JOURNAL*, VOL. 87, NO. 5, PP. 3547-3560, NOV 2004.
[246] G. R. HEATH *ET AL.*, "LAYER-BY-LAYER ASSEMBLY OF SUPPORTED LIPID BILAYER POLY-L-LYSINE MULTILAYERS," (IN ENGLISH), *BIOMACROMOLECULES*, ARTICLE VOL. 17, NO. 1, PP. 324-335, JAN 2016.
[247] A. R. DE BOER, C. H. HOKKE, A. M. DEELDER, AND M. WUHRER, "SERUM ANTIBODY SCREENING BY SURFACE PLASMON RESONANCE USING A NATURAL GLYCAN MICROARRAY," *GLYCOCONJ J*, VOL. 25, NO. 1, PP. 75-84, JAN 2008.
[248] R. J. GREEN, J. DAVIES, M. C. DAVIES, C. J. ROBERTS, AND S. J. B. TENDLER, "SURFACE PLASMON RESONANCE FOR REAL TIME IN SITU ANALYSIS OF PROTEIN ADSORPTION TO POLYMER SURFACES," (IN ENGLISH), *BIOMATERIALS*, ARTICLE VOL. 18, NO. 5, PP. 405-413, MAR 1997.
[249] C. R. EMMENEGGER, E. BRYNDA, T. RIEDEL, Z. SEDLAKOVA, M. HOUSKA, AND A. B. ALLES, "INTERACTION OF BLOOD PLASMA WITH ANTIFOULING SURFACES," (IN ENGLISH), *LANGMUIR*, ARTICLE VOL. 25, NO. 11, PP. 6328-6333, JUN 2009.
[250] A. AUBE, J. BREAULT-TURCOT, P. CHAURAND, J. N. PELLETIER, AND J. F. MASSON, "NON-SPECIFIC ADSORPTION OF CRUDE CELL LYSATE ON SURFACE PLASMON RESONANCE SENSORS," *LANGMUIR*, VOL. 29, NO. 32, PP. 10141-10148, AUG 2013.
[251] R. ALCALDE, A. GUTIERREZ, M. ATILHAN, J. L. TRENZADA, AND S. APARICIO, "INSIGHTS INTO GLYCOL ETHER-ALKANOL MIXTURES FROM A COMBINED EXPERIMENTAL AND THEORETICAL APPROACH," *JOURNAL OF PHYSICAL CHEMISTRY B*, VOL. 121, NO. 22, PP. 5601-5612, JUN 2017.
[252] L. CENCI *ET AL.*, "SURFACE PLASMON RESONANCE BASED ON MOLECULARLY IMPRINTED NANOPARTICLES FOR THE PICOMOLAR DETECTION OF THE IRON REGULATING HORMONE HEPCIDIN-25," (IN ENGLISH), *JOURNAL OF NANOBIOTECHNOLOGY*, ARTICLE VOL. 13, P. 15, AUG 2015, ART. NO. 51.
[253] R. ALCALDE, G. GARCIA, J. L. TRENZADO, M. ATILHAN, AND S. APARICIO, "CHARACTERIZATION OF AMIDE-ALKANEDIOL INTERMOLECULAR INTERACTIONS," *THE JOURNAL OF PHYSICAL CHEMISTRY. B*, VOL. 119, NO. 13, PP. 4725-38, 2015-APR-2 2015.
[254] Y. J. HUANG, P. KANNAN, L. ZHANG, T. CHEN, AND D. H. KIM, "CONCAVE GOLD NANOPARTICLE-BASED HIGHLY SENSITIVE ELECTROCHEMICAL IGG IMMUNOBIOSENSOR FOR THE DETECTION OF ANTIBODY-ANTIGEN INTERACTIONS," *RSC ADVANCES*, VOL. 5, NO. 72, PP. 58478-58484, 2015.
[255] J. L. RICHENS, E. A. M. LUNT, AND P. O'SHEA, "OPTIMISATION OF PROTEIN MICROARRAY TECHNIQUES FOR ANALYSIS OF THE PLASMA PROTEOME: MINIMISATION OF NON-SPECIFIC BINDING INTERACTIONS," (IN ENGLISH), *INTERNATIONAL IMMUNOPHARMACOLOGY*, ARTICLE VOL. 24, NO. 2, PP. 166-168, FEB 2015.
[256] D. RICHARDSON, "MEMBRANE MICRODOMAIN MODELLING WITH NASCN," *UNPUBLISHED OBSERVATIONS*, 2016.

[257] J. L. RICHENS, J. S. LANE, M. L. MATHER, AND P. O'SHEA, "THE INTERACTIONS OF SQUALENE, ALKANES AND OTHER MINERAL OILS WITH MODEL MEMBRANES; EFFECTS ON MEMBRANE HETEROGENEITY AND FUNCTION," *JOURNAL OF COLLOID AND INTERFACE SCIENCE*, VOL. 457, PP. 225-231, NOV 1 2015.

[258] P. J. BOOTH, R. H. TEMPLER, W. MEIJBERG, S. J. ALLEN, A. R. CURRAN, AND M. LORCH, "IN VITRO STUDIES OF MEMBRANE PROTEIN FOLDING," (IN ENGLISH), *CRITICAL REVIEWS IN BIOCHEMISTRY AND MOLECULAR BIOLOGY*, REVIEW VOL. 36, NO. 6, PP. 501-603, 2001.

[259] T. J. KNOWLES, R. FINKA, C. SMITH, Y. P. LIN, T. DAFFORN, AND M. OVERDUIN, "MEMBRANE PROTEINS SOLUBILIZED INTACT IN LIPID CONTAINING NANOPARTICLES BOUNDED BY STYRENE MALEIC ACID COPOLYMER," *JOURNAL OF THE AMERICAN CHEMICAL SOCIETY*, VOL. 131, NO. 22, PP. 7484-+, JUN 2009.

[260] J. KNOL, K. SJOLLEMA, AND B. POOLMAN, "DETERGENT-MEDIATED RECONSTITUTION OF MEMBRANE PROTEINS," *BIOCHEMISTRY*, VOL. 37, NO. 46, PP. 16410-16415, NOV 1998.

[261] L. YANG AND M. GLASER, "MEMBRANE DOMAINS CONTAINING PHOSPHATIDYLSERINE AND SUBSTRATE CAN BE IMPORTANT FOR THE ACTIVATION OF PROTEIN-KINASE-C," (IN ENGLISH), *BIOCHEMISTRY*, ARTICLE VOL. 34, NO. 5, PP. 1500-1506, FEB 1995.

[262] J. Y. KIM, M. MOSIOR, L. A. CHUNG, H. WU, AND S. MCLAUGHLIN, "BINDING OF PEPTIDES WITH BASIC RESIDUES TO MEMBRANES CONTAINING ACIDIC PHOSPHOLIPIDS," (IN ENGLISH), *BIOPHYSICAL JOURNAL*, ARTICLE VOL. 60, NO. 1, PP. 135-148, JUL 1991.

[263] I. VERMES, C. HAANEN, H. STEFFENSNAKKEN, AND C. REUTELINGSPERGER, "A NOVEL ASSAY FOR APOPTOSIS - FLOW CYTOMETRIC DETECTION OF PHOSPHATIDYLSERINE EXPRESSION ON EARLY APOPTOTIC CELLS USING FLUORESCEIN-LABELED ANNEXIN-V," *JOURNAL OF IMMUNOLOGICAL METHODS*, VOL. 184, NO. 1, PP. 39-51, JUL 1995.

[264] G. P. BATES *ET AL.*, "HUNTINGTON DISEASE," *NATURE REVIEWS DISEASE PRIMERS*, VOL. 15005, 2015.